

**INVESTIGATION OF ELECTROSTATIC CHARGING PHENOMENA IN DRY  
POWDER INHALERS AND THE EFFECT ON DEPOSITION**

Martin Jan Telko

A dissertation submitted to the faculty of the University of North Carolina at Chapel Hill in partial fulfillment of the requirements for the degree of Doctor of Philosophy in the Department of Pharmaceutical Sciences.

Chapel Hill  
2009

Approved by:

Advisor: Anthony J. Hickey, PhD., D.Sc

Chair: Philip C. Smith, PhD.

Reader: Lucila Garcia-Contreras, PhD.

Reader: J. Ed Hall, PhD.

Reader: David Leith, Sc.D.

©2009  
Martin Jan Telko  
ALL RIGHTS RESERVED

## **ABSTRACT**

MARTIN JAN TELKO

### INVESTIGATION OF ELECTROSTATIC CHARGING PHENOMENA IN DRY POWDER INHALERS AND THE EFFECT ON DEPOSITION

(Under the direction of Professor Anthony J. Hickey.)

Dry powder inhalers (DPI) are an important drug delivery option, for the treatment of respiratory diseases, and, increasingly, for the delivery of systemically acting drugs and vaccines. Most DPI formulations consist of micronized drug blended with larger carrier particles. The interactions between drug and carrier are a major determinant of DPI performance. Electrostatic interactions between particles are recognized as one mode of particle interaction. Simulations, *in vitro* and *in vivo* studies indicate that electrostatic charge affects the delivery and deposition of aerosol particles in the lung. Yet, the occurrence and origins of electrostatic charge on medicinal aerosol particles are poorly investigated and understood.

The major physicochemical properties of two drugs (albuterol sulfate and budesonide) and a number of excipients (lactose, glucose and calcium phosphate) were assessed. Deposition studies with model formulations using the electrical low pressure impactor showed that micronized drug particles are subject to significant triboelectrification. Particle charge levels were shown to be several orders of magnitude larger than had previously been estimated. A multivariate experimental design framework was employed to investigate the effects of various formulation factors on the charging of the two drugs; it was shown that several formulation variables, in particular the excipient, have profound effects on charge acquired by micronized drug particles available to the lungs. The charging behavior observed in deposition studies agreed largely with bulk electrostatic measurements conducted on the raw materials. It was thus concluded that the origin of the charge was contact charging between

particles of the formulation. The charging behavior was further elucidated through inverse gas chromatography measurements, in which the surface acid/base properties of the excipients were determined. Surface acid/base parameters, which characterize the tendency of a material to act as electron donor or acceptor in intermolecular interactions, correlated with the charges obtained in Faraday well experiments and particle charges acquired during DPI actuation, which suggests the three phenomena are closely related. The rank-order observed (from least to most electron withdrawing) was albuterol, lactose, glucose, calcium phosphate, budesonide. The study provides a mean of characterization that can be used to predict charging propensity which can assist the DPI product development process.

## **DEDICATION**

To my parents Miroslaw Jan and Magdalena Anna Telko, who have always encouraged and supported me.

## ACKNOWLEDGEMENTS

I gratefully acknowledge the helpful discussions with labmates, colleagues, as well as the faculty and students, past and present, of the Division of Molecular Pharmaceutics. In particular, I wanted to thank the members of the Hickey lab, with whom I have had the privilege of working over the last few years.

I thank my former Merck & Co. colleagues, in particular Bozena Matuszewska, Sunny Panmai, and Christopher Kemmerer for encouraging and supporting me in my decision to go to graduate school.

I thank Henna Isherwood and Jukka Kujanpaa of Dekati Ltd, as well as Tyler Beck of Particle Instruments LLC, for introducing me to the Electrical Low Pressure Impactor which has sparked my interest and propelled me down this avenue of research. I also thank them for the training, technical support, and discussion associated with the use of the instrument.

I thank my committee members, Professors Lucila Garcia-Contreras, J. Ed Hall, Anthony Hickey, David Leith, and Philip Smith for their time and effort in guiding me through this project. Their probing questions, insights, and suggestions have been tremendously helpful and are greatly appreciated.

I reserve special thanks to my advisor, Professor Anthony Hickey, who has been a teacher, mentor, and a friend to me. His perspective, humility, and intellect have impacted my work and have touched my life. I will remember the lessons I have learned working in his laboratory throughout my professional and personal life.

Finally, I would like to acknowledge the financial support of the U.S. Pharmacopeia and the PhRMA Foundation which have made this work possible. Receipt of their fellowships has not only been a source of funding, but also a major source of encouragement. I am grateful for further financial support and thoughtful input from John Langridge and Tako Mulder of DMV-Fonterra Excipients, as well as Dimitris Papadopoulos and Richard McLean of Pfizer.

## TABLE OF CONTENT

LIST OF TABLES .....	xii
LIST OF FIGURES .....	xiii
LIST OF ABBREVIATIONS AND SYMBOLS .....	xvii
1. INTRODUCTION .....	1
1.1. General Introduction .....	1
1.2. Formulation Development .....	2
1.3. Dry Powder Inhalers .....	3
1.3.1. Development of the DPI .....	3
1.3.2. Principles of Operation .....	5
1.4. Drug Properties and Manufacture .....	3
1.4.1. The Active Pharmaceutical Ingredient .....	7
1.4.2. API Preparation .....	9
1.5. Excipients .....	12
1.6. Powder and Aerosol Physics .....	13
1.6.1. Crystallinity and Polymorphism .....	14
1.6.2. Moisture Content and Hygroscopicity .....	17
1.6.3. Particle Size .....	18
1.6.4. Surface Area and Morphology .....	24
1.7. Interparticulate Forces of Interaction .....	26

1.7.1. Intermolecular Interactions.....	26
1.7.2. Electrostatic Forces .....	27
1.8. Previous Work .....	33
1.8.1. Faraday Cage.....	33
1.8.2. Single Particle Impact Electrostatics .....	34
1.8.3. Electrical Single Particle Aerodynamic Relaxation Time (E-SPART) .....	35
1.8.4. Electrical Low Pressure Impaction.....	35
1.9. Problem Statement .....	36
1.10. Hypotheses and Specific Aims .....	37
1.10.1. Hypotheses .....	37
1.10.2. Specific Aims .....	37
1.11. Conclusion .....	39
1.12. Acknowledgements.....	40
1.13. Literature Cited.....	41
<b>2. MATERIAL PREPARATION AND PHYSICOCHEMICAL CHARACTERIZATION .....</b>	<b>53</b>
2.1. Introduction.....	53
2.1.1 Selection of Drugs.....	54
2.1.2. Selection of Excipients.....	56
2.2. Materials .....	57
2.2.1. Drugs .....	57
2.2.2. Excipients .....	58
2.3. Methods .....	58
2.3.1. Excipient Sieving and Powder Preparation .....	58
2.3.2. Particle Size Analysis.....	59



2.3.3. Thermal Analysis: Differential Scanning Calorimetry.....	60
2.3.4. Electrostatic Material Characterization: Faraday Well Experiments .....	60
2.3.5. Formulation Manufacture and Content Uniformity Determination.....	61
2.4. Results and Discussion .....	62
2.4.1. Particle Size Distribution.....	62
2.4.2. Size and Shape Characterization of Powders .....	65
2.4.3. Differential Scanning Calorimetry .....	69
2.4.4. Electrostatic Material Characterization .....	70
2.5. Summary .....	73
2.6. Acknowledgements.....	74
2.7. Literature Cited .....	75
3. SURFACE ENERGY MEASUREMENTS .....	77
3.1. Introduction.....	77
3.2. IGC Theory and Experimental Conditions .....	78
3.2.1. Surface Free Energy .....	78
3.2.2. Dispersive and Specific Energy by IGC.....	79
3.3. Materials and Methods.....	82
3.3.1. Materials.....	82
3.3.2. Inverse Gas Chromatography Methodology .....	83
3.3.3. Differential Scanning Calorimetry .....	84
3.3.4. Data Analysis .....	85
3.4. Results and Discussion .....	85
3.4.1. Analysis of Lactose Monohydrate Batches .....	85
3.4.2. Analysis of Glucose Monohydrate .....	87

3.4.3. Analysis of Anhydrous Calcium Phosphate .....	89
3.4.4. Discussion .....	91
3.5. Summary and Conclusion .....	93
3.6. Acknowledgements .....	93
3.7. Literature Cited .....	94
4. AERODYNAMIC AND ELECTROSTATIC PROPERTIES DETERMINED BY ELECTRICAL LOW PRESSURE IMPACTION .....	97
4.1. Introduction .....	97
4.1.1. Electrostatic Low Pressure Impactor (ELPI™) .....	97
4.1.2. Preliminary Data .....	99
4.2. Experimental Design .....	100
4.2.1. Design Factors .....	101
4.2.2. Study Design .....	104
4.3. Materials and Methods .....	108
4.3.1. Materials .....	108
4.3.2. Methods .....	108
4.4. Results and Discussion .....	113
4.4.1. Reproducibility of ELPI Experiments .....	113
4.4.2. Remanufactured Product Variability .....	116
4.4.3. Surface Effects .....	117
4.4.4. Environmental Effects .....	120
4.4.5. Experimental Design Analysis: Effect of Formulation Factors on Fine Particle Mass (FPM) and Particle Size Distribution .....	122
4.4.6. Experimental Design Analysis: Effect of Formulation Factors on Electrostatic Charging of Drug .....	129
4.4.7. Triboelectric Series .....	140

4.4.8. Per Particle Charge Levels .....	142
4.4.9. Study Design Critique .....	144
4.5. Summary and Conclusion .....	145
4.6. Acknowledgements .....	148
4.7. Literature Cited .....	149
5. GENERAL CONCLUSIONS AND FUTURE WORK .....	152
5.1. Hypotheses .....	153
5.2. Specific Aims .....	153
5.3. Discussion .....	156
5.4. Future Work .....	158
5.5. Literature Cited .....	161
APPENDICES .....	164
APPENDIX A. FARADAY WELL CIRCUIT .....	165
APPENDIX B. CRITICAL ASSESSMENT OF INVERSE GAS CHROMATOGRAPHY AS MEANS OF ASSESSING SURFACE FREE ENERGY AND ACID-BASE INTERACTION OF PHARMACEUTICAL POWDERS .....	166
APPENDIX C. INVESTIGATION OF TRIBOELECTRIC CHARGING IN DRY POWDER INHALERS USING ELECTRICAL LOW PRESSURE IMPACTOR (ELPI™) .....	175
APPENDIX D. EFFECT OF STORAGE ON DISPERSION AND CHARGE .....	185

## LIST OF TABLES

Table 1.1. Dry powder inhaler vs. metered dose inhaler.....	4
Table 1.2. Mean physicochemical properties of marketed small-molecule drugs for oral inhalation....	8
Table 2.1. Select properties of albuterol sulfate and budesonide .....	55
Table 2.2. Select material properties of excipients used in these studies .....	57
Table 2.3. Particle size distribution summary for different excipient sieve fractions obtained (after sifting).....	65
Table 2.4. Triboelectric series, by excipient sieve fraction, from most negative to most positive.....	72
Table 3.1. Properties of IGC probes, values used in all IGC calculations .....	85
Table 3.2. Surface acid/base parameters of lactose monohydrate batches, SV and ML with corresponding square of correlation coefficient.....	87
Table 3.3. Specific surface free energies of adsorption between glucose monohydrate and the vapor probes listed in the table .....	89
Table 3.4. Summary of $K_A$ and $K_B$ data obtained in the IGC experiments .....	92
Table 4.1. Relevant fluid dynamic properties of standard entrainment tubes used in studies compared with previously used and commercially available inhalers.....	109
Table 4.2. Effect of last surface of contact on total charge for 1% albuterol in ML58 lactose, 45-75 um sieve fraction formulation, 20mg actuated from SET A, shown in Figure 4.9 .....	119
Table 4.3. Effect of last surface of contact on total charge for 0.5% budesonide in SV425 lactose, 45-75 um sieve fraction formulation, 40mg actuated from SET A.....	120
Table 4.4. Particle size distribution proxies for albuterol in 45-75um ML80 lactose formulation, shown in Figure 4.12 .....	123
Table 4.5. Effect of excipient, , drug concentration, and fluidization conditions on the PSD and FPF of deposited budesonide.....	126
Table 4.6. Effect of excipient, excipient sieve fraction, drug concentration, and fluidization conditions on the PSD and FPF of deposited albuterol .....	128
Table 4.7. Formulation variables contributing to the charging of budesonide.....	137
Table 4.8. Formulation variables contributing to the charging of albuterol.....	137
Table 4.9. Using formulation techniques to affect drug charging.....	147

## LIST OF FIGURES

Figure 1.1. Principle of dry powder inhaler design. The formulation, typically consisting of micronized drug blended with larger carrier particles is dispensed in a metering system. An active or passive dispersion system entrains the particles in the patient's airways where drug particles separate from the carrier and are carried into the lung .....	6
Figure 1.2. Crystal habit. Inhibition of growth in one of more spatial directions results particles with plate or needle morphology .....	16
Figure 1.3 Hygroscopic growth. Particles absorb moisture as they traverse the humid environment of the airways resulting in increased particle size.....	18
Figure 1.4. Strategies for altering the aerodynamic diameter. A. Aerodynamic diameter equation; B. Large, low density porous particles; C. Needle-shaped particles. Particles in both A and B are expected to have aerodynamic diameters that are smaller than their size would suggest.....	20
Figure 1.5. Particle sizing by laser light diffraction .....	23
Figure 1.6. Particle sizing by digital image analysis .....	24
Figure 2.1. Particle size distribution of budesonide (blue) and albuterol (red). Figure 2.1(a) shows the fraction of drug recovered on the midpoint of the given stage. Figure 2.1(b) shows the cumulative undersize at each interval.....	63
Figure 2.2. Particle size distribution of CP sample and the constituent sieve fractions after simple sieving, i.e. without additional fluidization. All samples clearly show the presence of very fine, single micron size particles. Dashed lines show the sieve fraction pore sizes.....	64
Figure 2.3. Particle size distribution of whole calcium phosphate sieve fractions after sieving and sifting. Compared to Figure 2.2, the proportion of fine particles is greatly reduced. Dashed lines show the sieve fraction pore sizes.....	64
Figure 2.4. Micronized drug particles at 5000x magnification. (a) Albuterol sulfate, (b) budesonide.	66
Figure 2.5. Electron micrographs showing the 45-75 $\mu$ m sieve cut, each at a magnification of 500x..	67
Figure 2.6. Lactose SV94 particles at 15,000x magnification. Fine particles in the single micron range are present at the particle surface. ....	68
Figure 2.7. Representative drug blends. (a) 1% albuterol on ML58 lactose particles (b) 0.5% Budesonide on CP particles. Drug was quite evenly distributed. ....	68
Figure 2.8. DSC thermograms of albuterol sulfate and budesonide used in formulations. ....	69
Figure 2.9. DSC thermograms of lactose ML58, ML80, SV94, SV425, and glucose. Samples were scanned at at 5°C/min from 50°C to 250°C.....	70
Figure 2.10. Electrostatic charge recorded after deposition of the powders in the Faraday well. Experiments were randomized and performed at a 23°C/24%RH ambient conditions. Averages of	

n=3 experiments with standard deviations in the error bar are shown.....	71
Figure 3.1. Plot used to determine the dispersive and specific surface energy of the solid, $\gamma_s^d$ and $\gamma_s^{sp}$ , respectively. ....	80
Figure 3.2. Dispersive surface free energies of sieved and milled lactose monohydrate vs. temperature. ....	86
Figure 3.3. Thermogram of glucose monohydrate before (blue) and after (blue) the IGC experiment. Prolonged exposure of glucose monohydrate packed into IGC column at 48°C results in dehydration and formation of $\beta$ -D-dextrose. Prolonged exposure of glucose monohydrate at 36°C results in dehydration of the material. Glucose monohydrate has a melting point of ~80°C, glucose anhydrate melts at ~145°C, while $\beta$ -glucose melts at ~150°C.....	88
Figure 3.4. Dispersive surface free energy of calcium phosphate from 60°C to 100°C. ....	90
Figure 4.1. (a) Standard ELPI configuration with corona charger in place. The aerosol particles are charged uniformly prior to deposition within the impactor, for real-time particle size determination. (b) Modified ELPI configuration with charger turned off. When the incoming aerosol is not charged uniformly, the ELPI determines native particle charges and records a charge distribution. ....	98
Figure 4.2. Ishikawa (cause-and-effect) diagram describing the function of dry powder inhalers. ...	101
Figure 4.3. Experimental framework developed to study the electrostatic effects of the variables. Each circle denotes a different experimental setting. The framework contains elements of factorial and central composite design but was developed to test specific hypotheses. The main elements of the design are denoted by red boxes. The design is described in detail in the text.....	106
Figure 4.4. Experimental set-up, adapted from Telko et al. 2007. ....	110
Figure 4.5. Six actuations of 1% albuterol in ML58 lactose, 45-75 $\mu$ m sieve fraction, 20mg actuated from SET A. The first three were performed on one day separated only by actuations of excipient, the next three performed 9 days later, also separated by excipient actuations (excipient actuations have been removed from this graph). Double line indicates temporal discontinuity. In each case, deposition on stages is complete in about 6 seconds. While there is some variability with regards to magnitude, the overall rank/order and polarity is highly preserved in each trial.....	114
Figure 4.6. Formulation (0.5% albuterol in 45-75 $\mu$ m ML80 lactose, 40mg) actuated from SET A (three times) on different days, separated by 5 days of storage. The differences in deposition (actual quantities shown) are minimal. Differences in charge distribution mirror the differences in deposition, and are within a standard deviation from one another. ....	115
Figure 4.7. Remade formulation (0.5% albuterol in 75-106 $\mu$ m ML58 lactose) actuated from SET A (three times). ....	116
Figure 4.8. Same formulation (0.5% budesonide in 45-75 $\mu$ m SV425 lactose) actuated from SET A (three times) on different days, separated by 36 days of storage. Also shown remade formulation, actuated day after it was made. The remade formulation has FPF similar to the old formulation without storage, while storage results in higher deposition. Charge deposition profiles are similar for all.....	117

Figure 4.9. 1% albuterol in ML58 lactose, 45-75 $\mu\text{m}$ sieve fraction, 20mg actuated from SET A, off different surfaces. The eight actuations were performed in a row with intermittent placebo actuations. There are minor magnitude differences but the charge deposition profiles are largely the same. This supports the hypothesis that the charges observed are the result of triboelectrification during actuation, when particles have undergone charge transfer and those charges are exposed. ....	118
Figure 4.10. 0.5% budesonide in SV425 lactose, 45-75 $\mu\text{m}$ sieve fraction, 20mg actuated from SET A, off different surfaces. The eight actuations were performed in a row with intermittent placebo actuations. There are minor magnitude differences but the charge deposition profiles are largely the same. This supports the hypothesis that the charges observed are the result of triboelectrification during actuation, when particles have undergone charge transfer and those charges are exposed. ....	120
Figure 4.11. 1% albuterol in ML58 lactose, 45-75 $\mu\text{m}$ sieve fraction, 20mg actuated from SET A, actuated at low RH, high RH, and then again at low RH. Brief exposure to high RH as might be experienced in a patient's lung does not lead to a dissipation of electrical charges. ....	121
Figure 4.12. Effects of drug concentration and actuation conditions (high pressure drop (SET A), low pressure drop (SET C) and very low pressure drop (SET D)) on the particle size distribution of albuterol in 45-75 $\mu\text{m}$ ML80 lactose formulations. ....	123
Figure 4.13. Effect of formulation excipient on FPM and charge distribution of albuterol. Mass depositions of drug ( $\mu\text{g}$ , yellow diamonds), charge distribution of formulation (fC, red rectangles, $n=3 \pm \sigma$ ), and excipient charging (fC, blue triangles) are shown. Each formulation is 0.5% albuterol in 45-75 $\mu\text{m}$ fraction of the excipient, 40mg actuated from SET A. ....	130
Figure 4.14. Effect of formulation excipient on FPM and charge distribution of budesonide. Mass depositions of drug ( $\mu\text{g}$ , yellow diamonds), charge distribution of formulation (fC, red rectangles, $n=3 \pm \sigma$ ), and excipient charging (fC, blue triangles) are shown. Each formulation is 0.5% albuterol in 45-75 $\mu\text{m}$ fraction of the excipient, 40mg actuated from SET A. ....	131
Figure 4.15. Charge distribution (average particle charge) for drug deposited in ELPI. Shown are 0.5% budesonide in ML80 lactose (45-75 $\mu\text{m}$ ) (blue diamonds), 0.5% albuterol in ML58 lactose (45-75 $\mu\text{m}$ ) (yellow diamonds), both actuated from SET A (high Re). For comparison, the graph shows the charge limit expected for the particles (green triangles) and the Boltzmann charge distribution (red squares). In both cases, over 80% of the deposited particles carry >100 charges per particle. ....	143
Figure A.1. Non-integrating circuit for Faraday well.....	165
Figure A.2. Photo of Faraday well .....	165
Figure D.1. Formulation (0.5% albuterol in 45-75 $\mu\text{m}$ ML80 lactose, 40mg) actuated from SET A (three times) on different days, separated by 5 days of storage. The differences in deposition (actual quantities shown) are minimal. Differences in charge distribution mirror the differences in deposition, and are within a standard deviation from one another.. ....	185
Figure D.2. Formulation (1% albuterol in 45-75 $\mu\text{m}$ ML58 lactose, 20mg) actuated from SET A (three times) on different days, separated by 9 days of storage. Reproducibility is very good.....	186

Figure D.3. Same formulation (1% budesonide in 45-75 $\mu$ m ML80 lactose) actuated from SET C (three times) on different days, separated by 6 days of storage. Differences in deposition (actual quantities shown) are minimal; differences in charge distribution are within standard deviation and follow deposition patterns..... 186

Figure D.4. Same formulation (0.5% budesonide in 45-75 $\mu$ m ML80 lactose) actuated from SET A (three times) on different days, separated by 33 days of storage. The differences in deposition (actual quantities shown) are quite large with significantly more deposition after storage. Despite these differences the charge distributions are virtually the same..... 187

Figure D.5. Same formulation (0.5% albuterol in 75-106 $\mu$ m ML80 lactose) actuated from SET A (three times) on different days, separated by 49 days of storage. .... 188

Figure D.6. Changes in (a) FPF and (b) charge as a result of storage. Each point in the graph represents a different formulation that was retested after a variable number of days in storage (x-axis). For most formulations, storage seems to increase the FPF, i.e. it results in an improvement of drug/carrier separation. The charge becomes more positive after storage, even though the magnitude remains unchanged..... 189

Figure D.7. The change in charge plotted against the change in deposited mass. Essentially, the ordinate data in Figures 5.10 (a) and (b) give the abscissa and ordinate in Figure 5.11. The figure indicates more clearly that the total charge becomes more positive but the sum of charges changes little in absolute magnitude..... 190



## LIST OF ABBREVIATIONS AND SYMBOLS

$\gamma$	surface (or interfacial) energy, J/m <sup>2</sup>
$\gamma_d$	dispersive surface energy
$\gamma_{sp}$	polar surface energy
$\lambda$	mean free path
$\epsilon$	permittivity
$\epsilon_0$	permittivity of vacuum, 8.85 x 10 <sup>-12</sup> C <sup>2</sup> /Nm <sup>2</sup>
$\epsilon_r$	relative permittivity, dielectric constant
$\phi$	work function
$\eta$	viscosity
$\rho_o$	unit density
$\rho_p$	particle density
$\sigma$	conductivity, Si/m; standard deviation
$\tau$	charge relaxation time
$\mu$	kinematic viscosity
X	shape factor
a	area, molecular surface area
ACI	Andersen cascade impactor
AN*	acceptor number, corrected
ANOVA	Analysis of variance
CMD	count median diameter
COPD	chronic obstructive pulmonary disease
CP	calcium phosphate
D	diffusion coefficient
d	diameter
d <sub>10</sub> , d <sub>50</sub> , d <sub>90</sub>	particle diameter, for which 10%, 50%, 90% particles are undersize
d <sub>ae</sub>	aerodynamic diameter
d <sub>eq</sub>	equivalent volume diameter
d <sub>p</sub>	particle diameter
DN	donor number
DPI	dry powder inhaler

DSC	differential scanning calorimetry
e	charge of an electron, $1.6 \times 10^{-19}$ C
ED	emitted dose
$E_L$	Surface field strength required for spontaneous emission, $9.0 \times 10^8$ V/m
ELPI	electrical low pressure impactor
E-SPART	electrical single particle aerodynamic relaxation time
F	force
$f_n$	fraction of particles having n charges
$F_E$	electrostatic force
$F_{\text{grav}}$	gravitational force
$F_{\text{vdw}}$	van der Waals force
FPF	fine particle fraction
FPM	fine particle mass
g	gravitational acceleration constant
G	Gibbs free energy
GLM	General linear model
GSD	geometric standard deviation
H	enthalpy
IGC	inverse gas chromatography
INN	International Nonproprietary Name
$K_A$	surface acid parameter, unitless
$K_B$	surface base parameter, unitless
$k_B$	Boltzmann constant, $1.381 \times 10^{-23}$ J/K
$K_E$	Coulomb's law constant
MW	molecular weight
MDI	metered-dose inhaler
ML	milled
MMAD	mass median aerodynamic diameter
MMD	mass median diameter
N	Avogadro's number
$\bar{n}$	average number (of charges)
$n_L$	negative charge limit (number of elementary charges)

P	pressure
$P_o$	saturation vapor pressure
Q	charge
r	radius, distance
R	gas constant, 8.314J/mol K
S	entropy
SEM	scanning electron microscopy
SET	standard entrainment tube
SV	sieved
T	temperature
t	time
$t_R$	retention time
THF	tetrahydrofuron, $C_4H_8O$
USAN	United States Adopted Name
USP	United States Pharmacopoeia
V	volume
VN	net retention volume
VMD	volume median diameter
$V_{TS}$	terminal settling velocity
v	velocity
$v_p$	particle velocity
$W_A$	work of adhesion
x	distance

## **1. INTRODUCTION**

### **1.1. General Introduction**

Dry powder inhalers (DPI) are an increasingly important drug delivery option, for the treatment of respiratory diseases, as well as for the fast and noninvasive delivery of systemically acting drugs and vaccines. Most DPI formulations consist of micronized drug blended with larger carrier particles, which enhance flow, reduce aggregation and aid in dispersion. During DPI actuation, the formulation is fluidized, dispersed into aerosol particles, and enters the patient's airways. Under the influence of inspiratory airflow, the drug particles separate from the carrier and are transported into the lungs while the larger carrier particles are deposited on the oropharyngeal surfaces and are cleared by dissolution and swallowing. If the forces acting between the particles of the formulation are too strong, the shear of the airflow may not be sufficient to separate drug from the carrier particles resulting in low deposition efficiency.

Significant effort is being expended in understanding the underlying physicochemical parameters influencing DPI performance. Numerous particle design and characterization techniques have been applied toward this end. The work has largely been aimed at controlling particle interactions to enhance dispersion, thereby decreasing variability and increasing delivery of drug to the lung periphery. Aerosol electrostatic properties have not been studied in this context. Particle charging is being used in a number of industries to control particle behavior. Charge may also be a design advantage for medicinal aerosols. It is postulated that triboelectric charging is a major factor in drug delivery from DPIs and that its characterization and control can be utilized to enhance DPI performance.

## 1.2. Formulation Development

Formulation development encompasses an array of processes in which an active pharmaceutical ingredient (API) is incorporated into a drug product. While biological activity of the API is a prerequisite for a successful dosage form, it is not the sole determinant of efficacy. Factors such as stability, processability, delivery and availability to target organ, contribute significantly to an efficacious pharmaceutical system. Optimization of these factors is a key development task, and the final product is often a compromise between pharmaceutical and practical (i.e. economic/engineering) considerations. Formulation development is challenging because molecules with pharmacological activity often display poor physicochemical properties. In fact, the same molecular characteristics that confer pharmacological activity, e.g. high receptor affinity, frequently limit a compound's pharmaceutical utility making it difficult or even unsuitable for delivery.<sup>1, 2</sup> This is particularly true for many of the compounds that are identified by high-throughput screening methods.<sup>2, 3</sup>

Development of pharmaceuticals for inhalation is a particular challenge, as it involves the preparation of a formulation and the selection of a device for aerosol dispersion. The lungs have lower buffering capacity than other delivery sites (e.g. the GI tract or the blood) which limits the range of excipients that could potentially enhance delivery outcomes. The patient is an additional variable, presenting unique barriers for pulmonary delivery, both in terms of respiratory tract anatomy and physiology, and mode of inhalation.<sup>4</sup> There are greater complexities in administering an inhaled aerosol than there are for oral administration of tablets or capsules, the dominant route and means of delivery. Variability in delivered dose to individual or populations of patients may be substantial.<sup>5, 6</sup> Consequently, reproducible therapeutic effect is difficult to assure.

Treatment of respiratory diseases using inhalers requires delivery of sufficient drug to the lungs to bring about a therapeutic response. For optimal efficacy, drug administration must be reliable, reproducible and convenient. This goal can be achieved by a combination of formulation, metering and inhaler design strategies.<sup>7</sup> The technical and clinical aspects of device design and selection have been extensively reviewed elsewhere.<sup>8-10</sup> The following discussion highlights the design of dry

powder inhaler formulations to achieve the delivery goals. To that end, an understanding of dry powder physics and surface chemistry is essential.

### **1.3. Dry Powder Inhalers**

#### 1.3.1. Development of the DPI

Inhaled drug delivery systems can be divided into three principal categories: pressurized metered dose inhalers (pMDIs), dry powder inhalers (DPI), and nebulizers, each class with its unique strengths and weaknesses. This classification is based on the physical states of dispersed phase and continuous medium and within each class further differentiation is based on metering, means of dispersion, or design. Nebulizers are distinctly different from both pMDIs and DPIs in that the drug is dissolved or suspended in a polar liquid, usually water. Nebulizers are used mostly in hospital or ambulatory care settings and are not typically used for chronic disease management because when considered with their auxiliary pump and tubing they are larger in size and less convenient. In addition, the aerosol is delivered continuously over an extended period of time. pMDIs and DPIs, bolus drug delivery devices, contain solid drug, suspended or dissolved in a nonpolar volatile propellant or in a dry powder mix (DPI) that is fluidized when the patient inhales. The clinical performance of different types of inhalation devices has been thoroughly examined in many clinical trials which have been reviewed by Barry and O'Callaghan and more recently by Dolovich et al.<sup>8, 10</sup> The authors of both papers conclude that no device is clinically superior to the next and that decisions regarding device selection should be directed by other factors, such as convenience, cost, and patient preference.

The pMDI, first approved in 1956, was also the first modern inhaler device.<sup>11</sup> With a global market share of ca. 80% in 2004 the pMDI remains the most widely used device.<sup>12</sup> The development of DPIs has been motivated by the desire for alternatives to pMDIs, to reduce emissions of ozone-depleting and greenhouse gases (CFCs and HFAs, respectively) used as propellants, and to facilitate the delivery of formulations of macromolecules and products of biotechnology. Concurrently, DPIs proved successful in addressing other, device and formulation-related shortcomings of the pMDI.

DPIs are, by their predominantly passive nature, easier to use, more stable, and highly efficient systems. pMDIs deliver their dose at high velocities, because they are pressurized at more than 5 atmospheres, which makes premature deposition in the oropharynx more likely.<sup>13, 14</sup> Thus pMDIs require careful coordination of actuation and inhalation. Despite enhancements to their design (e.g. use of spacers)<sup>15</sup>, incorrect use of pMDIs is still a prevalent problem; Giraud and Roche described poor coordination of actuation and inhalation that accounted for decreased asthma control in a significant portion of patients treated with corticosteroid pMDIs.<sup>16</sup> DPIs require little or no coordination of actuation and inhalation since they are activated by the patient's inspiratory airflow, This has frequently resulted in better delivery to the lungs than was achieved with comparable pMDIs.<sup>17</sup> Since DPIs are typically formulated as one-phase solid particle blends, they are also preferred from a stability and processing standpoint.<sup>18</sup> Dry powders are at a lower energetic state, which reduces the rate of chemical degradation and likelihood of reaction with contact surfaces. By contrast, pMDI formulations, which include propellant and cosolvents, may extract organic components from the device components.<sup>19</sup> The main advantages and disadvantages of the DPI (over the pMDI) are summarized in Table 1.1. For great detail on the evolution of delivery devices, excellent reviews are available.<sup>11, 20</sup>

The development of several new DPI devices, which have been reviewed elsewhere<sup>18, 21-23</sup> and the commercial success of the bronchodilator-corticosteroid combination product Advair<sup>®</sup> have further stimulated interest in and development of DPIs.<sup>7</sup>

**Table 1.1.** Dry powder inhalers vs. metered dose inhalers (Modified from Ashurst et al., 2000)

---

**Advantages of the DPI**

- Environmental sustainability, propellant-free design
- Little or no patient coordination required
- Formulation stability

**Disadvantages of the DPI**

- Deposition efficiency dependent on patient's inspiratory air flow
  - Potential for dose uniformity problems
  - Development and manufacture more complex/expensive
-

### 1.3.2. Principles of Operation

The principles of dry powder inhaler design are shown in Figure 1.1. Most DPIs contain micronized drug blended with larger carrier particles, which prevents aggregation, assists in metering and helps flow. The important role these carrier particles play will be discussed in depth in Section 1.6: Powder and Aerosol Physics. The dispersion of dry powder aerosols is conducted from a static powder bed. In order to generate the aerosol the particles have to be moved. Movement can be brought about by several mechanisms. Passive inhalers employ the inspiratory flow of the patient for fluidization and aerosol generation. When the patient activates the DPI by inhaling through it, airflow within the device creates shear and turbulence; and the generation of velocity gradients introduces air into the powder bed. Thus, the static powder blend is fluidized and enters the patient's airways. At the mouthpiece, the drug particles separate from the carrier particles and are carried deep into the lungs while the larger carrier particles impact in the oropharynx and are cleared. Thus, deposition in the lungs is determined by the patient's variable inspiratory airflow.<sup>24-26</sup> One of the main explanations for the low deposition efficiency encountered with DPIs is inadequate drug/carrier separation.<sup>27</sup> Dose uniformity is a challenge in the performance of DPIs. This is a greater concern with powders than with liquids because of the discrete nature of particulates.



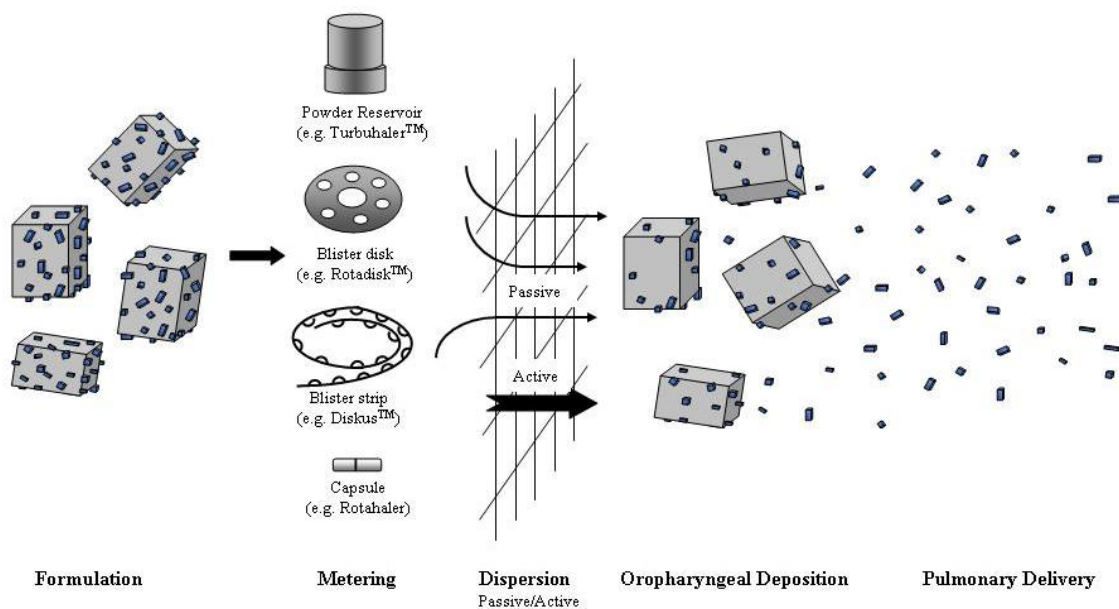


**Figure 1.1.** Principle of dry powder inhaler design. The formulation, typically consisting of micronized drug blended with larger carrier particles is dispensed in a metering system. An active or passive dispersion system entrains the particles in the patient’s airways where drug particles separate from the carrier and are carried into the lung.

Various dispersion mechanisms have been adopted for DPI designs.<sup>22</sup> While most DPIs are breath-activated, relying on the inhalation for aerosol generation, several power-assisted devices (pneumatic, impact force, vibratory) have been developed or are currently under development. These devices are being considered for the delivery of systemically acting drugs with narrow therapeutic windows.<sup>28</sup> It is important to note that these “active” inhalers are not subject to the same limitations as passive inhalers and have a different advantage/disadvantage profile. Moreover, it has been suggested that if shear and turbulence could be standardized by using a dispersion mechanism independent of the patient’s breath, high levels of delivery efficiency and reproducibility may be achieved. Thus, an active inhaler may provide formulation independent delivery.<sup>29</sup> Despite brief market entry of a compressed gas assisted device (Exubera®), the subsequent product withdrawal means there are no commercially available active dispersion DPIs. Therefore, in the interest of brevity, these devices are not discussed here; the reader is instead referred to other literature.<sup>28-30</sup>

## 1.4. Drug Properties and Manufacture

### 1.4.1. The Active Pharmaceutical Ingredient

The respiratory tract is both a therapeutic target and route for delivery. It is an attractive delivery route because it does not subject drugs to the same harsh conditions they may experience in the gastrointestinal tract (i.e. pH and enzyme levels)<sup>31</sup>, yet it remains noninvasive and convenient. Bioavailability for proteins and other macromolecules is greater than in any other noninvasive delivery route.<sup>32, 33</sup> For these reasons, oral inhalation is increasingly being explored for the delivery of systemically acting drugs, including therapeutic proteins such as recombinant human granulocyte colony-stimulating factor (rhG-CSF),<sup>34</sup> insulin,<sup>35-37</sup> drugs to treat bone disorders,<sup>38</sup> and vaccinations.<sup>39</sup> Systemically active drugs need to be absorbed into the circulation; therefore, they should be delivered to the alveoli, the terminal regions of the lung from which absorption is most efficient. Absorption through the alveolar-vascular membranes can take place via transcellular diffusion, paracellular diffusion (through tight junctions), and transcellular vesicular transport. The absorption mechanism depends on the drug.

Pulmonary drug delivery is also the most effective way of treating diseases of the airways. The majority of pulmonary drugs on the market are pharmaceuticals to treat obstructive airway ailments, such as asthma and chronic obstructive pulmonary disease (COPD). Most of these drugs fall into one of three therapeutic categories:

1.  $\beta_2$ -adrenergic agonists
2. Corticosteroids and cromones.
3. Anticholinergics

Tronde et al. found that of 34 inhaled drugs commercially available in 2001 (including anesthetics, but excluding lung surfactant preparations and macromolecules), 12 compounds were  $\beta_2$ -adrenergic agonists and six compounds were corticosteroids.<sup>40</sup> The chemistry and pharmacology of these molecules has been reviewed elsewhere.<sup>41</sup> For effective delivery, it is important to understand the pharmacology of the drug, so that the correct physiology can be targeted. Unlike systemically active

drugs, the three drug classes above need not be absorbed into the circulation to exert their pharmacological activity. Most  $\beta_2$ -adrenergic receptors are located in the alveoli.<sup>42</sup> Anticholinergics target muscarinic cholinergic receptors, which are moderately distributed throughout the airways and periphery. The trachea is more densely populated with  $M_3$  muscarinic cholinergic receptors than  $\beta_2$ -adrenergic receptors.<sup>43</sup> Corticosteroids target inflammatory cells, which are located throughout the airways and alveoli.<sup>42</sup> Having mentioned receptor distribution it is not clear which receptors must be targeted for maximal therapeutic effect.

In contrast to the oral route, for which various structure-bioavailability relationships have been developed<sup>3, 44-47</sup> and applied to the screening of drug candidates, the structure-bioavailability relationship for inhaled drugs remains largely unexplored. One notable exception is the publication by Tronde et al., in which the authors examined marketed inhaled pharmaceuticals for physicochemical similarities and have studied their absorption.<sup>40</sup> The range of physicochemical properties of these 34 small-molecule therapeutic agents incorporated in oral inhalation products in 2001 are listed in Table 1.2.

**Table 1.2.** Mean Physicochemical Properties of marketed small-molecule drugs for oral inhalation (Modified from Tronde et al., 2003)

Physicochemical Property	10 <sup>th</sup> to 90 <sup>th</sup> Percentile
cLogD (pH 7.4) - Logarithm of octanol/water distribution coefficient	-6.3 – 3.8
Molecular weight (Da)	225 – 482
Polar surface area (Å <sup>2</sup> )	65 – 178
cLogP - Logarithm of octanol/water partition coefficient	-1.0 – 4.1
Hydrogen bond donors	2 – 6
Hydrogen bond acceptors	4 – 11

Since the number of drugs is small, it is hard to establish guidelines analogous to Lipinski's Rule of Five, one of the prominent structure-absorption relationships for orally-active compounds.<sup>3</sup> As shown in Table 1.2, most properties examined varied widely, or were closely linked to the respective drug category. No extremes were noted for any of the properties, but inhaled drugs were generally more

polar than oral drugs. Several drugs that showed poor oral permeability were well absorbed in the lungs. Absorption appeared to be mostly related to the polar surface area of the molecule. However, overall, Tronde et al. concluded that the range of physicochemical properties acceptable for respiratory delivery was wider than for orally administered drugs. Tronde et al. did not, however, consider active transport which plays a role for several inhaled drugs.

Given the wide range of physicochemical properties that make a drug suitable for pulmonary absorption (compared to orally administered drugs), there is, nonetheless, one critical requirement a drug must meet to qualify for respiratory delivery; this requirement is potency. Current inhalation devices limit the quantity of drug that can be delivered to the lungs, in a single dose, to a few milligrams. Thus, in order to be considered for inhalation therapy, drugs need to be therapeutically effective in the microgram or milligram range. With the development of new inhalers, this quantity is likely to increase in the future. However, potency will continue to be a limiting factor. Moreover, it is questionable if the lungs are able to manage large single doses administered chronically. Anatomically, the lungs have evolved to prevent entry of airborne particulates. This sets a limit to the use of particularly large molecules and explains the success of receptor agonists and endogenous or endogenous-like molecules such as cromones.

The evolution of combination therapy using single inhaler , e.g. corticosteroid and long-acting  $\beta_2$ -adrenergic agonist<sup>48</sup> has brought about new formulation challenges. In designing combination inhalers, one must also consider drug-drug interaction, whether chemical, pharmacokinetic, or pharmacodynamic in nature, in addition to the other developmental aspects.<sup>49</sup>

#### 1.4.2. API Preparation

The final steps of bulk drug manufacture are crystallization from solution, followed by filtration, and drying. Typically the drug particle size is not well controlled during these steps. In order to be in the respirable size range (<5 $\mu\text{m}$  in diameter), the drug particle size must be reduced in a separate unit operation. The formulator has several options at his/her disposal, and may evaluate several methods

to find the one that works best for the specific drug. The size reduction technique most frequently employed is milling. There are many different mills, but only a few are able to mill dry powder to the required particle size range of 1 – 5 $\mu$ m. The three main types of mills used in DPI manufacture are fluid-energy mills such as the jet mill, high peripheral speed mills such as the pin-mill, and the ball mill. The basic designs are described here, more in-depth discussion of operation with detailed illustrations, capacity and performance are reviewed elsewhere.<sup>50</sup> Mechanical processing, such as milling, has been shown to affect the crystallinity of the material;<sup>51</sup> this effect must be considered.

The jet-mill<sup>52</sup> or air attrition mill, is the most useful technique; it reduces particle size via high velocity particle-particle collisions. Unmilled particles are introduced into the milling chamber. High-pressure nitrogen is fed through nozzles and accelerates the solid particles to sonic velocities. Inadvertently, particles collide and fracture. While moving around the mill, larger particles are subjected to higher centrifugal forces and are pushed to the outer perimeter of the chamber. Small particles because of their aerodynamic size exit the mill through the central discharge stream. Depending on nitrogen pressure and powder feed rate, particles down to the 1 $\mu$ m in diameter can be produced.

A pin mill uses mechanical impact to grind material by both particle-particle and particle-solid collisions. A pin mill is equipped with a series of concentrically mounted pins located on a spinning rotor and stationary stator plate. Powder is fed to the milling chamber and transported through the milling chamber by centrifugal force. Milled product is collected from the bottom. The pin mill can produce single-micron particles;<sup>53</sup> however, not as small as the jet mill. Conversely, its power consumption is lower than that of the jet mill.

The ball mill<sup>54</sup> is essentially a rotating cylinder loaded with drug and milling media, balls that grind the drug between each other as they tumble inside the mill. The size and material of the milling media can be varied. Ball milling is very slow and the process is poorly scalable, which is why tumbling ball mills are only used in the laboratory.

Other techniques for making micron-size particles involve direct particle formation from solution. Spray-drying and supercritical fluid crystallization are noteworthy approaches for controlling particle size. These techniques are distinctly different from milling, in that the particles are constructed (i.e. size is increased) whereas size is decreased during milling. In spray-drying,<sup>55, 56</sup> the drug is dissolved in water or solvent and sprayed as fine mist into a heated expansion chamber. The droplets dry leaving behind tiny particles of drug that are collected at the bottom of the chamber. Spray-drying can produce more spherical particles than milling; however, spray-dried particles are mostly amorphous in structure.<sup>57</sup>

A supercritical fluid (SCF) is a single phase with liquid-like density and gas-like transport properties. SCFs exhibit pressure-tunable solubility, which makes them well-suited for recrystallization operations. Several techniques have emerged that use supercritical fluids, most notably CO<sub>2</sub> or propane, as solvents (e.g. Rapid Expansion of Supercritical Solutions, RESS<sup>58</sup>) or as antisolvents (e.g. Solution-Enhanced Dispersion by Supercritical Fluids, SEDS<sup>59</sup>) for the formation of small particles. These methods have been used to prepare particles suitable for delivery to the lungs. Schiavone et al. noted that SEDS yielded smoother budesonide particles with reduced surface area compared to milled drug. This in turn resulted in higher emitted dose in the Turbospin.<sup>60</sup> “Particle engineering” using SCFs is the subject of intense research in the pharmaceutical industry; excellent reviews on this topic have been published.<sup>61</sup>

For each technique it is important to consider the effect it has on the drug. Spray-drying and SCF methods offer more flexibility and the possibility of morphology control in addition to size control, but they may often only yield amorphous material or an undesired polymorph. Milling remains the process of choice for micronization of drug, because it is simple, more predictable, easy to scale up, and inexpensive. However, spray-drying, SCF, and a few other techniques remain alternatives for the formulator to consider when milling does not produce the desired results.

## 1.5. Excipients

The particle size distribution affects the deposition of drug in the respiratory tract. However, before drug can be delivered to the lungs, drug particles must leave the DPI and separate from each other and from other components in the formulation. Thus, a DPI formulation must undergo flow, fluidization, deaggregation and aerosolization. However, micron-size particles, particularly those resulting from high-energy operations such as jet-milling have high surface areas and surface energies, which result in poor flow and a high tendency to aggregate. Formulation strategies aim at alleviating these problems.

One way to improve the non-pharmacological properties of a drug is through the addition of excipients. In general, excipients are used to enhance the physical or chemical stability of the API, its mechanical properties, and/or pharmaceutical properties such as dissolution and permeation. In DPI formulations, excipients function first and foremost as carrier particles. Usually no more than a few milligrams of drug need to be delivered, and excipients provide bulk, which improves handling, dispensing, and metering of the drug. Excipients also reduce drug cohesiveness by occupying the high energy sites of the drug particles.

The primary function of the lungs is respiration. To fulfill this purpose, the lungs have a large surface area and thin peripheral epithelia. Unlike the gastrointestinal tract, the lungs have limited buffering capacity. Many compounds that could enhance drug delivery outcomes, also have the potential to irritate or injure the lungs. Consequently, the array of potential excipients is limited to compounds that are endogenous to the lungs and can easily be metabolized or cleared.

Currently, lactose is the only excipient used in DPIs marketed in the USA. The reasons for this are both historical and physicochemical/ pharmaceutical in nature. Lactose had long been used as an excipient in oral dosage forms before being employed in DPIs. It has established safety and stability profile, manufacturing process with tight controls over purity and physical properties, and was available and inexpensive from the dairy industry. Lactose is highly crystalline, has smooth surfaces and satisfactory flow properties, which are desirable properties for a DPI carrier particle.<sup>7</sup> It is less

hygroscopic than other sugars and is quite versatile; several manufacturers offer excipient grade lactose of varying size and different morphologies. One drawback of lactose is that it is a reducing sugar, which makes it incompatible with drugs that have primary amine moieties.<sup>62</sup>

Other sugars, such as mannitol,<sup>63, 64</sup> have been shown to be feasible alternatives to lactose and it is expected that these sugars will eventually find their way into approved products. Glucose is already used in DPIs in Europe. Phospholipids, such as phosphatidyl choline and cholesterol have also been used in experimental liposomal formulations.<sup>65, 66</sup> Several other materials have been included in experimental DPI formulations with varying objectives and varying success rates.<sup>67-69</sup>

Excipients can make up over 99% of the product by weight, making them crucial determinants of overall DPI performance. Despite the limited excipient options they must be carefully selected; physicochemical properties, such as size and morphology have a profound effect of the performance of the formulation.<sup>70-74</sup> The adhesive forces must be carefully considered; inadequate separation of drug and carrier is the main reason for deposition problems. The formulator may also choose to modify the excipient before combining it with the drug. It should also be noted that excipients are not always required; the Pulmicort (budesonide) Turbuhaler<sup>®</sup> (Astra-Zeneca, Lund, Sweden) is an example of an excipient-free formulation.

## **1.6. Powder and Aerosol Physics**

The character of particulate systems is central to the performance of DPIs. Powders present unique design challenges. Powders are two-phase gas-solid systems. When they are static, they behave as solids, when they flow powders resemble liquids easily assuming the shape of the containing vessel.<sup>50</sup> When a powder is dispersed in air, as is the case after actuation of a DPI, in many ways it conforms to its carrier gas (though unlike gases or vapors, pharmaceutical powders are non-equilibrium systems). Whereas gas and liquid behavior is understood and accurately predicted by equations derived from first principles, physical equations governing powders are often empirical or rely on assumptions that are only approximations to real systems, such as homogeneity in size and



shape of particles. As a consequence, equations describing the behavior of solids are less predictive than their fluid counterparts. Various texts have been written on multiphase flow phenomena.<sup>75-79</sup>

Powder properties can vary widely. Powder features such as the physicochemical properties and morphology of its constituent particles and the distribution of particle sizes contribute to variability. Unlike liquid solutions or gas mixtures, powders are not completely homogeneous (at primary particulate scale) and segregation by size, a function of the action of external forces, is always a potential contributor to heterogeneity. The aerodynamic behavior, which has a profound effect on the disposition of drug from a DPI, is particularly sensitive to powder properties. This feature will invariably contribute to poor dose uniformity and variable efficiency and reproducibility of drug delivery.

#### 1.6.1. Crystallinity and Polymorphism

Many pure organic substances, including most drugs, are crystalline. A crystal is a solid in which the molecules or ions are arranged in an ordered, repeating pattern (the unit cell) extending in three spatial dimensions. Crystalline systems are defined by the intermolecular spacing, i.e. bond lengths and bond angles, of the unit cell, which can be determined by X-ray diffraction.<sup>80</sup> There are seven crystal classes, which yield fourteen distinct lattice structures.<sup>81</sup> The arrangement of molecules into crystals is governed by noncovalent interactions, including hydrogen bonding, van der Waals forces,  $\pi$ - $\pi$  stacking, and electrostatic interactions.<sup>82</sup>

Nearly one third of all drugs are known to display polymorphism,<sup>83</sup> the ability of a solid to exist in more than one crystal form. A prominent example of a polymorphic pharmaceutical is carbamazepine which has four known polymorphs, one of which was discovered almost 30 years after identification of the first polymorphs.<sup>84</sup> Determination of the polymorphic forms of a drug is an important part of the formulation development process, because polymorphic forms are not equivalent. Different polymorphs are at different energy states and thus have different properties,

including stability, solubility and even bioavailability.<sup>81</sup> Identification of all polymorphs of a drug also has important economic implications, because a separate patent can be granted for each polymorph.<sup>83</sup>

It is also possible to generate noncrystalline solid. In most cases this involves cooling a fluid so rapidly that its molecules lose mobility before assuming their lattice positions. A noncrystalline material is considered amorphous because it lacks long-range order. Amorphous materials have higher Gibbs free energies than crystals; the laws of thermodynamics predict that in the long-term materials will seek to minimize their free energies by transitioning to lower energetic states (e.g. crystallization). Whether this will occur at a timescale that need be of concern to the pharmaceutical scientist, is governed by the chemical kinetics (statistical thermodynamics) of the system.

Different polymorphs can be discerned in terms of a variety of physicochemical properties. Polymorphs usually differ in density, melting point, solubility and hygroscopicity. The most stable polymorph frequently has the highest density, melting point, and lowest solubility. Discriminating analytical methods to characterize polymorphs include X-ray diffraction and thermal analysis, such as differential scanning calorimetry.<sup>81</sup> To reduce the risk of transformation during processing or storage, the most stable polymorph is typically selected for development, provided its other properties are manageable.

While crystallinity refers to the geometry of the unit cell, crystal habit describes the morphology of particles, which can vary independently of the crystal lattice structure if growth rates (during precipitation) vary in some dimension.<sup>85</sup> This is shown in Figure 1.2. Crystal habit is important because different particle shape affects the aerodynamic behavior and, thus, the deposition in the lungs. Crystallization and crystal habit are influenced by a variety of factors, including identity of solvent,<sup>86, 87</sup> impurities present during crystallization,<sup>88</sup> and processing parameters, such as temperature, pH, and solution volume, viscosity.<sup>89</sup>

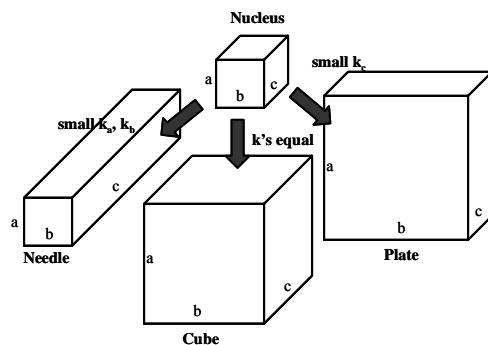


**Figure 1.2.** Crystal habit. Inhibition of growth in one of more spatial directions results particles with plate or needle morphology.

Some compounds will spontaneously incorporate solvent molecules into the lattice structure upon crystallization or storage at certain conditions. This phenomenon has been referred to as pseudopolymorphism, and is relevant for many drugs, which exist as solvates or hydrates.<sup>90</sup> It is important to understand the conditions that will result in hydration, because, as with true polymorphs, hydrates differ in their physicochemical properties.

Knowledge of crystallization and polymorphism is still unfolding and the ability to predict polymorphism remains imperfect. In most solids, a large number of different intermolecular interactions are possible but few are actually observed.<sup>91</sup> The difficulties involved in crystallization are illustrated by several reported cases of “disappearing polymorphs”. These cases were characterized by difficulty in resynthesis of a polymorph, after initial synthesis, despite the procedure and conditions appearing the same.<sup>92</sup> Controlling crystallization is at the heart of “particle engineering”, a term that is used with increasing frequency in the pharmaceutical and chemical literature. It has been suggested that adequate control over the crystallization process could yield particles with precisely engineered morphology; co-crystallization (inclusion of functional impurities into the crystal) could then become a formulation strategy, resulting in “supramolecular pharmaceuticals.”<sup>90</sup>

The recent discovery of the second aspirin polymorph has renewed interest and added new insight to the understanding of polymorphism. A second aspirin polymorph had long been suspected and the

feasibility of it was shown computationally<sup>93</sup> in 2004. Researchers have since reported having observed this polymorph after crystallization under specific conditions; the crystal was thought to be only transiently stable at ambient conditions.<sup>94</sup> A second group then discovered that the polymorph had not truly been observed; after careful examination Bond et al. discovered aspirin's ability to exist in a previously unknown "intergrowth" structure in which a single crystal contains domains with both crystal arrangements.<sup>95</sup> The discovery requires a new definition of polymorphism and may result in reexamination of other drug and excipient structures.

### 1.6.2. Moisture Content and Hygroscopicity

Hygroscopicity is the intrinsic tendency of materials to take on moisture from their surroundings. The hygroscopicity is affected by the crystallinity of the material and the morphology of the particles. Hygroscopic drugs present a greater risk of physical and chemical instability. Moisture uptake and loss due to changes in relative humidity can result in local dissolution and recrystallization leading to irreversible aggregation through solid bridge formation.<sup>22</sup> This, in turn, may adversely affect aerosol generation and deposition of particles in the lung.<sup>96</sup> Hygroscopicity may also alter the adhesive and cohesive properties or in more extreme situations induce significant increases in particle size, hygroscopic growth.<sup>97</sup> The latter phenomenon, shown schematically in Figure 1.3, involves the uptake of moisture, which will reach equilibrium in droplets as a function of the water activity of the solution formed and the surrounding atmosphere of water vapor; the Kelvin-Gibbs equation describes the phenomenon involved.<sup>98</sup> Hygroscopic growth has implications for the equilibrium moisture content of the particles in the dosage form prior to aerosol generation; it may cause either chemical or physical instability of the product. For aerosols the physical instability is of great significance since agglomeration may be irreversible and lead to an inability to generate aerosols in respirable sizes. As aerosol particles enter the lungs they experience a high humidity environment (99.5%RH at 37°C).<sup>99</sup> Although they may not reach equilibrium during transit susceptible aerosol particles may be subject to hygroscopic growth which will increase particle dimensions and affect lung deposition.<sup>99</sup>

Hygroscopic growth can be prevented by coating the drug particles with hydrophobic films.<sup>98</sup>

However, no such approach has been successfully implemented in a marketed formulation.

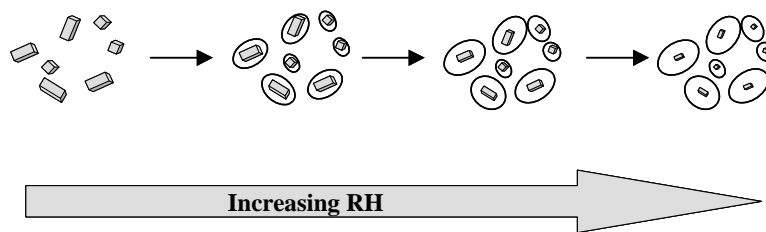


**Figure 1.3.** Hygroscopic growth. Particles absorb moisture as they traverse the humid environment of the airways resulting in increased particle size.

The equilibrium moisture content of a drug and excipient must be determined over a range of relative humidities, so that storage conditions can be defined and other protective measures considered. Excipients that modify the hygroscopic properties of a drug may need to be considered.

### 1.6.3. Particle Size

Particle size is the single most important design parameter of DPI formulations. Methods for the determination of particle size and distribution make use of different geometric features or physicochemical properties.<sup>50</sup> Among these, aerodynamic diameter is the most relevant to lung delivery and ultimately to therapeutic effect. There is significant literature in industrial hygiene, environmental and occupational medicine in addition to pharmaceutical sciences that links the probability of deposition in specific sites in the lungs to aerodynamic size and size distribution. The statistical basis for these relationships in terms of variability in airways geometry and lung physiology both between individuals and within individuals has been sufficient to allow the development of semi-empirical models correlating particle size with lung deposition.<sup>100</sup>

#### 1.6.3.1 Aerodynamic diameter and dynamic shape factor

Aerodynamic diameter is the most appropriate measure of aerosol particle size because it relates to particle dynamic behavior and describes the main mechanisms of aerosol deposition; both

gravitational settling and inertial impaction depend on aerodynamic diameter. In order to reach the peripheral airways where drug is most efficiently absorbed, particles need to be in the 1-5  $\mu\text{m}$  aerodynamic diameter range.<sup>101</sup> Larger particles usually deposit in the oral cavity or pharynx, from which they are easily cleared. In contrast, particles smaller than 0.5 $\mu\text{m}$  may not deposit at all, since they are subject to Brownian motion and settle very slowly. Moreover, they are inefficient, as a 0.5 $\mu\text{m}$  sphere delivers only 0.1% of the mass a 5 $\mu\text{m}$  sphere carries into the lungs. In a series of studies the optimal particle size of aerosol particles was examined for several different therapeutic agents in patients with different disease states. Although some differences due to patient lung function were noted, the optimal size was always in this 1-5 $\mu\text{m}$  size range.<sup>102-106</sup>

The aerodynamic diameter,  $d_{ae}$ , is defined by the diameter of an equivalent volume sphere of unit density  $d_{eq}$  with the same terminal settling velocity as the actual particle. For particles greater than about 1 $\mu\text{m}$  the following expression describes the relationship between these dimensions.

$$d_{ae} = d_{eq} \sqrt{\left(\frac{\rho_p}{\rho_o X}\right)} \quad (1.1)$$

where  $\rho_p$  and  $\rho_o$  are particle and unit densities, and X is the dynamic shape factor. Pharmaceutical powders are rarely spherical and shape factors are dimensionless measures of the deviation from sphericity. The dynamic shape factor in particular is the ratio of the actual resistance force experienced by the nonspherical falling particle to the resistance force experienced by a sphere having the same volume.<sup>107</sup> Dynamic shape factors are either determined experimentally or using more complex models that are beyond the scope of this chapter. A very thorough review of this concept with values for common shapes is provided by Hinds.<sup>107</sup>

Equation 1.1 merits closer examination. As discussed, it is the aerodynamic diameter ( $d_{ae}$ ) that determines lung disposition, irrespective of geometric particle size (to a certain point). The aerodynamic diameter can be decreased by decreasing particle size and particle density, or by

increasing the dynamic shape factor. This concept is shown graphically in Figure 1.4, and is discussed in more detail below. All three of these approaches have been applied.

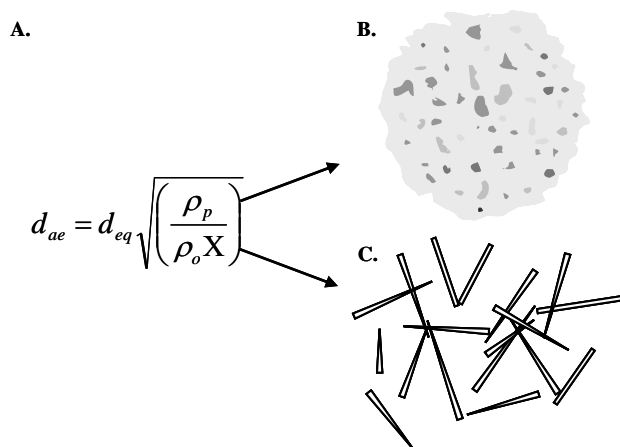


**Figure 1.4.** Strategies for altering the aerodynamic diameter. A. Aerodynamic diameter equation; B. Large, low density porous particles; C. Needle-shaped particles. Particles in both B and C are expected to have aerodynamic diameters that are smaller than their size would suggest.

### 1.6.3.2 Fine Particle Fraction

One expression that has been employed to allow general comparison of aerosols with respect to lung delivery is the fine particle mass/dose (dose, FPM/FPD) or fraction (usually percentage of nominal dose, FPF).<sup>108</sup> The fine particle component of aerosols is usually defined as the proportion less than 5 $\mu$ m (aerodynamic diameter) or in the case of particular sizing instruments a cut-off diameter that is close to this value. Quite often this may be in the 6-7 $\mu$ m range. The danger of adopting these values as definitive measures of equivalency is associated with the significance of particle size on deposition.<sup>109</sup> This is considered in more detail in section 1.6.3.3.

### 1.6.3.3 Polydispersity

For drug delivery it is the convention to consider the mass associated with each particle size as the frequency term in the distribution since this relates directly to dose. Conventional statistical properties apply to populations of particles (i.e. mode, mean and median). It is usual to define the central tendency of numbers of aerosol particles by the mass median aerodynamic diameter (MMAD)

which reflects the particle size dividing the distribution in half as a function of mass. Monomodal distributions may conform to log-normal mathematical interpretation in which case the breadth of the distribution can be expressed in terms of the geometric standard deviation which is usually derived by dividing the particle size at the 84<sup>th</sup> percentile by the median size to achieve a dimensionless number greater than 1.

When considering particle size, the degree of polydispersity, i.e. the range of particle sizes around the mode, is also important. The simplest and preferred system exhibits a single mode. However, many pharmaceutical aerosols will exhibit more than one mode. It is conceivable that two completely different aerosol distributions, i.e. small median size with narrow distribution or large median size with broad distribution could give exactly the same fine particle fraction. However, within the FPF the aerosol would exhibit different sizes leading to differences in regional lung deposition resulting in variations in therapeutic effect. Thus, degree of dispersity is an important consideration for both quality and efficacy of pharmaceutical aerosols.<sup>110</sup> The nature of the aerosol distribution must be established accurately if its implications for deposition and efficacy are to be understood.

Another consideration relates to the standard DPI formulation, which is frequently bimodal since it contains micronized drug and substantially larger carrier particles. Recognizing the potential for multimodal distributions is important to the application of statistical methods to the interpretation of the data. Traditional methods of data interpretation, i.e. log-normal mathematical fits to distributions,<sup>111</sup> may be superseded by other mathematical approaches<sup>112</sup> or non-linear curve fitting using calibration data.<sup>113</sup>

#### 1.6.3.4 Particle Sizing Techniques

Several techniques are available for the determination of particle size distributions; they have been described in depth elsewhere<sup>111</sup> and will be covered, briefly, here. The techniques used for sizing aerosols can be classified as either (1) inertial methods, (2) light scattering methods, or (3) imaging methods.



## Cascade Impactors

Cascade impactors (CIs),<sup>114, 115</sup> including multi-stage liquid impingers, are the most widely used instruments for sizing aerosols; they are recommended by both U.S. and European Pharmacopeias. Their utility stems from the fact that they directly measure aerodynamic size rather than equivalent volume diameter (based on cross-sectional area), like the other methods. The theory of CI operation has been described in-depth elsewhere.<sup>116</sup> Briefly, CIs contain several stages with orifices of decreasing size stacked on top of each other. Particles suspended in air are drawn through the CI and the particles deposit on different stages based on their inertia. After each run, the CI is disassembled and the mass of particles deposited on each stage is determined, mostly via analytical methods (dissolution in solvent, followed by chromatography or UV absorbance). A cutoff diameter is associated with each stage of the CI. This diameter varies with airflow, thus the CI must be calibrated for different flowrates. This airflow dependence allows investigation of the effect of different inspiratory flowrates on deposition.

At atmospheric conditions cascade impactors can only classify particles down to a size of approximately 0.1 $\mu$ m. Below this size particles are close to the mean free path of air (0.066 $\mu$ m at 1atm and 20°C)<sup>107</sup> and experience the air as a discontinuous medium; they experience 'slip'. The mean free path,  $\lambda$ , is the average distance traversed by air molecules between collisions with each other. The cutoff size range of cascade impactors can be extended downward by decreasing the air pressure, thereby increasing the distance between air molecules and thus the mean free path. Several low pressure impactors have been developed that have extended the cutoff size down to tens of nanometers; they have chiefly been used in the study of air pollution.<sup>117, 118</sup>

The Electrical Low-Pressure Impactor (ELPI),<sup>119</sup> is another rather recent modification of the CI. Particles passing through the ELPI are charged before traversing the cascade of stages. Their impact on the stages produces an electrical current that is detected and converted into particle size data that can be interpreted in real-time. Operating at reduced pressure the ELPI can classify particles down to

a size of 30nm. The device is extensively used in experiments and is discussed in more detail in Chapter 4.

#### Light Scattering – Laser Diffraction

Light scattering methods, especially laser light scattering, are quite commonplace in formulation development. The operating principle of laser light scattering is depicted in Figure 1.5. An expanded laser beam is passed through a sample that is being drawn through a measuring zone. Different size particles diffract the light at different angles. A computer algorithm, which varies between manufacturers, interprets the diffraction pattern and calculates a particle size distribution. The algorithms used are based on Fraunhofer or Mie Theory from which the particle sizes are determined. Since the algorithms vary among the different instruments, as does instrument geometry (e.g. size and position of detection) comparisons are difficult particularly for pharmaceutical particles, many of which deviate from sphericity.

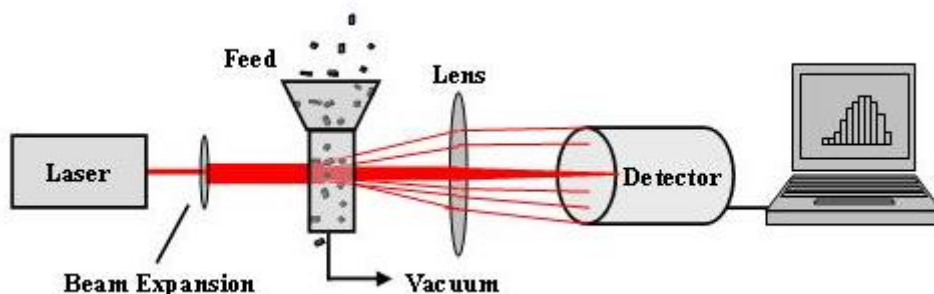


**Figure 1.5.** Particle sizing by laser light diffraction.

#### Image Analysis

The last method that is of importance in sizing particles is image analysis; it is illustrated schematically in Figure 1.6. An example of this method consists of taking digital images of particle samples, converting them to binary data, designating the key dimension, and deriving particle size data. The analyst can perform the steps individually or use an automated piece of equipment that samples particles and produces particle size distribution data. Software varies, thus conversion from

binary data to particle size can produce different results. However, this technique is very powerful in that it has the capability to account for the shape of the particles, though images are only 2-dimensional representations of 3-dimensional particles. Another limitation of this approach is low capacity. Since individual particles are imaged, it takes considerably more time than the other techniques.

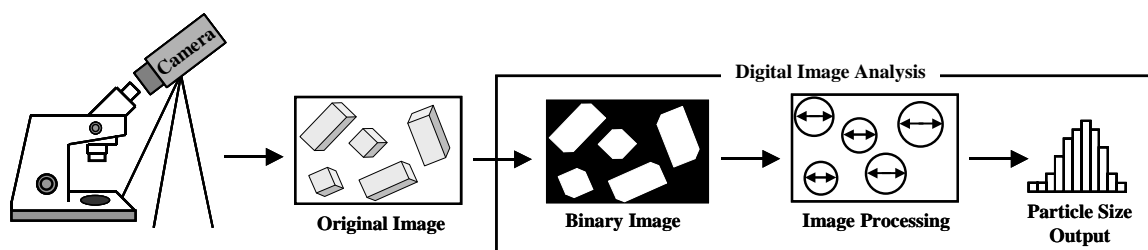


**Figure 1.6.** Particle sizing by digital image analysis.

While light scattering and imaging methods are very useful in the characterization of raw materials, i.e. drug particles or excipient particles alone, cascade impaction is the only method that allows the direct determination of the FPF, an aerodynamic property. Thus, it is a better measure of the performance of the formulation rather than the raw materials. The different methods complement each other. In the early stages of the formulation development process, it is not uncommon to use all methods at your disposal until good process control has been established or a methodology has been developed that is robust enough to describe all desired features.

#### 1.6.4. Surface Area and Morphology

Particle surfaces are important elements in particle interactions, stability and ease of dispersion. Since aerosol particles are small, the total surface area of a powder is very large. A large surface area renders the particles subject to greater potential for charging and moisture uptake. In addition, the size of the particles renders them more susceptible to the influence of van der Waals forces.

##### 1.6.4.1 Surface Morphology

Surface area is not solely determined by particle size and shape; the surface morphology also contributes to surface area: corrugated (i.e. rough) particles have more surface area than smooth particles occupying the same volume. Thus, particle morphology can also be exploited for DPI formulation design.<sup>120-122</sup> By creating drug particles with specific morphology or by selecting (modifying) carrier particles to obtain specific surface morphology the interparticulate forces can be modulated to enhance lung deposition. Ideally, the contact area and, thus, the forces should be adjusted to a level that provides enough adhesion between drug and carrier to provide a stable formulation, yet allows easy separation upon inhalation. Carrier particle surface morphology has been shown to affect the FPF in several studies.<sup>27, 70, 122-126</sup> However, the influence of surface corrugation on the FPF has not been firmly established. Smooth surface lactose carrier particles have been shown to increase the FPF and dispersibility of micronized drug,<sup>27</sup> while other studies showed that corrugated carrier particles increased the FPF.<sup>123-126</sup> These results appear contradictory, but may both be correct since the surface force balance is dependent on a number of variables not simply surface structure.

#### 1.6.4.2 Surface area and morphology measurements

Since surface area is highly correlated with particle interactions, measurements must be obtained as part of the DPI formulation development effort. Determining the powder surface area involves measuring the volume of gas adsorbed to the powder surface at a given pressure. Several models have been developed to describe gas-solid adsorption behavior, the most prominent one being the Brunauer, Emmett, and Teller (BET) equation.<sup>127</sup> Another important technique for examining particle morphology is scanning electron microscopy (SEM), which can provide high magnification, high resolution images of particles. However, the technique suffers from the shortcoming, that only a small portion of particles can be screened. Over the last few decades, new techniques for studying surfaces have emerged or have been borrowed from other scientific disciplines. One particularly noteworthy method is inverse gas chromatography (IGC), which is used extensively for surface energy measurements in this research project and which is discussed in detail in Chapter 3.

## 1.7. Interparticulate Forces of Interaction

Particle separation is the most significant performance requirement for effective aerosol generation. In order to separate particles specific forces of interaction must be overcome. There are four major physical interactions between particles: (1) mechanical interlocking; (2) capillary forces from the presence of water; (3) intermolecular interactions; and (4) electrostatic forces.

Mechanical interlocking, due to surface asperities, may prevent particles from dislodging and may thus prevent particle dispersion. Regular particle shapes with smooth surface morphology may reduce the propensity for particles to interlock. The presence of moisture, even in small quantities, may bring about capillary forces.<sup>128</sup> The magnitude of these forces is related to the diameter of the pores between particles and the interfacial tension due to hydrogen bonding of water. Controlling moisture content will aid in reducing capillary forces.

### 1.7.1. Intermolecular Interactions

Intermolecular interactions have two contributions, Lifshitz-van der Waals (LW) interactions and the acid-base (AB) interactions.<sup>129</sup> LW interactions consist of London dispersion forces, Debye dipole/ induced dipole forces, and Keesom dipole/dipole forces. London dispersion forces are independent of molecular polarity and result from natural electron cloud oscillations, which induce oscillations in adjacent molecules. Since London dispersion predominates LW interactions, they are frequently referred to as simply dispersive interactions, and the superscript 'disp' is used.

In contrast to the ubiquitous dispersive interactions, AB interactions are present only when proton or electron sharing or transfer occurs between functional groups of nearby molecules or surfaces. These interactions are specific to each system of interacting surfaces, which is why they are more commonly referred to as specific interactions and are designated herein by superscript 'spec'.

As stipulated by Fowkes, dispersive and specific interactions contribute to total intermolecular interactions independently.<sup>130, 131</sup> Consequently, work of adhesion ( $W_A$ ), a thermodynamic measure of

the work needed to separate two surfaces from contact, can be represented as the sum of dispersive and specific contributions according to equation 1.2<sup>132</sup>

$$W_A = W^{disp} + W^{spec} \quad (1.2)$$

Alternatively, work of adhesion can be defined by

$$W_A = \gamma_1 + \gamma_2 - \gamma_{12} \quad (1.3)$$

where  $\gamma_1$  and  $\gamma_2$  are the surface free energies of the individual materials that make up the interface, and  $\gamma_{12}$  is the interfacial free energy between them.<sup>132</sup>

Reducing the work of adhesion,  $W_A$ , is one approach to enhancing drug-carrier particle separation.  $W_A$  can be reduced by decreasing either  $W^{disp}$  and/or  $W^{spec}$ . While dispersive forces are always present between adjacent molecules, they can, nevertheless, be manipulated by reducing the particle contact area or increasing the distance between particles. Low density, high porosity particles achieve this goal.<sup>133</sup> Decreasing the specific contribution to work of adhesion requires matching the drug particles with a carrier particle with which it does not strongly interact. Alternatively, based on equation 1.3, adhesion can be modified by reducing surface free energy of the particles or increasing the interfacial free energy between them. While simple in theory, this approach is experimentally difficult because surface free energy determinations of powders are cumbersome; the commonly used contact angle approach requires compression of powder which could significantly alter the surface properties. One way to approach the problem is by inverse gas chromatography measurements which are discussed in detail in Chapter 3. IGC measurements allow determination of both dispersive and specific (acid-base) surface properties for powders.

## 1.7.2. Electrostatic Forces

### 1.7.2.1 Aerosol Electrostatics

Electrostatic charging has been known since Ancient Greece.<sup>134</sup> It has been studied in the context of powder handling,<sup>135</sup> where it was characterized as a nuisance<sup>136-138</sup> or explosion risk<sup>139</sup>.

Electrostatic particle charging has inspired a number of industrial applications, such as the electrostatic precipitator, electrostatic dry powder coating, and powder separation. Electrostatic charging is the basis of xerography, where charged toner particles attach to the latent image on the drum surface to create a visible toner image.<sup>140</sup> Despite these innovations, the electrostatic charging process is not fully understood, particularly for nonconducting materials; numerous factors affect the phenomenon and inconsistent experimental results have been reported.<sup>135</sup>

Electrostatic forces are described by Coulomb's Law, the natural starting point for a discussion of electrostatics. Coulomb's law is experimentally determined, but often treated as a mathematically derived fundamental relationship.<sup>141</sup> It states that a force between two point charges,  $F_{12}$ , is proportional to the magnitude of each charge  $Q_1$  and  $Q_2$ , inversely proportional to the square of the distance,  $r$ , between the charges, and is directed along the line connecting the charges

$$F_{12} = K_E \frac{Q_1 Q_2}{r^2}, \quad (1.4)$$

where the constant  $K_E$  is inversely related to permittivity  $\epsilon$ , via equation 1.5

$$K_E = \frac{1}{4\pi\epsilon} \quad (1.5)$$

In case of aerosols, the permittivity is the permittivity of vacuum,  $\epsilon_0 = 8.85 \cdot 10^{-12} \text{ C}^2/\text{N} \cdot \text{m}^2$ , so that  $K_E$  is  $9.0 \cdot 10^9 \text{ N} \cdot \text{m}^2/\text{C}^2$ .

Most atmospheric aerosol particles naturally carry a low level of charge in accordance with Boltzmann equilibrium charge distribution theory, which for particles greater than  $0.05\mu\text{m}$ , can be written as

$$f_n = \sqrt{\left(\frac{K_E}{\pi d_p k_B T}\right)} \exp\left(\frac{-K_E n^2 e^2}{d_p k_B T}\right) \quad (1.6)$$

where  $f_n$  is the fraction of particles of particle diameter  $d_p$  having  $n$  (positive or negative) elementary charges<sup>107</sup>.  $k_B$  is Boltzmann's constant. The average number of charges,  $\bar{n}$ , for aerosol particles can be estimated by

$$\bar{n} \approx 2.37\sqrt{d_p} \quad (1.7)$$

where  $d_p$  is given in  $\mu\text{m}$ . Equation 1.7 is an empirical relationship that is accurate to within  $\pm 5\%$  for particles greater than  $0.2\mu\text{m}$ .<sup>107</sup> The Boltzmann distribution predicts charges of less than  $\pm 5$  (elementary charges) for most particles with  $d_p < 5\mu\text{m}$ . Active charging mechanisms such as diffusion and field charging can produce particle charges 2-3 orders of magnitude larger than what is predicted by Boltzmann distribution.<sup>107</sup> According to the results of Bailey<sup>142</sup> and Fraser<sup>143</sup>, particle charges in the  $>100$  elementary charges range can enhance the deposition of micron-size particles in the lungs.

While the Boltzmann charge distribution gives the lower limit of charge for an aerosol, it is also important to consider the upper charge limits. The maximum number of negative charges that a particle can support,  $n_L$ , is given by the equation<sup>107</sup>

$$n_L = \frac{d_p^2 E_L}{4K_E e} \quad (1.8)$$

where  $d_p$  is the particle diameter,  $E_L$  is the surface field strength required for spontaneous electron emission ( $9.0 \times 10^8$  V/m),  $K_E$  is the Coulomb's law constant, and  $e$  is the charge of an electron,  $1.6 \times 10^{-19}$  C. The maximum number of charges is proportional to the surface area. Equation 1.8 assumes particles are spherical; nonspherical particles have larger surface area and would be expected to have higher charge limits. Since it is more difficult for a particle to emit a positive ion from its surface, the positive charge limit is also higher.

Aerosol particles can acquire charge by flame charging, static electrification, diffusion charging, and field charging.<sup>107</sup> Of these mechanisms, static electrification plays an important role during DPI actuation. Static electrification occurs when particles are detached from surfaces or the bulk phase



resulting in a separation of charges. In DPIs, this occurs naturally in the form of surface charging, or triboelectrification.

#### 1.7.2.2 Contact Charging and Triboelectrification

Triboelectrification is a form of contact charging in which materials come into contact and acquire electrical charge, which they retain after separation. Contact charging occurs due to differences in the work functions of different materials, i.e. electrons move from one material to the other more easily than in the reverse direction. When put into contact, almost any two solids will produce a voltage difference, referred to as a contact potential. The presence of an electric field is not required for charge transfer to occur.<sup>140</sup>

For metals, the contact charging process can be explained in terms of band theory: valence and conduction bands overlap so that a portion of the valence electrons can move through the metal. The work function,  $\phi$ , the minimum energy needed to extract an electron from a material (more precisely, it is the energy necessary to remove electrons from Fermi level to infinity), however differs between different metals. When two metals with differing work functions / Fermi levels are placed in contact, electrons are transferred from one to the other until the Fermi levels align. The result of the electron transfer is a potential difference, the material with the higher work function acquires a surplus of electrons and thus a negative charge. This has been experimentally validated.<sup>144</sup> The potential difference remains after the metals are separated, though some backflow may occur.

The situation is thought to be analogous for insulators.<sup>140</sup> However, the concept of work functions is more abstract since energy levels are poorly defined, and Fermi levels are not occupied. Ideal insulators are not expected to charge at all, but real materials do display contact charging because impurities and morphology defects produce additional energy levels into which charge can move.<sup>145</sup> As stated by Bailey,<sup>146</sup> for charge transfer to or from an insulator to occur, electron donor or acceptor sites need to be present at or near the surface of the material.

Insulators or dielectrics are defined as materials having low conductivity,  $\sigma$ . When thinking about the charging properties of insulators it is also useful to consider the times necessary for charge transfer.<sup>147</sup> The charge relaxation constant,  $\tau$ , is defined as

$$\tau = \frac{\varepsilon}{\sigma} \quad (1.9)$$

where  $\varepsilon$  is the permittivity, as already defined above. The permittivity can also be expressed in terms of the free space permittivity,  $\varepsilon_0$ , by

$$\varepsilon = \varepsilon_r \varepsilon_0 \quad (1.10)$$

where  $\varepsilon_r$  is the relative permittivity, which is also called the dielectric constant. The dielectric constant indicates the polarizability of a dielectric; dielectric constants for many materials can be obtained from handbooks. Insulators have high dielectric constants, low conductivities and therefore large time constants. Charge transfer between insulators is slow compared to conductors. The time scale of contact must, therefore, be considered in contact electrification processes involving insulators.<sup>147</sup> Charge relaxation times of insulators are in the order of seconds (0.5s for corn oil) to  $10^4$  seconds ( $5.1 \times 10^4$  s for mica), though they vary widely and may differ for different presentations of the same material.<sup>148</sup>

Tribocharging is a specific term applied to contact charging that results from materials being rubbed (tribo means “rub” in Greek) together. Friction in itself does not lead to triboelectrification, but increases the number of points of contact which facilitates charge transfer. Local heat gradients may evolve due to the rubbing, and heat also affects charging.<sup>146</sup> It is difficult to separate the effects of tribocharging from simple contact electrification, which is why the terms are often combined.<sup>140</sup> They are used interchangeably here as well.

Some researchers have suggested that adsorbed water and electrolytic ions play an important role in the surface charging process.<sup>149</sup> While surface contaminants are always present and may affect charging or promote surface leakage, it has been shown that they are not necessary for charging of insulators to occur. As cited by Harper,<sup>149</sup> Coehn and Lotz (1921) proved that triboelectric charging

occurs after surfaces have been thoroughly cleaned and water has been rigorously expelled. Nonetheless, for experimental purposes, surfaces must be considered contaminated.

Triboelectrification of insulators remains poorly understood.<sup>150</sup> Conflicting observations have been reported and consistency between labs has often been lacking. Clearly, cleanliness and environmental conditions play an important role; this has been shown experimentally.<sup>151</sup> However, discrepancies go beyond environmental control. As an example of the complexities involved in the charging process, consider that different crystal faces of quartz display different charging characteristics.<sup>149</sup> Similarly, polycrystalline ice has been shown to charge differently from monocrystalline ice.<sup>152</sup> Nonetheless, some general trends have been observed in the interaction of different materials; part of this information has been captured in triboelectric series, which rank materials in their propensity of acquiring positive (and negative) electric charge. There have been attempts at constructing triboelectric series for pharmaceutical materials as well.<sup>153</sup> Some investigators have also classified insulators in terms of “pseudo-work functions” by measuring charge transfer between insulators and metal surfaces,<sup>146</sup> a more quantitative approach to the construction of triboelectric series.

### 1.7.2.3 Aerosol Electrostatics and Particle Deposition

Electrostatics not only play a role in particle adhesion, but also in particle deposition. Computer simulations have indicated that electrostatic deposition is important for small particles in the lower lung regions, particularly the alveoli.<sup>154</sup> The alveolar region is the site of most  $\beta_2$ -adrenergic receptors<sup>42</sup> as well as the region from which systemic absorption is most efficient. Thus, it is an important site for targeting therapeutic aerosols. Deposition enhancement due to electric charge was also shown *in vivo*; using rabbits and silica particles of variable size, Fraser showed that the deposition of particles (0.4 – 3.5  $\mu\text{m}$  size range) in the respiratory system was significantly increased as particles were charged.<sup>143</sup> More recently, the effect of charge on deposition of both MDI and DPI products was shown in experiments involving a human oral-pharyngeal-laryngeal airways cast; again

deposition enhancement was observed in the presence of particle charge.<sup>155</sup> Despite these results, electrostatic charging is not exploited for the delivery of medicines.

## **1.8. Previous Work**

Electrostatic forces affect the adhesional properties and separation efficiency of particles in the formulation. They may influence the transport of particles and can result in undesirable adhesion of charged drug particles to a device or other surfaces, and they may also affect the trajectory and deposition of drug within the lungs. In light of these potential effects, electrostatic forces are clearly an important consideration in DPI formulation development. In recent years they have been the subject of a number of pharmaceutically relevant studies. Different techniques have been applied to the characterization of DPI electrostatics, with different aims and to varying degrees of success. Some of the important past studies of DPI charging phenomena are discussed in the context of the techniques that have been used.

### **1.8.1. Faraday Cage**

The majority of studies of medicinal aerosol electrostatics have made use of Faraday cages, or Faraday-cage based experimental apparatus. A Faraday cage (also Faraday pail or cup) consists of some receiving surface contained within a cup enclosure that shields the inside from the effect of external electric fields. As a charged object (e.g. powder) is deposited on the receiving plate within the cage, it dissipates its electric charges which in turn are detected by an electrometer. One of the first successful aerosol electrostatic characterizations can be credited to Byron et al.,<sup>156</sup> who developed an experimental apparatus based on an impinger and Faraday cage, which allowed the charge of DPI emissions to be measured. (Recently, more advanced impinger /Faraday cage based designs were described.<sup>157, 158</sup>) The study included bulk measurements of powders as well as emitted dose measurements of commercial DPI products. No effort was made in formulating the material; the study focused on triboelectrification of aerosolized pure compounds. While the study suffered from

these obvious drawbacks, the authors were nevertheless able to produce a triboelectric series of pure pharmaceutical compounds and estimate (using an overly simple assumption of monodisperse particle size) the per particle charge level, which was found to be high enough to affect deposition (approximately 200 electronic charges per aerosol drug particle).

Bennett et al.<sup>159</sup> used a design based on Faraday cage principles to determine the charge of pneumatically conveyed lactose powders. Importantly, the authors observed that the presence of various fractions of fine particles affected the charging propensity of the bulk powder.

Electrostatic charge carried by a DPI aerosol cloud has also been measured using a grid probe;<sup>160</sup> however, the particles were large and the system was of little pharmaceutical relevance. The effects of particle morphology and crystallinity on triboelectrification of DPIs have been studied, but particle deposition was not considered.<sup>161</sup> Moreover, use of the Faraday cage precluded analysis of different size fractions and charge distribution. Cassidy et al.<sup>162, 163</sup> have also studied the propensity of different pharmaceutical materials to acquire charge, though their interest pertained to pneumatic conveying and processing; the results of their work are not relevant to respiratory drug delivery. With a slightly different focus, Elajnaf et al.<sup>164</sup> recently used a corona charger with a Faraday cage based apparatus to study the electrostatic charge decay of charged pharmaceutical materials; the powders were compacted into 5mm discs, the discs were charged and the charge dissipation was measured inside a Faraday cage; the authors found dissipation times in the order of tens to hundreds of minutes, which seem extremely high and question the study's relevance to micron-size drug particles delivered from DPIs.

### 1.8.2. Single Particle Impact Electrostatics

A variation from the Faraday cage powder electrostatic measurements are the recent measurements of charges associated with single particle impacts.<sup>165, 166</sup> The studies were able to shed some light on the charge transfer experienced during particle-wall collisions. Moreover, unlike regular Faraday cage methods, which measure only the net charge of a larger powder sample and

hence may only provide rough charge-to-mass (Q/M) information, the single impact method can measure actual particle charges. However, the single particle method does not lend itself to particles in the single micron-size, and is more relevant to pneumatic conveying systems than to DPIs; as in previous studies the authors neglected to consider the contact charging process within the formulation which is a likely contribution to the aerosol charging in DPI.

### 1.8.3. Electrical Single Particle Aerodynamic Relaxation Time (E-SPART)

E-SPART measurements are also based on single particle measurements, but go further than the single particle impact device. As in previous electrical mobility measurements,<sup>167</sup> charge is measured indirectly by particle behavior within an electric field. The E-SPART Analyzer has been around since at least the 1980s and has been applied to the characterization of many electrostatic particulate systems, e.g. printer toner particles.<sup>168, 169</sup> The principles of operation are discussed elsewhere.<sup>170</sup> Briefly, the E-SPART samples aerosols at low flow rates (1L/min) and detects particles by laser Doppler velocimetry. An oscillating electric field within the device causes particles to oscillate and the particles' response to these oscillations supplies information on the particles' count mean aerodynamic diameter, and charge-to-mass ratio. Saini et al.<sup>171</sup> recently used the E-SPART to study MDI and DPI particle electrostatics. Inhalers were actuated into a collection chamber from which the E-SPART sampled particles over the course of several minutes. While the paper neglects to consider carefully the pharmaceutical implications of the experiments (e.g. it is unclear from the paper which drugs and inhalers were tested) the study showed differentiated and bipolar particle charging, and suggested charging was the result of inhaler and formulation.

### 1.8.4. Electrical Low Pressure Impaction

The ELPI, described briefly earlier and subject to more in-depth discussion in Chapter 4, is a cascade impactor in which charge depositions on the individual, electrically insulated stages can be measured. The ELPI can classify particle size fractions and measure the charge on each impactor

stage. Unlike the E-SPART it cannot obtain charges for individual particles but rather average charges for mass deposited on a given impactor collection plate. Using the ELPI, tribocharging within the formulation was implicated as the likely cause of the drug particle charge.<sup>172</sup> The studies also clearly showed for the first time that DPI charging of drug was subject to strong formulation and device effects.<sup>172</sup> Furthermore, since impactor stages are electrically isolated, size specificity of charging could be evaluated. However, the studies left a lot of questions unanswered, which is why a more thorough investigation is in order.

The studies herein rely heavily on the ELPI. They constitute a more comprehensive investigation of the DPI electrostatic phenomenon, with more variables, a more in-depth look at the accurate determination of magnitude and polarity of charge on particles in the respirable size range over time. Using complementary techniques the physicochemical origins of contact charging are probed.

### **1.9. Problem Statement**

The DPI formulation presents a system that lends itself to triboelectric charging: Drug and carrier particles are in close contact in the formulation and are separated during actuation; the contacts can lead to charge transfer resulting in net particle charge. DPI formulations are usually insulating materials maintained at low humidities; they experience significant friction during discharge which may further increase triboelectric charging.

Electrostatic charges play a significant role in the particle adhesion and separation process, as well as during deposition in the respiratory tract. There is evidence to suggest that tribocharging in the DPI is quite significant, yet the extent and the implications of DPI charging are not fully understood. However, it is clear that particle charging is being used in a number of other industries to control particle behavior. Charge may also be a design advantage for medicinal aerosols. Understanding the degree to which tribocharging occurs and the effect of formulation variables on the process could enhance the DPI formulation development process. It is postulated that triboelectric charging is a

major factor in drug delivery from DPIs and that its characterization and control can be utilized to maximize DPI performance.

## **1.10. Hypotheses and Specific Aims**

### 1.10.1. Hypotheses

1.10.1.1 Electrostatic charging is a consequence of triboelectrification during inhaler actuation.

1.10.1.2 Magnitude and polarity of charge on drug particles can be controlled by formulation variables, independently of the chemical identity of the drug being delivered.

1.10.1.3 The acid-base characteristics of a pharmaceutical material, as determined by inverse gas chromatography, are directly related to its triboelectric charging characteristics and its position in the triboelectric series.

1.10.1.4 By selecting formulation properties and inhaler, micronized drug can be made to acquire charges well beyond the Boltzmann equilibrium charge distribution theory.

### 1.10.2. Specific Aims

The following specific aims will be pursued in addressing the above hypotheses.

1.10.2.1 To elucidate the phenomenon of triboelectric charging during DPI actuation.

(a) The electrostatic properties of albuterol sulphate, budesonide and three excipients (lactose (disaccharide), glucose (monosaccharide), and inorganic salt (e.g. calcium phosphate)), including different batches, size fractions, and blends will be studied using Faraday cage experiments to determine charge in the absence of frictional triboelectrification.

(b) From Faraday well experiments, pseudo-work functions will be determined for the drugs, excipients, excipient batches and sieve fractions.

(c) The effect of last surface of contact will be established by using different materials during Faraday cage discharge.



- (d) The electrostatic charges of the above materials will be studied using the Electrical Low Pressure Impactor (ELPI), in conjunction with standard flow tubes and inhaler devices to determine the effect of inspiratory airflow on triboelectrification.
- (e) Charge and particle size deposition will be determined and fully characterized in each case using the ELPI.

1.10.2.2 To determine the contribution of specific formulation factors.

- (a) The effect of chemistry (drug and excipients), manufacture process, blend concentration, pressure drop, and materials (capsule and inhaler) on electrostatic charge will be determined in ELPI deposition experiments.
- (b) Materials and formulation components, including different excipient sieve fractions, and batches will be used to create a triboelectric series.

1.10.2.3 To determine the correlation between surface acid/base properties and triboelectric charging.

- (a) The dispersive surface free energy and specific acid/base surface characteristics of select drugs, excipients, blends, and sieve fractions will be studied by inverse gas chromatography.
- (b) The relationship between surface acid/base parameters and pseudo-work functions will be investigated, i.e. acid/base parameters will be related to charge sign and magnitude.

1.10.2.4 To determine if tribocharging can increase particle charge beyond Boltzmann distribution.

- (a) Using the developed triboelectric series, drugs will be formulated to give maximal charging.
- (b) Charge during deposition studies in ELPI will be measured and compared to Boltzmann distribution.

### 1.11. Conclusion

Dry powder inhalers are increasingly important respiratory delivery devices. Particle electrostatic charging is used in a number of applications to bring about specific particle behavior; its use in dry powder inhalers has not been studied. Simulations, *in vitro* and *in vivo* studies suggest that charge can increase the deposition of aerosol particles in the lung. Due to their design and material characteristics DPI devices and formulations lend themselves to triboelectric charging. The project aim is to characterize particle charging in the DPI to determine if tribocharging can be utilized for DPI formulation development and drug delivery. The research is likely to yield secondary results that will further our understanding of DPI formulations and behavior.

There have been few studies that probed aerosol electrostatics but none that has studied pharmaceutically relevant systems. There is no comprehensive model relating formulation variables with electrostatic charging and delivery. Use of the ELPI for this work has distinct advantages over other techniques as it allows concurrent determination of particle size and charge for particles in the respirable size range. Studies to date have focused on the entire discharge or on particles larger than what could be inhaled.

While it has been suggested that triboelectric charging of insulators is related to the presence of electron donor and electron acceptor sites on the surface,<sup>146</sup> this hypothesis has never been evaluated. The specific aim of linking specific surface energy data with charging holds promise to do that. If this hypothesis is supported by experimental data, our understanding of insulator charging would be significantly enhanced, and confounding data may be explained. The result would have implications not just to the field of pharmaceutical sciences, but could advance the entire field of particle electrostatics.

## **1.12. Acknowledgements**

The first part of this introduction chapter is based on an article published previously in *Respiratory Care*.<sup>173</sup> The publisher has kindly permitted use of the article in full or of passages but has requested that the sections not be altered. Several sections have been reproduced though the order in which they are presented has been changed and some sections and figures have been omitted.

### 1.13. Literature Cited

1. Di, L. & Kerns, E. H. Profiling drug-like properties in discovery research. *Current Opinion in Chemical Biology* 7, 402-408 (2003).
2. Lipinski, C. A. Drug-like properties and the causes of poor solubility and poor permeability. *Journal of Pharmacological and Toxicological Methods* 44, 235-249 (2000).
3. Lipinski, C. A., Lombardo, F., Dominy, B. W. & Feeney, P. J. Experimental and computational approaches to estimate solubility and permeability in drug discovery and development settings. *Advanced Drug Delivery Reviews* 23, 3-25 (1997).
4. Timsina, M. P., Martin, G. P., Marriott, C., Ganderton, D. & Yianneskis, M. Drug-Delivery to the Respiratory-Tract Using Dry Powder Inhalers. *International Journal of Pharmaceutics* 101, 1-13 (1994).
5. Aswania, O. et al. Intra-subject variability in lung dose in healthy volunteers using five conventional portable inhalers. *J Aerosol Med* 17, 231-8 (2004).
6. Cochrane, M. G., Bala, M. V., Downs, K. E., Mauskopf, J. & Ben-Joseph, R. H. Inhaled corticosteroids for asthma therapy: patient compliance, devices, and inhalation technique. *Chest* 117, 542-50 (2000).
7. Smyth, H. D. C. & Hickey, A. J. Carriers in drug powder delivery: Implications for inhalation system design. *American Journal of Drug Delivery* 3 (2005).
8. Dolovich, M. B. et al. Device selection and outcomes of aerosol therapy: Evidence-based guidelines: American College of Chest Physicians/American College of Asthma, Allergy, and Immunology. *Chest* 127, 335-71 (2005).
9. Crooks, P. A. & Al-Ghananeem, A. M. Drug targeting to the lung: chemical and biochemical considerations, in *Pharmaceutical inhalation aerosol technology*, edited by A. Hickey (M. Dekker, New York, 2004).
10. Barry, P. W. & O'Callaghan, C. The influence of inhaler selection on efficacy of asthma therapies. *Adv Drug Deliv Rev* 55, 879-923 (2003).
11. Rau, J. L. The inhalation of drugs: advantages and problems. *Respir Care* 50, 367-82 (2005).
12. O'Connor, B. J. The ideal inhaler: design and characteristics to improve outcomes. *Respir Med* 98 Suppl A, S10-6 (2004).
13. Newman, S. P. & Clarke, S. W. Bronchodilator delivery from Gentlehaler, a new low-velocity pressurized aerosol inhaler. *Chest* 103, 1442-6 (1993).
14. Ganderton, D. General factors influencing drug delivery to the lung. *Respiratory Medicine* 91, 13-16 (1997).
15. Newman, S. P. & Newhouse, M. T. Effect of add-on devices for aerosol drug delivery: deposition studies and clinical aspects. *J Aerosol Med* 9, 55-70 (1996).

16. Giraud, V. & Roche, N. Misuse of corticosteroid metered-dose inhaler is associated with decreased asthma stability. *Eur Respir J* 19, 246-51 (2002).
17. Borgstrom, L., Derom, E., Stahl, E., Wahlin-Boll, E. & Pauwels, R. The inhalation device influences lung deposition and bronchodilating effect of terbutaline. *Am J Respir Crit Care Med* 153, 1636-40 (1996).
18. Ashurst, I. I., Malton, A., Prime, D. & Sumby, B. Latest advances in the development of dry powder inhalers. *Pharm. Sci. Technol. Today* 3, 246-256 (2000).
19. Norwood, D. L. et al. Analysis of polycyclic aromatic hydrocarbons in metered dose inhaler drug formulations by isotope dilution gas chromatography/mass spectrometry. *J Pharm Biomed Anal* 13, 293-304 (1995).
20. Dalby, R. & Suman, J. Inhalation therapy: technological milestones in asthma treatment. *Adv Drug Deliv Rev* 55, 779-91 (2003).
21. Newman, S. P. & Busse, W. W. Evolution of dry powder inhaler design, formulation, and performance. *Respir Med* 96, 293-304 (2002).
22. Dunbar, C. A., Hickey, A. J. & Holzner, P. Dispersion and Characterization of Pharmaceutical Dry Powder Aerosols. *KONA* 16, 7-44 (1998).
23. Smith, I. J. & Parry-Billings, M. The inhalers of the future? A review of dry powder devices on the market today. *Pulm Pharmacol Ther* 16, 79-95 (2003).
24. Newman, S., Hollingworth, A. & Clark, A. Effect of different modes of inhalation on drug delivery from a dry powder inhaler. *International Journal of Pharmaceutics* 102, 127-132 (1994).
25. Cegla, U. H. Pressure and inspiratory flow characteristics of dry powder inhalers. *Respir Med* 98 Suppl A, S22-8 (2004).
26. Dunbar, C. A., Morgan, B., Van Oort, M. & Hickey, A. J. A comparison of dry powder inhaler dose delivery characteristics using a power criterion. *PDA J Pharm Sci Technol* 54, 478-84 (2000).
27. Zeng, X. M., Martin, A. P., Marriott, C. & Pritchard, J. The influence of carrier morphology on drug delivery by dry powder inhalers. *Int J Pharm* 200, 93-106 (2000).
28. Tobyn, M., Staniforth, J. N., Morton, D., Harmer, Q. & Newton, M. E. Active and intelligent inhaler device development. *Int J Pharm* 277, 31-7 (2004).
29. Crowder, T. M. Vibration technology for active dry-powder inhalers. *Pharmaceutical Technology* 28, 52-61 (2004).
30. Crowder, T. M., Louey, M. D., Sethuraman, V. V., Smyth, H. D. C. & Hickey, A. J. An odyssey in inhaler formulations and design. *Pharmaceutical Technology* 25, 99-113 (2001).
31. Crooks, P. A. & Damani, L. A. Drug Application to the Respiratory Tract: Metabolic and Pharmacokinetic Considerations. *Respiratory Drug Delivery I* 1, 61-90 (1990).

32. Patton, J. S. & Platz, M. P. Pulmonary delivery of peptides and proteins for systemic action. *Adv Drug Deliv Rev* 8, 179-196 (1992).
33. Byron, P. R. & Patton, J. S. Drug delivery via the respiratory tract. *J Aerosol Med* 7, 49-75 (1994).
34. Niven, R. W., Lott, F. D., Ip, A. Y. & Cribbs, J. M. Pulmonary delivery of powders and solutions containing recombinant human granulocyte colony-stimulating factor (rhG-CSF) to the rabbit. *Pharm Res* 11, 1101-9 (1994).
35. Cefalu, W. T. Concept, strategies, and feasibility of noninvasive insulin delivery. *Diabetes Care* 27, 239-46 (2004).
36. Owens, D. R., Zinman, B. & Bolli, G. Alternative routes of insulin delivery. *Diabet Med* 20, 886-98 (2003).
37. Patton, J. S., Bukar, J. & Nagarajan, S. Inhaled insulin. *Adv Drug Deliv Rev* 35, 235-247 (1999).
38. Patton, J. S. Pulmonary delivery of drugs for bone disorders. *Adv Drug Deliv Rev* 42, 239-48 (2000).
39. Roth, Y., Chapnik, J. S. & Cole, P. Feasibility of aerosol vaccination in humans. *Ann Otol Rhinol Laryngol* 112, 264-70 (2003).
40. Tronde, A. et al. Pulmonary absorption rate and bioavailability of drugs in vivo in rats: structure-absorption relationships and physicochemical profiling of inhaled drugs. *J Pharm Sci* 92, 1216-33 (2003).
41. Hickey, A. J. in *Drug Delivery: Principles and Applications* (eds. Wang, B., Siahaan, T. & Soltero, R. A.) pp 341-361 (John Wiley & Sons, Inc., Hoboken, N.J., 2005).
42. Labiris, N. R. & Dolovich, M. B. Pulmonary drug delivery. Part I: physiological factors affecting therapeutic effectiveness of aerosolized medications. *Br J Clin Pharmacol* 56, 588-99 (2003).
43. Howarth, P. H. Why particle size should affect clinical response to inhaled therapy. *J Aerosol Med* 14 Suppl 1, S27-34 (2001).
44. Bergstrom, C. A. et al. Absorption classification of oral drugs based on molecular surface properties. *J Med Chem* 46, 558-70 (2003).
45. Palm, K., Luthman, K., Ungell, A. L., Strandlund, G. & Artursson, P. Correlation of drug absorption with molecular surface properties. *J Pharm Sci* 85, 32-9 (1996).
46. Veber, D. F. et al. Molecular properties that influence the oral bioavailability of drug candidates. *Journal of Medicinal Chemistry* 45, 2615-2623 (2002).
47. Kerns, E. H. & Di, L. Pharmaceutical profiling in drug discovery. *Drug Discov Today* 8, 316-23 (2003).
48. Barnes, P. J. A single inhaler for asthma? *Am J Respir Crit Care Med* 171, 95-6 (2005).

49. Suarez, S. & Hickey, A. J. Drug properties affecting aerosol behavior. *Respir Care* 45, 652-66 (2000).
50. Snow, R. H., Allen, T., Ennis, B. J. & Litster, J. D. in *Perry's Chemical Engineers' Handbook* (eds. Perry, R. H. & Green, D. W.) (McGraw-Hill, New York, 1999).
51. Begat, P., Young, P. M., Edge, S., Kaerger, J. S. & Price, R. The effect of mechanical processing on surface stability of pharmaceutical powders: Visualization by atomic force microscopy. *Journal of Pharmaceutical Sciences* 92, 611-620 (2003).
52. Cheng, Y. S., Marshall, T. C., Henderson, R. F. & Newton, G. J. Use of a jet mill for dispersing dry powder for inhalation studies. *Am Ind Hyg Assoc J* 46, 449-54 (1985).
53. Drogemeier, R. & Leschonski, K. Ultra fine grinding in a two stage rotor impact mill. *International Journal of Mineral Processing* 44-5, 485-495 (1996).
54. Hu, G., Otaki, H. & Watanuki, K. Optimization of grinding performance of tumbling ball mill. *Jsmc International Journal Series C-Mechanical Systems Machine Elements and Manufacturing* 44, 267-274 (2001).
55. Steckel, H. & Brandes, H. G. A novel spray-drying technique to produce low density particles for pulmonary delivery. *Int J Pharm* 278, 187-95 (2004).
56. Chawla, A., Taylor, K. M. G., Newton, J. M. & Johnson, M. C. R. Production of Spray-Dried Salbutamol Sulfate for Use in Dry Powder Aerosol Formulation. *International Journal of Pharmaceutics* 108, 233-240 (1994).
57. Vidgren, M. T., Vidgren, P. A. & Paronen, T. P. Comparison of Physical and Inhalation Properties of Spray-Dried and Mechanically Micronized Disodium-Cromoglycate. *International Journal of Pharmaceutics* 35, 139-144 (1987).
58. Debenedetti, P. G., Tom, J. W., Kwauk, X. & Yeo, S. D. Rapid Expansion of Supercritical Solutions (RESS) - Fundamentals and Applications. *Fluid Phase Equilibria* 82, 311-321 (1993).
59. Velaga, S. P., Berger, R. & Carlfors, J. Supercritical fluids crystallization of budesonide and flunisolide. *Pharm Res* 19, 1564-71 (2002).
60. Schiavone, H., Palakodaty, S., Clark, A., York, P. & Tzannis, S. T. Evaluation of SCF-engineered particle-based lactose blends in passive dry powder inhalers. *International Journal of Pharmaceutics* 281, 55-66 (2004).
61. Jung, J. & Perrut, M. Particle design using supercritical fluids: Literature and patent survey. *Journal of Supercritical Fluids* 20, 179-219 (2001).
62. *Handbook of pharmaceutical excipients* (eds. Rowe, R. C., Sheskey, P. J. & Weller, P. J.) (Pharmaceutical Press, Chicago, 2003).
63. Steckel, H. & Bolzen, N. Alternative sugars as potential carriers for dry powder inhalations. *Int J Pharm* 270, 297-306 (2004).

64. Tee, S. K., Marriott, C., Zeng, X. M. & Martin, G. P. The use of different sugars as fine and coarse carriers for aerosolised salbutamol sulphate. *International Journal of Pharmaceutics* 208, 111-123 (2000).
65. Shah, S. P. & Misra, A. Development of liposomal amphotericin B dry powder inhaler formulation. *Drug Deliv* 11, 247-53 (2004).
66. Joshi, M. & Misra, A. N. Pulmonary disposition of budesonide from liposomal dry powder inhaler. *Methods Find Exp Clin Pharmacol* 23, 531-6 (2001).
67. Kawashima, Y., Serigano, T., Hino, T., Yamamoto, H. & Takeuchi, H. Design of inhalation dry powder of pranlukast hydrate to improve dispersibility by the surface modification with light anhydrous silicic acid (AEROSIL 200). *International Journal of Pharmaceutics* 173, 243-251 (1998).
68. Lucas, P., Anderson, K., Potter, U. J. & Staniforth, J. N. Enhancement of small particle size dry powder aerosol formulations using an ultra low density additive. *Pharmaceutical Research* 16, 1643-1647 (1999).
69. Kawashima, Y., Serigano, T., Hino, T., Yamamoto, H. & Takeuchi, H. A new powder design method to improve inhalation efficiency of pranlukast hydrate dry powder aerosols by surface modification with hydroxypropylmethylcellulose phthalate nanospheres. *Pharm Res* 15, 1748-52 (1998).
70. Zeng, X. M., Martin, G. P., Marriott, C. & Pritchard, J. Lactose as a carrier in dry powder formulations: the influence of surface characteristics on drug delivery. *J Pharm Sci* 90, 1424-34 (2001).
71. Podczeczek, F. The relationship between physical properties of lactose monohydrate and the aerodynamic behaviour of adhered drug particles. *International Journal of Pharmaceutics* 160, 119-130 (1998).
72. Islam, N., Stewart, P., Larson, I. & Hartley, P. Effect of carrier size on the dispersion of salmeterol xinafoate from interactive mixtures. *J Pharm Sci* 93, 1030-8 (2004).
73. Chew, N. Y. K. & Chan, H. K. The role of particle properties in pharmaceutical powder inhalation formulations. *Journal of Aerosol Medicine-Deposition Clearance and Effects in the Lung* 15, 325-330 (2002).
74. Sethuraman, V. V. & Hickey, A. J. Powder properties and their influence on dry powder inhaler delivery of an antitubercular drug. *AAPS PharmSciTech* 3, E28 (2002).
75. Crowe, C. T., Sommerfeld, M. & Tsuji, Y. *Multiphase flows with droplets and particles* (CRC Press, Boca Raton, Fla., 1998).
76. Kreith, F. *Fluid mechanics* (CRC Press, Boca Raton, Fla., 2000).
77. Gidaspow, D. *Multiphase flow and fluidization : continuum and kinetic theory descriptions* (Academic Press, Boston, 1994).
78. Kolev, N. I. *Multiphase flow dynamics* (Springer, Berlin ; New York, 2005).



79. Johnson, R. W. *The handbook of fluid dynamics* (CRC Press, Boca Raton, Fla., 1998).
80. Brittain, H. *Physical characterization of pharmaceutical solids* (Marcel Dekker Inc., New York, 1995).
81. Brittain, H. *Polymorphism in pharmaceutical solids* (Marcel Dekker Inc., New York, 1999).
82. Moulton, B. & Zaworotko, M. J. From molecules to crystal engineering: Supramolecular isomerism and polymorphism in network solids. *Chemical Reviews* 101, 1629-1658 (2001).
83. Henck, J. O., Griesser, U. J. & Burger, A. Polymorphism of drug substances - An economic challenge. *Pharmazeutische Industrie* 59, 165-169 (1997).
84. Grzesiak, A. L., Lang, M., Kim, K. & Matzger, A. J. Comparison of the four anhydrous polymorphs of carbamazepine and the crystal structure of form I. *J Pharm Sci* 92, 2260-71 (2003).
85. Cartensen, J. T. *Pharmaceutics of solids and solid dosage forms* (John Wiley and Sons, New York, NY, 1989).
86. Garekani, H. A., Sadeghi, F., Badiee, A., Mostafa, S. A. & Rajabi-Siahboomi, A. R. Crystal habit modifications of ibuprofen and their physicochemical characteristics. *Drug Development and Industrial Pharmacy* 27, 803-809 (2001).
87. Stoica, C. et al. Understanding the effect of a solvent on the crystal habit. *Crystal Growth & Design* 4, 765-768 (2004).
88. Wood, W. M. L. A bad (crystal) habit - and how it was overcome. *Powder Technology* 121, 53-59 (2001).
89. Rodriguez-Hornedo, N. & Sinclair, B. D. in *Encyclopedia of Pharmaceutical Technology* (eds. Swarbrick, J. & Boylan, J. C.) (Marcel Dekker, Inc., New York, 2002).
90. Rodriguez-Spong, B., Price, C. P., Jayasankar, A., Matzger, A. J. & Rodriguez-Hornedo, N. General principles of pharmaceutical solid polymorphism: a supramolecular perspective. *Adv Drug Deliv Rev* 56, 241-74 (2004).
91. Desiraju, G. R. Chemistry beyond the molecule. *Nature* 412, 397-400 (2001).
92. Dunitz, J. D. & Bernstein, J. Disappearing Polymorphs. *Accounts of Chemical Research* 28, 193-200 (1995).
93. Ouvrard, C. & Price, S. L. Toward crystal structure prediction for conformationally flexible molecules: The headaches illustrated by aspirin. *Crystal Growth & Design* 4, 1119-1127 (2004).
94. Vishweshwar, P., McMahon, J. A., Oliveira, M., Peterson, M. L. & Zaworotko, M. J. The predictably elusive form II of aspirin. *Journal of the American Chemical Society* 127, 16802-16803 (2005).

95. Bond, A. D., Boese, R. & Desiraju, G. R. On the polymorphism of aspirin: Crystalline aspirin as intergrowths of two "polymorphic" domains". *Angewandte Chemie-International Edition* 46, 618-622 (2007).
96. Braun, M. A., Oschmann, R. & Schmidt, P. C. Influence of excipients and storage humidity on the deposition of disodium cromoglycate (DSCG) in the Twin Impinger. *International Journal of Pharmaceutics* 135, 53-62 (1996).
97. Maggi, L., Bruni, R. & Conte, U. Influence of the moisture on the performance of a new dry powder inhaler. *Int J Pharm* 177, 83-91 (1999).
98. Hickey, A. J., Gonda, I., Irwin, W. J. & Fildes, F. J. Effect of hydrophobic coating on the behavior of a hygroscopic aerosol powder in an environment of controlled temperature and relative humidity. *J Pharm Sci* 79, 1009-14 (1990).
99. Hickey, A. J. & Martonen, T. B. Behavior of hygroscopic pharmaceutical aerosols and the influence of hydrophobic additives. *Pharm Res* 10, 1-7 (1993).
100. Rudolf, G., Gebhart, J., Heyder, J., Schiller, C. F. & Stahlhofen, W. An Empirical-Formula Describing Aerosol Deposition in Man for Any Particle-Size. *Journal of Aerosol Science* 17, 350-355 (1986).
101. Task Group on Lung Dynamics. *Health Physics* 12, 173-207 (1966).
102. Zanen, P., Go, L. T. & Lammers, J. W. Optimal particle size for beta 2 agonist and anticholinergic aerosols in patients with severe airflow obstruction. *Thorax* 51, 977-80 (1996).
103. Zanen, P., Go, L. T. & Lammers, J. W. J. The Optimal Particle-Size for Beta-Adrenergic Aerosols in Mild Asthmatics. *International Journal of Pharmaceutics* 107, 211-217 (1994).
104. Zanen, P., Go, L. T. & Lammers, J. W. J. The Optimal Particle-Size for Parasympatholytic Aerosols in Mild Asthmatics. *International Journal of Pharmaceutics* 114, 111-115 (1995).
105. Zanen, P., Go, L. T. & Lammers, J. W. J. Optimal particle size for beta(2) agonist and anticholinergic aerosols in patients with severe airflow obstruction. *Thorax* 51, 977-980 (1996).
106. Usmani, O. S., Biddiscombe, M. F., Nightingale, J. A., Underwood, S. R. & Barnes, P. J. Effects of bronchodilator particle size in asthmatic patients using monodisperse aerosols. *J Appl Physiol* 95, 2106-12 (2003).
107. Hinds, W. C. *Aerosol technology : properties, behavior, and measurement of airborne particles* (Wiley, New York, 1999).
108. Hickey, A. J., Martonen, T. B. & Yang, Y. Theoretical relationship of lung deposition to the fine particle fraction of inhalation aerosols. *Pharm Acta Helv* 71, 185-90 (1996).
109. Martonen, T. B., Katz, I., Fults, K. & Hickey, A. J. Use of analytically defined estimates of aerosol respirable fraction to predict lung deposition patterns. *Pharm Res* 9, 1634-9 (1992).

110. Chew, N. Y. K. & Chan, H. K. Effect of powder polydispersity on aerosol generation. *Journal of Pharmacy and Pharmaceutical Sciences* 5, 162-168 (2002).
111. Hickey, A. J. in *Pharmaceutical inhalation aerosol technology* (ed. Hickey, A. J.) 345-384 (Marcel Dekker, New York, 2004).
112. Dunbar, C. A. & Hickey, A. J. Evaluation of probability density functions to approximate particle size distributions of representative pharmaceutical aerosols. *Journal of Aerosol Science* 31, 813-831 (2000).
113. Raabe, O. G. A general method for fitting size distributions to multicomponent aerosol data using weighted least-squares. *Environ Sci Technol* 12, 1162-1167 (1978).
114. Marple, V. A. et al. Next generation pharmaceutical impactor: a new impactor for pharmaceutical inhaler testing. Part III. extension of archival calibration to 15 L/min. *J Aerosol Med* 17, 335-43 (2004).
115. Mitchell, J. P. & Nagel, M. W. Cascade impactors for the size characterization of aerosols from medical inhalers: their uses and limitations. *J Aerosol Med* 16, 341-77 (2003).
116. Marple, V. A., Rubow, K. L. & Olson, B. A. in *Aerosol Measurement: Principles, Techniques and Applications* (eds. Baron, P. A. & Willeke, K.) 229-260 (Wiley Interscience, New York, 2001).
117. Hering, S. V., Flagan, R. C. & Friedlander, S. K. Design and Evaluation of New Low-Pressure Impactor .1. *Environmental Science & Technology* 12, 667-673 (1978).
118. Hering, S. V., Friedlander, S. K., Collins, J. J. & Richards, L. W. Design and Evaluation of a New Low-Pressure Impactor .2. *Environmental Science & Technology* 13, 184-188 (1979).
119. Keskinen, J., Pietarinen, K. & Lehtimaki, M. Electrical Low-Pressure Impactor. *Journal of Aerosol Science* 23, 353-360 (1992).
120. Fults, K. A., Miller, I. F. & Hickey, A. J. Effect of particle morphology on emitted dose of fatty acid-treated disodium cromoglycate powder aerosols. *Pharm Dev Technol* 2, 67-79 (1997).
121. Hickey, A. J., Fults, A. K. & Pilliai, R. S. Use of particle morphology to influence the delivery of drug from dry powder aerosols. *J. Biopharm. Sci* 3, 107-113 (1992).
122. Young, P. M. et al. Characterization of a surface modified dry powder inhalation carrier prepared by "particle smoothing". *J Pharm Pharmacol* 54, 1339-44 (2002).
123. Chew, N. Y. K. & Chan, H. K. Use of solid corrugated particles to enhance powder aerosol performance. *Pharmaceutical Research* 18, 1570-1577 (2001).
124. Chew, N. Y. K., Tang, P., Chan, H. K. & Raper, J. A. How much particle surface corrugation is sufficient to improve aerosol performance of powders? *Pharmaceutical Research* 22, 148-152 (2005).

125. Heng, P. W., Chan, L. W. & Lim, L. T. Quantification of the surface morphologies of lactose carriers and their effect on the in vitro deposition of salbutamol sulphate. *Chem Pharm Bull (Tokyo)* 48, 393-8 (2000).
126. Chan, L. W., Lim, L. T. & Heng, P. W. Immobilization of fine particles on lactose carrier by precision coating and its effect on the performance of dry powder formulations. *J Pharm Sci* 92, 975-84 (2003).
127. Martin, A. *Physical Pharmacy* (Lippincott Williams & Wilkins, Baltimore, MD, 1993).
128. Israelachvili, J. N. *Intermolecular and surface forces* (Academic Press London, London, 1991).
129. Sun, C. H. & Berg, J. C. A review of the different techniques for solid surface acid-base characterization. *Advances in Colloid and Interface Science* 105, 151-175 (2003).
130. Fowkes, F. M. Determination of Interfacial Tensions, Contact Angles, and Dispersion Forces in Surfaces by Assuming Additivity of Intermolecular Interactions in Surfaces. *Journal of Physical Chemistry* 66, 382-& (1962).
131. Fowkes, F. M. Attractive forces at interfaces. *Ind. Eng. Chem.* 56, 40-52 (1964).
132. Mukhopadhyay, P. & Schreiber, H. P. Aspects of Acid-Base Interactions and Use of Inverse Gas-Chromatography. *Colloids and Surfaces a-Physicochemical and Engineering Aspects* 100, 47-71 (1995).
133. Edwards, D. A. et al. Large porous particles for pulmonary drug delivery. *Science* 276, 1868-1871 (1997).
134. Castle, G. S. P. Industrial applications of electrostatics: the past, present and future. *Journal of Electrostatics* 51, 1-7 (2001).
135. Matsusaka, S. & Masuda, H. Electrostatics of particles. *Advanced Powder Technology* 14, 143-166 (2003).
136. Yao, J. & Wang, C.-H. Granular size and shape effects on electrostatics in pneumatic conveying systems. *Chemical Engineering Science* 61, 3858-3874 (2006).
137. Adhiwidjaja, I., Matsusaka, S., Tanaka, H. & Masuda, H. Simultaneous phenomenon of particle deposition and reentrainment: Effects of surface roughness on deposition layer of striped pattern. *Aerosol Science and Technology* 33, 323-333 (2000).
138. Adhiwidjaja, I., Matsusaka, S., Yabe, S. & Masuda, H. Simultaneous phenomenon of particle deposition and reentrainment in charged aerosol flow - effects of particle charge and external electric field on the deposition layer. *Advanced Powder Technology* 11, 221-233 (2000).
139. Jones, T. B. & King, J. L. *Powder handling and electrostatics - Understanding and preventing hazards* (Lewis, London, 1991).
140. Hendricks, C. D. in *Electrostatics and its applications* (ed. Moore, A. C.) 57-85 (John Wiley & Sons, New York, 1973).

141. Hendricks, C. D. in *Electrostatics and its applications* (ed. Moore, A. C.) 29-56 (John Wiley & Sons, New York, 1973).
142. Bailey, A. G., Hashish, A. H. & Williams, T. J. Drug delivery by inhalation of charged particles. *Journal of Electrostatics* 44, 3-10 (1998).
143. Fraser, D. A. The deposition of unipolar charged particles in the lungs of animals. *Arch Environ Health* 13, 152-7 (1966).
144. Inculet, I. I. in *Electrostatics and its applications* (ed. Moore, A. C.) 86-114 (John Wiley & Sons, New York, 1973).
145. Murtomaa, M., Harjunen, P., Mellin, V., Lehto, V. P. & Laine, E. Effect of amorphicity on the triboelectrification of lactose powder. *Journal of Electrostatics* 56, 103-110 (2002).
146. Bailey, A. G. Charging of Solids and Powders. *Journal of Electrostatics* 30, 167-180 (1993).
147. Hendricks, C. D. in *Electrostatics and its applications* (ed. Moore, A. C.) 8-28 (John Wiley & Sons, New York, 1973).
148. Lectures of Electromagnetism, Chapter 7. Conduction and Electroquasistatic Charge Relaxation, [http://web.mit.edu/6.013\\_book/www/book.html](http://web.mit.edu/6.013_book/www/book.html)
149. Harper, W. R. *Contact and frictional electrification* (Oxford University Press, London, 1967).
150. Castle, G. S. P. Contact charging between particles; some current understanding. *Proc. ESA Annual Meeting on Electrostatics*, 1-3 (2008).
151. Eilbeck, J., Rowley, G., Carter, P. A. & Fletcher, E. J. Effect of contamination of pharmaceutical equipment on powder triboelectrification. *Int J Pharm* 195, 7-11 (2000).
152. Shio, H. Triboelectrification between polycrystalline and monocrystalline ice. *Journal of Electrostatics* 53, 185-193 (2001).
153. Elajnaf, A., Carter, P. & Rowley, G. Electrostatic characterisation of inhaled powders: effect of contact surface and relative humidity. *Eur J Pharm Sci* 29, 375-84 (2006).
154. Balachandran, W., Machowski, W., Gaura, E. & Hudson, C. Control of drug aerosol in human airways using electrostatic forces. *Journal of Electrostatics* 40-1, 579-584 (1997).
155. Ali, M., Mazumder, M. K. & Martonen, T. B. Measurements of Electrodynamic Effects on the Deposition of MDI and DPI Aerosols in a Replica Cast of Human Oral-Pharyngeal-Laryngeal Airways. *J Aerosol Med Pulm Drug Deliv* (2008).
156. Byron, P. B., Peart, J. & Staniforth, J. N. Aerosol electrostatics I: Properties of fine powders before and after aerosolization by dry powder inhalers. *Pharm Res* 14, 698-705 (1997).
157. Chow, K. T., Zhu, K., Tan, R. B. & Heng, P. W. Investigation of Electrostatic Behavior of a Lactose Carrier for Dry Powder Inhalers. *Pharm Res* (2008).

158. Zhu, K., Ng, W. K., Shen, S., Tan, R. B. & Heng, P. W. Design of a device for simultaneous particle size and electrostatic charge measurement of inhalation drugs. *Pharm Res* 25, 2488-96 (2008).
159. Bennett, F. S., Carter, P. A., Rowley, G. & Dandiker, Y. Modification of electrostatic charge on inhaled carrier lactose particles by addition of fine particles. *Drug Dev Ind Pharm* 25, 99-103 (1999).
160. Murtomaa, M., Strengell, S., Laine, E. & Bailey, A. Measurement of electrostatic charge of an aerosol using a grid-probe. *Journal of Electrostatics* 58, 197-207 (2003).
161. Murtomaa, M. et al. Effect of particle morphology on the triboelectrification in dry powder inhalers. *International Journal of Pharmaceutics* 282, 107-114 (2004).
162. Carter, P. A., Cassidy, O. E., Rowley, G. & Merrifield, D. R. Triboelectrification of fractionated crystalline and spray-dried lactose. *J Pharm Pharmacol* 4, 111-115 (1998).
163. Cassidy, O. E., Carter, P. A., Rowley, G. & Merrifield, D. R. Triboelectrification of spray-dried lactose prepared from different feedstock concentrations. *J Pharm Pharmacol* 52, 13-7 (2000).
164. Elajnaf, A., Carter, P. & Rowley, G. The effect of relative humidity on electrostatic charge decay of drugs and excipient used in dry powder inhaler formulation. *Drug Dev Ind Pharm* 33, 967-74 (2007).
165. Watanabe, H., Ghadiri, M., Matsuyama, T., Ding, Y. L. & Pitt, K. G. New instrument for tribocharge measurement due to single particle impacts. *Rev Sci Instrum* 78, 024706 (2007).
166. Watanabe, H. et al. Triboelectrification of pharmaceutical powders by particle impact. *Int J Pharm* 334, 149-55 (2007).
167. Knutson, E. O. & Whitby, K. T. Aerosol classification by electric mobility: apparatus, theory, and applications. *J Aerosol Sci* 6, 443-451 (1975).
168. Kitabatake, Y. Charge Spectra Measurement of Toner-Particles for Copier by E-Spart Analyzer. *Sharp Technical Journal*, 83-86 (1988).
169. Kutsuwada, N. et al. Tribocharging of Monocomponent Toner for Analyzing Charge-Distributions by E-Spart Analyzer. *Is&Ts Eighth International Congress on Advances in Non-Impact Printing Technologies*, 126-128, 529 (1992).
170. Mazumder, M. K. et al. E-Spart Analyzer - Its Performance in Real-Time Measurements of Particle-Size and Charge-Distributions. *Aerosol Science and Technology* 2, 240-240 (1983).
171. Saini, D., Biris, A. S., Srirama, P. K. & Mazumder, M. K. Particle size and charge distribution analysis of pharmaceutical aerosols generated by inhalers. *Pharm Dev Technol* 12, 35-41 (2007).
172. Telko, M. J., Kujanpaa, J. & Hickey, A. J. Investigation of triboelectric charging in dry powder inhalers using electrical low pressure impactor (ELPI). *Int J Pharm* 336, 352-60 (2007).

173. Telko, M. J. & Hickey, A. J. Dry powder inhaler formulation. *Respir Care* 50, 1209-27 (2005).

## **2. MATERIAL PREPARATION AND PHYSICOCHEMICAL CHARACTERIZATION**

### **2.1. Introduction**

Understanding triboelectrification in DPI formulations requires consideration of the interactions of the constituent materials, i.e. the drug and the excipient particles. Drugs vary from product to product. In the early stages of development, drug substance is usually in short supply, physical properties are estimated from limited testing and may then be modified in a narrow range, e.g. salt selection, to address regulatory, safety, and stability requirements more than formulation needs. The drug itself typically offers little flexibility in terms of formulation variables. The choice of excipient is, therefore, critically important. Carrier particles usually make up 98% or more of the product by weight, which makes them a crucial determinant of overall DPI performance.

As described in Chapter 1, a range of drug and carrier particle properties are considered to ensure bioavailability and stability. For aerosolized drugs, primary particle size and size distribution most profoundly affect aerosolization, delivery and availability to the target organ. Crystallinity, polymorphism, and moisture content are important with respect to drug stability. Carrier particles can moderate drug stability, handling, and aerosolization properties by manipulation of particle size and surface characteristics. Electrostatic particle interactions are thought to play a role as well, but are not routinely characterized in product preparation.

This chapter discusses the selection and characterization of the model drugs and excipients, and the preparation of the model formulations. The formulations are used in deposition studies which are described in detail in Chapter 4. Drugs and excipients are characterized in terms of their particle size, their thermal profiles (to establish their polymorphic makeup), and their electrostatic properties using Faraday cage experiments. Drugs are characterized in terms of their particle size and shape. To



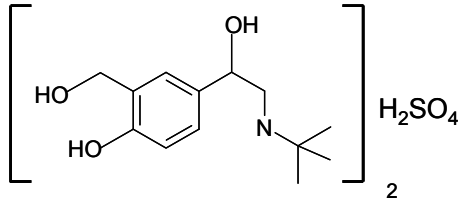
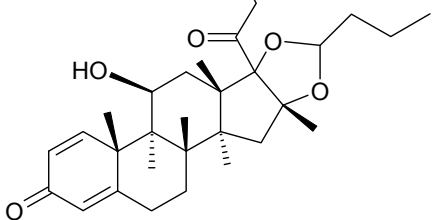
control for particle size related effects, excipients are sieved prior to blending with the drugs. Formulations are tested for content uniformity.

### 2.1.1. Selection of Drugs

Two drugs were selected for study, albuterol sulfate and budesonide. Albuterol (USAN) or salbutamol (INN) is a short-acting  $\beta_2$ -adrenergic receptor agonist used for the relief of bronchospasms in asthma and COPD. Albuterol (MW 239.3) is a common inhaled medicine and a frequently used model drug in medicinal aerosol research. Albuterol sulphate was the sole drug substance studied in the preliminary experiments.

Budesonide (MW 430.5) is a glucocorticoid steroid for the treatment of asthma, non-infectious rhinitis, and allergies. Budesonide is marketed as Pulmicort® with a Turbohaler DPI by AstraZenaca<sup>1</sup> and was selected because it is a different therapeutic category of drug and is structurally distinct from albuterol. While albuterol is a polar and hydrophilic drug, budesonide is hydrophobic. Since budesonide is protected from development as a patented product, few studies of its formulation for DPIs have been published. Select properties of albuterol and budesonide that pertain to this research project are summarized in Table 2.1.

**Table 2.1.** Select properties of albuterol sulfate and budesonide

Drug	Albuterol sulfate	Budesonide
<b>Chemical Name<sup>1</sup></b>	$\alpha$ 1[( <i>tert</i> -Butylamino)methyl]-4-hydroxy-mxylene- $\alpha$ , $\alpha'$ -diol sulfate	(RS)-11 $\beta$ , 16 $\alpha$ , 17, 21-tetrahydroxypregna-1, 4-diene-3, 20-dione cyclic 16, 17-acetal with butyraldehyde
<b>Proprietary name and manufacturer</b>	Generic, various manufacturers, e.g. Ventolin®, GlaxoSmithKline Proventil®, Schering-Plough ProAir®, Teva	Pulmicort®, Astra-Zeneca
<b>Therapeutic Category</b>	Short-acting $\beta_2$ -adrenergic receptor agonist	Glucocorticoid steroid
<b>Indication<sup>1</sup></b>	Bronchodilation, relief of bronchospasms. Asthma, COPD	Anti-inflammatory. Asthma, non-infectious rhinitis.
<b>Dose range<sup>1</sup></b>	120 $\mu$ g	0.25- 1.0 mg
<b>Empirical Formula</b>	$C_{13}H_{21}NO_3$ ( $C_{13}H_{21}NO_3$ ) <sub>2</sub> •H <sub>2</sub> SO <sub>4</sub>	$C_{25}H_{34}O_6$
<b>Structure</b>		
<b>Molecular Weight (g/mol)</b>	576.7 (239.3, albuterol)	430.5
<b>pKa</b>	5.9 <sup>2</sup>	High
<b>Partition Coefficient (log P)</b>	1.0 <sup>3</sup>	3.2 <sup>4</sup>
<b>Aq. Solubility<sup>5</sup></b>	Soluble, 3mg/L	Insoluble
<b>Melting point (°C)<sup>1</sup></b>	230-235 (151, <sup>5</sup> albuterol)	221-232 <sup>5</sup> (259 <sup>6</sup> )
<b>True density (g/cm<sup>3</sup>)</b>	1.34 <sup>7</sup>	1.25 <sup>8</sup>

### 2.1.2. Selection of Excipients

Lactose is the sole conventional carrier excipient used in DPI formulations in the United States and is, therefore, a primary focus of study. It has been shown that minute changes in morphology or particle size of lactose can produce dramatically different product performance. It is not surprising, therefore, that despite best efforts in process control, many problems with DPI performance have been associated with batch-to-batch variability of the excipient. Lactose material properties, including particle size, morphology, method of processing, crystallinity, surface energy have been studied in the context of elucidating batch-to-batch variability. The results of these studies have recently been discussed in two comprehensive publications.<sup>9, 10</sup> Since lactose is so important to DPI formulation development, it is available in different qualities (having undergone different manufacturing processes) from a number of different manufacturers. These differences are investigated in this research project using different lactose products as well as different batches of the same product. The products selected consist of the most stable polymorph  $\alpha$ -lactose monohydrate.

Glucose is the only the other excipient employed in marketed inhaled drug products<sup>11</sup> and, thus, is an important alternative excipient to study. However, like lactose, glucose is a carbohydrate. While one is a disaccharide and the other a monosaccharide, they share some chemical features.

In order to provide a more pronounced contrast, calcium phosphate (CP) was also employed. As an inorganic salt, it is physico-chemically an entirely different material from the sugars described previously. While CP is a physiologically biocompatible salt that is widely used in the formulation of oral dosage forms, it has not been used in DPI formulations. Nonetheless, as reported by Garcia-Contreras et al., CP has been used for lung delivery in animal studies with no adverse effects, and there is evidence to suggest it may be safe to use in humans as well.<sup>12</sup> However, it should be noted that any excipient is not intended to enter the lungs to any significant extent. Relevant physicochemical properties of the studied excipients are listed in Table 2.2.

**Table 2.2.** Selected material properties of excipients used in these studies

Excipient	Lactose monohydrate	Glucose monohydrate	Calcium Phosphate
Proprietary name and manufacturer	Respitose®, DMV-Fonterra	Lycadex® HD, Roquette	A-TAB®, Innophos
Chemical Name	4-(β-D-galactosido)-D-glucose monohydrate	D-(+)-Glucose monohydrate	Calcium hydrogen phosphate; Dicalcium phosphate, anhydrous
Empirical Formula	C <sub>12</sub> H <sub>22</sub> O <sub>11</sub> .H <sub>2</sub> O	C <sub>6</sub> H <sub>12</sub> O <sub>6</sub> .H <sub>2</sub> O	CaHPO <sub>4</sub>
Molecular Weight (g/mol)	360.3	198.2	136.1
Melting point <sup>13</sup>	201-202°C for α-lactose monohydrate 223°C for anhydrous α-lactose 252.2°C for anhydrous β-lactose	83°C for glucose monohydrate 146°C for anhydrous glucose 148-155°C for anhydrous β-D-dextrose	~1670°C Decomposes at ~425°C to form calcium pyrophosphate.
Polymorphism <sup>13</sup>	Several crystalline and amorphous forms. Differential scanning calorimetry can effectively be used to characterize the composition. α-lactose monohydrate becomes anhydrous at 120°C and has a melting point of 201-202°C; endothermic peaks occur at approximately 150°C and vary depending on particle size.	Below 50°C α-D-dextrose monohydrate is the stable crystalline form produced, above 50°C the anhydrous form is obtained, at still higher temperatures β-D-dextrose is formed.	Often contains other calcium phosphates, e.g. Ca <sub>3</sub> (PO <sub>4</sub> ) <sub>2</sub> .
True density <sup>13</sup> (g/cm <sup>3</sup> )	1.55	1.54	3.14
Specific Surface Area (m <sup>2</sup> /g)*	0.3 – 0.4 (SV) 0.9 (ML)	0.2 – 0.3	20-30 (A-Tab)
Aq Solubility <sup>13</sup>	Soluble (0.05-0.1g /mL at 20°C)	Highly soluble (0.9 g/ml at 25°C)	Sparingly soluble
Solubility in solvent <sup>13</sup>	Practically insoluble in alcohol	Soluble in alcohol (0.017g /ml at 20°C)	Practically insoluble in alcohol

\* Manufacturer furnished information

## 2.2. Materials

### 2.2.1. Drugs

Milled albuterol sulfate (median particle size 2µm) was obtained from Chemaco (Beetsterzwaag, NL) from drug manufactured by P.F.C. Italiana S.r.l, (Caronno Pertusella, Italy). Budesonide was obtained from Sigma-Aldrich (St. Louis, MO), and was jet-milled to a single-micron size range

(verified using laser diffraction light scattering). In accordance with manufacturer recommendations, both drugs were stored in glass bottles at ambient conditions (which are closely monitored within the laboratory and fluctuate modestly around  $23\pm 0.5^{\circ}\text{C}$  and  $30\pm 5\%\text{RH}$  throughout the year).

### 2.2.2. Excipients

Lactose monohydrate, Respitose™, was provided by DMV-Fonterra Excipients (Goch, Germany). Two batches of milled (ML001, batches 10136780 and 10138058), and two batches of sieved (SV003, batches 10134131 and 10135425) lactose were evaluated. Dextrose (D-glucose), Lycadex™, batch KDTLT, was provided by Roquette (Keokuk, IA). Calcium hydrogen phosphate, anhydrous, A-Tab™ (granular grade), lot WL00014930, was obtained from Innophos (Cranbury, NJ). In accordance with manufacturer recommendations, the excipients were stored in double-lined PE bags at ambient conditions  $23\pm 0.5^{\circ}\text{C}$  and  $30\pm 5\%\text{RH}$ .

## 2.3. Methods

### 2.3.1. Excipient Sieving and Powder Preparation

Excipients were sieved (Hogentogler & Co, Columbia, MD) prior to characterization and blending with micronized drug. This serves three purposes: (1) removal of fine particles which may confound later electrostatic analysis; (2) control of effects related to particle size between different excipients and (3) determination of particle size effects within a given batch of excipient.

The following sieve fractions are obtained:  $45 - 75\ \mu\text{m}$ ,  $75 - 105\ \mu\text{m}$ ,  $106 - 150\ \mu\text{m}$ . The sieves used were No. 100, 140, 200, and 325. In previous studies, milled lactose was shown to contain some fraction of surface-associated fines, which detached during DPI actuation and deposited on the stages of the ELPI. To remove these fine particles, simple sieving did not suffice and an element of fluidization was introduced; after sieving each size fraction was confined between two #325 sieves and sprayed with compressed air for 2 minutes. This facilitated dislodgement and removal of fine excipient particles that were associated with the surface of larger particles.

### 2.3.2. Particle Size Analysis

Assuming a cuboidal particle shape (i.e. rectangular prism), sieves retain particles whose second largest dimension exceeds the size of the sieve opening. Given that the excipient particles are of different and at times non-uniform shape, the mean volumetric or aerodynamic particle size of a sieve fraction is not necessarily confined to the size range of the sieves used. A dispersed sizing method provides mean volumetric particle sizes. It may also provide similarly turbulent conditions that separate particles and thus facilitate determination of the presence of fines, which can deposit on the stages of the ELPI. A microscopic method provides validation of the experiments and a visual assessment of the surface morphology.

#### 2.3.2.1 Laser Light Diffraction

To ascertain the size distributions of the sieve fractions and determine the level of fines after sieving, drugs and excipients were sized by Fraunhofer laser diffraction analysis (Malvern Series 2600c Droplet and Particle Sizer, Malvern, UK) using the liquid stir cell in the particle-in-liquid mode. A small quantity (~5mg) of drug or excipient were suspended in 2mL of non-solvent (light mineral oil or chloroform), stirred, then gradually added to the liquid-stir cell until obscuration reached approximately 15%. Depending on the expected particle size range, either the 63mm, 100mm, or 300mm focal length lens was used, corresponding to size ranges of 1.22 – 188  $\mu\text{m}$ , 1.9 – 188 $\mu\text{m}$ , 5.8 – 564 $\mu\text{m}$  (interval upper limits). Prior to addition to the liquid cells drug suspensions were sonicated for 10 seconds to promote deagglomeration into primary particle sizes.

#### 2.3.2.2 Scanning Electron Microscopy (SEM)

To complement the results of the laser diffraction light scattering measurements and to independently assess the particle size and morphology, electron micrographs were obtained for the micronized drugs and the excipient sieve fractions. To visualize the blend uniformity a number of

formulation blends were also assessed by SEM (Hitachi S-4700 Cold Cathode Field Emission Scanning Electron Microscope). An electron beam with an accelerating voltage of 2.0 kV was used at magnifications of 100x, 500x, 2000x, and 5000x (only micronized drug at this magnification). The powders were placed on double-sided adhesive carbon tabs (Ted Pella, Inc., Redding, CA) which were adhered to aluminum stubs (Ernest F. Fullam, Inc., Latham, NY) and were coated with gold-palladium alloy to a thickness of 3nm using a sputter-coater (Polaron 5200, Structure Probe Supplies, West Chester, PA) operating at 0.1 mmHg (under argon) for approximately 3min. The sputter coating conditions are commonly used and are not expected to result in drug evaporation from the lactose surface.

#### 2.3.3. Thermal Analysis: Differential Scanning Calorimetry

Differential scanning calorimetry (DSC) is a useful tool for discerning polymorphs and the presence of amorphous material in pharmaceutical solids. Thermal analyses (DSC-6, Perkin Elmer, Waltham, MA) were performed on the lactose, glucose and drugs. Samples of 3 mg were enclosed in crimped aluminum pans. Albuterol sulfate was scanned at a rate of 10°C/min under nitrogen purge to a temperature of 400°C, budesonide was scanned to 280°C.

Lactose samples were scanned at 5°C/min and from 30°C to 250°C under nitrogen purge to show the dehydration at approximately 140°C and melting at 210°C, and possibly thermal events at 170°C or 240°C, which would be indicative of the presence of unstable  $\alpha$ -lactose and  $\beta$ -lactose.<sup>14</sup> Glucose samples were scanned at 5°C/min from 30°C to 160°C to include the melting temperature of the  $\beta$ -glucose. CP was scanned at 5°C/min from 30°C to 450°C (max allowed with instrument).

#### 2.3.4. Electrostatic Material Characterization: Faraday well experiments

Faraday well experiments were conducted to determine the intrinsic electrostatic charge carrying propensity of drugs and excipients. A Faraday well was custom-manufactured at the UNC Dept of

Chemistry instrument shop. The well consists of a receiving pan contained within a metal enclosure that is open on top. The grounded enclosure shields the pan from the effects of external electric fields. The receiving pan is connected to a load resistor (current-to-voltage conversion) and transistor (amplification); when charges are deposited on the pan, the current generates a voltage difference which is then amplified. The amplified voltage signal is captured via a DI-154RS analog-to-digital converter (Dataq, Akron, OH) and recorded on a computer using Windaq data acquisition system (Dataq). Acquisition files are saved as a voltage vs. time binary code and then analyzed in Microsoft Excel. Charges were integrated to give the total electric charge for the sample of material deposited in the well. The circuit for the Faraday well and a picture of the device are shown in Appendix A.

Since the Faraday well was newly built and had no commercial equivalent, the first step in its use was developing a procedure that allowed materials to be characterized successfully. This type of characterization is not a standard technique and instrument and procedure are only poorly described in the literature; most experiments seem to have been conducted with improvised Faraday well type devices.<sup>15-17</sup> The limited work conducted in this area was summarized in Chapter 1.

Extensive initial trials were conducted to establish the charge measurement procedure. The initial trials differed in quantity of material, in the procedure for feeding the material, in use of grounding, and surface of last contact. The final procedure which results in a comparatively high level of reproducibility consists of weighing 50mg of material onto weighing paper and adding it to the Faraday well in a slow and steady manner. This procedure gave a high degree of reproducibility. Experiments were conducted at least three times in a randomized order over the course of several days.

#### 2.3.5. Formulation Manufacture and Content Uniformity Determination

Due to a limited supply of materials, the difficulty involved in preparing the raw materials, and the large number of experiments designed, formulations were manufactured in 1.0g batch sizes. This small batch size limited the methods and equipment that could be used for preparation. Formulations



were prepared using a combination of geometric dilution and tumbling within a vial. Drug and excipient were weighed out in appropriate quantities. Drug was distributed on a mixing pan and geometrically diluted with the excipient, then blended using a small stainless steel spatula for one minute. The blend was transferred to a 20mL glass vial, then tumbled for an additional two minutes by axial rotation of the vial.

Content uniformity of the blends was ascertained by withdrawing three samples (~15mg each) from different locations in the powder bed contained in the vial using a small stainless steel spatula; the powder was tumbled after each sample withdrawal. The samples were weighed and dissolved in 3mL water (albuterol formulations) or methanol (budesonide formulations). UV absorbance of the solutions was assessed at a wavelength of 225.5nm (albuterol) or 244nm (budesonide) (Shimadzu 160U spectrophotometer, Shimadzu Scientific Instruments, Columbia, MD). Excipients are either insoluble or have negligible absorbance at these wavelengths. Drug concentration and variability between samples were calculated; blend concentrations within 10% of nominal concentration and with relative standard deviation less than 10% were accepted, samples outside this range were remanufactured.

## **2.4. Results and Discussion**

### **2.4.1. Particle Size Distribution**

The particle size distributions of micronized albuterol and budesonide, obtained by laser diffraction light scattering are shown in Figure 2.1. The particles meet the size requirement of being in the unit-micron size range. Albuterol had an approximately log-normal distribution with a median diameter of 2.5 $\mu$ m and a geometric standard deviation of 1.4. Budesonide, which was previously jet-milled in the laboratory, had a highly monodisperse distribution with virtually all particles in the 1.9-2.6 $\mu$ m range and a  $d_{50}$  of 2.1 $\mu$ m. Note that the particle size distribution here, as in the following

figures, is not normalized for the width of the interval; this results in a distribution slightly skewed in favor of larger sizes. This presentation is simpler. Distributions are based on volume.

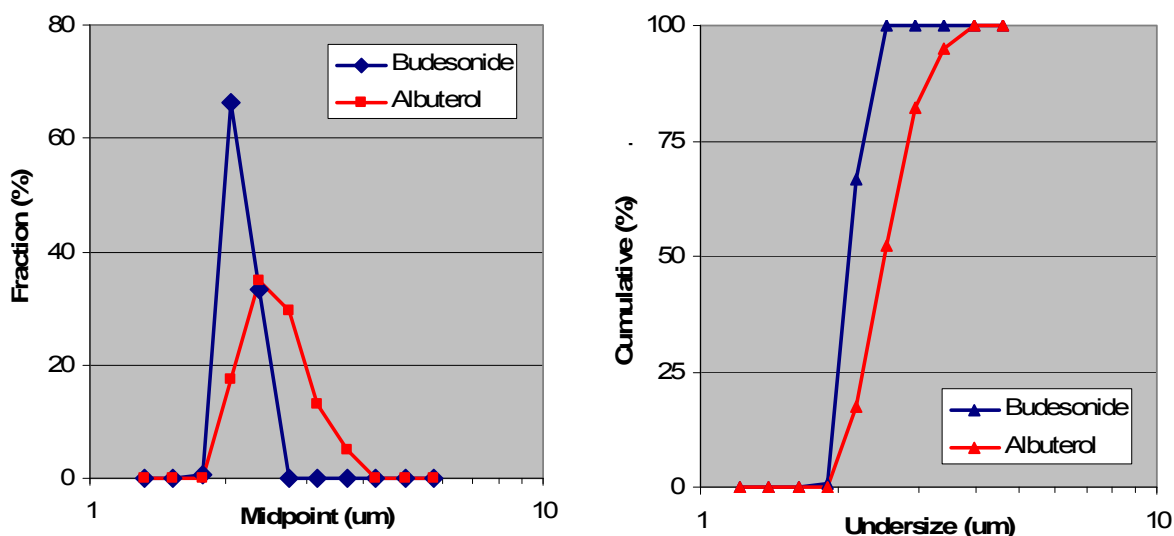


**Figure 2.1.** Particle size distribution of budesonide (blue) and albuterol (red). Figure 2.1(a) shows the fraction of drug recovered on the midpoint of the given stage. Figure 2.1(b) shows the cumulative undersize at each interval.

The excipient sieve fractions showed particle size distributions that extended outside the range of the sieves. As described earlier, this result is expected for sieved non-spherical particles (i.e. particles with an aspect ratio greater than 1). The sieves classify particles based on their second largest dimension, while light scattering methods determine mean particle diameters based on the assumption of sphericity. As a result, particles with diameters outside the boundaries of the sieves show up in a given sieve fraction. This is shown for the case of CP in Figure 2.2, where the particle size distributions of the entire sample and the constituent sieve fractions are shown. The dashed lines indicate the sieve boundaries. It is also evident, that each of the distributions is bimodal with a sizable fraction of fine particles. This observation cannot be explained by the sieving process. Rather, it suggests there is a portion of ultra-fine particles (in the single micron range) which are associated with the surface of the larger particles. They do not dislodge during sieving but detach from the surfaces of the larger particles after suspension and stirring in liquid media. The observation of surface associated fine particles has been made before, and has been described in the literature.<sup>18</sup>

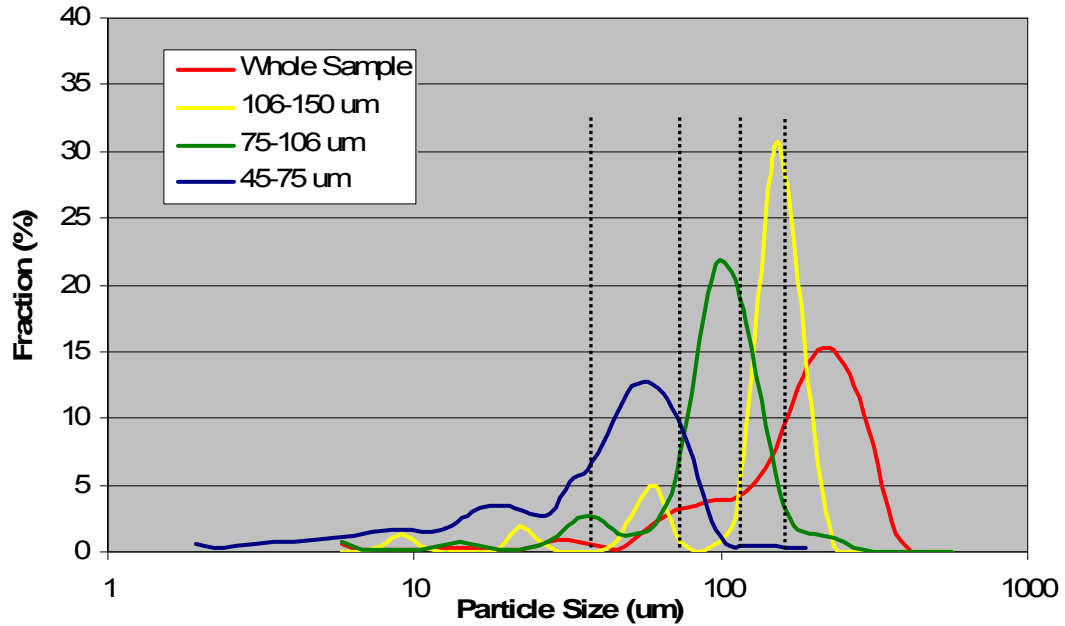


**Figure 2.2.** Particle size distribution of CP sample and the constituent sieve fractions after simple sieving, i.e. without additional fluidization. All samples clearly show the presence of very fine, single micron size particles. Dashed lines show the sieve fraction pore sizes.

Figure 2.2 also highlights the need for the additional processing step of "sifting" the sieve fractions. The result of this step is shown in Figure 2.3, for the same sieve fractions shown in Figure 2.2; clearly the presence of these fine particles has been greatly reduced.

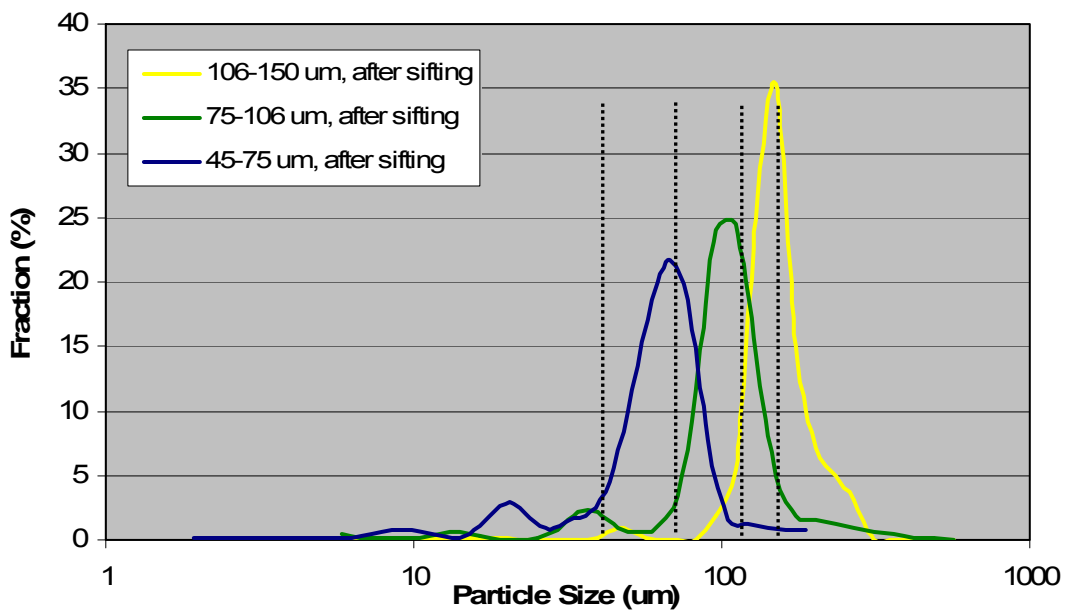


**Figure 2.3.** Particle size distribution of whole calcium phosphate sieve fractions after sieving and sifting. Compared to Figure 2.2, the proportion of fine particles is greatly reduced. Dashed lines show the sieve fraction pore sizes.

The behavior of other excipients with respect to sieve sizes was similar to that of CP, though it was somewhat less pronounced for lactose batches. The particle size distributions of the different sieve fractions are summarized by  $d_{10}$ ,  $d_{50}$ , and  $d_{90}$  values, span, and fraction of particles smaller than  $10\mu\text{m}$  in Table 2.3.

**Table 2.3.** Particle size distribution summary for the different excipient sieve fractions obtained (after sifting). Values are based on results from laser light diffraction experiments (average of  $n=3 \pm$  standard deviation). The  $d_{10}$ ,  $d_{50}$ , and  $d_{90}$  measures were determined through linear data interpolation, with no model assumptions.

Excipient	Excipient Sieve Fraction	$d_{10}$ ( $\mu\text{m}$ )	$d_{50}$ ( $\mu\text{m}$ )	$d_{90}$ ( $\mu\text{m}$ )	$d_{90} / d_{10}$	% < $10\mu\text{m}$
Calcium Phosphate	45-75 $\mu\text{m}$	44.9 $\pm$ 2.8	63.3 $\pm$ 1.9	80.5 $\pm$ 3.7	1.8 $\pm$ 0.2	1.4 $\pm$ 1.7
	75-105 $\mu\text{m}$	71.3 $\pm$ 8.6	102.2 $\pm$ 5.6	153.1 $\pm$ 8.4	2.2 $\pm$ 0.4	0.6 $\pm$ 0.4
	105-150 $\mu\text{m}$	115.8 $\pm$ 2.7	141.4 $\pm$ 3.0	183.5 $\pm$ 9.5	1.6 $\pm$ 0.1	0.0 $\pm$ 0.1
Glucose	45-75 $\mu\text{m}$	37.9 $\pm$ 6.3	73.7 $\pm$ 4.8	115.4 $\pm$ 1.8	3.1 $\pm$ 0.5	2.2 $\pm$ 0.4
	75-105 $\mu\text{m}$	78.8 $\pm$ 3.8	124.5 $\pm$ 4.0	199.4 $\pm$ 4.0	2.5 $\pm$ 0.1	1.2 $\pm$ 0.2
	105-150 $\mu\text{m}$	110.2 $\pm$ 1.2	181.4 $\pm$ 3.0	316.3 $\pm$ 18.9	2.9 $\pm$ 0.2	0.8 $\pm$ 0.0
Lactose ML80	45-75 $\mu\text{m}$	43.0 $\pm$ 1.3	64.3 $\pm$ 4.8	84.0 $\pm$ 6.9	2.0 $\pm$ 0.1	2.0 $\pm$ 0.2
	75-105 $\mu\text{m}$	82.8 $\pm$ 9.4	116.0 $\pm$ 5.4	165.5 $\pm$ 16.7	2.0 $\pm$ 0.0	1.2 $\pm$ 0.3
	105-150 $\mu\text{m}$	121.8 $\pm$ 2.0	167.9 $\pm$ 4.4	248.0 $\pm$ 15.8	2.0 $\pm$ 0.1	0.7 $\pm$ 0.1
Lactose ML58	45-75 $\mu\text{m}$	45.0 $\pm$ 0.7	63.6 $\pm$ 3.2	86.6 $\pm$ 13.6	1.9 $\pm$ 0.3	1.8 $\pm$ 0.2
	75-105 $\mu\text{m}$	84.8 $\pm$ 7.5	116.9 $\pm$ 5.8	172.9 $\pm$ 3.7	2.0 $\pm$ 0.2	1.0 $\pm$ 0.2
	105-150 $\mu\text{m}$	123.5 $\pm$ 1.2	170.7 $\pm$ 3.7	258.0 $\pm$ 14.0	2.1 $\pm$ 0.1	0.4 $\pm$ 0.3
Lactose SV425	45-75 $\mu\text{m}$	44.8 $\pm$ 0.1	66.1 $\pm$ 3.9	85.0 $\pm$ 6.5	1.9 $\pm$ 0.1	1.5 $\pm$ 0.3
Lactose SV94	45-75 $\mu\text{m}$	47.3 $\pm$ 2.1	71.1 $\pm$ 4.8	97.9 $\pm$ 12.5	2.1 $\pm$ 0.2	1.4 $\pm$ 0.2

#### 2.4.2. Size and Shape Characterization of Powders

SEM micrographs were obtained to: (1) ascertain that drug particles and excipients sieve fractions were in fact of the right particle size and thus independently verify the results of the laser light scattering experiments; (2) assess the results of the excipients fines removal procedure; and (3) assess the distribution of drug within the formulation blends. Figure 2.4 shows high magnification (5000x) images of micronized albuterol and budesonide. The particles appear to be in the required single micron range, which is consistent with the laser diffraction light scattering experiments. Albuterol had

a more disperse particle size distribution; particles from 1 to 5 $\mu\text{m}$  in size are visible in the micrographs. Budesonide is more uniformly distributed; particles have regular, approximately spherical shapes, and are in the 1-2 $\mu\text{m}$  range. These results are also consistent with laser diffraction light scattering.

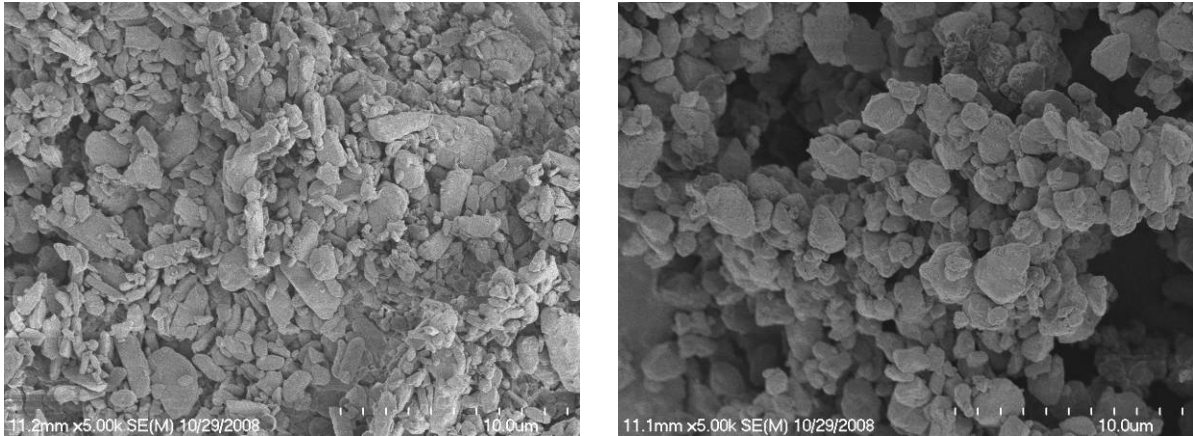
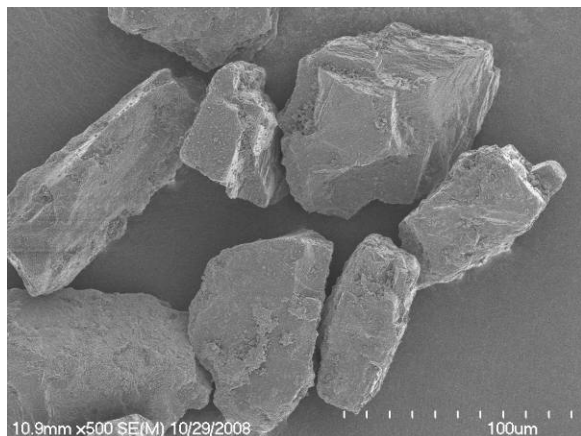
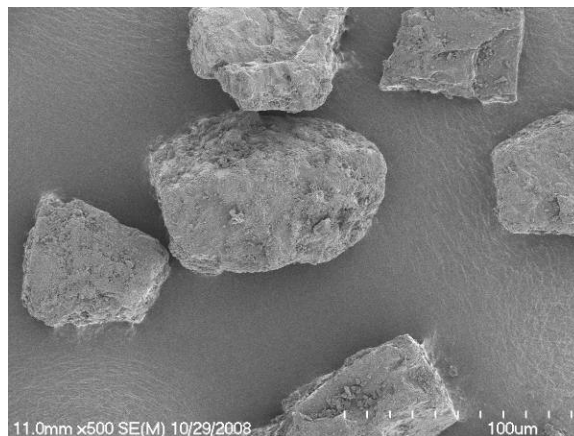


**Figure 2.4** Micronized drug particles at 5000x magnification. (a) Albuterol sulfate, (b) budesonide.

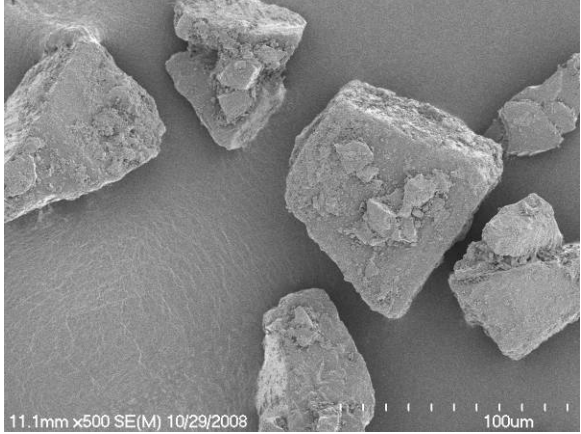
Figures 2.5(a) through (f) show the 45-75 $\mu\text{m}$  sieve fraction for each excipient at 500x magnification. Lactose particles display the characteristic tomahawk shape, glucose particles appear as flakes, while CP appears granular. These observations are consistent with what is known of the excipients. Compared to other SEM images of the same lactose excipients,<sup>18</sup> the fluidization procedure shows some success in removing surface associated fines. However, higher magnification images of lactose particles, SV94 shown in Figure 2.6, show the presence of some surface fines which might account for the approximately 1% of single-micron particles observed in most batches during laser light scattering experiments (shown in Table 2.3).



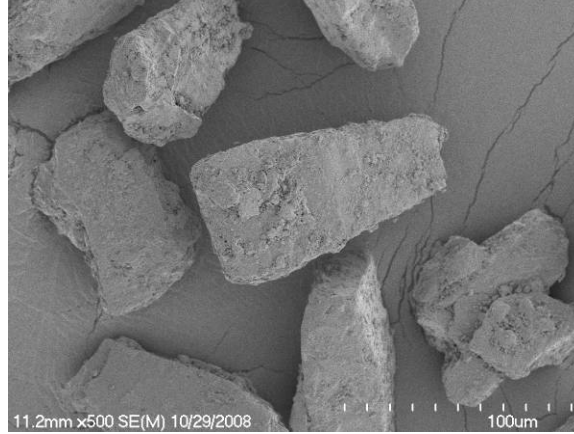
**(a)** ML80 lactose particles (45-75µm sieve fraction).



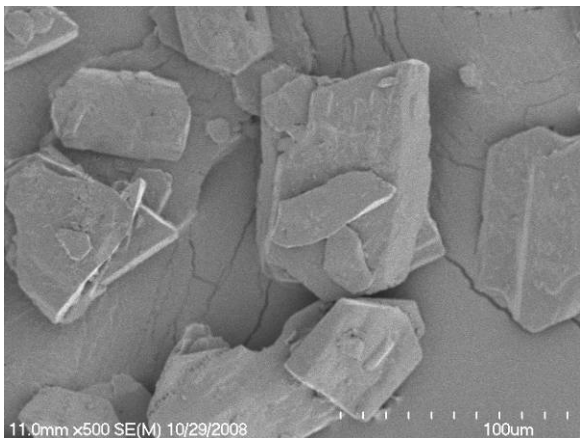
**(b)** ML58 lactose particles (45-75µm sieve fraction).



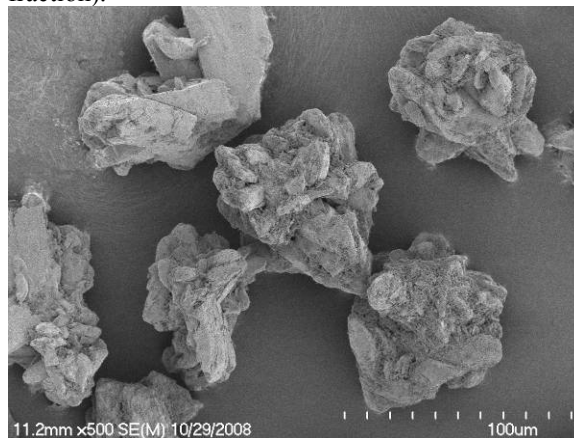
**(c)** SV94 lactose particles (45-75µm sieve fraction).



**(d)** SV 425 lactose particles (45-75µm sieve fraction).



**(e)** Glucose particles (45-75µm sieve fraction).



**(f)** CP particles (45-75µm sieve fraction).

**Figure 2.5.** Electron micrographs showing the 45-75µm sieve cut, each at a magnification of 500x.

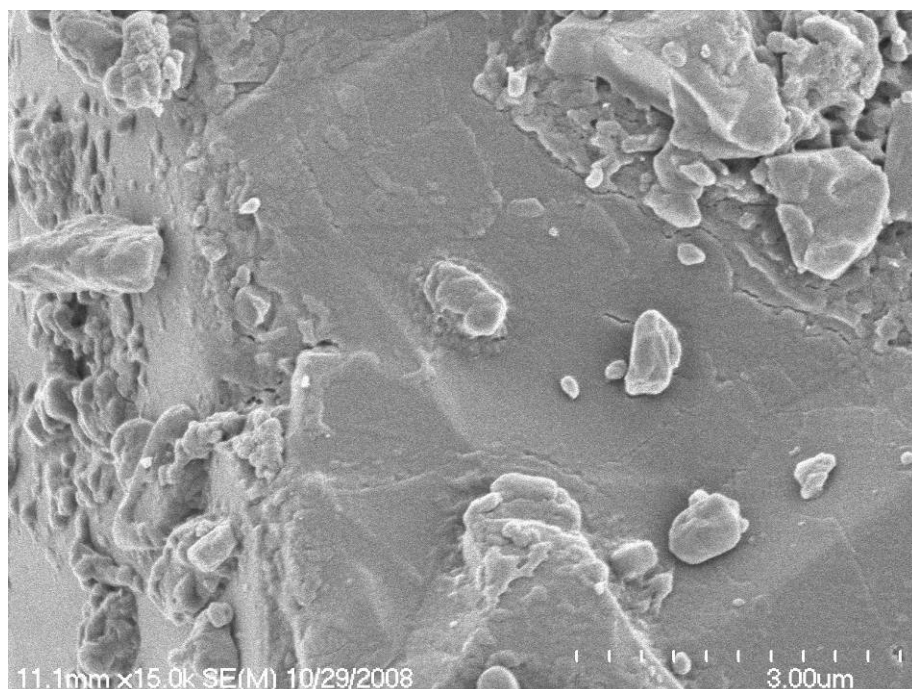


**Figure 2.6.** Lactose SV94 particles at 15,000x magnification. Fine particles in the single micron range are present at the particle surface.

In addition to a chemical assessment of formulation drug content uniformity (via UV assay), a number of blends were visually inspected by SEM for the presence of unique particle distribution patterns; none were noted. As shown in Figure 2.7, drug distribution across the surface of particles was uniform although distribution of drug across the population of different particles varied, i.e some excipient particles had a lot of drug on their surface, while other particles had little.

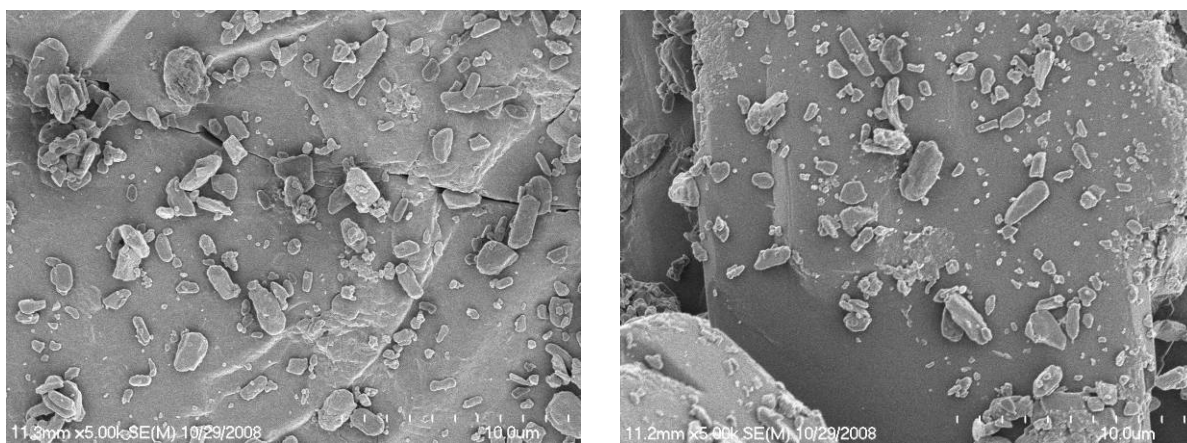


**Figure 2.7.** Representative drug blends. (a) 1% albuterol on ML58 lactose particles (b) 0.5% Budesonide on CP particles. Drug was quite evenly distributed.

### 2.4.3. Differential Scanning Calorimetry

The results of the thermal analysis of the drugs are shown in Figure 2.8. The DSC thermogram of the micronized budesonide showed a single endothermic melting transition at 256°C, which is in agreement with values reported in the literature.<sup>6, 19</sup> Various melting temperatures and thermograms can be found in the literature for albuterol sulfate. The manufacturer reports the melting point as 230-235°C,<sup>1</sup> so initially, albuterol sulfate was scanned to a temperature of 250°C which should have revealed this melting point. Instead, the thermogram revealed a sharp mixed endo/exo/endothermic event with a maximum endothermic peak at 206°C. This also contradicted other published results, e.g. a melting temperature of 185-195°C described by El Fattah et al.<sup>20</sup> Another sample of albuterol sulfate was scanned to a temperature of 400°C. This revealed two further endothermic peaks at 286 and 329°C, in agreement with observations made by Larhrib et al.<sup>21</sup> The explanation for the thermogram was recently provided by Palacio et al.; albuterol exists as two polymorphs, and the peaks show a decomposition pathway for the more stable Form I.<sup>22</sup>

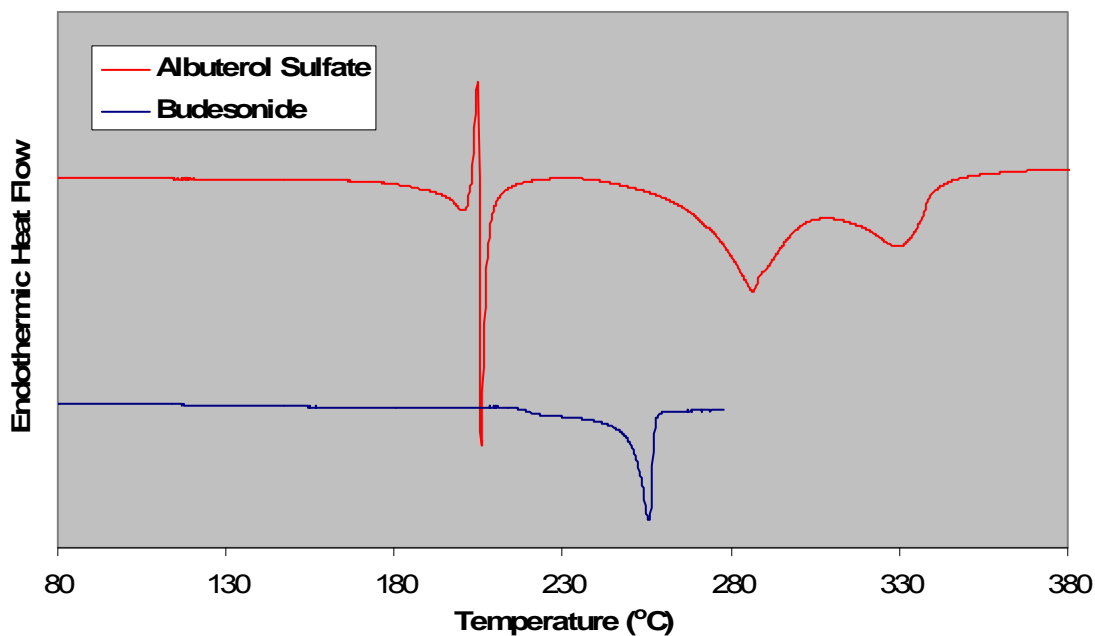


**Figure 2.8.** DSC thermograms of albuterol sulfate and budesonide used in formulations.

The DSC thermograms of the excipients are presented in Figure 2.9. All materials had thermal events as expected. Glucose monohydrate melts at 80°C. Slight curvature in the thermogram at 115°C



indicates the presence of some anhydrous glucose. Lactose monohydrate shows two endothermic events: the first endothermic transition corresponds to the loss of water of crystallization while the second transition shows the melting of the anhydrous material followed by its decomposition. These thermograms are in agreement with published data, e.g. Larhrib et al.<sup>21</sup> CP was scanned to 450°C, which is the highest temperature attainable on the DSC instrument used; as expected decomposition was observed at 425°C, which constituted the only thermal event. This is in agreement with Miyazaki et al., which have recently described the physical properties of dibasic calcium phosphate anhydrate and dehydrate.<sup>23</sup>

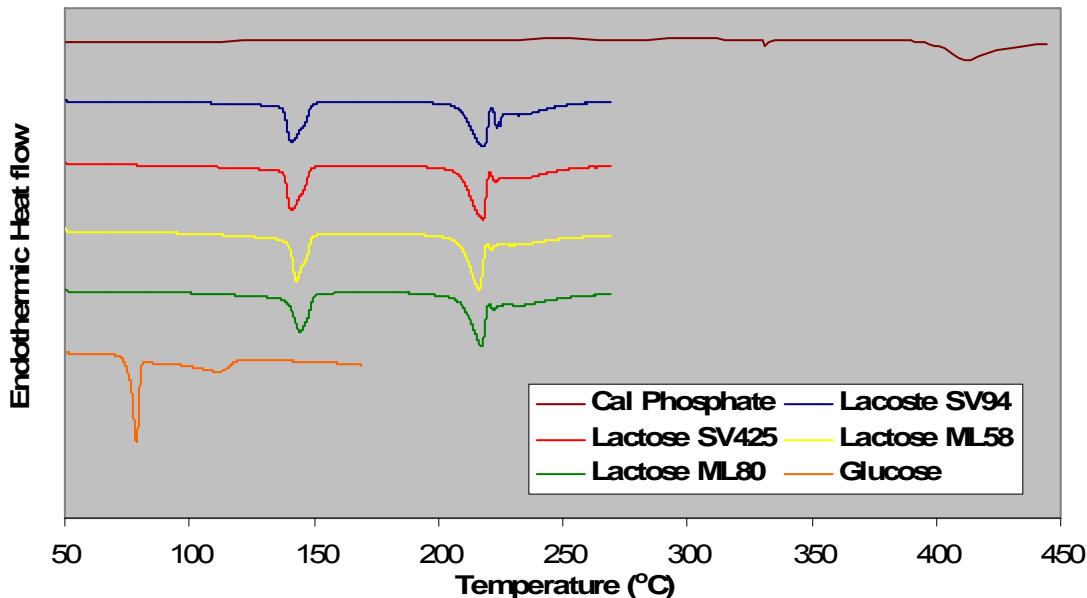


**Figure 2.9.** DSC thermograms of lactose ML58, ML80, SV94, SV425, and glucose. Samples were scanned at 5°C/min from 50°C to 250°C.

#### 2.4.4. Electrostatic Material Characterization

All materials, drugs and all excipient sieve fractions, were evaluated for their electrostatic properties. Experiments were randomized and conducted in triplicates (n=3) at 23°C/24%RH. Significant differences were observed in the charging behavior of drugs and excipients. Figure 2.10 summarizes the findings. Both CP and glucose consistently delivered a negative charge, in both cases in the order of -0.2 – -0.3 nC/g. By contrast, all lactose batches delivered positive charges to the

Faraday well, in the order of 0.4-0.6nC/g. While some differences between the lactose batches were noted, they were comparatively small and statistically insignificant. The micronized drugs showed the largest charges, whereby albuterol charged highly positive and budesonide charged highly negative. There were no significant differences between the size fractions of the excipients, except for ML58 lactose, where the finer sieve fractions delivered larger charges.

Since contact with the insulating paper was brief and affected only a small number of particles, the charges recorded are the result mostly of contact with the glass bottles, in which the formulations were stored. Thus, the charges are a relative measure of the effective work functions of the bulk materials; the negatively charged particles have acquired an excess of electrons from their environment; thus they have higher work functions than the positively charged materials which have given up their electrons.

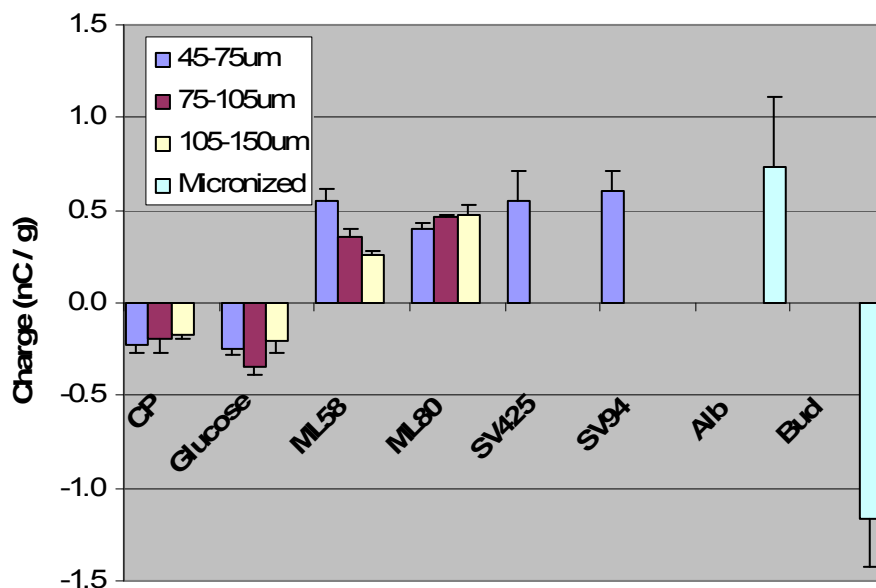


**Figure 2.10.** Electrostatic charge recorded after deposition of the powders in the Faraday well. Experiments were randomized and performed at a 23°C/24%RH ambient conditions. Averages of n=3 experiments with standard deviations in the error bar are shown.

Measurements were repeated for 45-75µm sieve fraction excipients at higher RH conditions (23°C, 37%RH). The same trend was observed at the higher RH conditions, with both CP and glucose

charging negative, and the lactose batches charging positive; the rank-order was even preserved among the lactose batches.

The results of the Faraday well experiments lend themselves to the creation of a triboelectric series. The series are presented, with the recorded charges, for different excipient fractions in Table 2.4.

**Tables 2.4.** Triboelectric series, by excipient sieve fraction, from most negative charge (left) to most positive charge (on right). Note that rank order is preserved across every sieve fraction.

Particle Size	----- Q (nC/g) -----							
	Budesonide	Glucose	CP	ML80	ML58	SV425	SV94	Albuterol
<b>Micronized</b>	-1.169 ± 0.260	-	-	<b>0±0</b>	-	-	-	+0.736 ± 0.378
<b>45 - 75µm</b>	-	-0.252 ± 0.025	-0.230 ± 0.043	<b>0±0</b>	+0.403 ± 0.031	+0.551 ± 0.061	+0.556 ± 0.161	+0.601 ± 0.107
<b>75-105µm</b>	-	-0.352 ± 0.049	-0.197 ± 0.070	<b>0±0</b>	+0.352 ± 0.049	+0.459 ± 0.015	-	-
<b>105 - 150µm</b>	-	-0.206 ± 0.060	-0.172 ± 0.019	<b>0±0</b>	+0.263 ± 0.015	+0.470 ± 0.059	-	-

While variability in the behavior clearly occurs, the results of the Faraday well experiments are highly consistent in a rank-order across the different sieve cuts. Assuming the sieved lactose batches were available in other larger sizes and fell into the same pattern, one general triboelectric series can be constructed as follows:

- Budesonide << Glucose ≤ CP < Paper/Glass < ML80 < ML58 < SV425 < SV94 < Albuterol +

Based on this series, we expect the strongest particle interactions to occur between albuterol and glucose as well as budesonide and SV94 lactose.

A number of drug/ excipient blends were also evaluated with the Faraday well method. The presence of drug, budesonide or albuterol, did not have a consistent effect on the bulk powder charging properties. This is not surprising as the drug content in the formulations is at or below 1% in all formulations.

## 2.5. Summary

The drugs and excipients in this study were carefully selected based on their relevance to respiratory drug delivery. Albuterol and budesonide are representatives of two important therapeutic categories,  $\beta_2$ -receptor adrenergic agonists and glucocorticosteroids, respectively. Lactose monohydrate and glucose are the sole DPI excipients in use. Calcium phosphate is a physiological salt that offers a useful contrast. The drugs were micronized and their particle size was independently confirmed using laser light scattering and scanning electron microscopy. To control for particle size effects that might confound later analysis, excipients were sieved into three sieve fractions. To aid the removal of surface-associated fines, excipients underwent fluidization procedures. Particle size and shape were verified by laser diffraction light scattering and scanning electron microscopy. The polymorphic makeup of the drugs and excipients was ascertained using differential scanning calorimetry. Excipients and drugs were combined in formulations by small-scale blending procedures. The blends were assayed for content uniformity and distribution of drug was assessed using SEM. The electrostatic properties of the materials were then characterized in Faraday well experiments and a triboelectric series was created. The triboelectric series follows the order (from most negative to most positive charge): Budesonide < glucose < calcium phosphate < milled lactose < sieved lactose < albuterol. Although the charging behavior was variable and the differences between the excipients were small, the charge behavior, in particular the rank-order, was preserved even as the experiments were repeated at different environmental conditions (higher RH).

Knowing the triboelectric series is of limited utility. However, the series will be helpful in determining the charging behavior of drug after release from the DPI formulation. This in turn will help test the hypothesis that aerosol charging is the result of contact charging between drug and excipient within the formulation. Based on the established triboelectric series, we can predict that albuterol will be most highly, positively charged when it is formulated with glucose and/or calcium phosphate and will be least positively charged when combined with sieved lactose. It is postulated that the reverse will be demonstrated with budesonide.

While the triboelectric series offers a chance to establish a causal relationship it does not explain why materials may behave one way or another. This question will be addressed in the next chapter after material characterization using inverse gas chromatography. Chapter 4 then presents the DPI actuation and deposition studies, in which the electrostatic properties of aerosolized drugs are probed.

## **2.6. Acknowledgements**

Colin McKinney, electronics designer and facility manager at the Dept of Chemistry Electronics Facility at UNC is gratefully acknowledged for building the Faraday well.

## 2.7. Literature Cited

1. Physicians' desk reference (Thomson PDR, Montvale, NJ, 2004).
2. Dougall, I. G., Harper, D., Jackson, D. M. & Leff, P. Estimation of the efficacy and affinity of the beta 2-adrenoceptor agonist salmeterol in guinea-pig trachea. *Br J Pharmacol* 104, 1057-61 (1991).
3. Kasprzyk-Hordern, B., Dinsdale, R. M. & Guwy, A. J. Multi-residue method for the determination of basic/neutral pharmaceuticals and illicit drugs in surface water by solid-phase extraction and ultra performance liquid chromatography-positive electrospray ionisation tandem mass spectrometry. *J Chromatogr A* 1161, 132-45 (2007).
4. Convention, U. S. P. The Pharmacopoeia of the United States of America (United States Pharmacopoeial Convention, Bethesda, MD, 2005).
5. Windholz, M., Budavari, S. & Merck & Co. The Merck index : an encyclopedia of chemicals, drugs, and biologicals (Merck & Co., Rahway, N.J., 1983).
6. Velaga, S. P., Berger, R. & Carlfors, J. Supercritical fluids crystallization of budesonide and flunisolide. *Pharm Res* 19, 1564-71 (2002).
7. Jashnani, R. & Byron, P. B. Dry powder aerosol generation in different environments: performance comparisons of albuterol, albuterol sulfate, albuterol adipate and albuterol stearate. *Int J Pharm* 130, 13-24 (1996).
8. Lobo, J. M. et al. SCF-engineered powders for delivery of budesonide from passive DPI devices. *J Pharm Sci* 94, 2276-88 (2005).
9. Hickey, A. J., Mansour, H. M., Telko, M. J. & Xu, Z. Physical Characterization of Component Particles included in Dry Powder Inhalers - II. Dynamic characteristics. *J Pharm Sci* 96, In Press (2007).
10. Hickey, A. J., Mansour, H. M., Telko, M. J. & Xu, Z. Physical Characterization of Component Particles included in Dry Powder Inhalers - I. Strategy Review and Static Characteristics. *J Pharm Sci* 96, In Press (2007).
11. Steckel, H. & Bolzen, N. Alternative sugars as potential carriers for dry powder inhalations. *Int J Pharm* 270, 297-306 (2004).
12. Garcia-Contreras, L., Morcol, T., Bell, S. J. & Hickey, A. J. Evaluation of novel particles as pulmonary delivery systems for insulin in rats. *AAPS PharmSci* 5, E9 (2003).
13. Kibbe, A. H. & American Pharmaceutical Association. Handbook of pharmaceutical excipients (American Pharmaceutical Association, Washington, D.C., 2000).
14. Lerk, C. F. et al. Alterations of alpha-lactose during differential scanning calorimetry. *J Pharm Sci* 73, 856-7 (1984).
15. Byron, P. B., Peart, J. & Staniforth, J. N. Aerosol electrostatics I: Properties of fine powders before and after aerosolization by dry powder inhalers. *Pharm Res* 14, 698-705 (1997).

16. Chow, K. T., Zhu, K., Tan, R. B. & Heng, P. W. Investigation of Electrostatic Behavior of a Lactose Carrier for Dry Powder Inhalers. *Pharm Res* (2008).
17. Murtomaa, M., Strengell, S., Laine, E. & Bailey, A. Measurement of electrostatic charge of an aerosol using a grid-probe. *Journal of Electrostatics* 58, 197-207 (2003).
18. Hickey, A. J. et al. Physical characterization of component particles included in dry powder inhalers. I. Strategy review and static characteristics. *J Pharm Sci* 96, 1282-301 (2007).
19. Vozzone, C. & Cabral Marques, H. Complexation of Budesonide in Cyclodextrin and Particle Aerodynamic Characterization of the Complex Form for Dry Powder Inhalation. *J Inclusion Phenomena and Macrocyclic Chemistry* 44, 111-115 (2002).
20. el Fattah, E. A., Grant, D. J., Gabr, K. E. & Meshali, M. M. Physical characteristics and release behavior of salbutamol sulfate beads prepared with different ionic polysaccharides. *Drug Dev Ind Pharm* 24, 541-7 (1998).
21. Larhrib, H., Martin, G. P., Marriott, C. & Prime, D. The influence of carrier and drug morphology on drug delivery from dry powder formulations. *Int J Pharm* 257, 283-96 (2003).
22. Palacio, M. A., Cuffini, S., Badini, R., Karlsson, A. & Palacios, S. M. Solid-state characterization of two polymorphic forms of R-albuterol sulfate. *J Pharm Biomed Anal* 43, 1531-4 (2007).
23. Miyazaki, T., Sivaprakasam, K., Tantry, J. & Suryanarayanan, R. Physical characterization of dibasic calcium phosphate dihydrate and anhydrate. *J Pharm Sci* (2008).

### 3. SURFACE ENERGY MEASUREMENTS

#### 3.1. Introduction

A principal goal of this project is to elucidate the triboelectrification process between the constituent particles of a DPI formulation. Contact charging is well understood for conducting materials, such as metals, where it is the result of electron transfer between materials of differing work functions. A work function is the minimum energy needed to extract an electron from a material (more precisely, it is the energy necessary to remove electrons from Fermi level to infinity at 0 K). Contact charging is less well understood for nonconducting materials, including most drugs and excipients, which have unoccupied Fermi levels and, thus no work functions, yet clearly are subject to contact charging.

The current theory, first proposed four decades ago by Harper<sup>1</sup>, is that the presence of crystal lattice defects, adsorbed gases, and impurities on the insulator surface produces additional energy levels into which charge can move.<sup>2</sup> This leads to the concept of an "effective" work function<sup>3</sup> or "pseudo-work function",<sup>4</sup> which is a material surface property rather than an intensive bulk physicochemical property. Stated more specifically, for charge transfer to or from an insulator to occur, electron donor or acceptor sites need to be present at or near the surface of the material.<sup>4</sup>

The important role of the material surface to contact charging highlights the need for specific surface characterization techniques. Inverse gas chromatography (IGC) permits powder surfaces to be studied without prior treatment (e.g. compression, as required in contact angle measurements). IGC methodology has been developed for characterizing the surface's tendency to interact with adjacent molecules, and to act as either an electron acceptor (acid) or electron donor (base) in the process.



### 3.2. IGC Theory and Experimental Considerations

IGC is a technique for studying particulate or fibrous solids or films using gas chromatography (GC) principles. The technique was used extensively in the characterization of polymers and fibers<sup>5</sup> before being applied to pharmaceutical material characterization. IGC is an effective technique for determining surface energy and surface acid/base properties and for the study of surface area,<sup>6</sup> porosity,<sup>5</sup> polymorphism,<sup>7</sup> and a host of other physical properties. It has some important advantages over other methods, which make IGC especially suitable for pharmaceutical work: the technique can be performed with small quantities of material; it is non-destructive, versatile and inexpensive, as it can be conducted with a standard gas chromatograph. Use of IGC in this work is tied primarily to the determination of surface energy and surface acid/base properties.

Use of the IGC technique has been extensively reviewed elsewhere.<sup>8-11</sup> Briefly, the technique is based on interactions of gaseous probe molecules with stationary phase in packed column which give a characteristic net retention volume,  $V_N$ . When measured at infinite dilution (where probe-probe interactions are negligible),  $V_N$  can be related to free energy of adsorption, which in turn can be used to calculate other thermodynamic parameters.

#### 3.2.1. Surface Free Energy

Surface free energy is a critical determinant of particle adhesion, which is an important factor in the performance of several pharmaceutical systems, including DPI formulations. Surface free energy is due the Lifshitz-van der Waals (LW) forces and acid-base interactions.<sup>12</sup> The LW component of surface energy is primarily due to dispersion forces and may be considered an intrinsic material property. Acid-base interactions are considered “specific” as they are only evident when surfaces interact with other molecules. Following Fowkes’ reasoning that different phenomena contribute to intermolecular forces independently,<sup>13, 14</sup> surface energy can be represented as the sum of dispersive and nondispersive (specific) contributions as

$$\gamma_S = \gamma_S^{disp} + \gamma_S^{spec} \quad (3.1)$$

where  $\gamma_S$  stands for the total surface free energy of the solid,  $\gamma_S^{disp}$  designates the dispersive surface free energy, and  $\gamma_S^{spec}$  the specific surface energy. (Note that  $\gamma_S^{spec}$  is sometimes referred to as  $\gamma_S^{AB}$ ; given the above rationale, the parameters are interchangeable.) Equation 3.1 is analogous to equation 1.2, which gives work of adhesion as a sum of its constituents.

### 3.2.2 Dispersive and Specific Energy by Inverse Gas Chromatography

From IGC measurements at infinite dilution (i.e. zero surface coverage of the adsorbent), Gray et al.<sup>15, 16</sup> proposed a relationship between the dispersive component,  $\gamma_S^{disp}$ , and the retention volumes of a series of n-alkanes (which only interact through dispersive forces). Using the work of adhesion concept and the Fowkes relationship,<sup>13</sup> Schultz et al.<sup>17</sup> expanded on this approach and derived an equation between net retention volume,  $V_N$  and free energy of adsorption

$$-\Delta G_A = RT \ln(V_N) + C \quad (3.2)$$

$$= 2 \cdot N_A \cdot a \cdot \sqrt{\gamma_S^{disp}} \sqrt{\gamma_L^{disp}} + C \quad (3.3)$$

where  $N_A$  is Avogadro's number,  $a$  is the effective surface area of the probe molecule,  $\gamma_S^{disp}$  and  $\gamma_L^{disp}$  are dispersive free energies of interacting solid and probe, and  $C$  is a constant that depends on the chosen reference state. Given that effective surface area and  $\gamma_L^{disp}$  increase linearly for the homologous series of alkanes, a plot of  $RT \ln V_N$  versus  $2 \cdot N_A \cdot a \cdot \sqrt{\gamma_L^{disp}}$ , shown in Figure 3.1, yields a straight line with slope  $\sqrt{\gamma_S^{disp}}$ . The dispersive surface energy,  $\gamma_S^{disp}$ , is the square of the slope of this line.

The specific free energy is determined from the retention of polar probes. When  $RT \ln V_N$  is plotted versus  $2 \cdot N_A \cdot a \cdot \sqrt{\gamma_l^D}$  for a polar probe the distance of the point from the n-alkane line is the

specific free energy of adsorption,  $-\Delta G^{spec}$ , between the surface of the stationary phase and the respective probe (shown in Figure 3.1). Other methods of determining  $-\Delta G^{spec}$  from retention volumes have also been described and were shown to give equivalent results.<sup>18</sup>

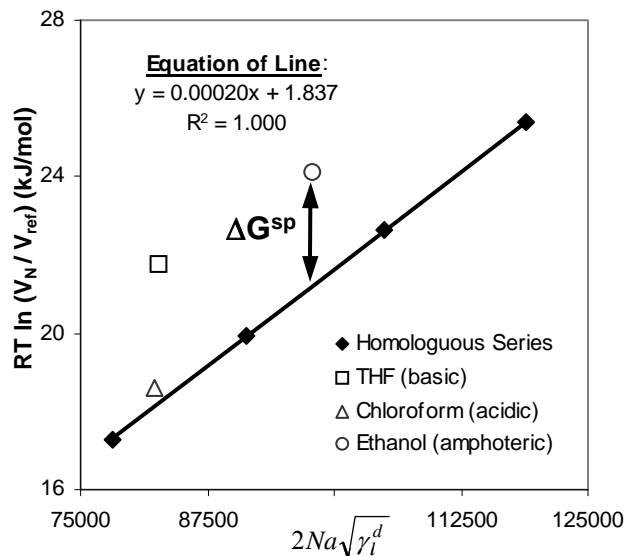


**Figure 3.1.** Plot used to determine the dispersive and specific surface energy of the solid,  $\gamma_s^d$  and  $\gamma_s^{sp}$ , respectively.

The specific free energies of different probes can be determined and correlated with the character of the interacting surface. This is most commonly done by way of the acid/base approach to molecular interactions,<sup>19</sup> based on which specific interactions are classified as either electron donor or acceptor type interactions. The approach allows the specific surface free energy values of any number of probes to be consolidated into two general parameters that characterize the tendency of the surface to act as an electron donor and acceptor. Donor and corrected acceptor numbers, DN and AN\*, have been determined for many different solvents; these values represent the ability of a probe to donate or accept electrons from reference acceptors and donors, respectively. Gutmann defined the DN as the molar enthalpy of a given substance with  $SbCl_5$ , a reference acid, in 1.0 mM dichloroethane solution ( $DN \equiv -\Delta H_{D \cdot SbCl_5}$ , kJ/mol).<sup>19</sup> AN\* was defined as the molar enthalpy of adduct formation of a substance with  $(CH_3CH_2)_3PO$ , a reference base ( $AN^* \equiv \Delta H_{A \cdot Et_3P=O}$ , kJ/mol).<sup>20</sup> This corrected the

initial AN definition by Gutmann.<sup>19</sup> Using said approach, the surface can be characterized by two constants related to the acid/base interactions via the equation

$$\Delta H_A^{sp} = K_A DN + K_B AN^* \quad (3.4)$$

where  $\Delta H_A^{sp}$  is the specific enthalpy of adsorption, and  $K_A$  and  $K_B$  are the acid (acceptor) and base (donor) parameters of the studied surface, respectively. Equation 3.4 is based on work to predict enthalpies of adduct formation<sup>21</sup> that was later extended to solid adsorption phenomena.<sup>17, 22</sup> It is a semi-empirical relationship, based on the observation that acid-base interactions are directly linked to changes in enthalpy. It was shown that heat of adsorption of basic probes onto an acidic surface can be accurately and quantitatively predicted based on acid/base parameters.<sup>23</sup> Since  $K_A$  and  $K_B$  of the absorbent are analogous to the DN and AN\* of the probes (which as shown are defined by enthalpy), they have the same reference.

Ticehurst et al.<sup>24</sup> and others<sup>8, 25-31</sup> have used an alternative expression based on surface free energy given by equation 3.5.

$$\Delta G_A^{sp} = K_A DN + K_B AN^* \quad (3.5)$$

The early literature stated that equation 3.5 is an approximation based on the assumption of negligible entropic effects. However, most subsequent papers no longer state this assumption, and in some cases erroneously cite the original Schultz et al. article as the source of this equation.

Use of equation 3.5 instead of 3.4 has important experimental consequences. Using equation 3.5 instead of 3.4 the experimenter can quickly determine  $K_A$  and  $K_B$  from one set of data at a single temperature, by plotting  $\Delta G_A^{sp} / AN^*$  versus  $DN/AN^*$  for a number of acidic and basic probes. By contrast, determination of  $K_A$  and  $K_B$  from equation 3.4 requires the IGC experiments to be repeated at several temperatures so that  $\Delta H_A^{sp}$  values can first be determined for the different probes from the intercept of the plot of  $\Delta G_A^{sp}$  versus temperature (by Gibb's equation). After that,  $K_A$  and  $K_B$  are determined from the slope and intercept of  $\Delta H_A^{sp} / AN^*$  versus  $DN/AN^*$  for the probes.

In preliminary work, the two approaches to characterizing surface acid/base interactions using IGC were compared and the validity of the assumptions behind equation 3.5 was evaluated.<sup>32</sup> Using the same set of data, the simplified approach (where  $\Delta G$  of adhesion is assumed to be equal to  $\Delta H$ ) that has been popular in the pharmaceutical literature was compared with a more rigorous approach for the determination of surface acid/base properties. While assuming  $\Delta G_A^{spec} \approx \Delta H_A^{spec}$  results in experimental simplification, it reduced the correlation since it depends strongly on method and experimental conditions. The values obtained were internally inconsistent and did not agree with those obtained in the rigorous analysis. This was an important result which justifies the rigorous approach applied in these studies. The study resulted in a publication,<sup>32</sup> which is included in Appendix B. This paper also provides a more detailed discussion of the methodology of the IGC approach.

### 3.3. Materials and Methods

#### 3.3.1. Materials

Two batches of milled (ML001, batches 10136780 and 10138058), and two batches of sieved (SV003, batches 10190094 and 10135425) Respitose™, lactose monohydrate, were selected for evaluation. (For convenience, the batches are referred to as ML80, ML58, SV94, and SV425, respectively.) Dextrose (D-glucose) monohydrate (batch KDTLT) Lycadex™, was provided by Roquette (Keokuk, IA). Calcium phosphate, Calipharm™ (powder grade) was obtained from Rhodia (Cranbury, NJ).

The IGC experiments utilized a number of apolar and polar probe vapors. The alkane probes used for dispersive free energy determination were hexane (>99%, Aldrich), heptane (>99%, Aldrich), octane (>99.5%, Fluka), nonane (>99%, Aldrich), and decane (>99%, Aldrich). Polar probes were chosen to cover a wide DN/AN\* range. The polar probes used were tetrahydrofuron (THF) (EM

Science, 99.99%), chloroform (100%, Mallinkrodt), acetone (99.7%, Mallinkrodt), ethyl acetate (99.9%, Mallinkrodt), diethyl ether (99%+, Acros), and ethanol (100%, Aaper).

### 3.3.2. Inverse Phase Gas Chromatography Methodology

IGC experiments were conducted with a Hewlett-Packard 5890 Series II GC with flame ionization detector. The chromatograph was modified to allow installation of 205mm, 4mm ID glass columns. Carrier gas employed was dry N<sub>2</sub> at a flowrate of 30mL/min. Lactose was packed into deactivated<sup>33</sup> glass columns and plugged with silanated glass wool. Corrections were made for pressure drop across column and temperature effects on flow rate. Injector and detector temperatures were set to 200°C to ensure immediate and complete probe evaporation and prevent eluted probe condensation at the detector. After installation and temperature changes, packed columns were allowed to equilibrate for at least 1 hour before subsequent injections were made. Injections were made with a 10µL-Hamilton syringe. Infinite dilution was ensured by detector response, detector signals below 10x limit of detection were permitted; this corresponds to injection volumes <0.01µL. The injection volumes were obtained by dipping the syringe needle briefly into the probe, and then waiting a few seconds for evaporation prior to injection. Each injection was made 2-3 times; the relative standard deviations in the retention times of these injections were <3% in each case. Each excipient was evaluated using three different packed columns. Since even inert probes can be somewhat retarded,<sup>34</sup> dead-times were calculated using a least squares approach involving the retention times of heptane, octane, nonane and decane.<sup>5</sup>

#### 3.3.2.1 Lactose Monohydrate

The oven temperatures used for analysis of the lactose samples were 60°C, 45°C, and 30°C, in that order. Previous experiments had shown that 60°C is the highest feasible temperature for analyzing lactose; prolonged exposure to higher temperatures can bring about polymorphic

transformations. The lowest temperature that can reliably be maintained in the GC oven without introducing an active cooling element is 26°C. However, operation at this temperature requires the oven door to remain opened, which creates air turbulence (generated by the oven fan) which in turn affects the stability of the FID signal. 30°C was chosen because it can be maintained in the GC oven with the oven door closed.

### 3.3.2.2 Glucose Monohydrate

An IGC method for glucose was required as all previous work had been conducted using lactose.  $\alpha$ -D-dextrose monohydrate is stable below 50°C, but may become anhydrous or form  $\beta$ -D-dextrose at higher temperatures.<sup>35</sup> As a result, in the initial experiments the oven temperatures for analysis were set to 48°C, 36°C, and 26°C, in that order to maximize the temperature range to obtain the most accurate  $\Delta H$  value recognizing that 26°C may result in some data variability.

### 3.3.2.3 Calcium Phosphate

In addition, the oven temperatures for calcium phosphate analysis required evaluation. Having a larger specific surface area than the other excipients ( $\sim 20\text{m}^2/\text{g}$ ) CP was expected to have longer retention times. Since the material is stable at higher temperatures, IGC experiments were performed at oven temperatures of 100°C, 80°C, and 60°C, in that order.

### 3.3.3. Differential Scanning Calorimetry

To assure that IGC experimental conditions did not induce physical instability, thermal analyses were performed on samples prior to and after the IGC experiment. Analyses were performed using DSC-6 (Perkin Elmer, Waltham, MA). Samples of 3 mg were enclosed in crimped aluminum pans and scanned across the relevant temperature ranges at a rate of 10°/min. (see Chapter 2 for details).

### 3.3.4. Data Analysis

Dead times, net retention times, and surface free energies at each temperature, and enthalpies were calculated in Excel 2003 (Microsoft Corp, Seattle, WA) in accordance with equations 3.1 through 3.3. Surface acid and base parameters,  $K_A$  and  $K_B$  respectively, were calculated using SPSS 16 (SPSS, Chicago, IL); enthalpy data for three columns was pooled and linear regression was performed. Results were plotted using Excel 2003. Differences between lactose batches were probed for statistical significance using the two-sample t-test for independent samples with unequal variances (Satterthwaite's method). Probe surface areas used in the analyses were obtained from Schultz et al.<sup>17</sup> Other properties, including surface tension, are readily available in chemistry handbooks.<sup>36</sup> Table 3.1 summarizes the relevant probe properties that were used in the calculations.

**Table 3.1.** Properties of IGC Probes, values used in all IGC calculations

<b>Probe</b>	<b>Molecular Surface Area (<math>\text{\AA}^2</math>)</b>	<b>DN (kJ/mol)</b>	<b>AN* (kJ/mol)</b>	<b>DN/AN*</b>	<b>Character</b>
n-Hexane	51.5	0	0		Neutral
n-Heptane	57.0	0	0		Neutral
n-Octane	62.8	0	0		Neutral
n-Nonane	68.9	0	0		Neutral
n-Decane	75.2	0	0		Neutral
THF	45	83.7	2.1	40.0	Base
Diethyl Ether	47	80.4	5.9	13.7	Base
Chloroform	44	0.0	22.6	0.0	Acid
Acetone	42.5	71.2	10.5	6.8	Amphoteric
Ethyl Acetate	48	71.6	6.3	11.4	Amphoteric
Methanol	42	83.7	50.2	1.7	Amphoteric
Ethanol	57	83.7	43.1	1.9	Amphoteric

Surface tension data as the relevant temperatures was obtained from CRC Handbook of Thermophysical and Thermochemical Data.<sup>36</sup>

## 3.4. Results and Discussion

### 3.4.1. Analysis of Lactose Monohydrate Batches

The dispersive surface free energies of the two ML and two SV batches were determined at 60, 45, and 30°C. Using DSC, the lactose samples were examined for physical changes after the IGC experiments but none were detected. While there do not appear to be any significant differences in the



dispersive surface free energies of the four batches at any of the temperatures, the milled and the sieved batches appear different when studied across the temperature range. This is evident in Figure 3.2. The slopes, which represent surface entropy, are larger for the sieved than the milled batches. As a result, higher surface enthalpies are obtained for the sieved than the milled lactose batches (106-110 mJ/m<sup>2</sup> versus 98-101 mJ/m<sup>2</sup>).

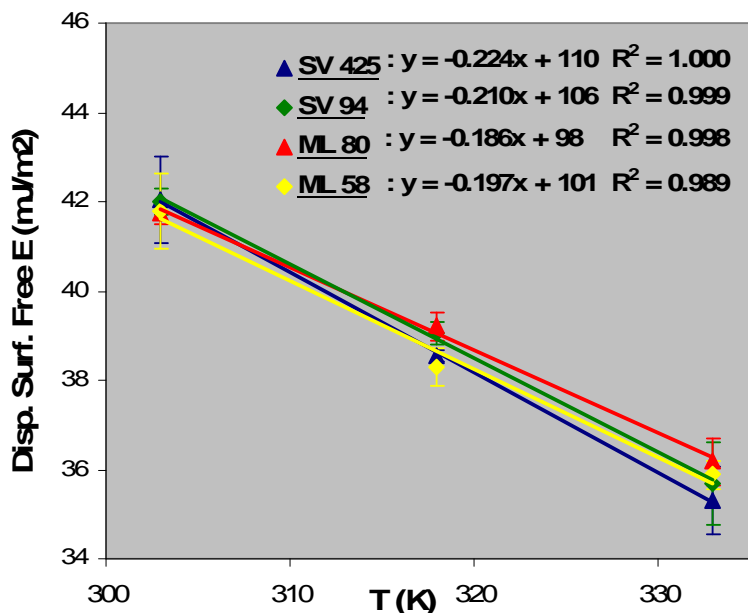


**Figure 3.2.** Dispersive surface free energies of sieved and milled lactose monohydrate vs. temperature. Relative standard deviation was < 2.5% in each case (n=4). While there are no statistically significant differences in dispersive surface free energy at any of the temperatures, the slope of the ML lactose batches (dashed lines) appears different from the two SV batches, resulting in lower slopes (entropy) and lower intercepts (enthalpy).

Examination of the specific interactions reveals differences between the milled and the sieved batches, and among the two sieved and two milled batches. These differences are presented in Table 3.2. In general, the batches appear to be quite similar, which is expected given that they are the same material from a single manufacturer (DMV-Fonterra). Since  $K_A$  and  $K_B$  values are unitless, differences between  $K_A$  and  $K_B$  for a material cannot be interpreted directly as signifying a more acidic or more basic surface. However, comparing  $K_A$  and  $K_B$  for different batches and materials allows these comparisons to be made. Lactose is known to be an acidic material and the differences in acidic parameter are small but significant as the sieved batches are similar to one another (0.146) but

differ from the milled batches (0.156 and 0.167). The differences in  $K_A$  between milled and sieved lactose batches are statistically significant ( $p < 0.05$ ). The differences in  $K_B$  are marked and indicative of material variations. Since lactose is an acidic material, the differences in  $K_B$  are likely tied to surface properties, perhaps the presence of impurities or certain crystal faces at the surface. However, due to the variability in this parameter, these differences lack statistical significance.

**Table 3.2.** Surface acid/base parameters of lactose monohydrate batches, SV and ML (mean  $\pm$  standard error of  $n \geq 3$  experiments) with corresponding square of correlation coefficient. The milled batches differ from the sieved batches in  $K_A$ ; they have more acidic surface. Sieved and milled batches differ from one another in  $K_B$  though variability in this parameter is high.

<b>Lactose Batch</b>	<b><math>K_A</math></b>	<b><math>K_B</math></b>	<b><math>R^2</math></b>	<b><math>K_A / K_B</math></b>
<b><u>SV</u></b>				
<b>094</b>	0.146 $\pm$ 0.006	0.419 $\pm$ 0.104	0.964	0.35
<b>425</b>	0.146 $\pm$ 0.003	0.357 $\pm$ 0.052	0.990	0.41
<b><u>ML</u></b>				
<b>58</b>	0.167 $\pm$ 0.003	0.374 $\pm$ 0.053	0.995	0.45
<b>80</b>	0.156 $\pm$ 0.004	0.311 $\pm$ 0.061	0.990	0.50

#### 3.4.2. Analysis of Glucose Monohydrate

A number of experimental IGC conditions were evaluated to determine the procedure best-suited for characterizing the surface energy of glucose. Initial experiments were performed at a maximum temperature of 48°C, below the temperature of 50°C at which polymorph instability may arise. Yet DSC experiments at the conclusion of the IGC experiment indicated that the material had been completely dehydrated and had formed anhydrous  $\beta$ -D-dextrose which has a melting temperature of 148-155°C (endotherm peak recorded at 151°C). This is shown in Figure 3.3. Experiments were repeated with 36°C as the highest temperature, but these conditions also resulted in dehydration of glucose monohydrate (though no  $\beta$ -D-dextrose formation); the melting endotherm characteristic of anhydrous glucose is observed at 146°C in Figure 3.3. Dehydration was so rapid, it could be observed during the experiments; changes in retention time of a given probe were noted in as little as ten minutes. Experiments were repeated with the injector temperature lowered to 50°C; dehydration of

the material persisted though the rate decreased. IGC measurements at 26°C with the injection temperature lowered to 50°C did not result in physical instability, but constitute a single temperature reading, which precludes determination of the surface enthalpy. As a result,  $K_A$  and  $K_B$  could not be determined using the conventional approach based on equation 3.4. Instead, the evaluation of the surface acid/base properties of glucose monohydrate is based on a single temperature setting and is qualitative in nature.

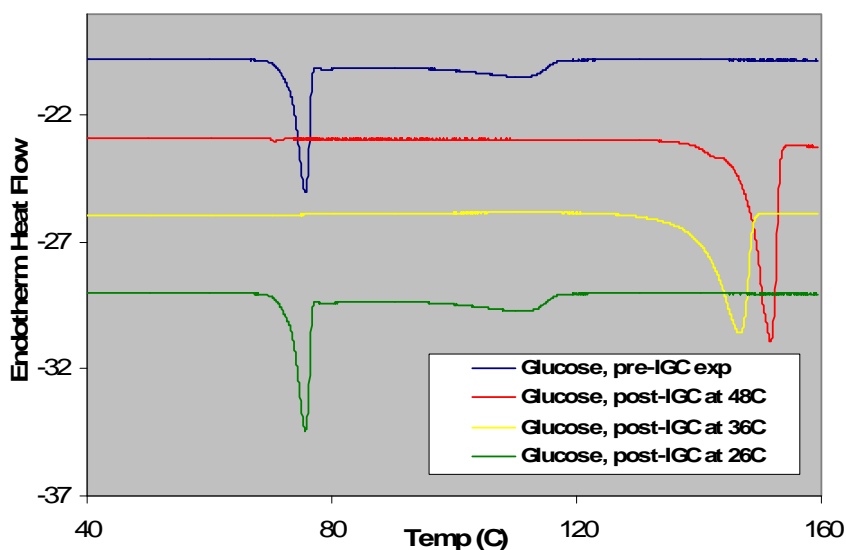


**Figure 3.3.** Thermogram of glucose monohydrate before (blue) and after (blue) the IGC experiment. Prolonged exposure of glucose monohydrate packed into IGC column at 48°C results in dehydration and formation of  $\beta$ -D-dextrose. Prolonged exposure of glucose monohydrate at 36°C results in dehydration of the material. Glucose monohydrate has a melting point of  $\sim 80^\circ\text{C}$ , glucose anhydrate melts at  $\sim 145^\circ\text{C}$ , while  $\beta$ -glucose melts at  $\sim 150^\circ\text{C}$ .

At 26°C, glucose monohydrate has a dispersive surface free energy of  $38.1 \pm 0.4 \text{ mJ/m}^2$ ; this value is approximately 10% lower than that of the lactose monohydrate batches. Table 3.3 summarizes the specific surface free energies of glucose monohydrate at 26°C compared to milled lactose monohydrate batch ML58, which had previously been determined using the same IGC method. Dispersive effects have been accounted for and have been subtracted; the specific free energy values listed account solely for specific interactions between the excipient and the given probes. The probes are listed along with their acidic/basic properties (DN/AN\* numbers). Comparing the values

of glucose and ML58 lactose, we can see that glucose has weaker interactions with the acidic chloroform probe but stronger interactions with the amphoteric and basic probes. This suggests that the glucose surface is itself more acidic or electron-accepting compared to lactose. Assuming the entropic contribution to the free energy were approximately the same for lactose and glucose, the results would imply higher  $K_A$  and lower  $K_B$  values for glucose than for this lactose batch.

**Table 3.3.** Specific surface free energies (average  $\pm$  standard deviation of n=3 columns) of adsorption between glucose monohydrate and the vapor probes listed in the table.

Probe (DN / AN*, kJ/mol)	$\Delta G_{sp}$ (kJ/mol)					
	Chloroform (0.0 / 22.6) Acidic	Methanol (83.7 / 50.2) Amphoteric	Ethanol (83.7 / 43.1) Amphoteric	Acetone (71.2 / 10.5) Amphoteric	Ethyl Ac. (71.6 / 6.3) Amphoteric	THF (83.7 / 2.1) Basic
<b>Glucose monohydrate</b>	0.28 $\pm$ 0.07	8.13 $\pm$ 0.38	5.40 $\pm$ 0.22	5.30 $\pm$ 0.12	5.94 $\pm$ 0.10	5.45 $\pm$ 0.09
<b>Lactose monohydrate ML58</b>	0.77 $\pm$ 0.02	6.16 $\pm$ 0.05	3.59 $\pm$ 0.02	3.81 $\pm$ 0.08	4.56 $\pm$ 0.05	3.87 $\pm$ 0.12

To estimate  $K_A$  and  $K_B$  numerically, equal entropic contribution was assumed and applied to the enthalpy of adsorption calculation of glucose. The entropic contribution to surface free energy of each lactose batch had already been estimated as part of the  $K_A$  and  $K_B$  calculation for the lactose batches. It was noted that the differences between the lactose batches were minor (max. difference was 20%) and the mean for all lactose batches and each probe was calculated.  $\Delta H^{sp}$  for each probe and glucose was then estimated, and  $K_A$  and  $K_B$  were calculated based on the  $\Delta H^{sp} / AN^*$  vs  $DN/AN^*$  best fit line. The parameter estimates were  $K_A = 0.18$  and  $K_B = 0.32$ , respectively, which does imply a more electron-withdrawing surface compared to lactose, recognizing that the differences are relatively minor.

### 3.4.3. Analysis of Anhydrous Calcium Phosphate

After preliminary studies to establish the IGC experimental conditions, the method described in section 3.3.2.3 was applied to the analysis of CP; IGC experiments, i.e. probe injections, were

performed at 100°C, 80°C, and 60°C. (The conditions that had been applied to lactose had resulted in extremely high retention times with severe peak spreading for all probes.) As shown in Figure 3.4, the dispersive surface free energies obtained varied from  $40.7 \pm 0.8 \text{ mJ/m}^2$  at 60°C to  $35.5 \pm 0.6 \text{ mJ/m}^2$  at 100°C. The 60°C free energy of  $40.7 \text{ mJ/m}^2$  is significantly higher than that of lactose, ca.  $36 \text{ mJ/m}^2$  across the different batches. Linear regression of the data provides the enthalpy of adsorption, approximately  $84 \text{ mJ/m}^2$ .

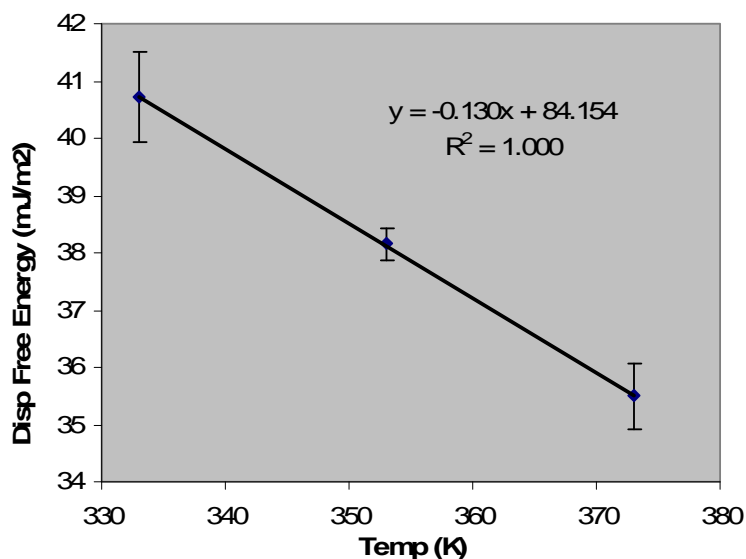


**Figure 3.4.** Dispersive surface free energy of calcium phosphate from 60°C to 100°C.

Injections of polar probes provided some unexpected results. While the injections of the n-alkane probes and chloroform resulted in the usual sharp chromatogram peaks, eluted after  $\leq 6$  minutes, all other polar probes did not elute at all. After the injections were repeated with increasing injection volumes (moving away from infinite dilution), extreme peak broadening, or rather solvent front development, were observed in the range of 10 minutes at 100°C to 40 minutes at 60°C. In each case the peak broadening was so severe, reliable and reproducible retention times could not be obtained, for either of the amphoteric or basic probes. Moreover, the condition of infinite dilution no longer applied to these chromatograms.

A survey of the literature did not provide any description, or explanation, of this observed retention behavior, with regard to calcium phosphate or other inorganic salts. Thus, the following explanation is proposed: The calcium phosphate material is highly acidic in nature and strongly interacts with the amphoteric and basic polar probes. Adsorption is clearly very strong resulting in extremely high retention times and severe dispersion and spreading. At low injection volumes, the spreading renders the concentrations at elution too low to be discerned from background effects.

The CP surface readily accepts electrons from the electron-donating probe vapors. Chloroform, on the other hand, which is an acidic probe with AN\* and DN of 22.6 and 0.0, respectively, does not interact strongly and is, thus, eluted after a short retention time. Specific free energies of adsorption were calculated for chloroform at each of the temperatures and an enthalpy of adsorption was thus obtained; it is  $4.8 \pm 0.2$  kJ/mol. Based on this one data point (albeit at the origin), the  $K_B$  was estimated from the y-intercept of the  $\Delta H_A^{sp} / \text{AN}^*$  versus  $\text{DN}/\text{AN}^*$  graph; it is  $0.213 \pm 0.007$ .  $K_A$  could not be determined but based on the very strong interactions of CP with the amphoteric and basic probes, it is clear that  $K_A$  is very high, higher than for either lactose monohydrate or glucose monohydrate. DSC performed on the CP samples prior to and after the IGC runs showed no differences, indicating no physical instability.

#### 3.4.4. Discussion

Physical adsorption, the principle of IGC, is a manifestation of interactions between molecules in the vapor probe and those in the solid surface.<sup>37</sup> The magnitude of the interactions is reflected in the adsorption processes, which in turn determine the retention times. While the IGC analysis did not result in  $K_A$  and  $K_B$  values for each surface studied, retention data provided sufficient information for a classification of the surface characteristics. The inability to generate  $K_A$  and  $K_B$  for glucose and  $K_A$  for CP was a result of experimental limitations due to the nature of the materials; it is not a failure of the technique or approach itself. The  $K_A$  and  $K_B$  data are summarized in Table 3.4.

**Table 3.4.** Summary of  $K_A$  and  $K_B$  data obtained in the IGC experiments.

<b>Excipient</b>	<b><math>K_A</math></b>	<b><math>K_B</math></b>
<b>Lactose SV094</b>	$0.146 \pm 0.006$	$0.419 \pm 0.104$
<b>Lactose SV425</b>	$0.146 \pm 0.003$	$0.357 \pm 0.052$
<b>Lactose ML 58</b>	$0.167 \pm 0.003$	$0.374 \pm 0.053$
<b>Lactose ML 80</b>	$0.156 \pm 0.004$	$0.311 \pm 0.061$
<b>Glucose monohydrate</b>	Higher than lactose	About the same as lactose
<b>Calcium Phosphate</b>	High	$0.213 \pm 0.007$

Based on these results, a rank-order correlation for the expected behavior of the excipient as either an electron donor or electron acceptor can be proposed. While the lack of precise data for calcium phosphate and glucose precludes an entirely quantitative comparison of the excipients, the results provide enough information to determine an ordinal, rank-order, comparison. Based on the results of the experiments, calcium phosphate, followed by glucose would be expected to act most electron withdrawing (acidic) in contact with other materials, such as drug. Based on  $K_A$  and  $K_B$ , sieved lactose (SV094, followed by SV425) is expected to be least electron-withdrawing and most electron donating. The following rank-order is thus given, from least to most electron withdrawing species:

$$SV094 < SV\ 425 < ML58 \approx ML80 < \text{Glucose} < \text{Calcium Phosphate}$$

If the surface acid / base properties are predictive of contact charging processes, drugs co-formulated with these respective excipients would be expected to charge in the following order:

$$\text{Negative drug charge} - SV094 < SV\ 425 < ML58 \approx ML80 < \text{Glucose} < \text{CP} - \text{Positive drug charge}$$

Note that this order is largely consistent with the order proposed based on Faraday well experiments at the conclusion of Chapter 2. The next chapter will demonstrate the charging of drugs when delivered from DPI formulations consisting of interactive blends with these excipients. The results of this chapter will be revisited in light of those findings.

### **3.5. Summary and Conclusion**

The IGC methodology was applied to the studied excipients, four batches of lactose monohydrate, glucose monohydrate, and anhydrous calcium phosphate. The technique was subject to several experimental limitations, most notably the physical instability of glucose monohydrate at elevated temperatures, and the extremely strong interactions of some probes with calcium phosphate. While these limitations have precluded a determination of all surface acid and base parameters for glucose and calcium phosphate, the experiments provided sufficient information to rank-order the excipient surfaces in their ability to act as electron donors or electron acceptors in physicochemical processes. The trend is in agreement with that proposed from Faraday well experiments in Chapter 2. The next chapter will demonstrate if the relationship is predictable of formulation behavior.

A principal goal of this project is to elucidate the triboelectrification process between the constituent particles of a DPI formulation. While Faraday well experiments in Chapter 2 provided a macroscopic view of bulk powder charging, and Chapter 4 will examine drug particle charging upon delivery from a DPI, this chapter has focused on the explanation of the charge transfer phenomenon by linking it with material surface properties. Inverse gas chromatography (IGC) permits the characterization of a surface's tendency to interact with adjacent molecules, and to act as either an electron acceptor (acid) or electron donor (base) in the process.

### **3.6. Acknowledgements**

Some of the discussion presented in the introduction is based on an article previously published in the Journal of Pharmaceutical Sciences; the publisher has granted me permission, as author, to use the material in any form.<sup>32</sup>



### 3.7. Literature Cited

1. Harper, W. R. Contact and frictional electrification (Oxford University Press, London, 1967).
2. Murtomaa, M., Harjunen, P., Mellin, V., Lehto, V. P. & Laine, E. Effect of amorphicity on the triboelectrification of lactose powder. *Journal of Electrostatics* 56, 103-110 (2002).
3. Castle, G. S. P. Contact charging between particles; some current understanding. Proc. ESA Annual Meeting on Electrostatics, 1-3 (2008).
4. Bailey, A. G. Charging of Solids and Powders. *Journal of Electrostatics* 30, 167-180 (1993).
5. Conder, J. R. & Young, C. L. Physicochemical measurement by gas chromatography (Wiley, Chichester ; New York, 1979).
6. Almazan-Almazan, M. C., Perez-Mendoza, M., Fernandez-Morales, I., Domingo-Garcia, M. & Lopez-Garzon, F. J. Use of specific surface areas in inverse gas chromatography studies at zero surface coverage. *Journal of Chromatography A* 1190, 271-277 (2008).
7. Tong, H. H., Shekunov, B. Y., York, P. & Chow, A. H. Influence of polymorphism on the surface energetics of salmeterol xinafoate crystallized from supercritical fluids. *Pharm Res* 19, 640-8 (2002).
8. Grimsey, I. M., Feeley, J. C. & York, P. Analysis of the surface energy of pharmaceutical powders by inverse gas chromatography. *Journal of Pharmaceutical Sciences* 91, 571-583 (2002).
9. AlSaigh, Z. Y. Review: Inverse gas chromatography for the characterization of polymer blends. *International Journal of Polymer Analysis and Characterization* 3, 249-291 (1997).
10. Bolvari, A. E., Ward, T. C., Koning, P. A. & Sheehy, D. P. in *Inverse gas chromatography : characterization of polymers and other materials* (eds. Lloyd, D. R., Ward, T. C. & Schreiber, H. P.) 12-19 (American Chemical Society, Washington, DC, 1989).
11. Lloyd, D. R. et al. *Inverse gas chromatography : characterization of polymers and other materials* (American Chemical Society, Washington, DC, 1989).
12. Sun, C. H. & Berg, J. C. A review of the different techniques for solid surface acid-base characterization. *Advances in Colloid and Interface Science* 105, 151-175 (2003).
13. Fowkes, F. M. Attractive forces at interfaces. *Ind. Eng. Chem.* 56, 40-52 (1964).
14. Fowkes, F. M. Determination of Interfacial Tensions, Contact Angles, and Dispersion Forces in Surfaces by Assuming Additivity of Intermolecular Interactions in Surfaces. *Journal of Physical Chemistry* 66, 382-& (1962).
15. Katz, S. & Gray, D. G. The Adsorption of Hydrocarbons on Cellophane .1. Zero Coverage Limit. *Journal of Colloid and Interface Science* 82, 318-325 (1981).

16. Dorris, G. M. & Gray, D. G. Adsorption of Normal-Alkanes at Zero Surface Coverage on Cellulose Paper and Wood Fibers. *Journal of Colloid and Interface Science* 77, 353-362 (1980).
17. Schultz, J., Lavielle, L. & Martin, C. The role of the interface in carbon fibre-epoxy composites. *J Adhesion* 23, 45-60 (1987).
18. Panzer, U. & Schreiber, H. P. On the Evaluation of Surface Interactions by Inverse Gas-Chromatography. *Macromolecules* 25, 3633-3637 (1992).
19. Gutmann, V. The donor-acceptor approach to molecular interactions (Plenum Press, New York, 1978).
20. Riddle, F. L. & Fowkes, F. M. Spectral Shifts in Acid-Base Chemistry .1. Vanderwaals Contributions to Acceptor Numbers. *Journal of the American Chemical Society* 112, 3259-3264 (1990).
21. Drago, R. S., Vogel, G. C. & Needham, T. E. 4-Parameter Equation for Predicting Enthalpies of Adduct Formation. *Journal of the American Chemical Society* 93, 6014-& (1971).
22. Fowkes, F. M. & Mostafa, M. A. Acid-Base Interactions in Polymer Adsorption. *Industrial & Engineering Chemistry Product Research and Development* 17, 3-7 (1978).
23. Joslin, S. T. & Fowkes, F. M. Surface-Acidity of Ferric Oxides Studied by Flow Microcalorimetry. *Industrial & Engineering Chemistry Product Research and Development* 24, 369-375 (1985).
24. Ticehurst, M. D., Rowe, R. C. & York, P. Determination of the surface properties of two batches of salbutamol sulphate by inverse gas chromatography. *Int J Pharm* 111, 241-249 (1994).
25. Feeley, J. C., York, P., Sumbly, B. S. & Dicks, H. Determination of surface properties and flow characteristics of salbutamol sulfate, before and after micronization. *Int J Pharm* 172, 89-96 (1998).
26. Ohta, M. & Buckton, G. The use of inverse gas chromatography to assess the acid-base contributions to surface energies of cefditoren pivoxil and methacrylate copolymers and possible links to instability. *International Journal of Pharmaceutics* 272, 121-128 (2004).
27. Ohta, M. & Buckton, G. Determination of the changes in surface energetics of cefditoren pivoxil as a consequence of processing induced disorder and equilibration to different relative humidities. *International Journal of Pharmaceutics* 269, 81-88 (2004).
28. Ohta, M. & Buckton, G. A study of the differences between two amorphous spray-dried samples of cefditoren pivoxil which exhibited different physical stabilities. *Int J Pharm* 289, 31-8 (2005).
29. Planinsek, O. & Buckton, G. Inverse gas chromatography: Considerations about appropriate use for amorphous and crystalline powders. *Journal of Pharmaceutical Sciences* 92, 1286-1294 (2003).

30. Planinsek, O. et al. Influence of inverse gas chromatography measurement conditions on surface energy parameters of lactose monohydrate. *International Journal of Pharmaceutics* 256, 17-23 (2003).
31. Traini, D., Rogueda, P., Young, P. & Price, R. Surface energy and interparticle forces correlations in model pMDI formulations. *Pharm Res* 22, 816-25 (2005).
32. Telko, M. J. & Hickey, A. J. Critical assessment of inverse gas chromatography as means of assessing surface free energy and acid-base interaction of pharmaceutical powders. *J Pharm Sci* 96, 2647-54 (2007).
33. Mohammad, H. A. H. & Fell, J. T. Contact Angles of Powder Mixtures Consisting of Spherical-Particles. *International Journal of Pharmaceutics* 11, 149-154 (1982).
34. Smith, R. J., Haken, J. K. & Wainwright, M. S. Evaluation of mathematical procedures for the calculation of dead-time. *J Chromatography* 147, 65-73 (1978).
35. Kibbe, A. H. & American Pharmaceutical Association. *Handbook of pharmaceutical excipients* (American Pharmaceutical Association, Washington, D.C., 2000).
36. Lide, D. R. & Kehiaian, H. V. *CRC Handbook of Thermophysical and Thermochemical Data* (CRC Press, Boca Raton, 1994).
37. Paryjczak, T. *Gas chromatography in adsorption and catalysis* (Ellis Horwood Limited, Chichester, 1986).

## **4. AERODYNAMIC AND ELECTROSTATIC PROPERTIES DETERMINED BY ELECTRICAL LOW PRESSURE IMPACTION**

### **4.1. Introduction**

DPI formulations and devices have characteristics that can give rise to surface charging, or triboelectrification, as described in Chapter 1. When the patient actuates a DPI the formulation is fluidized and dispersed; drug and carrier particles separate from each other. Charges can be transferred during this process resulting in net particle charges which may affect particle trajectory and deposition. Particles experience significant friction during DPI discharge which tends to amplify these effects.

Chapter 2 describes Faraday well experiments which provide the bulk material charging properties of the drugs and excipients. This chapter describes the aerodynamic and electrical property experiments required for elucidating the aerosol behavior of the formulation. Using the electrical low pressure impactor (ELPI), the experimental apparatus permits the simultaneous determination of particle size and charge distribution of the fine particle fraction of the emitted aerosol, which are important prerequisites for understanding formulation behavior and testing hypotheses 1, 2, and 4.

#### **4.1.1. The Electrical Low Pressure Impactor (ELPI<sup>TM</sup>)**

The experimental apparatus relies on the Electrical Low Pressure Impactor (ELPI<sup>TM</sup>, Dekati Ltd, Tampere, Finland), an aerodynamic particle sizer that detects particles by charge.<sup>1</sup> The ELPI has primarily been used in the automotive industry<sup>2-5</sup> and in industrial hygiene applications.<sup>6, 7</sup> Only recently has it been applied to the evaluation of electrostatic phenomena in medicinal aerosols, including MDIs<sup>8</sup> and DPIs<sup>9</sup>.

A detailed discussion of the ELPI is available elsewhere.<sup>10</sup> Briefly, the ELPI is composed of a low-pressure cascade impactor and a unipolar corona aerosol charger that charges the incoming aerosol uniformly prior to entry into the cascade impactor. Operating at a reduced pressure (10kPa on the final stage) the ELPI collects particles down to size of 30nm, the cutoff diameter of the bottom stage (stage 1). The cutoff diameters of the other 12 stages are 10.2, 6.56, 4.09, 2.52, 1.66, 1.02, 0.66, 0.41, 0.27, 0.17, 0.11, and 0.06 $\mu\text{m}$ , respectively. As is the case in other impactors, deposition inside the ELPI is dependent on particle aerodynamic diameter. But unlike conventional cascade impactors which are disassembled after operation for chemical or gravimetric assay of the stages, an ELPI detects particle deposition by measuring the current resulting from dissipation of the particles' electrical charges. The collected particles can be measured simultaneously on all stages using a multichannel electrometer and reported in real-time on a computer. Thus, when operated with charger turned on, the ELPI functions as a real-time particle sizer; this is the standard ELPI configuration and it is shown in Figure 4.1(a).

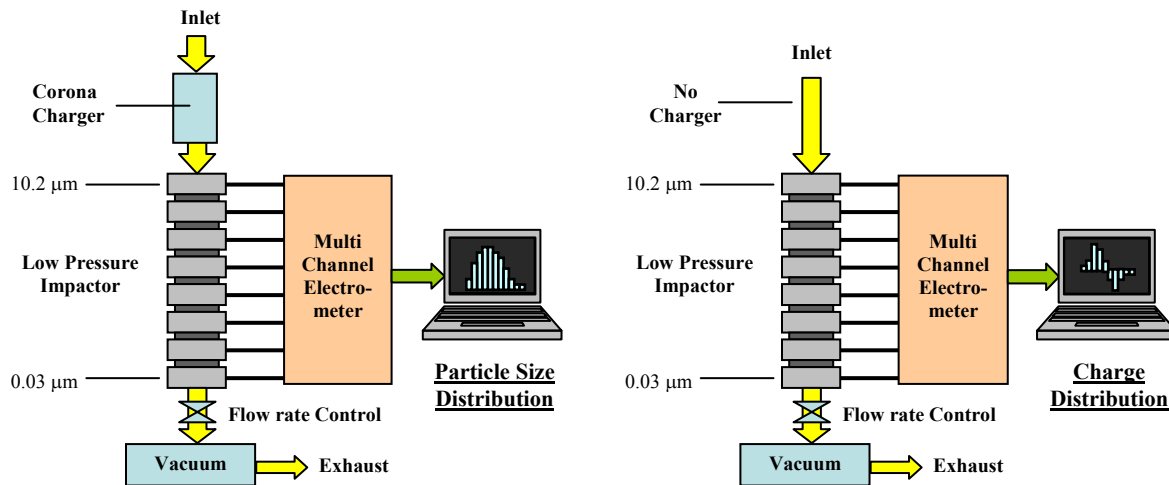


**Figure 4.1. (a)** Standard ELPI configuration with corona charger in place. The aerosol particles are charged uniformly prior to deposition within the impactor, for real-time particle size determination.

**(b)** Modified ELPI configuration with charger turned off. When the incoming aerosol is not charged uniformly, the ELPI determines native particle charges and records a charge distribution.

The ELPI can also be operated with the charger turned off, as shown schematically in Figure 4.1(b). In this configuration, the incoming aerosol is not charged within the ELPI and the electrometer measures only native particle charges. Since each impactor stage is electrically isolated from the next, charges can be measured across individual stages, allowing the evaluation of size specific charging with accurate determination of charge magnitude and polarity on particles in the respirable size range over time.

#### 4.1.2. Preliminary Data

Studies of medicinal aerosol electrostatics have been attempted previously. Electrostatic charge carried by a DPI aerosol cloud has been measured using a grid probe,<sup>11</sup> however, the particles were rather large and the system was of little pharmaceutical relevance. The effects of particle morphology and crystallinity on triboelectrification of DPIs have also been studied, but particle deposition was not considered.<sup>12</sup> Moreover, the studies relied solely on Faraday cage charge measurements, which precluded analysis of fine particle sizes and size-dependent charge distribution.

A preliminary analysis of DPI electrostatics in a pharmaceutically relevant system was conducted by the author and has recently been published; it is included in Appendix C.<sup>9</sup> The preliminary studies provide the foundation for the work described in this chapter, and can be summarized as follows:

- (1) An experimental apparatus was developed that allowed inhalers to be tested at an airflow rate of 60L/min, as recommended by the FDA and US Pharmacopeia<sup>13</sup>, and the electrical charge of the respirable fraction to be determined. The same setup is used in the present work.
- (2) Initial experiments assessed the ability of the ELPI to classify therapeutic aerosols consistently and in accord with a conventional inertial impactor, i.e. the Andersen eight stage nonviable impactor. ELPI particle size distributions were in agreement with those determined from ACI deposition measurements.

- (3) The particle size distributions acquired by ELPI were compared to those obtained from gravimetric analysis of the stages; agreement was good with almost superimposable particle size distributions and same  $d_{25}$ ,  $d_{50}$ , and  $d_{75}$  values. The ELPI system proved more precise and reproducible in the lower particle size ranges due to the limited resolution of the analytical balance used in the gravimetric analysis.
- (4) The study showed that particle deposition within the ELPI was consistent and reproducible for a given set of conditions. However, deposited particle charge was shown to vary significantly between different particle size fractions of a given formulation as well as between formulations.
- (5) The study revealed that pharmaceutical product properties such as excipient, inhaler type, and metering system (capsule material) significantly affect the extent to which formulations experience triboelectrification. Both charge magnitude and polarity were affected consistently.

The experiments constituted the most comprehensive study of DPI triboelectrification phenomena to date. They proved unequivocally that triboelectrification is a significant phenomenon in DPI actuation. Yet, the study had several shortcomings that needed to be considered in follow-up work. Charging effects are confounded by particle size distribution and mass depositions since the stages of the ELPI were not assayed for drug and excipient deposition during individual actuations. Moreover, excipients contained sizeable proportions of fine particles that were deposited together with the micron-size drug after formulation actuation. As a result, it is unclear which material contributed to charge on each stage; tribocharging could not be conclusively linked with fine particulate drug, and the magnitude of particle charge could not be established. However, this information is needed to determine whether particles carry sufficient charge to affect delivery.

#### **4.2. Experimental Design**

The goal of the experiments was to elucidate the phenomenon of electrostatic charging in a DPI (specific aim 1) by simultaneously studying charge and mass deposition following DPI actuation.

Establishing which formulation variables contribute to charging (specific aim 2) has consequences for product development. However, the number of possible variables to study in this context was potentially large. The choice of a discriminating experimental design with appropriate input factors and responses was critical.

#### 4.2.1. Design Factors

Preliminary experiments suggested which factors might merit closer scrutiny. At the same time the scope of the study needed to be expanded to consider previously neglected factors that might allow generalized conclusions. The Ishikawa (cause-and-effect) diagram in Figure 4.2 lists the factors that affect the performance of a DPI. The following section describes which of these factors were selected for study and how the experimental design was developed to test the contribution of the factors to triboelectric charging:

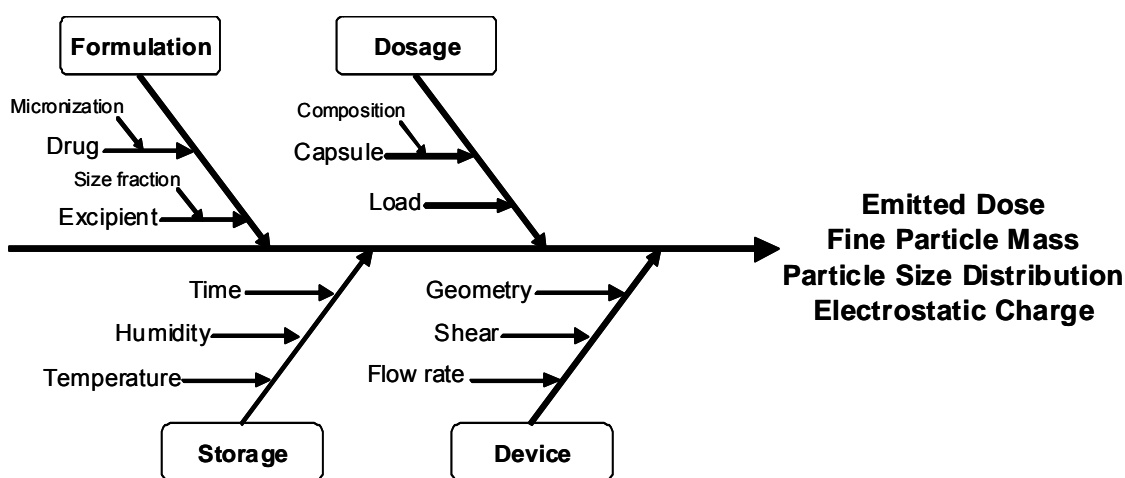


**Figure 4.2.** Ishikawa (cause-and-effect) diagram describing the function of dry powder inhalers.

(1) Drugs: Albuterol sulfate, Budesonide

Albuterol (USAN) or salbutamol (INN) is a short-acting  $\beta_2$ -adrenergic receptor agonist used for the relief of bronchospasms in asthma and COPD. Albuterol (MW 239.3) is a commonly inhaled medicine, available in many drug products, and frequently used as a model drug in medicinal



aerosol research. Albuterol sulfate was the sole drug substance studied in the preliminary experiments.

A second model drug, budesonide, was selected to determine if preliminary results could be extended beyond albuterol alone. Budesonide (MW 430.5) is a glucocorticoid steroid for the treatment of asthma, non-infectious rhinitis, and allergies. Budesonide is marketed as Pulmicort® with a Turbohaler DPI by AstraZenaca.<sup>14</sup> It was selected because it is a different therapeutic category of drug and is structurally very distinct from albuterol. Since it is a newer and still patented product, budesonide has not been studied to a large extent.

(2) Excipients: Lactose monohydrate, Glucose, Calcium Phosphate (CP)

Lactose is the most common excipient in DPI formulations. It was the only excipient used in the preliminary experiments and is the primary excipient in the formulations tested in this study. In addition to lactose, glucose was tested. It is the only other excipient employed in DPI formulations,<sup>15</sup> and is thus a relevant substance to compare. CP was chosen for study because it is chemically an entirely different material (inorganic salt), which offers a contrast. While it is a physiological salt that is widely used in the formulation of oral dosage forms, it has not been used in DPI formulations.

(3) Excipient Sieve Fractions: 45–75  $\mu\text{m}$ , 75–105  $\mu\text{m}$ , 105–150  $\mu\text{m}$

Different excipient sieve fractions were obtained and used in individual formulations. Since different size fractions of micronized albuterol have shown different charging characteristics in preliminary experiments, it is postulated that excipients may also show size dependent behavior. Three sieve fractions were selected because they were size ranges available for most excipients (all but the sieved lactose batches, where all particles are smaller than 75  $\mu\text{m}$ ). A lower limit of 45 $\mu\text{m}$  was selected to allow the most complete removal of excipient fines which might otherwise be deposited on the stages of the ELPI, confounding the analysis.

(4) Excipient Batch-to-Batch Variability (Lactose only): 2 milled (ML) 2 sieved (SV) lactose products

Since batch-to-batch variability is a well-known problem, several lactose products and batches were used to make formulations. Sieved lactose batches (SV) have undergone sieving as the only process step after crystallization while milled batches (ML) have been milled after crystallization at the manufacture site.

(5) Drug Concentration: 0.25%, 0.50%, 1.0%

DPI formulations are interactive powder blends containing low drug concentrations, often at the 0.5-2% mass/mass range. These concentrations ensure that drug particles remain separated from one another and, thus, maintain their primary particle size, i.e. they do not aggregate significantly. Drug concentrations are an important determinant of drug/carrier particle interactions. The drug concentration was examined at three levels to evaluate particle separation and charging. Carrier particle surfaces are heterogeneous with a number of particularly energetic “active sites”;<sup>16</sup> using different drug concentrations these active sites may be probed. The presence of active sites would likely be manifested in particle association resulting in deposition differences that are in non-linear with respect to drug concentration.

(6) Dose: 10mg, 20mg, 30mg, 40mg

The dose range is relevant to DPI formulations. Nonlinear responses of charging and drug deposition to changes in dose may elucidate the fluidization and charging pattern.

(7) Fluidization Conditions: Standard Entrainment Tubes

Preliminary studies were conducted using two different inhaler devices, the Rotahaler<sup>®</sup> (GlaxoSmithKline, RTP, NC) and the Inhalator<sup>®</sup> (Boehringer Ingelheim, Germany) single capsule inhaler, were a high pressure drop and a low pressure drop device, respectively.<sup>17</sup> The study results indicated a strong correlation between choice of inhaler and both magnitude and polarity of acquired charge. However, this correlation could not be firmly linked to a change in pressure drop or device resistivity, because the devices also differed in material and operational principles, which confounded comparisons between the devices. To eliminate this source of variability, standardized entrainment tubes (SETs) replaced DPI devices as aerosol dispersion

systems. SETs are simple steel tubes of specific dimensions in which well characterized air flow patterns are established.<sup>18</sup>

#### (8) Product Batch-to-Batch Variability (variability in manufacture)

Manufacture of select batches was repeated to determine if the observed phenomena were the result of fundamental material properties (as postulated) or whether they were the result of environmental or random effects that might arise in the process of manufacture.

#### 4.2.2. Study Design

Having established the design factors and their most useful levels, experiments must be structured to satisfy the study's aims. The mere combination of excipient, batch, and sieve fractions results in 14 different excipient building blocks. Were each of these to be tested at two levels, the total number of individual formulations would be  $14 \times 2$  (drugs)  $\times 2$  (conc) = 56 formulations. Tested at 2 doses and 2 fluidization conditions would require 224 experiments which does not account for the allocation of replicates (to test reproducibility and manufacture consistency). Were all levels discussed above tested the study would require  $14 \times 2 \times 3 \times 4 \times 3 \times 4 \times 3 = 12,096$  experiments (again excluding allocations for reproducibility and manufacture consistency). Efficient experimental allocation is crucially important.

In determining the appropriate statistical design, several competing objectives were weighed. Picking a standard design scheme, such as a fractional factorial or central composite design is attractive because it provides the ability to interpret all generated data simultaneously using well established statistical tools and generate response surfaces that may allow interpolation and extrapolation. However, given the large number of factors (in particular categorical factors such as the 14 different excipient building blocks) this design would be difficult to construct and in the end would still require sufficient trials to be impractical. Consequently a different approach was required.

The experimental design developed was a series of experiments in a design framework rather than a purely statistical design scheme. While it contains elements of both half and full-factorial designs it

was structured to test specific (if conditional) hypotheses rather than to determine a multidimensional response surface. Using this experimental framework the results cannot be interpreted generally but must be considered discretely. Specific hypotheses, represented by the design factors listed in section 4.2.1 were tested using a 2-level design with a number of intermittent or extreme points at various positions to gauge the response surface curvature where it appeared to play a role. The design, which is shown schematically in Figure 4.3, is based on the assumption that most factors are independent, and that marginal effects are more important than interaction effects. While many effects in this design can only be considered conditionally, understanding the system may allow more general statements to be formulated. In all, the design required 33 formulations to be tested in 63 experiments, which provided sufficient time for the repetition of a sizable portion of experiments, thereby increasing statistical power. In figure 4.3, each circle denotes an experiment, for which three sets of electrical charge data and one set of mass deposition data were determined.

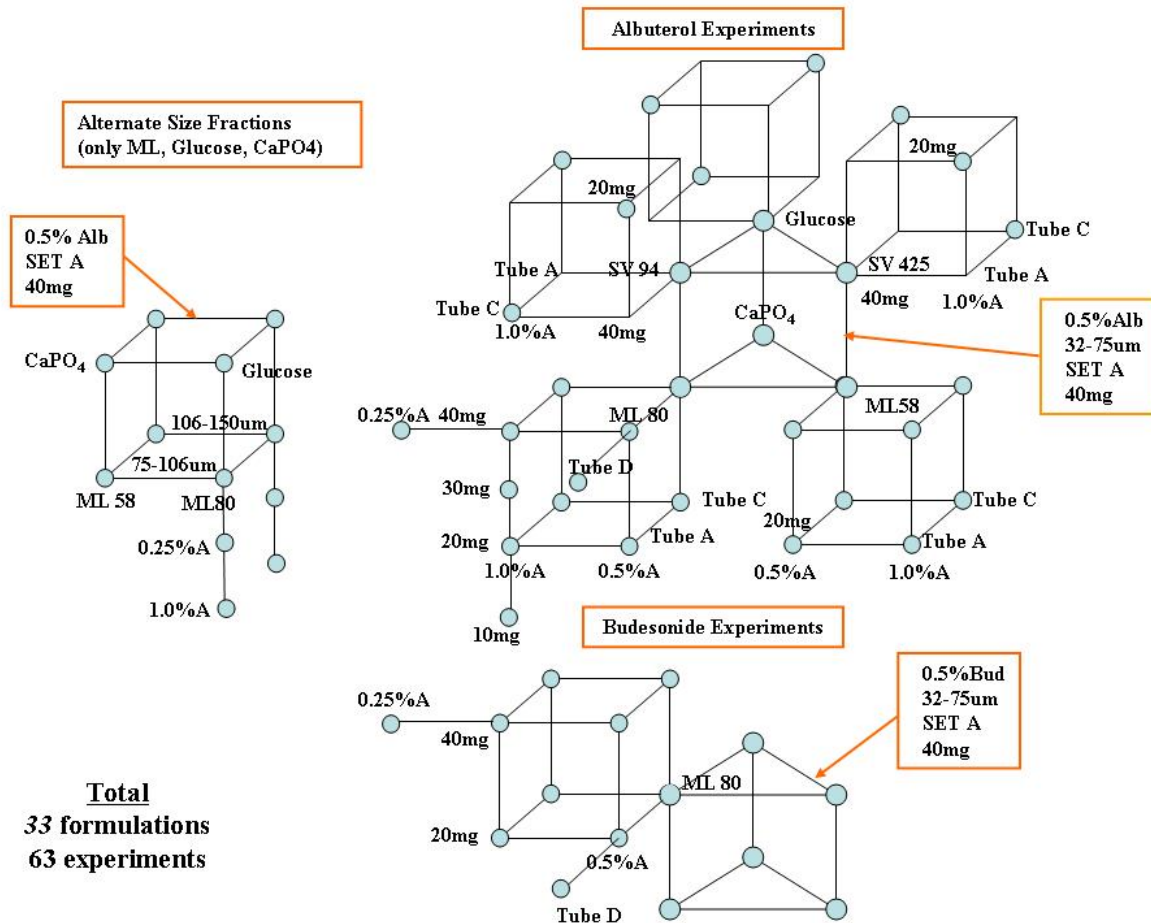


**Figure 4.3.** Experimental framework developed to study the electrostatic effects of the variables. Each circle denotes a different experimental setting. The framework contains elements of factorial and central composite design but was developed to test specific hypotheses. The main elements of the design are denoted by red boxes. The design is described in detail in the text.

The design is built around a central set of experiments that compares each excipient in a standard formulation (0.5% albuterol in 45-75 $\mu$ m sieve fraction of excipient) to the other five excipients using a common set of actuation conditions (40mg, SET A). There are two full-factorial experimental sets using the two milled lactose batches (ML80 and ML58) aimed at gauging the effects of drug concentration (0.5% and 1.0%), fluidization conditions (SET A vs. SET C), and dose (20mg vs. 40mg), and half-factorial designs for each of the other excipients. The purpose of collecting 2 full-factorial sets for ML80 and ML58 is that the differences between the batches are assumed to be minute (batch-to-batch variability), much smaller than the differences expected between the different materials. A full-factorial design has greater potential to discriminate differences. Using ML80 only,

the effects of drug concentration (0.25% albuterol), fluidization conditions (SET D), and dose (10mg, 30mg) were further investigated. These experiments were to provide insight on the response surface curvature with respect to these variables. The central design (triangular prism) with a full-factorial assessment around ML80 is repeated for budesonide; this should allow a comprehensive comparison of drug identity for each excipient, as well as confounded effects (interactions between drug, drug concentration, fluidization conditions, and dose) for ML80 lactose formulations. Finally, the cube on the left provides comparisons of the different sieve fractions for each of the four excipients for which the larger sieve fractions are obtainable, that is the two milled lactose batches (ML80, ML58), glucose, and CP. Once again, using ML80 lactose, the confounding effects of sieve fraction and drug concentration may be examined. While this is one of the afore-mentioned conditional tests, if an effect is observed it may well exist for some of the other excipients.

Of the 63 experiments that were conducted in this framework, 28 involve ML80 lactose (12 out of 33 formulations). Thus, a very thorough study of ML80 lactose behavior is obtained, allowing a complete examination of all possible interactions of the different variables. Examinations of the other excipients are less comprehensive. ML80 lactose stands at the center of this study because it presents the pharmaceutically most relevant excipient.

To ensure that formulations would be tested within a week after manufacture, the order of the formulations was randomized first, and then the different actuations were randomized within blocks of ~5 formulations. Formulations were then manufactured. This ensured that formulations were not subject to different storage effects.

To evaluate the reproducibility and possible storage effects, 20 of the 63 experiments were randomly selected for retesting, several of these would be retested several times after varying periods of storage. To evaluate the variability associated with the manufacture seven formulations were randomly selected for remanufacture and were subsequently retested using the same experimental conditions and settings. In addition, several formulations were selected to check the effect of environmental conditions, including the effect of high RH and the effect of the last surface of contact.

### 4.3. Materials and Methods

The following discussion focuses on the description of the materials and methods directly related to the actuation experiments. A complete discussion of drug and excipient and formulation preparation (sieving, particle size analysis, etc.) and characterization is provided in Chapter 2.

#### 4.3.1. Materials

##### 4.3.1.1 Excipients

Lactose monohydrate, Respitose™, was provided by DMV-Fonterra Excipients (Goch, Germany). Two batches of milled (ML001, batches 10136780 and 10138058), and two batches of sieved (SV003, batches 10190094 and 10135425) lactose were evaluated. (For convenience, the batches will be referred to as ML80, ML58, SV94, and SV425, respectively.) Dextrose (D-glucose), Lycadex™, was provided by Roquette (Keokuk, IA). Calcium phosphate, A-Tab™ was obtained from Innophos (Cranbury, NJ). To control for differences in particle size in the experiments, all excipient batches were sieved prior to use in the formulations and experiments.

##### 4.3.1.2 Drugs

Milled albuterol sulfate (median particle size 2µm) was obtained from Chemaco (Beetsterzwaag, NL) from drug manufactured by P.F.C. Italiana S.r.l, (Caronno Pertusella, Italy). Budesonide was obtained from Sigma-Aldrich (St. Louis, MO), and was jet-milled to a single-micron size range (verified using laser light scattering, described in Chapter 2).

##### 4.3.1.3 Dispersion Devices

To understand the effects of fluid dynamics on triboelectrification three standard entrainment tubes (SET) were used, giving low, intermediate, and high specific resistance values of 0.021, 0.046, and 0.140 cm H<sub>2</sub>O<sup>1/2</sup> / (L/min), respectively<sup>18</sup>. The relevant properties of these SETs in comparison with the two previously tested devices are shown in Table 4.1; SETs A, C, and D provide high, low

(corresponding to Inhalator and Rotahaler), and very low resistivity devices, likely to provide evidence of a range of performance of the formulations in response to airflow conditions.

**Table 4.1.** Relevant fluid dynamic properties (at 60L/min) of standard entrainment tubes used in studies compared with previously used and commercially available inhalers.

SET	Specific Resistance ( $R_D$ ) cm H <sub>2</sub> O <sup>0.5</sup> / (L/ min)	$Re$	$\Delta P$ (N/m <sup>2</sup> )	Power (Watt)	Shear Stress (N/m <sup>2</sup> )
A	0.140	18440	6920	6.92	13.14
C	0.046	11070	747	0.747	2.20
D	0.021	7720	156	0.156	0.62
Rotahaler	0.040	N/A			
Inhalator	0.180	N/A			

#### 4.3.2. Methods

##### 4.3.2.1 ELPI Experimental Apparatus

The experimental apparatus was developed during preliminary studies to overcome two major obstacles, (1) operation at 30L/min and (2) pre-separation of large agglomerates (of no therapeutic importance). (1) The ELPI operates at 30L/min, but DPIs are typically tested at 60L/min airflow rates which more closely approximates the inspiratory air flowrate; (2) unlike the ACI (ThermoAnderson, Smyrna, GA), the ELPI does not have a pre-separator capable of removing large quantities of coarse material. However, initial trials made clear that failure to remove carrier particles and agglomerates from the aerosol prior to introduction into the ELPI could result in flooding the top stages after a single inhaler actuation. The setup that was devised to address these issues is shown in Figure 4.4. An SET is connected to the standard USP induction throat, which is connected to the ACI pre-separator (loaded with 15mL water or methanol) (cut-off size of 8.6 $\mu$ m at 60L/min). A custom-manufactured aluminum connector from the pre-separator split the 60L/min stream in two equal streams; 40cm Tygon<sup>TM</sup> tubing (R3603) was used to connect the two outlets with ELPI and ACI, each employing a vacuum pump operating at 30L/min. Tygon tubing is commonly used in aerosol research because, unlike other materials, Tygon has negligible electrostatic effects.<sup>19</sup> Deposition of drug in different



parts of the experimental apparatus was determined in preliminary studies; deposition in the custom-made part and tubing accounted for <5% of deposition in the ELPI and ACI. To prevent particle bounce ACI collection plates were coated with silicone oil. Coated aluminum foils were used with the ELPI stages. The apparatus was leak tested prior to each experiment. In accordance with manufacturer recommendations, the ELPI was switched on at least 1 hour prior to measurement. Inlet air was not filtered and baseline measurements of charge were collected.

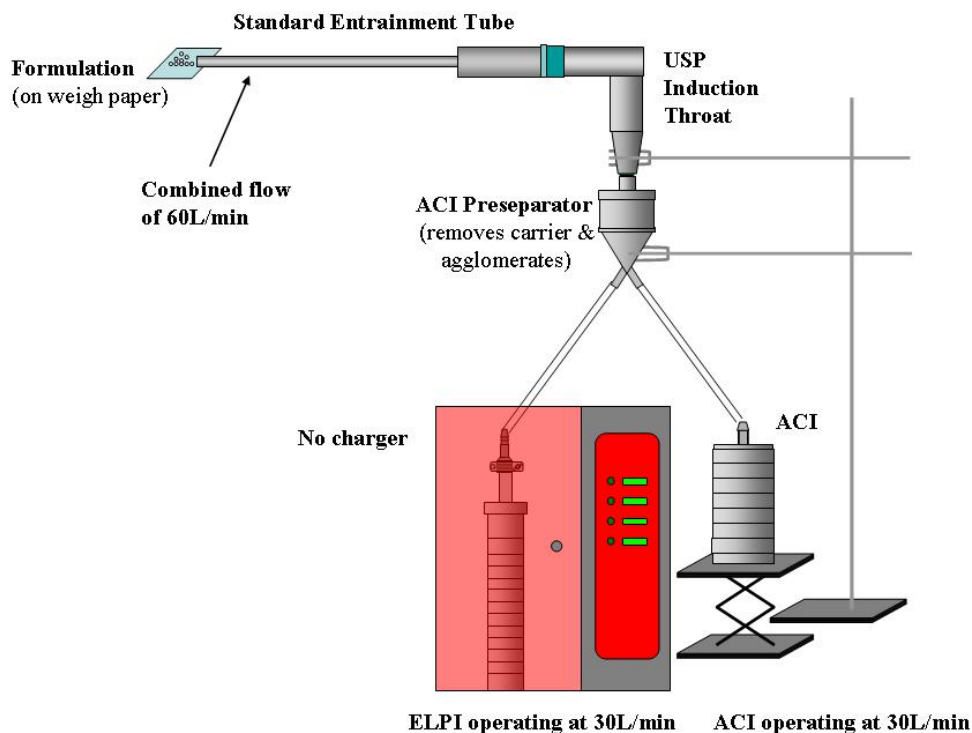


**Figure 4.4.** Experimental set-up, adapted from Telko et al. 2007.

#### 4.3.2.2 Actuators

Formulations were weighed on an analytical balance, dispensed onto weighing paper and placed in front of the entrainment tube for actuation into the experimental apparatus. Preliminary studies indicated that three actuations were required to ensure sufficient material deposited on all ELPI stages. To determine the charge contribution of excipient only, for each experimental setting the three

formulation actuations were preceded by three actuations of excipient only. In sequence, for each setting, the apparatus was turned on, the electrometer channels were zeroed, and once the signal stabilized, the actuations proceeded in the order: placebo; active formulation; placebo; active formulation; placebo; and active formulation. All active and placebo formulations were weighed out prior to the experiment and approximately 10 seconds were allowed between actuations. Electrical charge across twelve stages during actuations was recorded using the ELPI V acquisition software.

#### 4.3.2.3 Analysis of Drug Deposition on ELPI Stages

After each set of three actuations for a given formulation the ELPI was turned off and the apparatus was disassembled and washed. The coated aluminum foils were removed from the ELPI stages and washed with 3mL water (albuterol formulations) or 3mL methanol (budesonide formulations). CP formulations (limited aqueous and methanol solubility) were centrifuged to separate any undissolved excipient. UV absorbance of the supernatant solutions was assessed at a wavelength of 224.5nm (albuterol) or 244nm (budesonide) using a Shimadzu 160U spectrophotometer. The excipients have negligible absorbance at this wavelength.

#### 4.3.2.4 Environmental conditions

The extent to which triboelectric charging occurs depends, in part, on the environmental conditions. Triboelectrification is only observed at relative humidities of less than 65%.<sup>20</sup> Hence, conditions must be monitored closely. The experiments were performed in the climate-controlled laboratory over the course of several months; the conditions during blending, storage, and actuation were constant at a temperature of  $23 \pm 0.5^\circ\text{C}$  and a relative humidity of  $35 \pm 5\%$ .

#### 4.3.2.5 Environmental Effects Study

When a patient actuates an inhaler and the drug particles enter the airways, they are entering a high humidity (100% RH) environment. High RH is known to inhibit triboelectrification. However, it

is unclear if the environmental conditions in the airways, to which drug particles are briefly exposed can also dissipate the particles' charges. This was determined using a modified apparatus which is similar to Figure 4.4 with an ultrasonic humidifier (Vicks V-5100, Procter & Gamble, Cincinnati, OH) generating water vapor immediately next to the SET inlet, so that humid air instead of ambient air is drawn into the apparatus.

#### 4.3.2.6 Surface Effects Study

Triboelectrification is a surface effect; different surfaces interact with materials and result in specific charging behavior. It is important to understand the choice of surface from which the formulation is actuated. Two formulations were actuated into the experimental apparatus from a series of different surfaces, including weighing paper, PE weighing dish, aluminum weighing dish, a gelatin capsule, carageenan capsule. Only the ELPI charge deposition data was recorded for these and was subsequently compared.

#### 4.3.2.7 Storage

Raw materials were stored in double-lined PE bags and PE containers. Once the excipients were sieved, they were stored in 60mL Wheaton glass bottles with plastic snap caps. After blending formulations were stored in 20mL Wheaton glass vials with PE-lined screw caps. Since ambient conditions in the laboratory were well controlled, no specific storage conditions were used. For consistency, drug/excipient blends were stored no longer than one week between manufacture and initial actuation.

#### 4.3.2.8 Data Analysis

Charge data were collected by the ELPI data acquisition software, ELPIVI 4.0 (Dekati, Tampere, Finland). Raw data were transferred to, and analyzed using Excel software (Microsoft, Seattle, WA). Each actuation was isolated and charge was integrated over the time the actuation had occurred. Since

there were three actuations of active formulation for each experiment, the charges were averaged and standard deviations determined. Drug deposition was determined from chemical assay of the ELPI stages and plotted in Excel.

The set of 63 experiments provides a large dataset. However, the data represents a custom design; containing elements of factorial and central composite design. Data were transferred to statistical software SPSS 16.0 for Windows (SPSS Inc., Chicago, IL) and analyzed using the general linear model multivariate analysis feature. The response elements examined included  $d_{25}$ ,  $d_{50}$ ,  $d_{75}$ , fine particle fraction, as well as total charge magnitude and polarity (summed across all stages), absolute magnitude of the charges recovered, and charges recovered on stages 1-3, 4-6, 7-9, 10-12. Another response variable tested was charge/fine particle mass. Assuming the particles were perfect spheres of a uniform size at the midpoint between two stages, the average particle charge was determined and adapted as a response variable. All of the response variables were examined with respect to each of the formulation factors in a series of statistical tests.

#### **4.4. Results and Discussion**

##### **4.4.1. Reproducibility of ELPI Experiments**

Preliminary experiments had shown good reproducibility of charge distribution profiles for a given formulation performed at constant conditions.<sup>21</sup> Using the same formulation/ capsule/ inhaler combination gave consistent charge distributions, which differed from those of other formulation/ capsule/ inhaler combinations. This consistency was also observed in the current trials, as is highlighted in Figure 4.5. 20mg of 1% albuterol in ML58 lactose, 45-75  $\mu\text{m}$  sieve fraction, was actuated from SET A three times (separated by actuations of placebo formulation); the procedure was repeated 9 days later. As is evident in Figure 4.5, the actuations were consistent within a given day, and consistent over the course of several days. There were some differences in magnitude, by as much as 20%, but some portion of this is a result of drug concentration variations in the blend.

Moreover, even as differences in magnitude are observed, polarity and rank/order of the stages was retained in all trials.

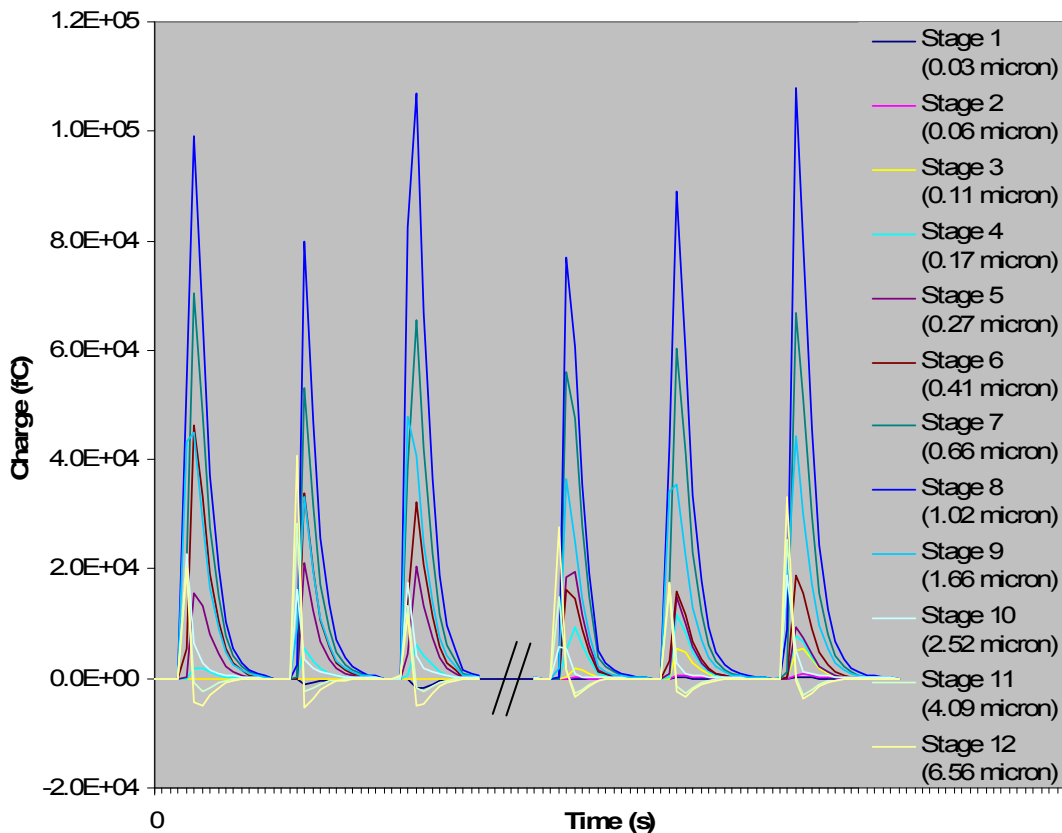


**Figure 4.5.** Six actuations of 1% albuterol in ML58 lactose, 45-75  $\mu\text{m}$  sieve fraction, 20mg actuated from SET A. The first three were performed on one day separated only by actuations of excipient, the next three performed 9 days later, also separated by excipient actuations (excipient actuations have been removed from this graph). Double line indicates temporal discontinuity. In each case, deposition on stages is complete in about 6 seconds. While there is some variability with regards to magnitude, the overall rank/order and polarity is highly preserved in each trial.

In some instances, the variability was in excess of the approximately 20% shown in Figure 4.5. However, even where the variability was greater, the charge deposition patterns remained discernable for given formulations actuated at specific conditions (compared to other formulations and/or conditions).

The two experiments shown in Figure 4.5 were separated by nine days of storage. However, since the current experimental plan was completed over the course of months rather than days the

consistency was evaluated in more detail, including an assessment of the reproducibility of charge and particle size distribution after storage. Storage times of less than two weeks generally resulted in highly reproducible charge and particle size distributions with variability similar in magnitude to intra-experimental variability observed when experiments were performed in sequence (on the same day). Figure 4.6 represents a case, where a formulation was retested five days after the original sample was examined; this formulation (0.5% albuterol in 45-75 $\mu$ m ML80 lactose) showed very good reproducibility in both mass deposited (FPM and FPF) and charge distributions.

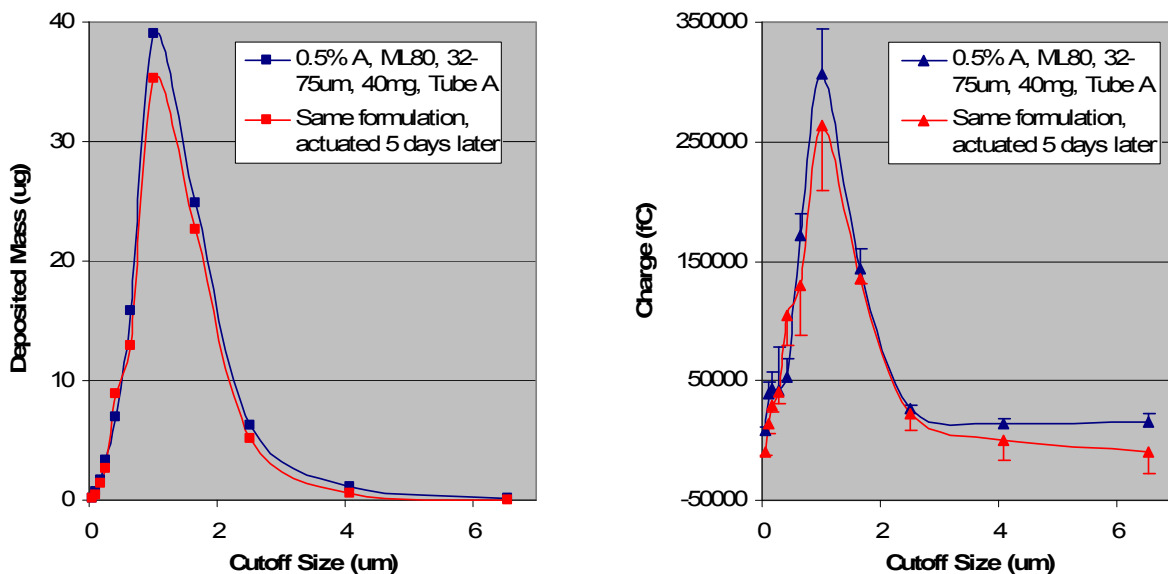


**Figure 4.6.** Formulation (0.5% albuterol in 45-75 $\mu$ m ML80 lactose, 40mg) actuated from SET A (three times) on different days, separated by **5 days of storage**. The differences in deposition (actual quantities shown) are minimal. Differences in charge distribution mirror the differences in deposition, and are within a standard deviation from one another.

However, variability in mass and charge deposition profiles increased after more than two weeks of storage (at ambient but constant conditions). In many cases, the differences observed after storage were so dramatic that the replicates were no longer representative of the original system. In other words, many of the formulations were subject to significant storage effects. Surprisingly, in most cases, the dispersion of drug had improved upon storage. A complete discussion of the storage effects

is given in Appendix D. As a result of these effects, all replicates subject to storage effects, i.e. those with storage times exceeding two weeks, were excluded from the experimental analysis.

#### 4.4.2. Remanufactured Product Variability

Another aspect of variability that requires elucidation is the variability associated with the manufacture. While the same process of manufacture is applied to all formulations, the major processing step of blending is by its nature a random process. If the variability associated with the product manufacture results in significant differences in formulation behavior, variability from other factors would be difficult to discern. In light of the observations made with respect to storage, understanding the variability of the manufacture process is essential.

Figure 4.7 shows the mass and charge deposition profiles for a formulation (0.5% albuterol, ML58 lactose, 75-106 $\mu$ m sieve fraction) manufactured twice. Both mass and charge deposition profiles are almost superimposable, indicating a high level of reproducibility.

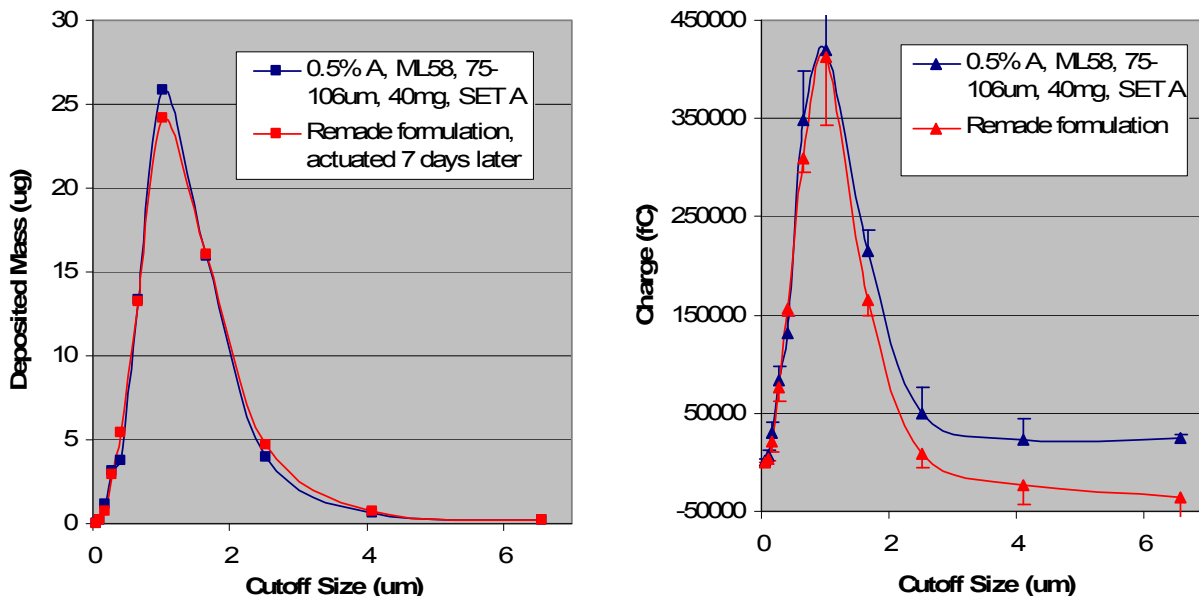
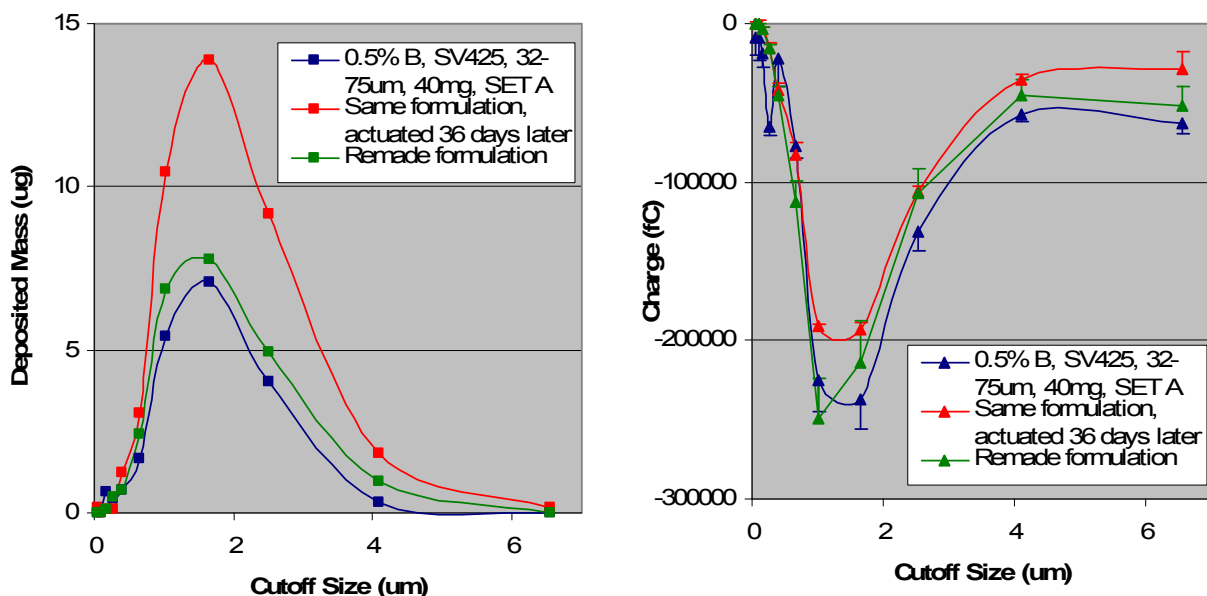


Figure 4.7. Remade formulation (0.5% albuterol in 75-106 $\mu$ m ML58 lactose) actuated from SET A (three times).

Figure 4.8 compares two batches of product, one actuated soon after manufacture (blue) as well as after 36 days of storage (red) and a remanufactured formulation actuated two days after manufacture. Clearly, the remanufactured formulation is more similar to the original formulation than to the formulation that has undergone storage. This suggests that the variability in the process is not significant, and that the storage effects are real.



**Figure 4.8.** Same formulation (0.5% budesonide in 45-75 $\mu$ m SV425 lactose) actuated from SET A (three times) on different days, separated by **36 days of storage**. Also shown remade formulation, actuated day after it was made. The remade formulation has FPF similar to the old formulation without storage, while storage results in higher deposition. Charge deposition profiles are similar for all.

#### 4.4.3. Surface Effects

Two formulations were actuated into the experimental apparatus from a series of different surfaces, including weighing paper, a polyethylene (PE) weighing dish, a gelatin capsule, and a carageenan capsule. Figure 4.9 shows the results of one of these experiments, charge depositions over time for a formulation of 1% albuterol in ML58 lactose, 45-75  $\mu$ m sieve fraction, 20mg actuated from SET A; the formulation had been dispensed onto each of the different surfaces and had been kept there for at least 30 minutes prior to actuation. The choice of surface did not appear to have a significant effect on the charging properties of the FPF within the ELPI in either case; the charging



recorded on the individual stages follows the same pattern in each case, and the differences in overall magnitude are in the order of inter-actuation variability.

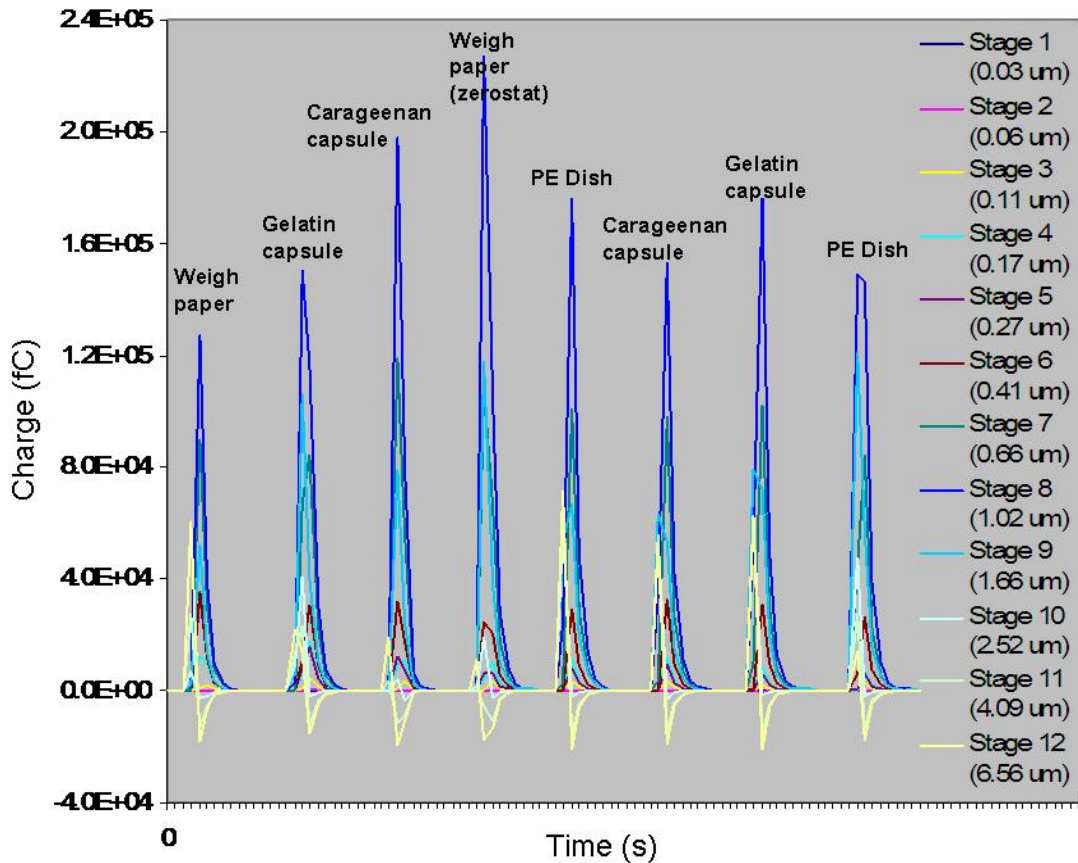


**Figure 4.9.** 1% albuterol in ML58 lactose, 45-75  $\mu\text{m}$  sieve fraction, 20mg actuated from SET A, off different surfaces. The eight actuations were performed in a row with intermittent placebo actuations. There are minor magnitude differences but the charge deposition profiles are largely the same. This supports the hypothesis that the charges observed are the result of triboelectrification during actuation, when particles have undergone charge transfer and those charges are exposed.

The results in Figure 4.9 are important because they support the hypothesis that the electrical charges are the result of tribocharging, i.e. charge transfers between the particles of the formulation. These charges are the result of electron transfer during particle contact which occur during and after the blending process; the charges are exposed when the particles are separated from one another during the actuation process. This point in particular can be deduced from the fourth actuation shown, in which the blend was actuated from weigh paper after it had been treated with Zerostat<sup>®</sup> antistatic gun,

which removes static charges by releasing a stream of bipolar ions. This treatment ensures that the system as a whole is uncharged. The charges, shown in Figure 4.9 were integrated over time and summed across the stages; the results of this are shown in Table 4.2. Differences in charge (actual and absolute magnitude) are within the normal variability.

**Table 4.2.** Effect of last surface of contact on total charge (sum across all stages, and sum of absolute magnitudes across all stages) for 1% albuterol in ML58 lactose, 45-75  $\mu\text{m}$  sieve fraction formulation, 20mg actuated from SET A, shown in Figure 4.9. Range is given, except in last row which gives actuation average  $\pm$  standard deviation.

<b>Last Surface of Contact</b>	<b>Sum of Charges (pC)</b>	<b>Charge Magnitude (pC)</b>
<b>Paper (n=1)</b>	559	663
<b>Carageenan Capsule</b>	646 – 714	758 – 813
<b>PE Dish</b>	781 – 821	886 – 908
<b>Paper w/ Zerostat (n=1)</b>	806	922
<b>Gelatin Capsule</b>	829 – 860	934 – 941
<b>AVERAGE</b>	752 $\pm$ 104	853 $\pm$ 100

As shown in Figure 4.10 and Table 4.3, another formulation containing budesonide in sieved lactose displayed the same behavior, i.e. charge distribution was independent of the surface of last contact, even as the actual charging was very different from the previous formulation. In this case, highly negative charges were recorded for all actuations, suggesting that the milled budesonide had a higher pseudo work function than the sieved lactose leaving its particles with an excess of electrons after separation from the sieved lactose.

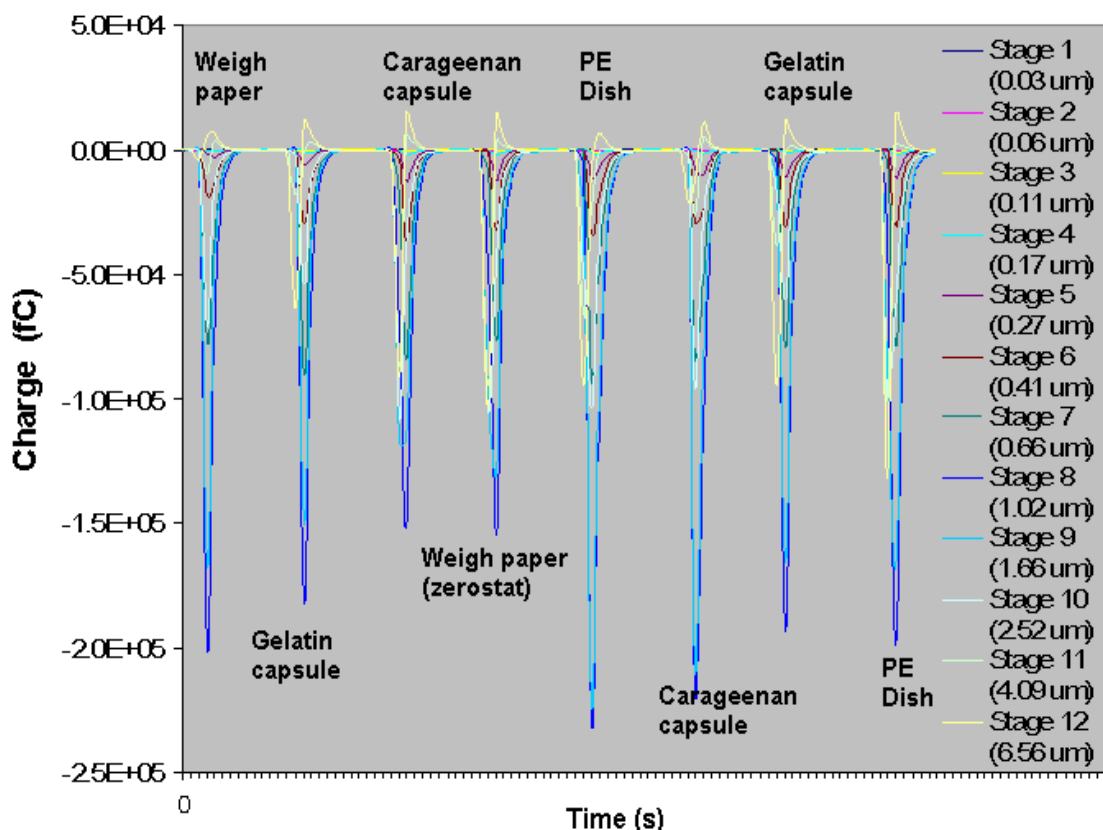


**Figure 4.10.** 0.5% budesonide in SV425 lactose, 45-75  $\mu\text{m}$  sieve fraction, 20mg actuated from SET A, off different surfaces. The eight actuations were performed in a row with intermittent placebo actuations. There are minor magnitude differences but the charge deposition profiles are largely the same. This supports the hypothesis that the charges observed are the result of triboelectrification during actuation, when particles have undergone charge transfer and those charges are exposed.

**Table 4.3.** Effect of last surface of contact on total charge (sum across all stages, and sum of absolute magnitudes across all stages) for 0.5% budesonide in SV425 lactose, 45-75 $\mu\text{m}$  sieve fraction formulation, 40mg actuated from SET A. Range is given, except in last row which gives actuation average  $\pm$  standard deviation.

Last Surface of Contact	Sum of Charges (pC)	Charge Magnitude (pC)
Paper (n=1)	-795	834
Carageenan Capsule	-1080 – -1086	1125 – 1136
PE Dish	-1209 – -1426	1254 – 1447
Paper w/ Zerostat (n=1)	-1077	1129
Gelatin Capsule	-822 – -959	873 – 1003
<b>AVERAGE</b>	<b>-1057 <math>\pm</math> 205</b>	<b>1100 <math>\pm</math> 199</b>

#### 4.4.4. Environmental Effects

When drug particles enter the airways during inhaler actuation they are entering a high humidity environment. Although high RH can inhibit triboelectrification, it is unclear if brief exposure is

sufficient to dissipate particle charges. To determine the effect of high RH during aerosol transport, an ultrasonic humidifier was operated adjacent to the SET inlet, so that humid air was drawn into the apparatus. Actuations of 1% albuterol in ML58 lactose, 45-75  $\mu\text{m}$  sieve fraction, 20mg actuated from SET A (same as Figure 4.9) were performed. The charges recorded on the stages of the ELPI are shown in Figure 4.11. The first two peaks show previous experiments performed at ambient humidity (35% RH), the next three were performed at high humidity (95% RH). Then the humidifier was turned off and another two actuations were performed at ambient humidity. While the high humidity greatly increases the noise on the stages, the actuations are essentially unchanged. Charge distribution and magnitude are the same as in a low humidity environment. This confirms that charging is a relevant phenomenon during clinical DPI use. Whether there is sufficient triboelectrification to affect particle trajectory and deposition will be determined in later experiments.

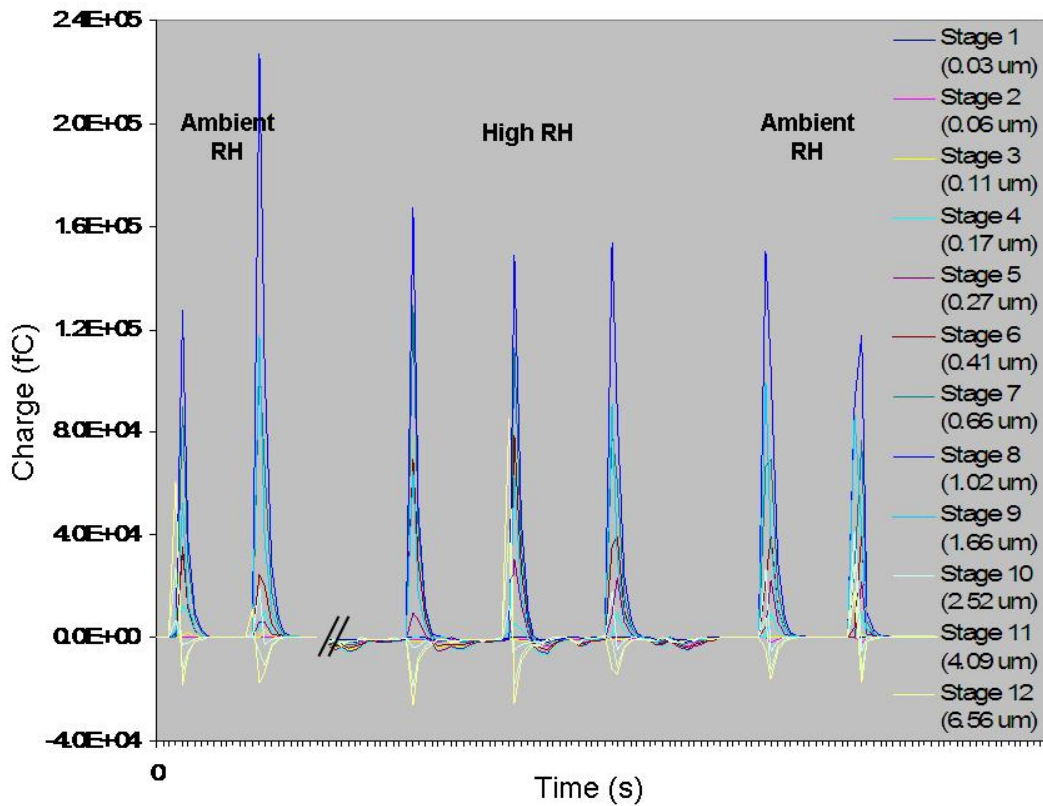


**Figure 4.11.** 1% albuterol in ML58 lactose, 45-75  $\mu\text{m}$  sieve fraction, 20mg actuated from SET A, actuated at low RH, high RH, and then again at low RH. Brief exposure to high RH as might be experienced in a patient's lung does not lead to a dissipation of electrical charges.

#### 4.4.5. Experimental Design Analysis: Effect of Formulation Factors on Fine Particle Mass (FPM) and Particle Size Distribution

As discussed in the introduction (Section 4.1.2), mass depositions for individual actuation were not determined in the preliminary studies.<sup>9</sup> Instead, a number of initial screens were performed and assumptions about deposition applied to the other actuations. This was a valid approach given the goal of the study was to assess the overall prevalence of electrostatic charging. However, in the absence of accurate deposition data, the effects of the formulation variables on the charging characteristics are confounded by presumed differences in mass deposition. In order to understand how particle charge is affected by formulation and actuation factors the charge levels need to be considered relative to the mass of the deposited aerosol particles. In the current project charge distributions were recorded using the ELPI, then the mass deposition on each stage were determined by chemical assay. (Since the single depositions were close to the limit of detection on some stages mass was assayed for a pooled set of 3 subsequent depositions of the same formulation and averaged.) As a result we can discern how the formulation variables affect drug deposition and apply the results to the analysis of charging.

After each actuation experiment, the ELPI was disassembled and the stages assayed. The mass on each individual ELPI stage was determined, total deposited mass and FPF were calculated, and particle size distributions (PSDs) were generated. These measures are used in conjunction with the charging data, but it is also instructive to consider them individually, since they present a rich data set of formulation effects on PSD. The PSDs are first discussed qualitatively, then in context of the statistical analysis.

##### 4.4.5.1 Qualitative Analysis

The effects of drug concentration, fluid dynamic conditions, excipient, and excipient sieve fraction on particle size were evaluated. While the fine particle mass (FPM) varied for many of these variables (as might be expected), only the **fluidization conditions** (pressure drop or Re) had a visible

effect on the particle size distribution of the deposited drug. This is shown in Figure 4.12, in which different albuterol in ML80 lactose formulations (0.25%, 0.50%, 1.0%) actuated under different fluid dynamic conditions represented by SET A (Re=18440), SET C (Re=11070), and SET D (Re=7720) are shown. Table 4.4 gives the corresponding  $d_{25}$ ,  $d_{50}$ , and  $d_{75}$  values. The figure and table show clearly that the actuation conditions affect the particle size distribution; more intense actuation conditions (SET A, triangles) shift the particle size distribution to lower values by dislodging and delivering more fine drug particles (in the  $1\mu\text{m}$  range), which may not separate under less turbulent conditions. Mass depositions were higher under the more vigorous conditions which supports this conclusion. In turn, the very low pressure drop actuation conditions (SET D, rectangles) shift the particle size distribution to a higher size range. The **concentration of drug** does not appear to have any effect on the relative particle size distribution, though higher concentrations resulted in correspondingly more drug on the stages of the ELPI (as expected). The effect of **sieve fraction** or the **excipient** was more difficult to discern and is discussed in the context of the experimental design analysis.

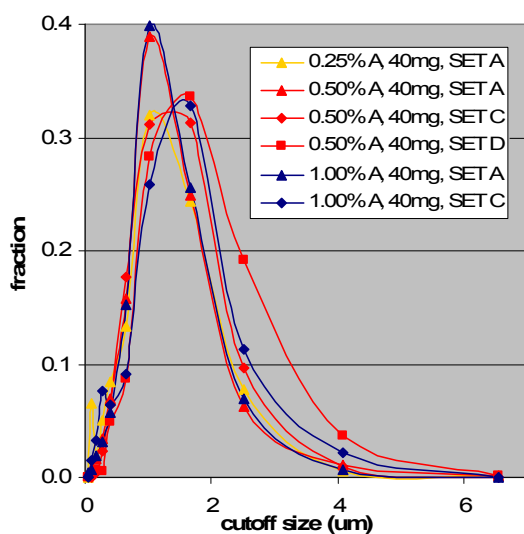


**Figure 4.12.** Effects of drug concentration and actuation conditions (high pressure drop (SET A), low pressure drop (SET C) and very low pressure drop (SET D)) on the particle size distribution of albuterol in 45-75 $\mu\text{m}$  ML80 lactose formulations.

**Table 4.4.** Particle size distribution proxies for albuterol in 45-75 $\mu\text{m}$  ML80 lactose formulations, shown in Figure 4.12.

Formulation & Actuation Conditions	$d_{25}$ ( $\mu\text{m}$ )	$d_{50}$ ( $\mu\text{m}$ )	$d_{75}$ ( $\mu\text{m}$ )
0.25%A, SET A	0.86	1.32	1.88
0.50%A, SET A	0.94	1.37	1.92
0.50%A, SET C	0.98	1.49	2.13
0.50%A, SET D	1.24	1.83	2.47
1.0%A, SET A	0.98	1.39	1.94
1.0%A, SET C	0.97	1.52	2.20

#### 4.4.5.2 Statistical Analysis: General

For the experimental design analysis, the PSD data were reduced to a smaller number of descriptive parameters consisting of  $d_{25}$ ,  $d_{50}$ ,  $d_{75}$ , (determined by linear interpolation of the particle size distribution data) and FPF which were evaluated by multivariate statistics.

An initial evaluation of the entire data set showed very strong codependency of the results on the identity of the drugs. This is expected, since, as shown in the preliminary analysis (Chapter 2), the drugs have different primary particle sizes. As a result, all significant effects contained the drug as a cofactor. Moreover, since the two drugs differed in their behavior and response to formulation variables the statistical software (SPSS) could not find a converging model that accounted for all effects on both drugs simultaneously. To circumvent this problem, the datasets for the two drugs were analyzed separately. The results of this analysis are summarized in Table 4.5 (budesonide) and Table 4.6 (albuterol).

Table 4.5 summarizes the significant effects of the formulation variables on the particle size and mass distribution of budesonide actuated from different formulations. Since the table follows the same format and gives the same kind of information as the subsequent results tables, a short description of the procedure is in order:

The first two rows in the table describe the data in terms of the mean ( $\pm$  standard deviation) and the range for the entire data set. Subsequent rows show the results of the statistical analysis. The statistical analysis was conducted in SPSS using the general linear model (GLM) multivariate procedure. The procedure provides regression analysis and analysis of variance (ANOVA) for the dependent variables (i.e.  $d_{25}$ ,  $d_{50}$ ,  $d_{75}$ , and FPF) by factor variables (i.e. excipient, drug conc., fluidization conditions). The effects of factor variables on the means of dependent variable groupings were tested, and the interactions between factors and the effects of individual factors were probed. Only the effects of individual factors are reported in Table 4.5 and subsequent result tables, because these are general and apply to different systems. The tables also provide effect size estimates based on the unbalanced full factorial model (unbalanced because, as described above, certain factor

combinations were not tested). The effect size describes the proportion of total variability attributable to a given factor. The confidence interval for each test is also given; the significance level was set to  $\alpha=0.05$ , and only effects with lower p-values are reported. For each category of factor (underlined) the cells to the right indicate whether the effect on the given response was significant. Where the effects are statistically significant, the p-value is indicated and the rows below give the individual factor contribution (parameter) estimates; again, where these contributions are significantly different from the other variables of the category, the p-value is indicated. One of the variables serves as a basis of comparison in each case and is assigned a contribution of 0; the effects of the other variables are given relative to it. The basis of comparison is SV94 lactose, 45-75 $\mu\text{m}$  sieve fraction, 1.0% drug concentration, and the highly turbulent actuation conditions (SET A,  $\text{Re}=18440$ ). The model intercept is also given in the tables. This intercept provides the default response value in absence of the factor effects. Thus, to highlight an example from Table 4.5, the  $d_{25}$  of budesonide after release from a 0.25% drug in ML80 formulation, actuated at  $\text{Re}=18440$  is expected to be  $0.96-0.16+0.28+0.00=1.08\mu\text{m}$ ; this result is consistent with the raw data: the actual recorded value from experiments is  $1.08\pm 0.03\mu\text{m}$ .

#### 4.4.5.3 Statistical Analysis: Budesonide

Table 4.5 shows that the particle size distributions and FPFs have wide ranges. Yet neither **excipients** nor **drug concentrations** of the formulation have a significant effect on the particle size distribution of the deposited drug. Only  $d_{25}$  is affected by the excipient, suggesting that the particle size distribution is most sensitive to formulation and actuation conditions in the smallest particle size range. Use of ML80 lactose and CP **excipients** results in the most dramatic shift in the  $d_{25}$  to a higher particle size (compared to SV94 lactose), suggesting relatively less separation of smaller drug particles. When considering the FPF of CP, which is significantly higher than that of the other excipients, one can see that the shift in the particle size is likely due to an overall increase in the



release of drug, most of which is larger in size. Varying the drug concentration, on the other hand, does not have a statistically significant effect on the  $d_{25}$  of budesonide.

**Table 4.5.** Effect of excipient (all 45-75 $\mu\text{m}$  sieve cut), drug concentration and fluidization conditions on the PSD (using  $d_{25}$ ,  $d_{50}$ ,  $d_{75}$  as surrogate markers) and FPF of deposited **budesonide**. In the model, created by SPSS software, the default value is given by the model intercept and the contribution for each factor is given in each column. Thus, for example, the  $d_{25}$  of budesonide from a 0.25% drug in ML80 actuated at  $Re=18440$  would be expected to be  $0.96-0.16+0.28+0.00= 1.08\mu\text{m}$  (actual recorded value from experiments is  $1.08\pm 0.03\mu\text{m}$  ( $n=2$ )).

<b>Factor / Response</b>	<b><math>d_{25}</math> (<math>\mu\text{m}</math>)</b>	<b><math>d_{50}</math> (<math>\mu\text{m}</math>)</b>	<b><math>d_{75}</math> (<math>\mu\text{m}</math>)</b>	<b>FPF</b>
Data Average $\pm \sigma$	$1.38 \pm 0.28$	$1.99 \pm 0.22$	$2.73 \pm 0.31$	$0.056 \pm 0.061$
Data Range	1.04 – 2.05	1.75 – 2.56	3.34 – 2.39	0.002 – 0.219
Model Intercept	0.96	1.83	2.59	0.093
<u>Excipient</u>	Significant ( $p=0.034$ )	Not Sign.	Not Sign.	Significant ( $p=0.001$ )
Lactose, SV94	0			0
Lactose, SV425	+ 0.19			- 0.042
Lactose, ML58	+ 0.22			- 0.056
Lactose, ML80	+ 0.28 ( $p=0.028$ )			- 0.054
Glucose	+ 0.11			+ 0.037
Calcium Phosphate	+ 0.38 ( $p=0.005$ )			+ 0.127 ( $p=0.001$ )
<u>Drug Concentration</u>	Not Sign.	Not Sign.	Not Sign.	Not Sign.
<u>Fluidization Conditions</u>	Significant ( $p=0.000$ )	Significant ( $p=0.000$ )	Significant ( $p=0.019$ )	Not Sign.
Re = 18440	0	0	0	
Re = 11070	+ 0.25	+ 0.29	+ 0.55	
Re = 7720	+ 0.73	+ 0.70	+ 0.89	

As could be gauged from Figure 4.12 and Table 4.4, the **fluidization conditions** shift the entire particle size distribution; Table 4.5 confirms that  $d_{25}$ ,  $d_{50}$ , and  $d_{75}$  of budesonide are all affected. Use of less turbulent (less energetic) actuation conditions, represented by a lower  $Re$ , results in the release of fewer fine particles and consequently an increase of all three particle size indicators to higher values. Remarkably, the actuation conditions did not have statistically significant effects on the FPF of budesonide, though this is in part the result of relatively few data points and high data variability for budesonide formulations. Changing the **excipient** appears to be a more reliable way of increasing the FPF than increasing the pressure drop during DPI actuation. The effects of **excipient size fraction**

on budesonide delivery were not considered since only 45-75 $\mu$ m sieve fractions were used for all excipients. (They were, however, examined for albuterol formulations.) The  $d_{50}$  value observed in the experiments ( $\sim 2\mu$ m) was in good agreement with the primary particle size measured by light scattering, described in Chapter 2.

#### 4.4.5.4 Statistical Analysis: Albuterol

The same analysis of particle size and FPF effects was conducted for albuterol; the results are shown in Table 4.6. As explained in Section 4.2.2 more experiments in the experimental design involved albuterol formulations, and excipient particle size was varied as well; hence the additional rows in the results table and more effects. Varying the **excipient**, has a significant effect on each of the response variables, the entire particle size distribution as well as the FPF. For  $d_{25}$  and FPF, the observed trends are largely in agreement with those observed for budesonide. Again, some of the most significant increases in particle size and FPF are observed for CP, indicating more efficient release of drug compared to the other excipients. Glucose provides another interesting result; the entire particle size distribution is shifted to higher particle sizes, while the FPF registers a decrease. This suggests that separation of fine particulate drug is limited, which supports prior suggestions that the small particles are most strongly affected by formulation changes. While the **size fraction of the excipient** does have statistically significant and consistent effects, the effects on the particle size are relatively minor. Use of the intermediate excipient sieve fraction (75-106 $\mu$ m) appears to result in higher FPF in most cases. The **concentration of drug** has a significant effect on the FPF, with the 1% drug concentration resulting in significantly higher FPF than the 0.5% concentration. (The comparison to 0.25% is less significant, perhaps once more due to the limited number of experiments using 0.25% drug concentration.) This result supports the active site hypothesis, whereby the drug first adheres to the most energetic ("active") sites of the carrier particles, and then (after active site saturation) distributes around the less energetic sites of the carrier particle. Thus, at higher drug concentrations active sites have been saturated and a larger fraction of drug is in contact at less

energetic carrier surface sites, from which it can detach more easily. In contrast to budesonide, for which particle size and FPF were barely affected, albuterol formulations are significantly affected by the fluidization conditions. Using more turbulent actuation conditions (higher Re) gives reliably smaller particle size and higher FPF. This result suggests once more that primarily the separation of small particles is enhanced during actuation.

**Table 4.6.** Effect of excipient, excipient sieve fraction, drug concentration, and fluidization conditions on the PSD (using  $d_{25}$ ,  $d_{50}$ ,  $d_{75}$  as surrogate markers) and FPF of deposited **albuterol**. In the model, created using SPSS software, the default value is given by the model intercept and the contribution for each factor is given in each column.

<u>Factor</u> / <u>Response</u>	<u><math>d_{25}</math> (um)</u>	<u><math>d_{50}</math> (um)</u>	<u><math>d_{75}</math> (um)</u>	<u>FPF</u>
Data Average $\pm \sigma$	0.94 $\pm$ 0.18	1.47 $\pm$ 0.16	2.10 $\pm$ 0.25	0.101 $\pm$ 0.051
Data Range	0.64 – 1.24	1.29 – 1.97	1.80 – 3.12	0.015 – 0.194
Model Intercept	1.05	1.32	1.80	0.193
<u>Excipient</u>	Significant (p=0.000)	Significant (p=0.000)	Significant (p=0.000)	Significant (p=0.004)
Lactose, SV94	0	0	0	0
Lactose, SV425	+ 0.30	+ 0.29 (p=0.003)	- 0.08	- 0.036
Lactose, ML58	+ 0.01	+ 0.03	+ 0.05	+ 0.134 (p=0.014)
Lactose, ML80	- 0.11	+ 0.05	+ 0.10	- 0.019
Glucose	+ 0.17	+0.31 (p=0.033)	+ 0.58 (p=0.006)	- 0.088
Calcium Phosphate	+ 0.49 (p=0.054)	+ 0.46 (p=0.001)	+ 0.65 (p=0.001)	+ 0.051
<u>Excipient Size Fraction</u>	Not Sign.	Significant (p=0.015)	Significant (p=0.001)	Significant (p=0.006)
45-75 $\mu\text{m}$		0	0	0
75-106 $\mu\text{m}$		- 0.02	- 0.04	+ 0.090 (p=0.005)
106-150 $\mu\text{m}$		+ 0.04	+ 0.09	+ 0.025
<u>Drug Concentration</u>	Not Sign.	Not Sign.	Not Sign.	Significant (p=0.003)
1.00%				0
0.50%				- 0.149 (p=0.001)
0.25%				- 0.041
<u>Fluidization Conditions</u>	Not Sign.	Significant (p=0.000)	Significant (p=0.000)	Significant (p=0.015)
Re = 18440		0	0	0
Re = 11070		+ 0.18 (p=0.065)	+ 0.35 (p=0.013)	- 0.041
Re = 7720		+ 0.46 (p=0.000)	+ 0.57 (p=0.000)	- 0.109 (p=0.000)

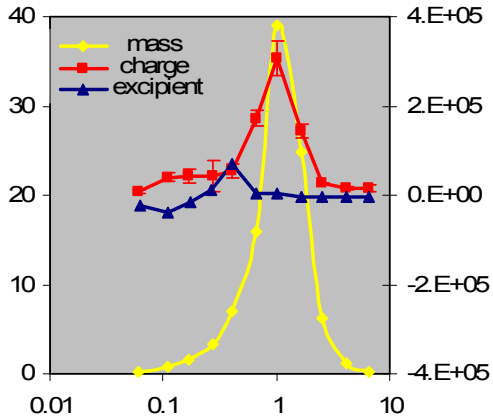
#### 4.4.6. Experimental Design Analysis: Effect of Formulation Factors on Electrostatic Charging of Drug

##### 4.4.6.1 Qualitative Analysis

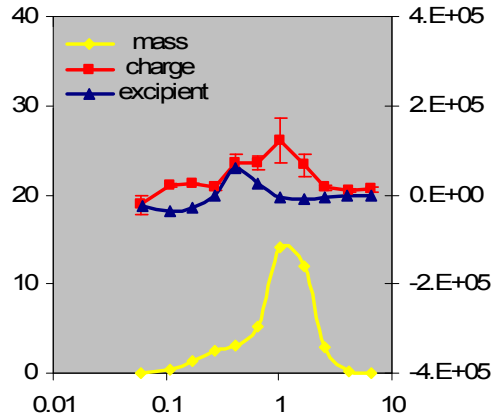
As in the previous case, it is instructive to first look at the effects on drug charging qualitatively. Figure 4.13 (a) through (f) show the effects of varying the excipient on the mass deposition and the charge deposition of 0.5% albuterol in 40mg of 45-75 $\mu$ m sieve fraction excipient formulations, actuated from SET A (at high sheer conditions). Figure 4.14 (a) through (f) show the same effects for budesonide formulations. The mass depositions of drug are shown in yellow diamonds (left axis), and the charge distribution (right axis) is shown in red squares.

From Figures 4.13 (a) through (f) it is evident that the FPM and the deposited charges vary significantly from excipient to excipient. While the charge deposition is largely positive for albuterol drug actuated from milled lactose (a and b) and glucose (e), sieved lactose formulations (Figures c and d) and the CP formulation (f) show bipolar charging. Clearly the mass depositions vary, but the overall shapes of the particle size distributions are similar (as might be expected, since it is the same drug). Yet the charge distribution is unique for each formulation. This clearly shows that the formulation has a profound effect on the charging behavior of the drug. Figure 4.14 makes the same point for formulations containing budesonide. The conditions are the same as in Figure 4.13, i.e. 0.5% budesonide in a 45-75 $\mu$ m fraction of the excipient, 40mg actuated from SET A. Note that in this case, the charge is mostly negative, with some bipolar charging observed for the formulation containing CP. Milled lactose formulations also show slight positive peaks in the 0.5 $\mu$ m range, which, however, are likely due to the deposition of some residual excipient particles in that size range (actuatiions of excipient only are shown in blue triangles). Unlike albuterol, the charge distributions of the different budesonide formulations are much more similar to one another, suggesting that the formulation has a smaller impact.

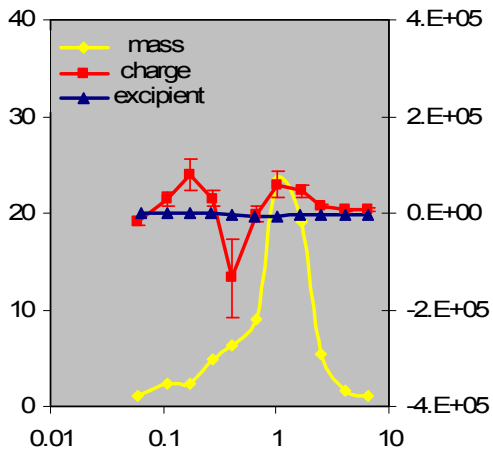
**Figure 4.13.** Effect of formulation excipient on FPM and charge distribution of albuterol. Mass depositions of drug ( $\mu\text{g}$ , yellow diamonds, axis on left), charge distribution of formulation (fC, red rectangles,  $n=3 \pm \sigma$ , axis on right), and excipient charging (fC, blue triangles, right axis) are shown. Each formulation is 0.5% albuterol in 45-75 $\mu\text{m}$  fraction of the excipient, 40mg actuated from SET A. Lines drawn between points for better visibility.



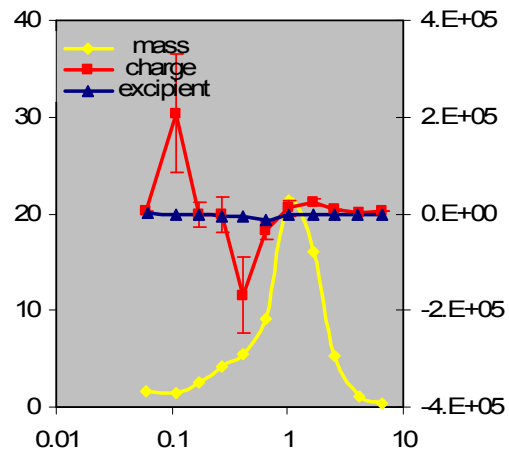
(a) 0.5% albuterol in 45-75 $\mu\text{m}$  sieve fraction ML80 lactose, 40mg, actuated from SET A.



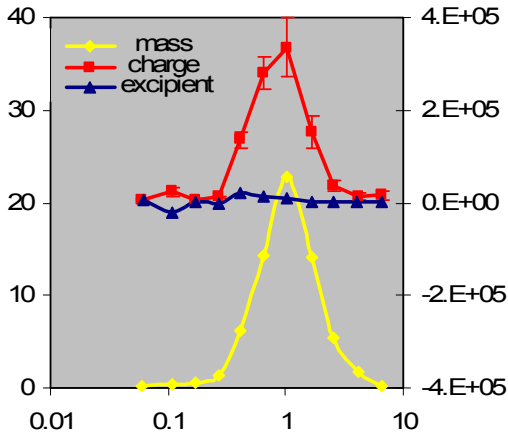
(b) 0.5% albuterol in 45-75 $\mu\text{m}$  sieve fraction ML58 lactose, 40mg, actuated from SET A.



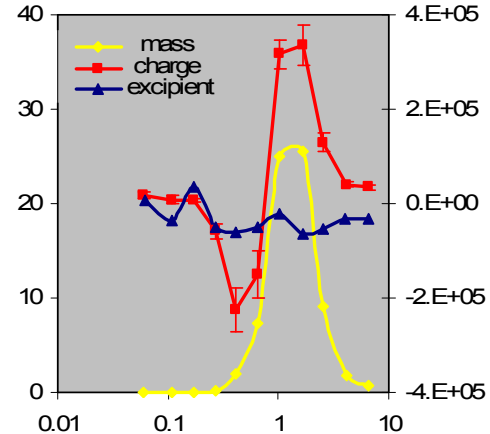
(c) 0.5% albuterol in 45-75 $\mu\text{m}$  sieve fraction SV425 lactose, 40mg, actuated from SET A.



(d) 0.5% albuterol in 45-75 $\mu\text{m}$  sieve fraction SV94 lactose, 40mg, actuated from SET A.

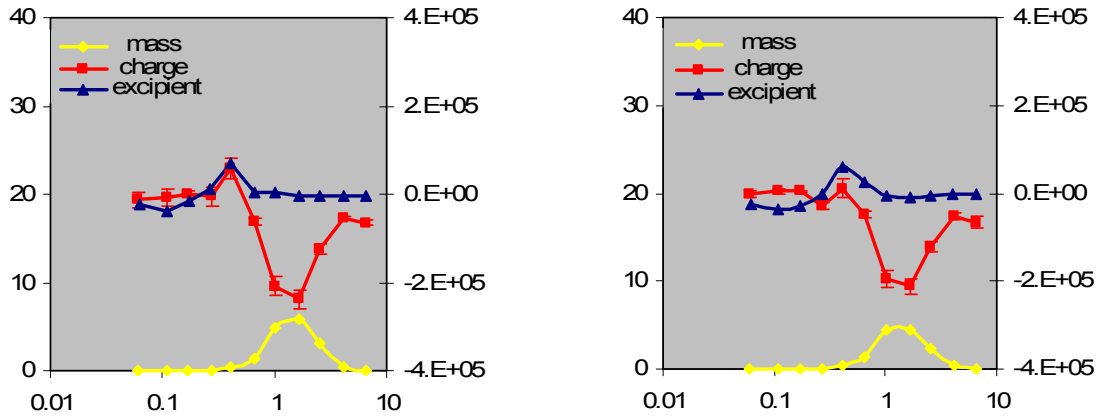


(e) 0.5% albuterol in 45-75 $\mu\text{m}$  sieve fraction glucose, 40mg, actuated from SET A.



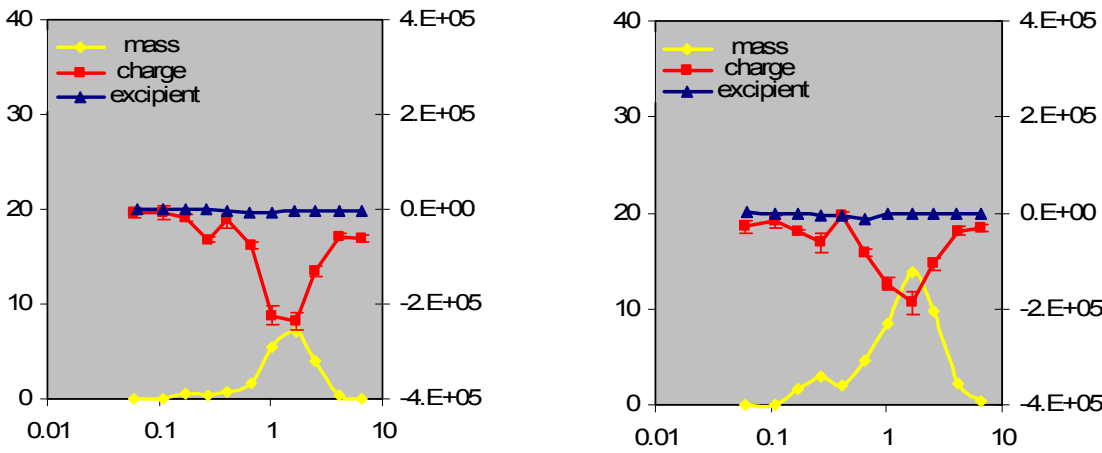
(f) 0.5% albuterol in 45-75 $\mu\text{m}$  sieve fraction Calcium phosphate, 40mg, actuated from SET A.

**Figure 4.14.** Effect of formulation excipient on FPM and charge distribution of budesonide. Mass depositions of drug ( $\mu\text{g}$ , yellow diamonds, left axis), charge distribution of formulation (fC, red rectangles,  $n=3 \pm \sigma$ , axis on right), and excipient charging (fC, blue triangles, right axis) are shown. Each formulation is 0.5% albuterol in 45-75 $\mu\text{m}$  fraction of the excipient, 40mg actuated from SET A. Lines drawn between points for better visibility.



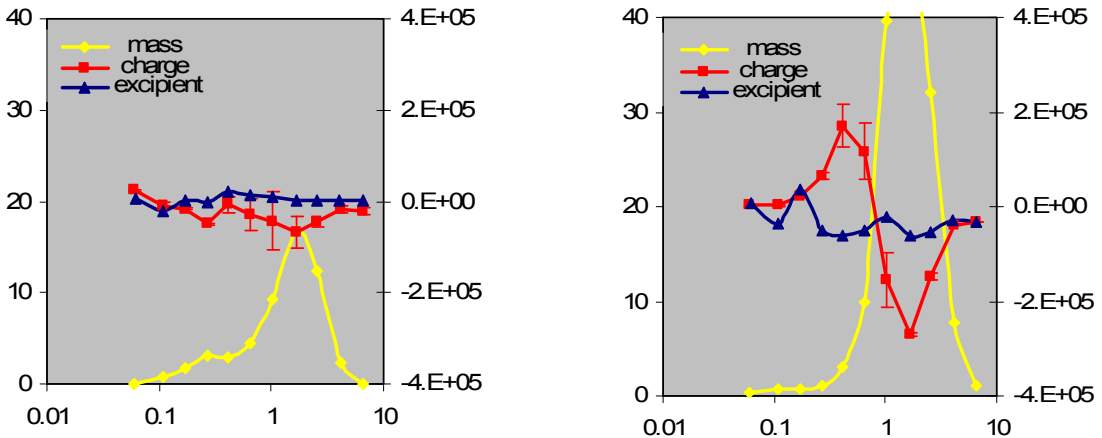
**(a)** 0.5% budesonide in 45-75 $\mu\text{m}$  sieve fraction ML80 lactose, 40mg, actuated from SET A.

**(b)** 0.5% budesonide in 45-75 $\mu\text{m}$  sieve fraction ML58 lactose, 40mg, actuated from SET A.



**(c)** 0.5% budesonide in 45-75 $\mu\text{m}$  sieve fraction SV425 lactose, 40mg, actuated from SET A.

**(d)** 0.5% budesonide in 45-75 $\mu\text{m}$  sieve fraction SV94 lactose, 40mg, actuated from SET A.



**(e)** 0.5% budesonide in 45-75 $\mu\text{m}$  sieve fraction glucose, 40mg, actuated from SET A.

**(f)** 0.5% budesonide in 45-75 $\mu\text{m}$  sieve fraction Calcium phosphate, 40mg, actuated from SET A.

#### 4.4.6.2 Charging Differences between Polydisperse Particles

One striking feature observed throughout Figures 4.13 and 4.14 is that different drug particle size fractions show differences in charging behavior. The charging behavior does not follow the particle size distribution, and cannot be explained by mass depositions on the given stages. For instance, when delivered from SV425 lactose (Figure 4.13(c)), albuterol particles smaller than  $\sim 0.5\mu\text{m}$  charge positive, particles between  $0.5\mu\text{m}$  and  $1.0\mu\text{m}$  charge negative, whereas particles above  $1\mu\text{m}$  charge positive again. Based on the small size of the error bars (showing standard deviation of  $n=3$  actuations), this charging pattern is quite reproducible. The effect is not related to the deposition of fine excipient particles either, which is minimal as shown by the blue graphs in the figures. Clearly, different drug size fractions have different charging properties.

The phenomenon of charging between particles within a polydisperse mixture of a material having the same chemical composition (and thus presumably the same effective work function) has been observed in other natural and industrial settings.<sup>22-24</sup> In polydisperse mixtures with many surface contacts, it was found that smaller particles typically acquire an excess of negative charge while the larger particles tend to charge more positive.<sup>23-25</sup> The phenomenon has recently been explained using a largely statistical argument in conjunction with particle dynamics simulations;<sup>26</sup> it was postulated that high energy electrons are initially uniformly distributed, and during a mixing process concentrate on the surface of the smaller particle fraction, leaving the smaller particles with an excess of electrons relative to larger particles in the mixture.

However, this explanation does not adequately describe the DPI system, where the larger drug particles are not necessarily more positively charged. Moreover, in the DPI formulation, the drug particles are primarily in contact with the excipient. Both drug and excipient are somewhat disperse within some defined particle size ranges (in the figures it is  $0.1\text{-}8\mu\text{m}$  for the drug, and  $\sim 45\text{-}75\mu\text{m}$  for the excipient particles). The bimodal charging phenomena observed in this study are more complicated and no adequate explanation can be offered. However, given the small drug particle size and the low concentration, the drug particles cannot be controlled directly. Instead, the formulation

components and variables offer the better opportunity for drug particle control so we now turn to the statistical analysis of the contributions of the formulation variables to drug triboelectrification.

#### 4.4.6.3 Statistical Analysis: General

As was the case for the particle size and mass deposition data, the charge distribution data (consisting of charge distribution data for each ELPI stage over time) were consolidated into a smaller number of descriptive parameters and analyzed using SPSS. As before, the general linear model multivariate procedure was applied. The data in the results tables, Tables 4.7 (budesonide) and 4.8 (albuterol) are organized as previously discussed as well. As in the previous results tables, the average and the data range are shown in the first two rows. Note that the data average is just the simple, non-weighted average of all measurements of a given response. This is important to remember because the statistical design is unbalanced, that is more experiments were conducted around a central set of conditions (e.g. milled lactose excipient) than for the other formulations and conditions; this explains part of the variability.

It is clear that for both budesonide and albuterol formulations the data variability is very large. Some of this variability is due to the natural variability of the observed phenomena, i.e, the random element in charging phenomena. However, it is important to recognize that some of the extreme data points may be subject to experimental error. Nonetheless, to prevent the introduction of bias into the analysis, no data points were removed from the analysis. Since the dataset is extensive, the analysis should not be overwhelmed by the influence of outliers.

Two important response variables were the total charge and the dominant polarity. However, to understand the strength of the charging phenomena it is important to determine charge effects relative to the quantity of drug that is delivered. Charge deposition was recorded using the ELPI and deposition of drug was determined from chemical assay of the ELPI stages. Having this data, there are a number of different ways in which the two measures could be correlated. Several different response factors were evaluated in this analysis. Each response variable correlates charge to quantity



of drug in a different way using a different set of assumptions; as discussed below the response variables used are normalized for mass (sum of charge per mass, average per particle charge), or normalized for surface area (charges per surface area). The different response factors are described in detail:

- (1) Polarity of Charge is determined by summing all the charges recorded for a given deposition across all the stages and then, depending on the polarity of the charge, assigned a -1 or a +1. This response variable is very simple and requires no assumptions. However, since the value can only be either +1 or -1, the response is nominal and thus not scalable.
- (2) The total of absolute charge (Sum  $|Q|$ ), given in units of nC, is simply the total of the absolute values of charge recorded across the different ELPI stages. This response does not take into account the quantity of material delivered. It is nevertheless considered as a first step, since the charging phenomena could also turn out to be a property of the actuation process, relatively independent of mass.
- (3) Absolute charge per mass (Sum  $|Q| / m$ ), given in units of  $\mu\text{C/g}$ , is determined by summing all the absolute values of the charges recorded across all the ELPI stages and then dividing by the total mass that was recovered from all the stages. The calculation makes no assumptions, but may oversimplify and skew the charging response, which depends more on surface area than mass.
- (4) Charges/Area, given in elementary charges ( $1 e^- = 1.6 \times 10^{-19}\text{C}$ ) per  $\mu\text{m}^2$  is the sum of charges divided by the surface area of the deposited drug particles. This response variable assumes that the deposition of drug on each stage consists of spheres with particle size exactly at the midpoint between the cutoff sizes of the corresponding and the previous stage. Clearly, this is an oversimplification; the drug particles are not uniform spheres, but are prismatic in shape and present a distribution of sizes. The assumption of sphericity underestimates the true surface area, which is likely to be a factor larger; thus, the true charges / area measures are likely to be smaller. But this inaccuracy should not affect the outcome of the analysis, since it applies the simplifying assumption to all size fractions for each drug. The two drugs are not analyzed jointly, so

differences in particle shape should not bias the outcome of the statistical analysis either. Since charging is a surface effect, differences in the magnitude of this measure are probably the most physically meaningful indications of charging strength.

(5) Average charges per particle (stages 7-10) is the estimated per-particle charge (in elementary charges) for drug deposited on stages 7-10, which includes particles from 0.655 $\mu\text{m}$  (cutoff size of stage 7) to 4.09 $\mu\text{m}$  (cutoff size of stage 11). These four stages account for at least 70% (and in most cases over 85%) of total drug deposited inside the ELPI. Due to the high material depositions on these stages there is a high level of confidence associated with the mass determinations. Using the material densities (1.3g/cm<sup>3</sup> for albuterol, 1.25g/cm<sup>3</sup> for budesonide)<sup>27</sup> and basic geometric assumptions (particles are uniform spheres of average size for a given stage) the mass depositions on each stage are converted into numbers of particles. The charge collected on each stage is divided into elementary charges, which are divided by the number of particles. This measure is an oversimplification and is likely a source of some error, though the approach is uniform and does not introduce any bias into the statistical analysis. While the charge density (charge per area, in (4)) is physically the most important response, the per particle charge is probably the most clinically relevant measure. It is, after all, the total charge on a particle that determines how the particle experiences the forces of other charges, including image forces of neutral surfaces, and how it is affected in its trajectory and deposition. Furthermore, this measure is an important intermediate in addressing Hypothesis 4, as will be discussed in more detail in the next section.

While the three normalized response variables (3-5) use different assumptions and correlate data in different ways, they follow the same basic trends in most cases. As a result, not all of them need to be discussed individually in detail.

#### 4.4.6.4 Statistical Analysis: Budesonide

Table 4.7 summarizes the effects of formulation variables on the charging behavior of budesonide particles. The drug consistently charged negatively and the polarity was not affected by the identity of the excipient. On the other hand, every single other response was significantly affected by the choice of **excipient**, the **concentration** of the drug, the **fluidization conditions** and even the **dose**. The effects of drug concentration, fluidization conditions, and dose on the absolute magnitude of the charge are expected and are related in part to the larger drug depositions. However, as the mass normalized charge measures show, the effects are smaller than might be expected based on mass depositions alone. On a per particle basis, the milled lactose batches result in the strongest (negative) charging of the drug particles, while glucose and CP result in least charge per particle. The lower **drug concentrations** of 0.25% and 0.50% produce higher particle charges than the higher 1% drug concentration formulations. This may be the result of stronger contact charging due to closer drug-excipient contact in lower concentration drug blends. (The smallest charge contribution of the 0.25% formulation does not support this conclusion, though the effect of this variable is variable and lacks statistical significance.) The charge contribution associated with the drug concentration is minor compared with the effects of excipient or fluidization conditions. **Fluidization conditions** significantly affect the charge. The parameter estimates for this effect are counterintuitive: the analysis reveals higher per particle charges for the less intense fluidization conditions ( $Re=11070$  and  $7720$ ) than the more turbulent conditions ( $Re=18440$ ). A possible explanation is that when fewer particles are dispersed, the likelihood of contact and charge backflow in transit is smaller, i.e. it is less likely that opposite charges cancel each other. This explanation is supported by the fact that the smaller actuation **dose** also gives rise to more highly charged particles. Additionally, as shown in the previous section, the lower  $Re$  fluidization conditions result in the release of fewer fine particles shifting the distribution to larger particles, which have larger surface areas and can accommodate more charges.

To see if these results hold for albuterol, we turn to the results of the statistical analysis of the albuterol formulations.

**Table 4.7.** Formulation variables contributing to the charging of **budesonide**. Effect of excipient, excipient size fraction, drug concentration, fluidization conditions, and dose on the charging behavior of fine particulate albuterol. In the model, created using SPSS software, the default value is given by the model intercept and the contribution for each factor is given in each column. Also shown is the significance level of the formulation variable (from ANOVA), as well as the level of significance for each individual variable level (where  $p \leq 0.05$ ).

<b>Factor / Response</b>	<b>(1) Polarity of Charge</b>	<b>(2) Sum  Q  (nC)</b>	<b>(3) Sum  Q  / m (<math>\mu\text{C/g}</math>)</b>	<b>(4) Charges/Area (<math>\text{e}^-/\mu\text{m}^2</math>)</b>	<b>(5) Avg charges per particle (stages 7-10)</b>
Data Average $\pm \sigma$	-1 $\pm$ 0	0.73 $\pm$ 0.27	64.8 $\pm$ 76.4	1333 $\pm$ 2003	6112 $\pm$ 7930
Data range	-1	0.35 – 1.31	6.9 – 304.1	70 - 8054	363 - 32312
Model Intercept	-1	1.20	-8.8	-294	-296
<u>Excipient</u>	Not Sign.	Significant (p=0.008)	Significant (p=0.000)	Significant (p=0.000)	Significant (p=0.003)
Lactose, SV94		0	0	0	0
Lactose, SV425		+ 0.11	+ 23.3 (p=0.006)	+ 379 (p=0.005)	+ 1640 (p=0.039)
Lactose, ML58		+ 0.00	+ 40.7 (p=0.001)	+ 759 (p=0.000)	+ 3210 (p=0.005)
Lactose, ML80		+ 0.11	+ 38.6 (p=0.001)	+ 762 (p=0.000)	+ 2690 (p=0.011)
Glucose		- 0.31 (p=0.020)	- 9.8	- 104	- 971
Calcium Phosphate		+ 0.24 (p=0.047)	- 7.6	- 76	- 874
<u>Drug Concentration</u>	Not Sign.	Significant (p=0.000)	Significant (p=0.000)	Significant (p=0.000)	Significant (p=0.000)
1.00%		0	0	0	0
0.50%		- 0.43 (p=0.010)	+ 25.4 (p=0.008)	+ 487 (p=0.003)	+ 1690 (p=0.056)
0.25%		- 0.90 (p=0.000)	+ 0.2	- 156	+ 773
<u>Fluidization Conditions</u>	Not Sign.	Significant (p=0.003)	Significant (p=0.006)	Significant (p=0.000)	Significant (p=0.000)
Re = 18440		0	0	0	0
Re = 11070		- 0.37 (p=0.010)	+ 10.2	+ 258 (p=0.022)	+ 2040 (p=0.018)
Re = 7720		- 0.52 (p=0.004)	+ 248.8 (p=0.000)	+ 7100 (p=0.000)	+ 2820 (p=0.000)
<u>Dose</u>	Not Sign.	Significant (p=0.003)	Significant (p=0.006)	Significant (p=0.010)	Significant (p=0.041)
40mg		0	0	0	0
20mg		- 0.33 (p=0.028)	+ 2.0	+ 38.6	+ 158

#### 4.4.6.5 Statistical Analysis: Albuterol

**Table 4.8.** Formulation variables contributing to the charging of **albuterol**. Effect of excipient, excipient size fraction, drug concentration, fluidization conditions, and dose on the charging behavior of fine particulate albuterol. In the model, created using SPSS software, the default value is given by the model intercept and the contribution for each factor is given in each column. Also shown is the significance level of the formulation variable (from ANOVA), as well as the level of significance for each individual variable level (where  $p \leq 0.05$ ).

<b>Factor / Response</b>	<b>(1) Polarity of Charge</b>	<b>(2) Sum  Q  (nC)</b>	<b>(3) Sum  Q  / m (<math>\mu\text{C/g}</math>)</b>	<b>(4) Charges/Area (<math>\text{e}^-/\mu\text{m}^2</math>)</b>	<b>(5) Avg charges per particle (stages 7-10)</b>
Data Average $\pm \sigma$	0.74 $\pm$ 0.68	0.77 $\pm$ 0.52	6.3 $\pm$ 12.9	142 $\pm$ 80	542 $\pm$ 381
Data Range	-1 – +1	0.89 – 2.12	1.5 – 30.5	16.5 – 395.3	43 – 2092
Model Intercept	0	0.72	- 6.1	- 49.9	-277
<u>Excipient</u>	Significant (p=0.011)	Significant (p=0.013)	Significant (p=0.001)	Significant (p=0.000)	Significant (p=0.000)
Lactose, SV94	-1	0	0	0	0
Lactose, SV425	$\pm$ 0	+ 0.26	+ 10.6 (p=0.008)	+ 127.2 (p=0.002)	+ 138
Lactose, ML58	+ 1 (p=0.000)	+ 2.10 (p=0.009)	+ 16.2 (p=0.026)	+ 207.3 (p=0.005)	+ 842 (p=0.01)
Lactose, ML80	+ 1 (p=0.000)	+ 0.63	+ 13.2 (p=0.002)	+ 117.1 (p=0.002)	+ 597 (p=0.03)
Glucose	+ 1 (p=0.000)	- 0.08	+ 16.4 (p=0.016)	+ 191.1 (p=0.005)	+ 1236 (p=0.000)
Calcium Phosphate	+ 1 (p=0.000)	+ 1.47 (p=0.012)	+ 19.2 (p=0.002)	+ 316.9 (p=0.000)	+ 1599 (p=0.000)
<u>Excipient Size Fraction</u>	Not Sign.	Significant (p=0.015)	Significant (p=0.000)	Significant (p=0.001)	Significant (p=0.006)
45-75 $\mu\text{m}$		+ 0.34	+ 9.6 (p=0.018)	+ 96.4 (p=0.013)	+ 216
75-106 $\mu\text{m}$		0	0	0	0
106-150 $\mu\text{m}$		- 0.91 (p=0.028)	- 5.2	- 47.2	- 135
<u>Drug Concentration</u>	Not Sign.	Significant (p=0.007)	Significant (p=0.001)	Significant (p=0.005)	Significant (p=0.002)
1.00%		0	0	0	0
0.50%		- 0.61	+ 13.8 (p=0.014)	+ 86.9	+ 245
0.25%		- 0.87 (p=0.035)	+ 6.1	+ 72.2 (p=0.048)	+ 216
<u>Fluidization Conditions</u>	Not Sign.	Significant (p=0.002)	Not Sign.	Significant (p=0.010)	Significant (p=0.000)
Re = 18440		0		0	0
Re = 11070		- 0.79		- 3.7	+ 267
Re = 7720		- 0.78 (p=0.030)		+ 110.5 (p=0.003)	+ 65
<u>Dose (mg)</u>	Not Sign.	Significant (p=0.004)	Significant	Not Sign.	Not Sign.
40		0	0		
20		- 0.50	+ 2.59		

The effects that the formulation variables have on the charging of albuterol are summarized in Table 4.8. With a larger number of trials conducted, the dataset around albuterol is richer (it includes an analysis of excipient size fractions as well), and as a result there is more confidence in the individual parameter estimates. The **excipient** clearly impacts the polarity of charge. Whereas budesonide always charged negatively, albuterol charged either positive or negative, depending on the excipient in the formulation. Formulated with SV94 lactose, albuterol particles were predominantly negatively charged. Formulated with the other sieved lactose batch, SV425, albuterol particles were either negatively or positively charged, whereas in combination with glucose and CP albuterol primarily charged positively. It can be deduced that albuterol has a pseudo work function that is somewhere in between that of sieved lactose and glucose. No other variables affected charge polarity significantly. However, all formulation variables, i.e. excipient, excipient size fraction, drug concentration, and fluidization conditions had effects on absolute and relative charge magnitudes. In the case of **drug concentration**, **fluidization conditions**, and **dose**, larger charges were associated with increased deposition of drug, that is higher concentration, more turbulent charging, and larger dose resulted in higher charge depositions. However, a look at the normalized responses shows that increased mass delivery does not fully account for the additional charge. As seen before with budesonide, smaller drug concentrations and less turbulent actuation conditions result in higher per particle charges. The positive effect of the smaller drug concentration on charge supports the active site hypothesis, i.e. that lower drug concentrations result in closer particle contact (possibly at active surface sites) and thus stronger contact charging. The lower Re actuation conditions also result in higher per particle charges, though the effects are variable and the individual parameter contributions lack statistical significance. Nevertheless, this result is in agreement with the results for budesonide. As stated previously, one explanation for this is the shift towards larger particle sizes which can accommodate larger charges. Another reason for this result is that fewer dispersed particles create fewer opportunities for charge neutralization or backflow. **Excipient particle size** also contributes to particle charging. The charge of the delivered drug decreases as the excipient particles increase in

size. While the overall contribution of the effect is modest, the effect is nonetheless consistent with a surface area effect; as the carrier particles become larger, their specific surface area decreases and the drug particles reach a higher degree of surface saturation on the carrier particle surface. The drug particles become less charged, because there is less surface area available with which to exchange electrons. This explanation may be seen as an extension of the active site hypothesis, provided the highly energetic surface sites are also more prone to electron exchange.

Comparing the charging effect of the excipient reveals an apparent paradox: CP and glucose result in the least charged budesonide particles, but they give rise to the most highly charged albuterol particles. These observations seem at odds, but are actually consistent with each other when the polarities of the charges are considered: in both instances, CP and glucose result in the most positive drug charges. This allows CP and glucose to be placed at the very top of the triboelectric series. Construction of a triboelectric series for the materials and the ramifications thereof are discussed in the next section.

#### 4.4.7. Triboelectric series

Based on the observed charging behavior we can construct triboelectric series for the excipients and drugs. As discussed in Chapter 1, a triboelectric series ranks materials in order of polarity of charge after contact charging and separation from another material, in this case contact charging between the drug and an excipient. Triboelectric series are constructed for insulators for which work functions cannot be measured reliably.

Based on charges/area data ( $\text{Sum } Q / A$ ), albuterol acquires charge in the following order after separation from the given excipients:

Albuterol: (most positive) CP > Glucose > ML58  $\approx$  ML80 > SV425 ( $\pm 0$ ) > SV94 (negative)

Note that this order is slightly different from what might be expected based on individual contributions in Table 4.8 because the results of the statistical analysis were obtained by treating charge magnitude and polarity strictly separated to avoid cancellation of opposite charges recorded on

different stages in the summation process. Given these charges on albuterol, and assuming the charges resulted in equal but opposite countercharges on the excipient particles, the triboelectric series looks as follows:

(+) SV94 > SV425 ≈ Albuterol > ML80 ≈ ML58 > Glucose > CP (-)

Similarly, based on charges/area raw data (Sum Q / A), budesonide acquires charges in the following order in the given excipients:

Budesonide: (least negative) CP > Glucose > SV94 > SV425 > ML58 > ML80 (most negative)

Based on this charging order, the triboelectric series would look like this:

(+) ML80 > ML58 > SV425 > SV94 > Glucose > CP > Budesonide (-).

It is difficult to reconcile these triboelectric series and consolidate them into one. Doing so would result in the following triboelectric series:

(+) ML80 ≈ ML58 ≈ SV425 ≈ SV94 ≈ Albuterol > Glucose > CP > Budesonide (-).

While CP and glucose consistently seem to result in the most positively (or least negatively) charged drug, the lactose excipients behave less predictably; the differences between them are less pronounced. This seems reasonable given the lactose batches are the same material and batch-to-batch differences are expected to be relatively smaller. Another reason for the difficulty in creating a consolidated triboelectric series is the fact that the charges associated with budesonide particles are about an order of magnitude larger than those associated with albuterol. Differences in excipient size fraction were not considered since they are insignificant compared to inter-excipient differences.

In an attempt to create a consolidated triboelectric series the data were also analyzed using SPSS. Using a reduced data set, containing actuations involving both drugs, but only the 45-75um sieve fractions of the excipients, and only two of the fluidization conditions, the program converged to a model and provided parameter contribution estimates. The results, indicated a high degree of co-dependency between the factors, resulting in strong secondary effects involving drug-lactose batch combinations. Even when the two ML and two SV batches were combined into one ML and SV batch each, the codependency persisted. This shows that while different lactose batches can be



differentiated from one another using charge deposition studies in the ELPI, their behavior is hard to predict *a priori* when combined with a different drug. This may also indicate simply that the effective work function of albuterol is close to that of the lactose batches, resulting in more variable behavior. On the other hand, CP and glucose behave in a way consistent with their relative position in the triboelectric series. Moreover, the results are largely consistent with the results from Faraday well experiments and surface free energy measurements, which suggested budesonide, CP, and glucose charged most negatively (Faraday well experiments) and CP and glucose had most electron accepting surface characteristics. The agreement among the three measurements is a very important result.

#### 4.4.8. Per Particle Charge Levels

One of the primary aims of this research project was to determine the role electrostatic charging plays in DPI particle interactions. Knowing that it arises from triboelectric charging and that it is highly dependent on formulation factors is important, but before this knowledge can be exploited to advance the formulation development of DPIs, it is necessary to understand the impact of charging. A number of simulation<sup>28</sup> and *in vivo*<sup>29</sup> studies have suggested that micron-size particles need to have charges in the 100s of elementary charges range to be affected in their trajectory and their deposition in the respiratory tract. Using Faraday cage data and some basic geometric assumptions, Byron et al.<sup>30</sup> estimated DPI particles could have charges in the 200e per particle range.

The results of this study indicate triboelectric charging in the DPI can give rise to significant charging with charge levels that are much higher than previously estimated. Surveying the data range for budesonide formulations (Table 4.7) and albuterol formulations (Table 4.8), the data indicate per particle charge levels of  $542 \pm 381$  and  $6112 \pm 7930$  elementary charges per particle (unbalanced, non-weighted means of entire dataset  $\pm$  standard deviation) on albuterol and budesonide particles in the  $0.655\mu\text{m}$  (stage 7) to  $4.09\mu\text{m}$  (stage 10) range, respectively. Particles in this size range account for the bulk of the drug delivered to the lungs. Figure 4.15 shows the entire charge distribution (absolute magnitude) for two representative formulations, 0.5% budesonide in ML80 lactose (45-

75 $\mu$ m sieve fraction) and 0.5% albuterol in ML58 lactose, as well as the upper and lower charge limits. The lower limit is the Boltzmann equilibrium charge distribution, which is the charge level expected for naturally occurring aerosols; it was calculated using equation 1.7. The upper limit is the negative charge limit for solid particles, above which spontaneous emission of electrons from a surface is expected; the points in this graph were determined using equation 1.8. The graphs indicate very high charges, well into the 1,000s and even 10,000s of elementary charges per particle range. These charges, which are by no means the highest charge levels recorded in these experiments, far exceed the Boltzmann equilibrium charge distribution. They are clearly the result of an active charging process, specifically contact charging in the formulation. Yet, as indicated in Tables 4.7 and 4.8, the formulation variables have significant effects on the charge distribution and can in fact produce much higher particle charge levels.

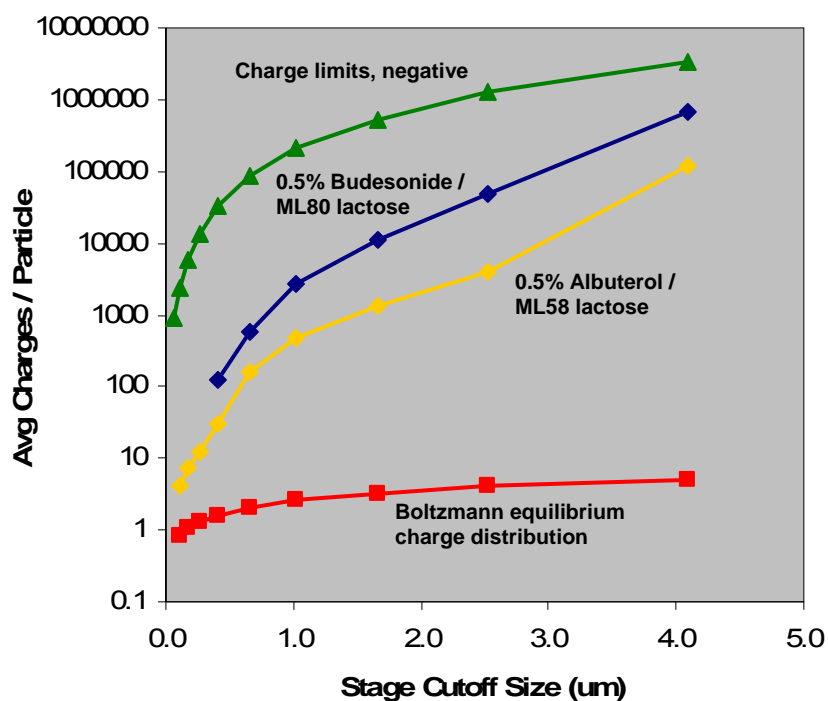


**Figure 4.15.** Charge distribution (average particle charge) for drug deposited in ELPI. Shown are 0.5% budesonide in ML80 lactose (45-75 $\mu$ m) (blue diamonds), 0.5% albuterol in ML58 lactose (45-75 $\mu$ m) (yellow diamonds), both actuated from SET A (high Re). For comparison, the graph shows the charge limit expected for the particles (green triangles) and the Boltzmann charge distribution (red squares). In both cases, over 80% of the deposited particles carry >100 charges per particle.

An important question is how this charging compares to other processes. As cited by Johnston et al.<sup>31</sup>, Kosenko conducted studies of aerosol charging in industrial processes and found the most highly charged aerosol particles (resulting from sandblasting operations) to have mean charge levels in the order of 30 elementary charges per  $\mu\text{m}^2$ . This level is much lower than the mean charge of  $142 \pm 80e$  observed for albuterol particles and  $1333 \pm 2003e$  per  $\mu\text{m}^2$  observed for budesonide particles. Johnston et al. conducted their own studies in the laboratory and found mean charges of  $550e$  for  $4\mu\text{m}$  quartz particles dispersed in a fluid bed dryer.<sup>32</sup> Again, these charges are much smaller than those that can be generated during DPI actuation. The reason for this is likely the close and prolonged contact of the drug and excipient particles in the formulation, followed by the vigorous separation.

#### 4.4.9. Study Design Critique

Considerable thought went into developing an efficient experimental framework that effectively tested the hypotheses using a relatively small number of experiments in a comprehensive manner. The experimental scheme developed used only 33 formulations and 63 experiments (not counting replicates that were employed to challenge the intrinsic variance) to examine a large number of possible interactions. Including duplicates and auxiliary experiments designed to test specific conditions, over 100 ELPI experiments were conducted. The large dataset generated by these experiments elucidate the contributions of different formulation variables to charge of delivered drug.

However, the experimental design has some weaknesses. Insufficient experiments were allocated to the low fluidization conditions ( $Re=7720$ ) and the low drug concentration (0.25%) for the results to be useful in determining trends. Clearly, the inherent variability of the triboelectric charging process has been underestimated. Similarly, only one experiment each was assigned to the intermediate and boundary conditions of dosing 30mg and 10mg of formulation, respectively. The data set consisting of 10mg, 20mg, 30mg, and 40mg formulation 1% albuterol in 45-75um ML80 lactose does not show

a consistent trend with respect to any of the charge measures. More experiments should have been conducted for these conditions.

An additional flaw was an underestimation of the potential of the strong storage effects which provide very interesting insight into the storage process but effectively reduce the number of replicates and, thus, reduce the statistical power that could be applied towards the analysis of formulation effects, which were the primary objective of the study.

Last, while the study clearly shows differences in the dispersion and charging behavior of the different lactose batches, the differences are smaller and more variable than those seen between different materials. As a result the different lactose batches cannot be applied towards the creation of a triboelectric series.

#### **4.5. Summary and Conclusion**

The ELPI offers significant advantages for studying electrostatic interaction between the particles in DPI formulations. The most significant advantage, which sets the instrument apart from other scientific instruments or experimental apparatuses, is its ability to measure particle size and charge distributions simultaneously for particles in the single-micron range, the size range required for respiratory drug delivery. An experimental apparatus was developed that allowed different DPI formulations to be tested at the commonly used 60L/min flow rate and deposition to be measured within the ELPI. An experimental framework was devised to test which formulation factors contribute to triboelectric charging in DPI formulations. The framework included roughly 100 experiments (including replicates and auxiliary experiments), of which a number of replicates had to be excluded due to storage effects.

The remaining experiments offer an extensive data set of charge and mass deposition data that give insight into which formulation factors contribute to triboelectric charging in the DPI. The choice of excipient is clearly important and most profoundly affects the charge characteristics of the deposited drug. Batch to batch variability in the behavior of the four lactose batches was clearly

indicated. However, a consolidated triboelectric series for all materials could not be established; it is clear that some excipients behave differently when combined with albuterol or budesonide, which shows the difficulty in determining certain effects *a priori*.

The particle size of the excipient also appears to have an effect on the charge profile of deposited drug, with smaller particles (with increased surface area) giving rise to stronger charging interactions.

The concentration of drug in the DPI formulation was also shown to affect the particle charge; lowering the drug concentration results in lower fine particle fractions with more highly charged drug particles, a result that adds weight to the often cited "active site hypothesis": due to lower surface coverage drug particles are concentrated around more energetic carrier particle surface sites where forces are stronger and electron exchange may be more extensive; as a result fewer particles separate from the carrier.

The actuation conditions also have a strong effect on the particle size and charge distribution of drug. Contrary to expectations, however, the more turbulent conditions result in somewhat lower per particle charge levels. This result is consistent with the idea that contact charging is the cause of the particle charge and that fluidization merely affects the particle separation process. A lower delivered dose also slightly raises the particle charge level. An explanation for these unexpected results is that a smaller amount of dispersed drug decreases the chance of opposite charges canceling each other during transit or deposition.

While the study provided statistically strong evidence to show the profound effect of some formulation variables, the study design also had some drawbacks. The inherent variability of the charging phenomena was underestimated; as a result some of the marginal conditions that were written into the design to test response surface curvature lacked sufficient data and, thus, statistical power to give conclusive results: the very low drug concentration of 0.25% and the very low Re actuation conditions have too few response points and too much variability to provide trends.

The results indicate that particle charging in DPI formulations is highly significant. Charging is at least one order of magnitude higher than had previously been estimated, and greater particle charges

are generated during DPI actuation than in other industrial or laboratory processes studied thus far. The particle charge levels are indicative of the active contact charging process, and provide a scientific basis for the problems with electrostatic charging which have been observed in the clinical use of respiratory delivery devices, MDIs and DPIs.

The charge levels are high enough to have clinical consequences, either due to change in trajectory, adhesion to device, or modified *in vivo* deposition patterns. It is clear, electrostatic interactions should be studied as part of the DPI formulation development and characterization process. Failure to consider the process presents a significant liability for product performance. At best it is a lost opportunity to moderate a phenomenon that can be affected through formulation considerations. Table 4.9 summarizes how charging can be affected.

Table 4.9. Using formulation techniques to affect drug charging.

<b>To minimize drug particle charge</b>	<b>To maximize drug particle charge</b>
- Increase drug coverage (drug concentration) of excipient particle	- Reduce drug concentration
- Increase excipient particle size	- Decrease excipient particle size
- Use excipients with similar effective work function (i.e. close position in triboelectric series)	- Use excipients with different effective work function (i.e. further removed from drug in triboelectric series)

Finally, it is particularly noteworthy that the charging behavior brought about by the different excipients is consistent with observations stemming from Faraday well experiments and IGC studies. The triboelectric series, developed based on drug charge levels measured in the deposition studies agrees with the triboelectric series constructed from raw material bulk electrostatic charging studies, and with a ranking of the materials based on measured surface acid/base properties. While the comparison is based on semi-quantitative rank-order correlations, it is nevertheless a strong indication that the three processes are correlated.

The next chapter discusses these results in a wider framework and in combination with the results of the IGC studies and Faraday well data, which complete our understanding and help evaluate the hypotheses. The hypotheses are revisited and recommendations for future studies are made.

#### **4.6 Acknowledgements**

Dr. Chris Wiesen, Statistical Consultant at the UNC Odum Institute is gratefully acknowledged for valuable discussions of the experimental design and help with the analysis.

#### 4.7 Literature Cited

1. Keskinen, J., Pietarinen, K. & Lehtimäki, M. Electrical Low-Pressure Impactor. *Journal of Aerosol Science* 23, 353-360 (1992).
2. Lehmann, U., Niemela, V. & Mohr, M. New method for time-resolved diesel engine exhaust particle mass measurement. *Environ Sci Technol* 38, 5704-11 (2004).
3. Maricq, M. M., Chase, R. E., Xu, N. & Podsiadlik, D. H. The effects of the catalytic converter and fuel sulfur level on motor vehicle particulate matter emissions: gasoline vehicles. *Environ Sci Technol* 36, 276-82 (2002).
4. Sanders, P. G., Xu, N., Dalka, T. M. & Maricq, M. M. Airborne brake wear debris: size distributions, composition, and a comparison of dynamometer and vehicle tests. *Environ Sci Technol* 37, 4060-9 (2003).
5. Holmen, B. A. & Qu, Y. Uncertainty in particle number modal analysis during transient operation of compressed natural gas, diesel, and trap-equipped diesel transit buses. *Environ Sci Technol* 38, 2413-23 (2004).
6. Brouwer, D. H., Gijssbers, J. H. & Lurvink, M. W. Personal exposure to ultrafine particles in the workplace: exploring sampling techniques and strategies. *Ann Occup Hyg* 48, 439-53 (2004).
7. Ferge, T., Maguhn, J., Felber, H. & Zimmermann, R. Particle collection efficiency and particle re-entrainment of an electrostatic precipitator in a sewage sludge incineration plant. *Environ Sci Technol* 38, 1545-53 (2004).
8. Kwok, P. C. L., Glower, W. & Chan, H.-K. Electrostatic charge characteristics of aerosols produced from metered dose inhalers. *J Pharm Sci* 94, 2789-2799 (2005).
9. Telko, M. J., Kujanpää, J. & Hickey, A. J. Investigation of triboelectric charging in dry powder inhalers using electrical low pressure impactor (ELPI). *Int J Pharm* 336, 352-60 (2007).
10. Marjamäki, M., Keskinen, J., Chen, D. R. & Pui, D. Y. H. Performance evaluation of the electrical low-pressure impactor (ELPI). *Journal of Aerosol Science* 31, 249-261 (2000).
11. Murtomaa, M., Strengell, S., Laine, E. & Bailey, A. Measurement of electrostatic charge of an aerosol using a grid-probe. *Journal of Electrostatics* 58, 197-207 (2003).
12. Murtomaa, M. et al. Effect of particle morphology on the triboelectrification in dry powder inhalers. *International Journal of Pharmaceutics* 282, 107-114 (2004).
13. Convention, U. S. P. in *The United States pharmacopeia. The national formulary 1765* (United States Pharmacopoeial Convention, Bethesda, MD, 1995).
14. *Physicians' desk reference* (Thomson PDR, Montvale, NJ, 2004).
15. Steckel, H. & Bolzen, N. Alternative sugars as potential carriers for dry powder inhalations. *Int J Pharm* 270, 297-306 (2004).



16. Ganderton, D. The generation of respirable clouds from coarse powder aggregates. *J. Biopharm. Sci.* 3, 101–105 (1992).
17. Clark, A. R. & Hollingworth, A. M. The Relationship between Powder Inhaler Resistance and Peak Inspiratory Conditions in Healthy-Volunteers - Implications for in-Vitro Testing. *Journal of Aerosol Medicine-Deposition Clearance and Effects in the Lung* 6, 99-110 (1993).
18. Louey, M. D., van Oort, M. & Hickey, A. J. Standardized entrainment tubing for the evaluation of pharmaceutical dry powder dispersion. *J Aerosol Sci* 37, 1520-1531 (2006).
19. Liu, B. Y., Pui, D. Y., Rubow, K. L. & Szymanski, W. W. Electrostatic effects in aerosol sampling and filtration. *Ann Occup Hyg* 29, 251-69 (1985).
20. Hinds, W. C. *Aerosol technology : properties, behavior, and measurement of airborne particles* (Wiley, New York, 1999).
21. Telko, M. J., Kujanpaa, J. & Hickey, A. J. Investigation of triboelectric charging in dry powder inhalers using electrical low pressure impactor (ELPI™). *Int J Pharm* 336, 352-60 (2007).
22. Cartwright, S., Singh, S., Bailey, A. G. & Rose, L. J. Electrostatic Charging Characteristics of Polyethylene Powder During Pneumatic Conveying. *IEEE Trans. on Ind. Appl.* 21, 541-546 (1985).
23. Zhao, H., Castle, G. S. P. & Inculet, I. I. The Measurement of Bipolar Charge in Poly-disperse Powders Using a Vertical Array of Faraday Pail Sensors. *J. Electrostatics* 55, 261-278 (2002).
24. Zhao, H., Castle, G. S. P., Inculet, I. I. & Bailey, A. G. Bipolar Charging of Poly-Disperse Polymer Powders in Fluidized Beds. *IEEE Trans. on Ind. Appl.* 39, 612-618 (2003).
25. Lacks, D. J. & Levandovsky, A. Effect of Particle Size Distribution on the Polarity of Triboelectric Charging in Granular Insulator Systems. *J. Electrostatics* 65, 107-112 (2007).
26. Duff, N. & Lacks, D. J. Particle dynamics simulations of triboelectric charging in granular insulator systems. *J. Electrostatics* 66, 51-57 (2008).
27. Lobo, J. M. et al. SCF-engineered powders for delivery of budesonide from passive DPI devices. *J Pharm Sci* 94, 2276-88 (2005).
28. Bailey, A. G., Hashish, A. H. & Williams, T. J. Drug delivery by inhalation of charged particles. *Journal of Electrostatics* 44, 3-10 (1998).
29. Fraser, D. A. The deposition of unipolar charged particles in the lungs of animals. *Arch Environ Health* 13, 152-7 (1966).
30. Byron, P. B., Peart, J. & Staniforth, J. N. Aerosol electrostatics I: Properties of fine powders before and after aerosolization by dry powder inhalers. *Pharm Res* 14, 698-705 (1997).
31. Johnston, A. M., Vincent, J. H. & Jones, A. D. Measurements of Electric Charge for Workplace Aerosols. *Annals of Occupational Hygiene* 29, 271-284 (1985).

32. Johnston, A. M., Vincent, J. H. & Jones, A. D. Electrical Charge Characteristics of Dry Aerosols Produced by a Number of Laboratory Mechanical Dispensers. *Aerosol Science and Technology* 6, 115-127 (1987).

## 5. GENERAL CONCLUSIONS AND FUTURE WORK

Dry powder inhalers (DPI) are an important drug delivery option, for the treatment of respiratory diseases, and, increasingly, for fast and noninvasive delivery of systemically acting drugs and vaccines.<sup>1, 2</sup> Most DPI formulations consist of micronized drug blended with larger carrier particles. The interactions between drug and carrier particles are one of the major determinants of DPI performance and have therefore been one of the main pursuits in inhaled drug delivery research. Much of the research in this area has focused on particle design, both the design of drugs and the design of carriers<sup>3-6</sup> with specific surface properties, that should enhance their dispersion. Studies have included the use of large porous particles,<sup>7, 8</sup> particles coated with surface modifying agents,<sup>9-14</sup> "mechano-fused" particles,<sup>9, 15-17</sup> needle-shaped particle agglomerates,<sup>18</sup> particles crystallized from supercritical fluids,<sup>19-25</sup> spray-freeze dried particles,<sup>26</sup> and spray-dried<sup>27</sup> particles with varying levels of corrugation<sup>26, 28-30</sup> to list just a few recent examples.

Far less research has been conducted aimed at understanding the interactions between particles independently of specific systems. The major physical interactions between particles include mechanical interlocking, capillary forces, intermolecular interactions, and electrostatic forces. Mechanical interlocking, due to surface asperities, may prevent particles from dislodging and may thus inhibit particle dispersion. Regular particle shapes with smooth surface morphology may reduce the propensity for particles to interlock. The presence of moisture, even in small quantities, may bring about capillary forces. Electrostatic interactions between particles are recognized as playing an important role. Simulations,<sup>31-34</sup> *in vitro*<sup>35, 36</sup> and *in vivo*<sup>37</sup> studies suggest that electrostatic charge can affect the delivery and deposition of aerosol particles in the lung. Due to their design and material characteristics DPI devices and formulations lend themselves to triboelectric charging. Yet, the

importance of electrostatic charge on the behavior of medicinal aerosols has not been extensively investigated and is poorly understood. This project is the first classification of these electrostatic interactions, to estimate their magnitude and prevalence, and finally understand how they arise and whether they can be predicted from physical measurements of the raw materials.

## **5.1. Hypotheses**

It was postulated that electrostatic charge is a major factor in drug delivery from DPIs and that charging can be controlled through the selection of formulation variables. Furthermore, it was proposed that the charging characteristics of a pharmaceutical material are related to the specific material surface properties and could thus be determined *a priori*. In detail, the hypotheses proposed were as follows:

*5.1.1. Electrostatic charging is a consequence of triboelectrification during inhaler actuation.*

*5.1.2. Magnitude and polarity of charge on drug particles can be controlled by formulation variables, independently of the chemical identity of the drug being delivered.*

*5.1.3. The acid-base characteristics of a pharmaceutical material, as determined by inverse gas chromatography, are directly related to its triboelectric charging characteristics and its position in the triboelectric series.*

*5.1.4. By selecting formulation properties and inhaler, micronized drug can be made to acquire charges well beyond the Boltzmann equilibrium charge distribution theory.*

## **5.2. Specific Aims**

A series of specific aims were adopted to address the hypotheses and the conclusions derived from the previous chapters were as follows.

*5.2.1. To elucidate the phenomenon of triboelectric charging during DPI actuation.*

The electrostatic properties of albuterol sulfate, budesonide and three excipients (lactose, glucose, and calcium phosphate), including different batches, size fractions, and blends were studied. Materials were characterized (Chapter 2) using a combination of techniques, including Faraday well experiments to determine their charging characteristics in the absence of frictional triboelectrification. The experiments indicated a low level of charge, in the order of  $\pm 0.5 \text{ nC/g}$  for excipients to  $\pm 1 \text{ nC/g}$  for the micronized drugs. From the results of the Faraday well experiments, the materials were organized in a triboelectric series, which arranged the materials from highest to lowest work function (most electron accepting to most electron donating material) as follows:

- Budesonide  $\gg$  Glucose  $\geq$  CP  $>$  ML80  $>$  ML58  $>$  SV425  $>$  SV94  $>$  Albuterol +

Formulations of different drug/excipient combinations were prepared and tested using the electrical low pressure impactor (ELPI) in conjunction with standard entrainment tubes (Chapter 4). The mass depositions were assayed, and the charges of the delivered drug particles were measured and analyzed with respect to their magnitude and charge polarity. The analysis showed charges in the 1-300  $\mu\text{C/g}$  range depending of the formulation and actuation conditions, which are 3-5 orders of magnitude larger than the charges recorded in Faraday well experiments. This large difference in charge clearly indicates an active charging mechanism in connection with the aerosolized drug particles. A triboelectric series was constructed based on the ELPI recovered charges. From highest to lowest work function (most electron accepting to most electron donating material) the series is as follows:

- Budesonide  $>$  CP  $>$  Glucose  $>$  ML80  $\approx$  ML58  $\approx$  SV425  $\approx$  SV94  $\approx$  Albuterol +

In general, differences between the lactose batches were less pronounced, which is expected given that they are the same chemical substance. However, CP and glucose consistently resulted in the most positively (or least negatively) charged drug, which was in agreement with the results of the Faraday well experiments. This is strong evidence in support of the hypothesis that the charge of

aerosolized drug particles is the result of contact charging between particles of the formulation followed by separation of particles during the DPI actuation process.

*5.2.2. To determine the contribution of specific formulation factors.*

The effect of chemistry (drug and excipients), manufacturing process, blend concentration and pressure drop on electrostatic charge were determined in ELPI deposition experiments. Formulation factors had significant effects on both the magnitude and the polarity of the charge. The choice of excipient has the most profound effect on the charge characteristics of the deposited drug; lactose batch to batch variability was also indicated. In addition, the particle size of the excipient appears to have an effect on the charge profile of deposited drug, with smaller particles giving rise to stronger charging. Drug concentration in the formulation had an effect consistent with the active site hypothesis. The effect of the actuation conditions was strong but contrary to expectations, turbulent conditions result in somewhat lower individual particle charge levels. This result is further evidence that contact charging is the cause of the particle charge and that fluidization merely affects the particle separation process.

The results of the ELPI deposition study show clearly that the drug charge can be affected through formulation factors. Per particle or per mass charge levels differed by as much as two orders of magnitude depending on how the drug was presented, i.e. what excipient was used in the formulation and what fluidization conditions were used in delivery.

*5.2.3. To determine the correlation between surface acid/base properties and triboelectric charging.*

The dispersive surface free energy and specific acid/base surface characteristics of the excipients were studied by inverse gas chromatography (Chapter 3). The excipients were arranged in order of most electron accepting to most electron donating; the rank order is as follows:

- CP > Glucose > ML58  $\approx$  ML80 > SV 425 > SV094 +

This order is in agreement with the triboelectric series derived from Faraday well experiments and mostly in agreement with ELPI deposition studies. This result strongly suggests bulk electrostatic charging (Faraday well experiments), electron exchange between surfaces (IGC experiments), and contact charging (ELPI studies) are all closely related, perhaps different manifestations of the same physical phenomenon. The variability of the data precludes establishment of a quantitative relationship but the rank-order relationship is highly preserved across the experiments and supports this conclusion.

#### *5.2.4 To determine if tribocharging can increase particle charge beyond Boltzmann distribution.*

The ELPI deposition studies allowed calculation of approximate per particle charge levels for drug deposited in the ELPI (Chapter 4). The results showed very high particle charge levels, often in the 1,000s and even 10,000s of elementary charges per particle range. These charges were several orders of magnitude higher than charge levels predicted by the Boltzmann charge distribution. The charge levels are considerably higher than had previously been estimated (ca. 200e per particle<sup>38</sup>), and substantially higher than what had been observed in other laboratory and industrial processes, in which aerosol charging is known to occur.

### **5.3. Discussion**

The study relies heavily on two techniques not commonly used in pharmaceutical research, IGC and ELPI. As outlined in earlier chapters, both techniques have been used previously, but this is the first study in which the techniques have complemented each other. IGC is increasingly being used to study the surface energy of powders, which is thought to play an important role in adhesive processes. The acid/base parameters have so far, however, not been related to electrostatic material properties and/or charging. The ELPI has only recently been applied to the study of DPI products,<sup>39</sup> with two recent studies examining the effects of storage humidity on charging.<sup>40, 41</sup> A search of the National

Center for Biotechnology Information database (PubMed ) still returns only 21 citations with "ELPI" as keyword, with a majority pertaining to environmental aerosols.

The results of this work clearly show that triboelectric charging is an important consideration in DPI product development and clinical inhaler use. Charge levels observed in these studies were significantly higher than had previously been estimated and higher than what is needed to affect the trajectory and the deposition of drug particles in the respiratory tract. Ignoring this phenomenon will result in reduced design control and formulation variability, resulting in performance inconsistencies and potentially failure of product to meet specification. This is particularly true in light of the fact that the occurrence of tribocharging is neither a random nor an uncontrollable process. The results of this project show that drug charging is highly dependent upon formulation variables and that it can be affected by formulation variables such as the choice of excipient or the drug concentration in the formulation. Results from Faraday cage experiments show that relative charge magnitude can be predicted from material properties prior to combining them in the formulation, though more work is needed here to develop a mean of quantitative prediction. Finally, IGC experiments offer a physical explanation for the charging phenomena by linking the position of a given material in the triboelectric series to measurable surface characteristics, i.e. surface acid and base parameters,  $K_A$  and  $K_B$ , respectively. This is a first; while it has been suggested that triboelectric charging of insulators is related to the presence of electron donor and electron acceptor sites on their surface, this hypothesis had previously not been tested. The data set in support of this hypothesis is small and the connection drawn is semi-quantitative (rank-order relationship). Yet, the results from IGC experiments are consistent with those from Faraday well experiments and, for the most part, ELPI deposition studies. This suggests that these phenomena are linked, or perhaps different manifestations of the same physical process. Extending this work would increase understanding of insulator charging, and confounding data in the literature may be explained. The result would have implications not just to the field of pharmaceutical sciences, but could advance the field of particle electrostatics.



Finally, it is worth noting, that the results of this dissertation project have direct and immediate applicability to the DPI formulation development process. And unlike many of the techniques cited in the introduction to this chapter, exploiting the lessons of this project does not require the use of specialized or proprietary equipment or techniques, of complicated manufacturing process, or of materials not approved for respiratory drug delivery. The project has clearly shown that electrostatic charge can be affected by conventional formulation techniques such as the choice of excipient or the concentration of drug. All that is required is a thorough characterization of the raw materials and an understanding of contact charging, which is provided herein.

#### **5.4. Future Work**

The study indicates that electrostatic charging is an important interaction in DPI formulations. But the results have been limited to two drugs and six excipients, whereby four of these excipients were different batches of the same material (lactose monohydrate) from the same manufacturer. While the two drugs, albuterol and budesonide, are chemically distinct from each another, they do not cover the range of different compounds that are currently used or are being developed for use in DPIs. Moreover, while batch-to-batch variability was investigated in lactose, it may also play a role for drugs. Current research effort in the field of inhaled drug pharmaceuticals focuses on drug particle design techniques, e.g. supercritical fluid crystallization. Testing the electrostatic properties of particles in Faraday well experiments and ELPI deposition studies may add to the understanding of how different particle properties (or manufacture methods) affect their propensity to charge. Similarly, a larger set of excipients should be tested, including lactose and glucose products of different origin, or different polymorphs or anhydrides.

This project has shown that triboelectric charging plays a significant role in DPI formulations. Using well defined systems charge was shown to be highly dependent on the formulation factors. In order to elucidate the importance of these effects for all applications, it is important to acknowledge that the number of potential system variables is much larger than addressed here. Storage effects were

omitted from the analysis but some auxiliary data (presented in the appendix) indicate they have an important effect on the performance of DPIs. In an effort to decouple air flow from the other variables that make up an inhaler, standard entrainment tubes were used in the experiments in lieu of inhaler devices. This, too, is a simplification of the system. Thus, a natural extension of this work would be the measurement of charging in more complicated systems, with more variables, which more closely approximate real use situations for the inhaler. One important experiment might be to test several commercially available inhaled products.

A principal aim in this project has been to elucidate the triboelectrification process between the constituent particles of a DPI formulation. Contact charging is well understood for conducting materials, such as metals, but not for insulators, such as the constituents of a pharmaceutical formulation. This has been the first such time surface acid/base parameters, which are readily measurable, have been linked with triboelectrification. However, the data have only allowed for a rank-order type correlation, not a fully quantitative approach. This has two reasons which could be addressed in follow-up work: (1) variability in the Faraday well experiments, (2) the IGC method. Contact charging between insulators is an inherently variable process that makes it difficult to obtain data that is statistically unequivocal. The approach and the methodology could likely be improved, but, importantly, the data set must be expanded. (2) The IGC equipment did not allow a complete characterization of all materials.  $K_A$  and  $K_B$  could not be determined for glucose monohydrate because the material is subject to dehydration and physical instability at elevated temperatures. If a cooling element were added to the equipment, experiments could be performed at lower temperatures, which would allow calculation of  $\Delta H^{sp}$  and thus determination of  $K_A$  and  $K_B$ . The IGC equipment also makes characterization of micronized drug difficult. Micronized particles are difficult to pack and would require carrier gas pressures that are higher than the glass column and the Swagelok fittings can sustain. However, some development work on equipment and method might overcome this limitation. Another problem associated with the IGC method is that it requires quantities of material that are often not available for developmental drugs. (Typical material requirement for IGC

is 2.0g while 1.5g of budesonide were available for the entire project, of which a portion was lost in the jet-milling process). One approach to solve both of the problems (high pressure and quantity required) would be to blend drug with inert beads (e.g. deactivated glass beads) and pack the column with the blend.

The ultimate goal in this research as well as that of any pharmaceutical or biomedical sciences research project must be the improvement of clinical outcomes. Based on the measurements of per particle charge levels and the previous work of other scientists, it was suggested that the electrostatics arising from DPI formulation and actuation could affect deposition in the respiratory tract. It would be useful to determine, first by modeling, what the clinical significance of the charge levels is.

This study has focused on particle interactions in the formulation. By showing that charges are present even at highly humid conditions, the study was shown to be relevant to physiological systems. However, that experiment does not replace actual *in vivo* studies. To determine the true effect of particle charging on drug deposition, there is no substitute for initial animal or ultimately clinical experiments.

In conclusion, future work can be grouped into several major categories: (1) expanding the scope / extending the conclusion to a larger number of systems, including a larger number of drugs and excipients; (2) testing the electrostatic properties of real systems, e.g. in a setting more approximating clinical conditions; (3) improving IGC technique to allow characterization of more materials; (4) improving Faraday well technique to decrease data variability and allow more quantitative results; (5) modeling to understand the clinical significance and, ultimately, (6) testing actual deposition effects *in vivo*.

#### 5.4. Literature Cited

1. Son, Y. & MConville, J. Advancements in dry powder delivery to the lung. *Drug Dev Ind Pharm* 34, 948-59 (2008).
2. Lu, D. & Hickey, A. J. Pulmonary vaccine delivery. *Expert Rev Vaccines* 6, 213-26 (2007).
3. Young, P. M., Kwok, P., Adi, H., Chan, H. K. & Traini, D. Lactose Composite Carriers for Respiratory Delivery. *Pharm Res IN PRESS*, DOI: 10.1007/s11095-008-9779-9 (2008).
4. Iida, K., Hayakawa, Y., Okamoto, H., Danjo, K. & Leuenberger, H. Preparation of dry powder inhalation by surface treatment of lactose carrier particles. *Chem Pharm Bull (Tokyo)* 51, 1-5 (2003).
5. Iida, K. et al. Effects of surface processing of lactose carrier particles on dry powder inhalation properties of salbutamol sulfate. *Chemical & Pharmaceutical Bulletin* 52, 938-942 (2004).
6. Gilani, K., Rouholamini Najafabadi, A., Barghi, M. & Rafiee-Tehrani, M. Aerosolisation of beclomethasone dipropionate using spray dried lactose/polyethylene glycol carriers. *Eur J Pharm Biopharm* 58, 595-606 (2004).
7. Edwards, D. A. et al. Large porous particles for pulmonary drug delivery. *Science* 276, 1868-1871 (1997).
8. Vanbever, R. et al. Formulation and physical characterization of large porous particles for inhalation. *Pharm Res* 16, 1735-42 (1999).
9. Begat, P. et al. The role of force control agents in high-dose dry powder inhaler formulations. *J Pharm Sci* (2008).
10. Coowanitwong, I. et al. Laser-ablated nanofunctional polymers for the formulation of slow-release powders for dry powder inhalers: physicochemical characterization and slow-release characteristics. *J Pharm Pharmacol* 59, 1473-84 (2007).
11. Chan, L. W., Lim, L. T. & Heng, P. W. Immobilization of fine particles on lactose carrier by precision coating and its effect on the performance of dry powder formulations. *J Pharm Sci* 92, 975-84 (2003).
12. Hickey, A. J., Gonda, I., Irwin, W. J. & Fildes, F. J. Effect of hydrophobic coating on the behavior of a hygroscopic aerosol powder in an environment of controlled temperature and relative humidity. *J Pharm Sci* 79, 1009-14 (1990).
13. Kawashima, Y., Serigano, T., Hino, T., Yamamoto, H. & Takeuchi, H. Design of inhalation dry powder of pranlukast hydrate to improve dispersibility by the surface modification with light anhydrous silicic acid (AEROSIL 200). *International Journal of Pharmaceutics* 173, 243-251 (1998).
14. Kawashima, Y., Serigano, T., Hino, T., Yamamoto, H. & Takeuchi, H. A new powder design method to improve inhalation efficiency of pranlukast hydrate dry powder aerosols by surface

- modification with hydroxypropylmethylcellulose phthalate nanospheres. *Pharm Res* 15, 1748-52 (1998).
15. Kumon, M. et al. Application and mechanism of inhalation profile improvement of DPI formulations by mechanofusion with magnesium stearate. *Chem Pharm Bull (Tokyo)* 56, 617-25 (2008).
  16. Kumon, M., Suzuki, M., Kusai, A., Yonemochi, E. & Terada, K. Novel approach to DPI carrier lactose with mechanofusion process with additives and evaluation by IGC. *Chem Pharm Bull (Tokyo)* 54, 1508-14 (2006).
  17. Kumon, M. et al. Applicability of DPI formulations for novel neurokinin receptor antagonist. *Int J Pharm* 356, 102-9 (2008).
  18. Ikegami, K. et al. A new agglomerated KSR-592 beta-form crystal system for dry powder inhalation formulation to improve inhalation performance in vitro and in vivo. *J Control Release* 88, 23-33 (2003).
  19. Jung, J. & Perrut, M. Particle design using supercritical fluids: Literature and patent survey. *Journal of Supercritical Fluids* 20, 179-219 (2001).
  20. Hooton, J. C. et al. Characterization of particle-interactions by atomic force microscopy: effect of contact area. *Pharm Res* 20, 508-14 (2003).
  21. Reverchon, E., Della Porta, G. & Pallado, P. Supercritical antisolvent precipitation of salbutamol microparticles. *Powder Technology* 114, 17-22 (2001).
  22. Schiavone, H., Palakodaty, S., Clark, A., York, P. & Tzannis, S. T. Evaluation of SCF-engineered particle-based lactose blends in passive dry powder inhalers. *International Journal of Pharmaceutics* 281, 55-66 (2004).
  23. Tong, H. H., Shekunov, B. Y., York, P. & Chow, A. H. Influence of polymorphism on the surface energetics of salmeterol xinafoate crystallized from supercritical fluids. *Pharm Res* 19, 640-8 (2002).
  24. Velaga, S. P., Berger, R. & Carlfors, J. Supercritical fluids crystallization of budesonide and flunisolide. *Pharm Res* 19, 1564-71 (2002).
  25. Young, P. M. & Price, R. The influence of humidity on the aerosolisation of micronised and SEDS produced salbutamol sulphate. *Eur J Pharm Sci* 22, 235-40 (2004).
  26. Columbano, A., Buckton, G. & Wikeley, P. Characterisation of surface modified salbutamol sulphate-alkylpolyglycoside microparticles prepared by spray drying. *Int J Pharm* 253, 61-70 (2003).
  27. Steckel, H. & Brandes, H. G. A novel spray-drying technique to produce low density particles for pulmonary delivery. *Int J Pharm* 278, 187-95 (2004).
  28. Adi, S. et al. Micro-particle corrugation, adhesion and inhalation aerosol efficiency. *Eur J Pharm Sci* 35, 12-8 (2008).

29. Chawla, A., Taylor, K. M. G., Newton, J. M. & Johnson, M. C. R. Production of Spray-Dried Salbutamol Sulfate for Use in Dry Powder Aerosol Formulation. *International Journal of Pharmaceutics* 108, 233-240 (1994).
30. Chew, N. Y. K. & Chan, H. K. Use of solid corrugated particles to enhance powder aerosol performance. *Pharmaceutical Research* 18, 1570-1577 (2001).
31. Balachandran, W., Machowski, W., Gaura, E. & Hudson, C. Control of drug aerosol in human airways using electrostatic forces. *Journal of Electrostatics* 40-1, 579-584 (1997).
32. Bailey, A. G. The inhalation and deposition of charged particles within the human lung. *Journal of Electrostatics* 42, 25-32 (1997).
33. Bailey, A. G., Hashish, A. H. & Williams, T. J. Drug delivery by inhalation of charged particles. *Journal of Electrostatics* 44, 3-10 (1998).
34. Hashish, A. H., Bailey, A. G. & Williams, T. J. Modeling the Effect of Charge on Selective Deposition of Particles in a Diseased Lung Using Aerosol Boli. *Physics in Medicine and Biology* 39, 2247-2262 (1994).
35. Cohen, B. S., Xiong, J. Q., Asgharian, B. & Ayres, L. Deposition of Inhaled Charged Ultrafine Particles in a Simple Tracheal Model. *Journal of Aerosol Science* 26, 1149-1160 (1995).
36. Cohen, B. S., Xiong, J. Q., Fang, C. P. & Li, W. Deposition of charged particles on lung airways. *Health Physics* 74, 554-560 (1998).
37. Fraser, D. A. The deposition of unipolar charged particles in the lungs of animals. *Arch Environ Health* 13, 152-7 (1966).
38. Byron, P. B., Peart, J. & Staniforth, J. N. Aerosol electrostatics I: Properties of fine powders before and after aerosolization by dry powder inhalers. *Pharm Res* 14, 698-705 (1997).
39. Telko, M. J., Kujanpaa, J. & Hickey, A. J. Investigation of triboelectric charging in dry powder inhalers using electrical low pressure impactor (ELPI). *Int J Pharm* 336, 352-60 (2007).
40. Kwok, P. C. & Chan, H. K. Effect of relative humidity on the electrostatic charge properties of dry powder inhaler aerosols. *Pharm Res* 25, 277-88 (2008).
41. Young, P. M. et al. Influence of humidity on the electrostatic charge and aerosol performance of dry powder inhaler carrier based systems. *Pharm Res* 24, 963-70 (2007).

## **APPENDICES**

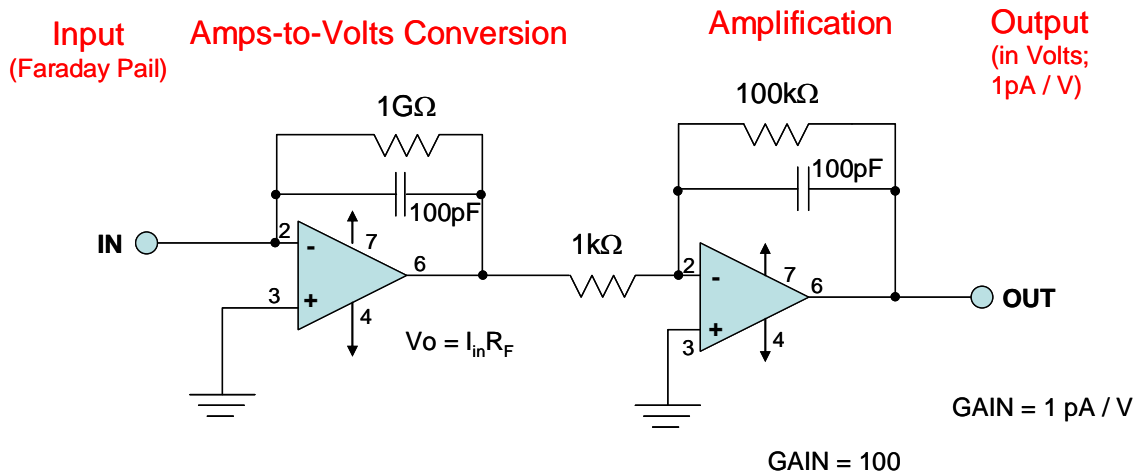
**APPENDIX A. FARADAY WELL CIRCUIT**

**APPENDIX B. CRITICAL ASSESSMENT OF INVERSE GAS CHROMATOGRAPHY AS MEANS OF ASSESSING SURFACE FREE ENERGY AND ACID-BASE INTERACTION OF PHARMACEUTICAL POWDERS**

**APPENDIX C. INVESTIGATION OF TRIBOELECTRIC CHARGING IN DRY POWDER INHALERS USING ELECTRICAL LOW PRESSURE IMPACTOR (ELPI™)**

**APPENDIX D. EFFECT OF STORAGE ON DISPERSION AND CHARGE**

**APPENDIX A.  
FARADAY WELL DEVICE AND OPERATING CIRCUIT**



Current integrating amplifier converts charge  $Q$  into voltage  $V$ , where  $Q$  is given by  $-C_f \times V$ .

**Figure A.1.** Non-integrating circuit for Faraday well.

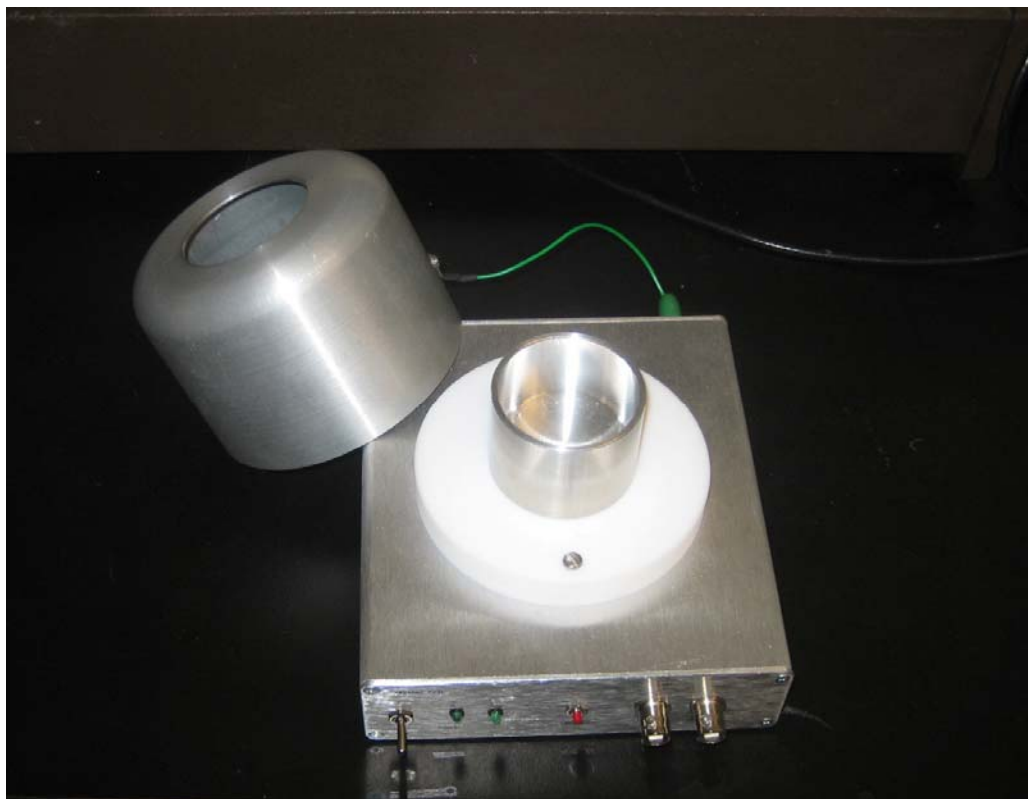


**Figure A.2.** Photo of Faraday well. The removable aluminum pan rests on top of a Teflon disc, the grounded enclosure (note the green cable which grounds the enclosure), can be slid on and off the disc. The outlet in the front feeds into a DI-154RS analog-to-digital converter (Dataq, Akron, OH) and which is connected to a computer where voltage over time is recorded using the Windaq data acquisition system.



**APPENDIX B.**

**CRITICAL ASSESSMENT OF INVERSE GAS CHROMATOGRAPHY AS MEANS OF  
ASSESSING SURFACE FREE ENERGY AND ACID-BASE INTERACTION OF  
PHARMACEUTICAL POWDERS**

# Critical Assessment of Inverse Gas Chromatography as Means of Assessing Surface Free Energy and Acid–Base Interaction of Pharmaceutical Powders

MARTIN J. TELKO, ANTHONY J. HICKEY

Division of Molecular Pharmaceutics, School of Pharmacy, CB# 7360, The University of North Carolina, Chapel Hill, North Carolina 27599

Received 28 August 2006; revised 16 November 2006; accepted 29 December 2006

Published online in Wiley InterScience (www.interscience.wiley.com). DOI 10.1002/jps.20897

**ABSTRACT:** Inverse gas chromatography (IGC) has been employed as a research tool for decades. Despite this record of use and proven utility in a variety of applications, the technique is not routinely used in pharmaceutical research. In other fields the technique has flourished. IGC is experimentally relatively straightforward, but analysis requires that certain theoretical assumptions are satisfied. The assumptions made to acquire some of the recently reported data are somewhat modified compared to initial reports. Most publications in the pharmaceutical literature have made use of a simplified equation for the determination of acid/base surface properties resulting in parameter values that are inconsistent with prior methods. In comparing the surface properties of different batches of  $\alpha$ -lactose monohydrate, new data has been generated and compared with literature to allow critical analysis of the theoretical assumptions and their importance to the interpretation of the data. The commonly used (simplified) approach was compared with the more rigorous approach originally outlined in the surface chemistry literature. © 2007 Wiley-Liss, Inc. and the American Pharmacists Association *J Pharm Sci* 96:2647–2654, 2007

**Keywords:** inverse gas chromatography; surface free energy; acid–base interactions; lactose; batch-to-batch variability

## INTRODUCTION

Inverse gas chromatography (IGC) applies gas chromatography principles to the surface analysis of powders, fibers, or coatings. Techniques for determining surface energy and acid/base interactions of surfaces by IGC were developed by Schultz et al. who studied polymers and composite materials.<sup>1</sup> Subsequent work was largely based on

this approach, though some experimenters have deviated from the method. The first use of IGC for surface energy measurements of pharmaceutical powders appears to be by Ticehurst et al. where chemically and structurally equivalent batches of salbutamol sulfate were differentiated by IGC.<sup>2</sup> Since this article, IGC has been used to characterize a number of different pharmaceutical systems, and surface energy and acid–base parameters were correlated with various material performance characteristics, including the dispersion of drugs from dry powder inhaler (DPI) formulations.<sup>3–6</sup>

In determining the acid–base parameters of salbutamol, Ticehurst et al. assumed that entropic

Correspondence to: Anthony J. Hickey (Telephone: 919-962-0223; Fax: 919-966-0197; E-mail: ahickey@unc.edu)

*Journal of Pharmaceutical Sciences*, Vol. 96, 2647–2654 (2007)  
© 2007 Wiley-Liss, Inc. and the American Pharmacists Association



JOURNAL OF PHARMACEUTICAL SCIENCES, VOL. 96, NO. 10, OCTOBER 2007 **2647**

contributions to Gibb's free energy of adsorption could be neglected.<sup>2</sup> This assumption has been adopted in many subsequent publications, and some investigators appear to have lost sight of the fact that this simplifying assumption results in an approximation. Unlike Ticehurst, they frequently have not acknowledged this deviation from Schultz' original method. Assuming negligible entropy simplifies the IGC experiment and analysis of data, but does not always hold true and can lead to erroneous interpretation of data. As IGC use continues to grow and surface forces are linked to an increasing number of performance criteria, the correct analysis of data may be critically important.

### Inverse Gas Chromatography

IGC has been extensively reviewed.<sup>7-9</sup> In brief, the technique is based on interactions of gaseous probe molecules with stationary phase in a packed column which give rise to a characteristic net retention volume,  $V_N$ , which can be related to free energy of adsorption, and used to calculate various other thermodynamic parameters.

### Surface Free Energy

Surface free energy is a critical determinant of particle adhesion, which is an important factor in the performance of several pharmaceutical systems, including compressed tablet strength and dry powder aerosol dispersion. Surface free energy is due to Lifshitz-van der Waals (LW) forces and acid-base interactions.<sup>10</sup> The LW component of surface energy is primarily the result of dispersion forces and may be considered an intrinsic material property. Acid-base interactions are considered "specific" as they are only evident when surfaces interact with other molecules. Following Fowkes' reasoning that different phenomena contribute to intermolecular forces independently,<sup>11,12</sup> surface energy can be represented as the sum of dispersive and nondispersive (specific) contributions as

$$\gamma_S = \gamma_S^D + \gamma_S^{sp} \quad (1)$$

where  $\gamma_S$  stands for the total surface free energy of the solid,  $\gamma_S^D$  designates the dispersive surface free energy, and  $\gamma_S^{sp}$  the specific surface energy.

### Dispersive and Specific Free Energy by Inverse Gas Chromatography

Net retention volume,  $V_N$  and free energy of adsorption,  $-\Delta G_A$ , are related by the following equations

$$-\Delta G_A = RT \ln V_N + C \quad (2)$$

$$= 2N_A A \sqrt{\gamma_S^D} \sqrt{\gamma_L^D} + C \quad (3)$$

where  $N_A$  is the Avogadro's number,  $A$  the effective surface area of the probe molecule,  $\gamma_S^D$  and  $\gamma_L^D$  the dispersive free energies of interacting solid and probe, and  $C$  is a constant that depends on the chosen reference state.<sup>1</sup> Based on Eqs. (2) and (3), surface free energy can be found from a plot of  $RT \ln V_N$  versus  $2N_A A \sqrt{\gamma_L^D}$  for a series of *n*-alkanes.

Specific free energy,  $\gamma_S^{sp}$ , is determined from polar probe retention times. When  $RT \ln V_N$  is plotted versus  $2N_A A \sqrt{\gamma_L^D}$  the distance above the alkane line is the specific free energy of adsorption,  $\Delta G_A^{sp}$ , between the surface of the stationary phase and the respective probe.

Determination of dispersive and specific free energies is well established and mostly straightforward. Since it is difficult to correlate the specific free energies of different probes individually to the character of the interacting surface, Schulz et al. developed a method for consolidating specific free energies into two comprehensive and descriptive parameters. The method is based on the acid/base approach to molecular interactions,<sup>13</sup> based on which specific interactions are classified as either electron donor or electron acceptor type interactions. Donor and (corrected) acceptor numbers, DN and AN\*, have been determined for different solvents; these values represent the ability of a probe to donate or accept electrons from reference acceptors and donors, respectively. Gutmann defined the DN as the molar enthalpy of a given substance with  $\text{SbCl}_5$ , a reference acid, in 1.0 mM dichloroethane solution ( $\text{DN} \equiv -\Delta H_{\text{DSbCl}_5}$ ).<sup>13</sup> AN\* was defined as the molar enthalpy of adduct formation of a substance with  $(\text{CH}_3\text{CH}_2)_3\text{PO}$ , a reference base,<sup>14</sup> a correction over the initial AN definition.<sup>13</sup>

Using this approach, the surface can be characterized by two constants related to the acid/base interactions via the equation

$$\Delta H_A^{sp} = K_A \text{DN} + K_B \text{AN}^* \quad (4)$$

where  $\Delta H_A^{\text{sp}}$  is the specific enthalpy of adsorption, and  $K_A$  and  $K_B$  are the acid (acceptor) and base (donor) parameters of the studied surface, respectively. Eq. (4) originated from work to predict enthalpies of adduct formation<sup>15</sup> that was extended to solid adsorption phenomena.<sup>1,16</sup> It is a semi-empirical relationship, based on the observation that acid-base interactions are linked to changes in enthalpy. It has been shown that heat of adsorption of a basic probe onto an acidic surface can be accurately and quantitatively predicted based on acid/base parameters.<sup>17</sup> Since  $K_A$  and  $K_B$  of the adsorbent are analogous to the DN and AN\* of the probes (which as shown are defined by enthalpy), they are considered relative to the same reference state.

Ticehurst<sup>2</sup> and others<sup>5,8,18-24</sup> have used an alternative expression based on surface free energy given by equation

$$\Delta G_A^{\text{sp}} = K_A \text{DN} + K_B \text{AN}^* \quad (5)$$

Early literature clearly stated that Eq. (5) is based on the assumption of negligible entropic effects.<sup>2</sup> Most subsequent papers no longer state this assumption, and in some cases erroneously cite the original Schultz et al. article as the source of this equation. Tong et al. compared the two approaches for polymorphs of salmeterol, and concluded they were not equivalent.<sup>25</sup> Despite these results, many authors continue to use the simplified approach.

Use of Eq. (5) instead of (4) has important experimental consequences. Using Eq. (5) the experimenter can quickly determine  $K_A$  and  $K_B$  from data at a single temperature, by plotting  $\Delta G_A^{\text{sp}}/\text{AN}^*$  versus DN/AN\* of a number of acidic and basic probes. By contrast, determination of  $K_A$  and  $K_B$  from eq. (4) requires IGC measurements at several temperatures so that  $\Delta H_A^{\text{sp}}$  can first be determined via Gibb's equation.

Lactose monohydrate is examined because it is the main component of most DPI formulations.<sup>26</sup> Efforts to predict and/or improve dispersion of drug from DPI have focused on the selection or design of lactose batches.<sup>3,5,27-33</sup> IGC measurements of surface free energy of lactose have been used extensively in this context, and results were often based on the simplified specific free energy approach.<sup>3,5</sup> This paper compares the simplified to the more rigorous approach using different batches of  $\alpha$ -lactose monohydrate, one milled and two in sieved form.

## MATERIALS

Lactose monohydrate, Respitose<sup>TM</sup>, was provided by DMV-Fonterra Excipients. One batch of milled (ML001, batch 10136780), designated ML A and two batches of sieved (SV003, batches 10190094 and 10135425) lactose, designated SV A and SV B were evaluated. The alkane probes used for dispersive free energy determination were hexane (99+%, Aldrich), heptane (99+%, Aldrich), octane (99.5+%, Fluka), nonane (99+%, Aldrich), and decane (99+%, Aldrich). Polar probes were chosen to cover a wide DN/AN\* range. The probes used were tetrahydrofuran (THF) (EM Science, 99.99%), chloroform (100%, Mallinkrodt), acetone (99.7%, Mallinkrodt), ethyl acetate (99.9%, Mallinkrodt), diethyl ether (99%+, Acros), and ethanol (100%, Aaper).

## METHOD

IGC experiments were conducted with a Hewlett-Packard 5890 Series II GC with flame ionization detector. The chromatograph was modified to allow installation of 205 mm, 4 mm ID glass columns. Carrier gas employed was dry N<sub>2</sub> at a flowrate of 30 mL/min. Oven temperatures used were 60°C, 45°C, and 30°C in that order. Lactose was packed into deactivated<sup>34</sup> glass columns and plugged with silanated glass wool. Necessary corrections for pressure drop across column and temperature effects on flow rate were made. After installation and temperature changes, packed columns were allowed to equilibrate for 6 h before subsequent injections were made. Injections were made with a 1  $\mu$ L-Hamilton syringe. Infinite dilution was ensured by detector response, detector signals below 10 $\times$  limit of detection were permitted; this corresponds to injection volumes <0.01  $\mu$ L. Each injection was made at least three times; the relative standard deviations in the retention times of these injections were <1% in each case. Each batch was examined with four different packed columns. Since even inert probes can be somewhat retarded,<sup>35</sup> dead-times were calculated using the retention times of heptane, octane, and nonane.<sup>36</sup> Data were analyzed using SigmaStat 2.03 (SPSS, Chicago, IL) and plotted using Excel 2000 (Microsoft, Seattle, WA). Differences between batches were probed for statistical significance using the two-sample *t*-test for independent samples with unequal variances

(Satterthwaite's method). Probe surface areas were taken from Schultz et al.<sup>1</sup> Other properties, including surface tension, are readily available from chemistry handbooks.<sup>37</sup>

## RESULTS AND DISCUSSION

In preliminary work, experiments were conducted in a temperature range of 30°C–80°C. However, differential scanning calorimetry showed structural changes occurred in lactose monohydrate after prolonged exposure to 80°C. Specifically, dehydration and polymorphic changes were observed.<sup>38</sup> A temperature range of 30°C–60°C did not modify the lactose.

Dispersive surface free energy was calculated at each temperature as discussed above;  $RT \ln V_N$  versus  $2N_A A \sqrt{\gamma_L^D}$  was plotted and straight lines were fitted to the data. The fit was excellent in each case ( $R^2 > 0.999$ ). Table 1 shows the dispersive free energies determined at each temperature; the dispersive free energies are similar for the three batches and agree with published data.<sup>23,30,32,39</sup> When the dispersive free energies are plotted against temperature, straight lines with excellent correlation coefficients ( $R^2 > 0.99$ ) can be fitted to each data set.

Specific interactions were analyzed (a) assuming negligible entropic effects, (b) using the approach of Schultz et al. which requires prior determination of enthalpy of adsorption. Figures 1 and 2 contrast the two methods; for clarity only one batch (milled lactose) is shown in the figures. Results for all batches are presented in Table 2 (negligible entropy) and Table 3 (including entropic contribution).

Since Eq. (5) does not account for the temperature dependent contributions ( $-T\Delta S$ ) to  $\Delta G_A^{sp}$ , analysis at different temperatures yields separate sets of results. As shown in Figure 1 and Table 2,

**Table 1.** Dispersive Free Energies (Standard Deviation) of Sieved and Milled Lactose Monohydrate at the Respective Temperature

Dispersive Surface Free Energy, $\gamma_S^D$ (mJ/m <sup>2</sup> )	30°C	45°C	60°C
SV A	42.0 (1.0)	38.5 (0.1)	35.3 (0.8)
SV B	42.0 (0.3)	39.1 (0.2)	35.7 (0.9)
ML A	41.7 (0.3)	39.2 (0.3)	36.2 (0.5)

Relative standard deviation was <2.5% in each case ( $n = 4$ ).

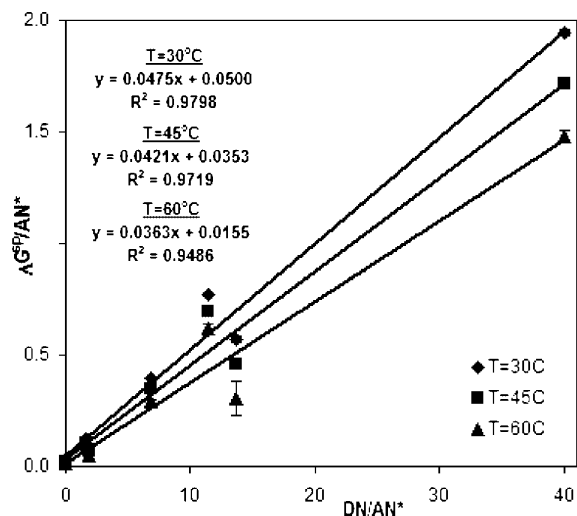


**Figure 1.** Estimating  $K_A$  and  $K_B$  for milled lactose monohydrate, ML A assuming negligible entropic effects.  $\Delta G_A^{sp}/AN^*$  is plotted over  $DN/AN^*$  for each polar probe at four temperatures. Each point is average of  $n = 4$  columns  $\pm$  standard deviation. The fitted lines miss several points (ethanol, ethyl acetate, ether), even though the standard deviations on those points are very small. Acid and base parameters based on this approach are shown in Table 2.

these results are quite distinct at different temperatures; each best-fit (least squares) trendline results in a different intercept and slope, which give different  $K_A$  and  $K_B$  values at every temperature. Magnitude varies and not even rank-order of  $K_A$  and  $K_B$  is preserved. The method differentiates the two sieved batches (which are intrinsically similar) from the milled batch;  $K_A$  and  $K_B$  of the two sieved batches are more similar to each other than to the milled batch. However, the large standard error of  $K_B$  ( $RSD \geq 50\%$  for all  $K_B$ ) precludes inferring the relative magnitudes of the basic properties. The ratio of  $K_A$  to  $K_B$ , which has sometimes been used to contrast materials, also varies widely, from 0.80 at 30°C to 1.12 at 60°C for sieved lactose, and from 0.95 at 30°C to 2.34 at 60°C for the milled lactose. However, the large standard error once again precludes a comparison of this ratio between the batches.

The more rigorous ( $\Delta H_A^{sp}$ -based) analysis produces different results, both in terms of absolute parameter magnitudes and relative rank-order. When entropic contributions ( $-T\Delta S$ ) are included, we arrive at a single set of acid/base parameters, independent of temperature. As shown in Figure 2(B) and by the correlation

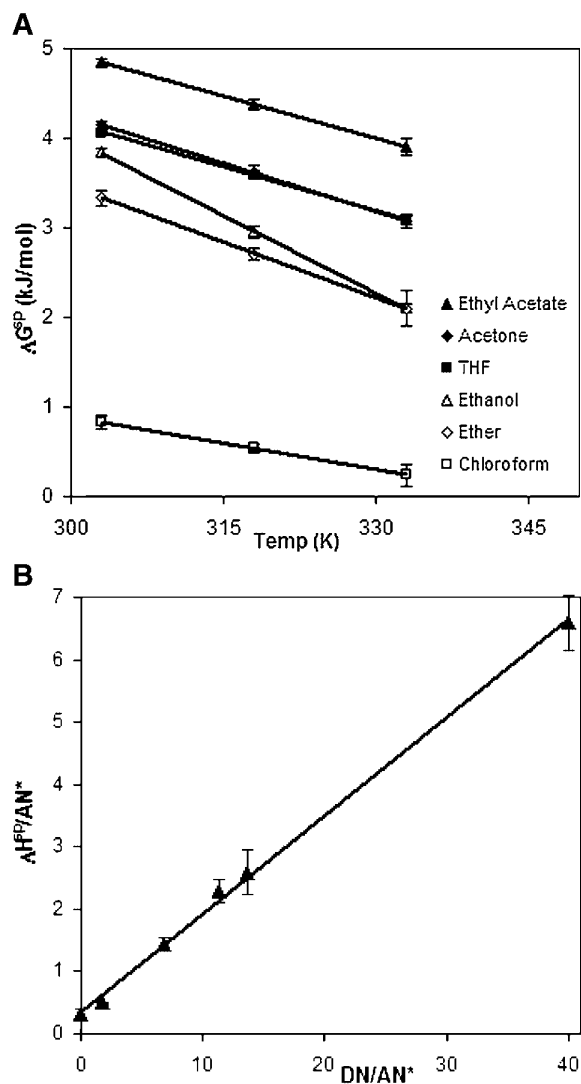


**Figure 2.** Determination of  $K_A$  and  $K_B$  for milled lactose monohydrate, ML A following the approach of Schultz et al. (A)  $\Delta H_A^{sp}$  for each polar probe is first determined from a plot of  $\Delta G_A^{sp}$  vs. Temperature; (B)  $K_A$  and  $K_B$  are determined from a plot of  $\Delta H_A^{sp}/AN^*$  vs.  $DN/AN^*$ . The straight line fit is very good ( $R^2 = 0.998$ ), with points evenly distributed around it (i.e. no bias). Each point is average of  $n = 4$  columns  $\pm$  standard deviation. Acid and base parameters with correlation coefficient of each lactose batch are shown in Table 3.

coefficients ( $R^2$ ) in Table 3, the data fit the linear relationship represented by Eq. (4) very well. The data allow a more meaningful interpretation than was proposed previously. The acidic parameters  $K_A$  of the two sieved batches are essentially

identical but differ from the milled batch ( $p < 0.05$ ). This is consistent with the  $\Delta G$  analysis, though there is no ambiguity, since there is only one value. The analysis suggests that  $K_B$  varies between SV A and the other two batches. This result is not apparent from the simplified correlation. The  $K_A/K_B$  ratio is also more meaningful and shows differences among all three batches. These differences are not detectable from the  $\Delta G$ -based analysis at any one temperature.

Note the correlation coefficients for the best fit straight lines obtained for the rigorous analyses ( $R^2 > 0.99$ ). In the case of the analyses based on  $\Delta G$ , the correlation coefficients ( $R^2$ ) also suggest strong correlations, with  $R^2 > 0.95$  in each case. However, upon closer examination, several probes clearly do not fall onto the regression line. Ether, which has a  $DN/AN^*$  ratio of 13.7, does not fit the line at all, at any temperature. This may explain why ether has been used infrequently in these analyses, although it has favorable probe properties (volatility and single functional group) and a useful  $DN/AN^*$  in the intermediate range. (Note that  $\Delta H_A^{sp}/AN$  for ether is predicted very well.) A strong correlation is obtained nonetheless because some of the points are so close together. The best-fit line is determined almost entirely by THF and chloroform, the most basic and the most acidic probes used, respectively. In fact, determining the trendline based solely on chloroform and THF results in an almost identical fit, giving similar  $K_A$  and  $K_B$ .

The discrepancy between the rigorous and the simplified approach was also observed by Tong et al.<sup>25</sup> However, they obtained more precise data using the simplified correlation, whereas we show much lower standard errors for the enthalpy based correlation. In fact, estimation of  $K_B$  appears impossible with the reduced correlation. As shown by Figure 1 the data suggest that the assumption of negligible entropy does not hold for all probes. Tong et al. do not plot their data and do not provide measures of "goodness of fit". When plots are constructed from their  $\Delta G$  data, linearity is poor. Within the limits of their experimental observations their conclusions were correct. However, we appear to have improved technique that supports a different conclusion.

It is worth noting that the assumption of negligible entropic effects has found little use outside the pharmaceutical literature, even while there have been numerous publications in the interfacial chemistry and chromatography disciplines. It seems reasonable that as a

**Table 2.** Lactose Surface Acid–Base Constants (Standard Error) with Corresponding Correlation Parameters Assuming Negligible Entropic Contributions, According to Eq. (5)

Lactose Batch	Temperature (°C)	$K_A$	$K_B$	$R^2$	$K_A/K_B$
SV A	30	0.0439 (0.0016)	0.0552 (0.0275)	0.970	0.80 (0.43)
	45	0.0389 (0.0016)	0.0343 (0.0285)	0.958	1.13 (0.98)
	60	0.0336 (0.0015)	0.0314 (0.0275)	0.958	1.07 (0.98)
SV B	30	0.0442 (0.0015)	0.0551 (0.0269)	0.968	0.80 (0.42)
	45	0.0388 (0.0014)	0.0383 (0.0262)	0.959	1.01 (0.73)
	60	0.0340 (0.0015)	0.0304 (0.0282)	0.951	1.12 (1.09)
ML A	30	0.0475 (0.0014)	0.0500 (0.0234)	0.980	0.95 (0.47)
	45	0.0421 (0.0014)	0.0353 (0.0246)	0.972	1.19 (0.87)
	60	0.0363 (0.0017)	0.0155 (0.0300)	0.944	2.34 (4.64)

The parameters in the table correspond to the slopes and intercepts of the lines in Figure 1, determined with four columns each, with  $n \geq 3$  injections each. Note that the results are highly dependent on the temperature at which the IGC experiment has been conducted. Despite high number of data points (with column RSD < 5%) the correlation parameter is only  $\sim 0.96$ .

technique is being established for a new application, assumptions might be made. However, given the present interest in IGC and numerous attempts to correlate the data with performance measures, the pharmaceutical literature should strive for the same level of accuracy in experimentation and data interpretation as others. There are recent examples of meaningful results obtained with the rigorous approach,<sup>40</sup> though publications using the  $\Delta G$  approach still predominate.

Lastly, the most significant short-comings of the acid–base approach to specific surface free energy relate to the determination of  $K_B$ , which is determined from the intercept of the correlation, whether the rigorous or the simplified approach is used. One potential way to overcome this problem is to concurrently plot  $\Delta H_A^{sp}/DN$  versus  $AN^*/DN$ , in addition to  $\Delta H_A^{sp}/AN^*$  versus  $DN/AN^*$  and determine  $K_B$  from the slope of the line. The limitation of this approach is the lack of probes which display a useful  $DN/AN^*$  range. However, the analysis is possible if in addition to the commonly used probes, benzene ( $AN^*/$

$DN = 1.7$ ) and/or nitromethane ( $AN^*/DN = 1.6$ ) are used.

## CONCLUSION

Using the same set of data obtained for three batches of lactose monohydrate, two sieved and one milled, two approaches to characterizing surface acid/base interactions using IGC were compared. A simplified approach (where  $\Delta G$  of adhesion is assumed to be equal to  $\Delta H$ ) that has been popular in the pharmaceutical literature was compared with a more rigorous approach for the determination of surface acid/base properties. While assuming  $\Delta G_A^{sp} \approx \Delta H_A^{sp}$  results in immense experimental simplification, it gives a reduced correlation that strongly depends on method and experimental conditions. The values obtained are internally inconsistent, as displayed by temperature dependence, and do not agree with those obtained in the rigorous analysis. While the simplification may be useful for the comparison of different materials, a rigorous analysis of

**Table 3.** Sieved and Milled Lactose Monohydrate Surface Acid–Base Constants (Standard Error) with Corresponding Correlation Parameters Based on the Approach of Schultz et al., in Accordance with Eq. (4)

Lactose Batch	$K_A$	$K_B$	$R^2$	$K_A/K_B$
SV A	0.146 (0.007)	0.463 (0.120)	0.991	0.315 (0.097)
SV B	0.146 (0.003)	0.354 (0.053)	0.996	0.412 (0.070)
ML A	0.158 (0.003)	0.331 (0.057)	0.998	0.477 (0.091)

The parameters in the last row of the table (ML A) correspond to the slope and intercept of the line in Figure 2(B). The sieved batches appear to have a more basic surface, particularly batch SV A, which has a significantly larger  $K_B$  than the other two batches.

similar materials (such as for the detection of batch-to-batch variability of a single product, where differences are presumed to be minute) may require the more exact correlation.

## ACKNOWLEDGMENTS

M. Telko gratefully acknowledges receipt of a U.S. Pharmacopeia Fellowship. The authors are grateful for additional financial support and thoughtful input from John Langridge and Tako Mulder of DMV-Fonterra Excipients, and Dimitris Papadopoulos and Richard McLean of Pfizer.

## REFERENCES

- Schultz J, Lavielle L, Martin C. 1987. The role of the interface in carbon fibre-epoxy composites. *J Adhesion* 23:45–60.
- Ticehurst MD, Rowe RC, York P. 1994. Determination of the surface properties of two batches of salbutamol sulphate by inverse gas chromatography. *Int J Pharm* 111:241–249.
- Cline D, Dalby R. 2002. Predicting the quality of powders for inhalation from surface energy and area. *Pharm Res* 19:1274–1277.
- Columbano A, Buckton G, Wikeley P. 2003. Characterisation of surface modified salbutamol sulphate-alkylpolyglycoside microparticles prepared by spray drying. *Int J Pharm* 253:61–70.
- Kumon M, Suzuki M, Kusai A, Yonemochi E, Terada K. 2006. Novel approach to DPI carrier lactose with mechanofusion process with additives and evaluation by IGC. *Chem Pharm Bull (Tokyo)* 54:1508–1514.
- Sethuraman VV, Hickey AJ. 2002. Powder properties and their influence on dry powder inhaler delivery of an antitubercular drug. *AAPS Pharm Sci Tech* 3:E28.
- AlSaigh ZY. 1997. Review: Inverse gas chromatography for the characterization of polymer blends. *Int J Polym Anal Character* 3:249–291.
- Grimsey IM, Feeley JC, York P. 2002. Analysis of the surface energy of pharmaceutical powders by inverse gas chromatography. *J Pharmaceut Sci* 91:571–583.
- Lloyd DR, Ward TC, Schreiber HP, American Chemical Society, Division of Polymeric Materials: Science and Engineering, Chemical Institute of Canada, Macromolecular Science Division, American Chemical Society, Meeting. 1989. *Inverse Gas Chromatography: Characterization of Polymers and other Materials*. ed., Washington, DC: American Chemical Society. p xii, 331.
- Sun CH, Berg JC. 2003. A review of the different techniques for solid surface acid–base characterization. *Adv Colloid Interf Sci* 105:151–175.
- Fowkes FM. 1962. Determination of interfacial tensions, contact angles, and dispersion forces in surfaces by assuming additivity of intermolecular interactions in surfaces. *J Phys Chem* 66:382.
- Fowkes FM. 1964. Attractive forces at interfaces. *Ind Eng Chem* 56:40–52.
- Gutmann V. 1978. *The Donor–Acceptor Approach to Molecular Interactions*. New York: Plenum Press.
- Riddle FL, Fowkes FM. 1990. Spectral shifts in acid–base chemistry .1. Van der Waals contributions to acceptor numbers. *J Am Chem Soc* 112:3259–3264.
- Drago RS, Vogel GC, Needham TE. 1971. 4-Parameter equation for predicting enthalpies of adduct formation. *J Am Chem Soc* 93:6014–6026.
- Fowkes FM, Mostafa MA. 1978. Acid–base interactions in polymer adsorption. *Ind Eng Chem Prod Res Dev* 17:3–7.
- Joslin ST, Fowkes FM. 1985. Surface-acidity of ferric oxides studied by flow microcalorimetry. *Ind Eng Chem Prod Res Dev* 24:369–375.
- Feeley JC, York P, Sumbly BS, Dicks H. 1998. Determination of surface properties and flow characteristics of salbutamol sulfate, before and after micronization. *Int J Pharm* 172:89–96.
- Ohta M, Buckton G. 2004. The use of inverse gas chromatography to assess the acid–base contributions to surface energies of cefditoren pivoxil and methacrylate copolymers and possible links to instability. *Int J Pharm* 272:121–128.
- Ohta M, Buckton G. 2004. Determination of the changes in surface energetics of cefditoren pivoxil as a consequence of processing induced disorder and equilibration to different relative humidities. *Int J Pharm* 269:81–88.
- Ohta M, Buckton G. 2005. A study of the differences between two amorphous spray-dried samples of cefditoren pivoxil which exhibited different physical stabilities. *Int J Pharm* 289:31–38.
- Planinsek O, Buckton G. 2003. Inverse gas chromatography: Considerations about appropriate use for amorphous and crystalline powders. *J Pharm Sci* 92:1286–1294.
- Planinsek O, Zadnik J, Rozman S, Kunaver M, Dreu R, Srcic S. 2003. Influence of inverse gas chromatography measurement conditions on surface energy parameters of lactose monohydrate. *Int J Pharm* 256:17–23.
- Traini D, Rogueda P, Young P, Price R. 2005. Surface energy and interparticle forces correlations in model pMDI formulations. *Pharm Res* 22:816–825.



25. Tong HH, Shekunov BY, York P, Chow AH. 2002. Influence of polymorphism on the surface energetics of salmeterol xinafoate crystallized from supercritical fluids. *Pharm Res* 19:640–648.
26. Telko MJ, Hickey AJ. 2005. Dry powder inhaler formulation. *Respir Care* 50:1209–1227.
27. Harjunen P, Lehto VP, Martimo K, Suihko E, Laninen T, Paronen P, Jarvinen K. 2002. Lactose modifications enhance its drug performance in the novel multiple dose Taifun DPI. *Eur J Pharm Sci* 16:313–321.
28. Iida K, Inagaki Y, Todo H, Okamoto H, Danjo K, Luenberger H. 2004. Effects of surface processing of lactose carrier particles on dry powder inhalation properties of salbutamol sulfate. *Chem Pharmaceut Bull* 52:938–942.
29. Louey MD, Mulvaney P, Stewart PJ. 2001. Characterisation of adhesional properties of lactose carriers using atomic force microscopy. *J Pharm Biomed Anal* 25:559–567.
30. Newell HE, Buckton G, Butler DA, Thielmann F, Williams DR. 2001. The use of inverse phase gas chromatography to measure the surface energy of crystalline, amorphous, and recently milled lactose. *Pharm Res* 18:662–666.
31. Steckel H, Markefka P, teWierik H, Kammelar R. 2006. Effect of milling and sieving on functionality of dry powder inhalation products. *Int J Pharm* 309:51–59.
32. Ticehurst MD, York P, Rowe RC, Dwivedi SK. 1996. Characterization of surface properties of  $\alpha$ -lactose with inverse gas chromatography, used to detect batch variation. *Int J Pharm* 141:93–99.
33. Zeng XM, Martin GP, Marriott C, Pritchard J. 2001. Lactose as a carrier in dry powder formulations: the influence of surface characteristics on drug delivery. *J Pharm Sci* 90:1424–1434.
34. Mohammad HAH, Fell JT. 1982. Contact angles of powder mixtures consisting of spherical-particles. *Int J Pharm* 11:149–154.
35. Smith RJ, Haken JK, Wainwright MS. 1978. Evaluation of mathematical procedures for the calculation of dead-time. *J Chromatography* 147:65–73.
36. Conder JR, Young CL. 1979. *Physicochemical Measurement by Gas Chromatography*. ed., Chichester, New York: Wiley. p xix, 632.
37. Lide DR, Kehiaian HV. 1994. *CRC Handbook of Thermophysical and Thermochemical Data*. Boca Raton: CRC Press. 518p.
38. Lerk CF, Andreae AC, de Boer AH, de Hoog P, Kussindrager K, van Leverink J. 1984. Alterations of alpha-lactose during differential scanning calorimetry. *J Pharm Sci* 73:856–857.
39. Ahfat NM, Buckton G, Burrows R, Ticehurst MD. 2000. An exploration of inter-relationships between contact angle, inverse phase gas chromatography and triboelectric charging data. *Eur J Pharm Sci* 9:271–276.
40. Baumgartner S, Planinsek O, Srcic S, Kristl J. 2006. Analysis of surface properties of cellulose ethers and drug release from their matrix tablets. *Eur J Pharm Sci* 27:375–383.

**APPENDIX C.**

**INVESTIGATION OF TRIBOELECTRIC CHARGING IN DRY POWDER INHALERS  
USING ELECTRICAL LOW PRESSURE IMPACTOR (ELPI™)**

## Investigation of triboelectric charging in dry powder inhalers using electrical low pressure impactor (ELPI™)

Martin J. Telko<sup>a</sup>, Jukka Kujanpää<sup>b</sup>, Anthony J. Hickey<sup>a,\*</sup>

<sup>a</sup> Division of Molecular Pharmaceutics, School of Pharmacy, CB 7360, The University of North Carolina, Chapel Hill, NC 27599, USA

<sup>b</sup> Dekati Ltd., Tampere, Finland

Received 1 November 2006; received in revised form 13 December 2006; accepted 14 December 2006

Available online 20 December 2006

### Abstract

Electrostatics and triboelectrification phenomena in dry powder inhalers (DPI) are not well understood, but as shown in this study they may play an important role. Using model formulations of albuterol in lactose, the extent of triboelectrification in the operation of DPI was investigated using an electrical low pressure impactor (ELPI™). An experimental apparatus was developed, the performance of the ELPI™ was evaluated for consistency and reproducibility, and compared to a conventional inertial impactor. Using a statistical experimental design the effects of lactose type, drug load, capsule fill, capsule material, and inhaler were assessed. DPI formulations appear to be subject to strong triboelectric effects. Charge separation can occur between different size fractions, i.e. different fractions can carry charges of different sign. In particular, lactose type, inhaler, and capsule material have a strong effect on the magnitude and polarity of the charge developed during DPI operation. The study suggests that the polarity of the aerosol can be controlled by choice of lactose type, capsule material, and inhaler, which could be exploited for targeting different lung physiologies.

© 2006 Elsevier B.V. All rights reserved.

**Keywords:** Triboelectrification; Dry powder inhaler (DPI); Electrical low pressure impactor (ELPI™); Formulation

### 1. Introduction

Electrostatic attraction between particles is a well-known event. It is of particular importance to small particles which have comparatively large surface areas. For particles smaller than 10 μm in size electrostatic forces can be many times larger than gravitational, fluid-dynamic forces, and other forces acting upon them. The property is exploited by various air-cleaning and aerosol sampling equipment, such as the electrostatic precipitator and the electrical mobility analyzer. While particle charging has been studied in a manufacturing and environmental context, its effects on the delivery of therapeutic aerosols have yet to be fully elucidated.

Dry powder inhalers (DPI) are important delivery devices for respirable medicines (Timsina et al., 1994). As the name suggests, DPI formulations consist of dry blends, typically consisting of micronized drug and larger carrier particles (Telko and

Hickey, 2005). Carriers, often lactose monohydrate, reduce drug agglomeration and aid in metering and dispersion. For effective delivery to the peripheral lungs, drug particles need to be ≤5 μm in aerodynamic diameter. Particles in this size range have specific surface areas in the order of several square meters per gram. Since charging is a surface phenomenon, particles in the respirable size range can accommodate large charges. In addition, most drugs and pharmaceutical excipients are organic molecules with high resistivity maintained at low humidities, which makes them prone to electrostatic charging.

Deposition in the lungs occurs by inertial impaction, diffusion, interception, and electrostatic deposition (Gonda, 2004). Computer simulations have indicated that electrostatic deposition dominates in the lower lung regions, particularly the alveoli (Balachandran et al., 1997). The alveolar region is the site of most β-adrenergic receptors (Labiris and Dolovich, 2003) as well as the region from which systemic absorption is most efficient, thus it is an important site for targeting therapeutic aerosols.

Aerosol particles can acquire charge by flame charging, static electrification, diffusion charging, and field charging (Hinds,

\* Corresponding author. Tel.: +1 919 962 0223; fax: +1 919 966 0197.  
E-mail address: [ahickey@unc.edu](mailto:ahickey@unc.edu) (A.J. Hickey).

1999). Of these mechanisms, static electrification plays the predominant role during DPI actuation. Static electrification occurs when particles are detached from surfaces or the bulk phase resulting in a separation of charges. In DPIs, this takes the form of surface charging, or triboelectrification. When drug and carrier particles are separated from each other or the surfaces of the dosage form or inhaler, charge can be transferred resulting in a net charge on the particles. Particles experience significant friction during DPI discharge which tends to amplify this effect. The extent to which triboelectrical charging in DPIs occurs, however, has not been investigated from a formulation perspective.

The studies described here evaluate the influence of triboelectrical charging of simple two-component DPI model formulations; magnitude and polarity of resulting currents are measured over time and the effects of lactose type, drug load, capsule fill weight, capsule material, and inhaler type are investigated in the framework of a comprehensive experimental design scheme. The experimental setup makes use of the electric low pressure impactor (ELPI™), a particle sizing device that detects particles by charge (Keskinen et al., 1992).

The ELPI™ has been used primarily in the analysis of environmental effects in the automotive industry (Holmen and Qu, 2004; Lehmann et al., 2004; Maricq et al., 2002; Sanders et al., 2003) and in industrial hygiene applications (Brouwer et al., 2004; Ferge et al., 2004). Only recently it has been applied to the evaluation of metered dose inhaler electrostatics (Kwok et al., 2005).

A detailed discussion and evaluation of the ELPI™ is available elsewhere (Marjamaki et al., 2000). The ELPI™ is composed of a unipolar corona aerosol charger and a low pressure cascade impactor. Deposition inside the impactor is dependent on particle aerodynamic diameter. Unlike conventional cascade impactors which are disassembled and the stages assayed chemically or gravimetrically after operation, ELPI™s detect deposited particles by measuring the current resulting from dissipation of the particles' electrical charge. The collected particle fractions can be measured simultaneously on all stages using a multichannel electrometer. Thus, when the ELPI™ is operated with charger turned on, it functions as a near real-time particle sizer. However, when operated with the charger off, particle charge is measured (main focus in this paper). The ELPI™ is a low pressure impactor; operation at reduced absolute pressures (10 kPa on the final stage) allows collection of particles down to a size of 30 nm (with filter stage to 7 nm). (By contrast, the Anderson cascade impactor operates at ambient pressures with a pressure drop of ~5 kPa across the device at flowrates of 30 L/min.)

Studies of medicinal aerosol electrostatics have been attempted before. Electrostatic charge carried by a DPI aerosol cloud has been measured using a grid probe (Murtomaa et al., 2003); however, the particles were rather large and the system was of little pharmaceutical relevance. The effects of particle morphology and crystallinity on triboelectrification of dry powder inhalers have also been studied, but particle deposition was not considered (Murtomaa et al., 2004). Moreover, a Faraday cage was used for the charge measure-

ment, which precluded analysis of different size fractions and charge distribution. Use of the ELPI™ for studying DPI electrostatics allows a more comprehensive investigation of the phenomenon, with accurate determination of magnitude and polarity of charges on particles in the respirable size range over time. Furthermore, since each impactor stage is electrically isolated from the next, charges can be measured across individual stages, allowing size specificity of charging to be evaluated.

## 2. Materials and methods

### 2.1. Materials

Lactose monohydrate, Respitose™, was provided by DMV-Fonterra Excipients. One batch of milled (ML001), and one batch of sieved (SV003) lactose, were used. Milled albuterol sulfate (median particle size 2 µm) was supplied by Chemaco (Beetsterzwaag, NL) from drug manufactured by P.F.C. Italiana S.r.l (Caronno Pertusella, Italy). Hard gelatin capsules (Capsugel Coni-snap™, lot 70016321) and carrageenan capsules (Capsugel NPcaps™, lot 38611), both #3 and transparent, were used in the study.

Two different inhalers were tested; both deliver their doses from capsules, but have otherwise different operational principles. The Rotahaler® (GlaxoSmithKline, RTP, NC) is a low resistance device; the capsule is discharged after separation of the cap from the capsule body. The Inhalator® single capsule inhaler (Boehringer Ingelheim, Germany) is a high resistance device in which drug is removed from the capsule through punctured holes (Dunbar et al., 1998). Specific device resistance of Inhalator® and Rotahaler® are 0.180 and 0.040 cm H<sub>2</sub>O 1/2/(L/min), respectively (Clark and Hollingworth, 1993).

### 2.2. Blending

Four formulations were manufactured in 5.0 g batch sizes using a method that had previously been validated in the laboratory. Drug and lactose were sieved prior to blending using a #125 mesh to promote deagglomeration. Albuterol was geometrically diluted to concentrations of 0.5% or 1% with lactose, then blended for 2 min in a 60 mL vial using a custom made small-scale planetary mixer operating at 150 rpm.

### 2.3. Blend uniformity

Content uniformity of the blends was ascertained by withdrawing 5 samples (~10 mg each) from different locations in the powder bed using a 1 mm inner diameter sample thief. Four of the locations were at ~90° to one another, close to the vial wall; the fifth sample was withdrawn from the center. Use of the narrow bore thief allowed lateral sampling of small material quantities representing powder from varying bed heights. The samples were weighed and dissolved in water. UV absorbance of the solutions was assessed at a wavelength of 224.6 nm using a Shimadzu 160U spectrophotometer. Lactose has negligible absorbance at this wavelength.

#### 2.4. Capsule filling

Capsules were hand-filled with  $15 \pm 1$  mg or  $30 \pm 1$  mg of formulation. Actual net fill weight averages were  $15.2 \pm 0.3$  mg and  $30.2 \pm 0.4$  mg. Empty capsule and net-fill weights were determined for each capsule. Each capsule was stored in an individual, labeled container. Since capsules were filled immediately prior to dosing, no capsule was stored for more than 2 h. After dosing each empty capsule was removed from the inhaler and placed back into its weigh boat; empty (post-dosing) capsules were weighted and weight delivered was determined. Actual material delivered averages were  $14.6 \pm 0.7$  mg (15 mg nominal fill weight) and  $29.2 \pm 1.2$  mg (30 mg nominal fill weight). When more than 10% of the fill weight was retained in the capsule (select cases), the recorded ELPI™ data were excluded from the analysis. No significant differences in emitted dose were observed between the different inhalers, formulations, or capsules.

#### 2.5. ELPI™ experimental apparatus

The experimental apparatus was developed to overcome two major obstacles: (1) operation at 30 L/min and (2) pre-separation of agglomerates. (1) The ELPI™ (Dekati Ltd., Tampere, Finland) operates at 30 L/min, but inhalers are typically tested at 60 L/min airflow rates; (2) unlike the Anderson cascade impactor (ACI, ThermoAnderson, Smyrna, GA), the ELPI™ does not have a preseparator capable of removing large quantities of material. However, initial work made clear that failure to remove carrier particles and agglomerates from the aerosol prior to introduction into the ELPI™ could result in flooding of the top stages after a single inhaler actuation. The setup that was devised to address these issues is shown in Fig. 1. The DPI is connected to the mouthpiece and standard USP induction

port, which is connected to the ACI pre-separator (loaded with 15 mL water) (cut-off size of  $8.6 \mu\text{m}$  at 60 L/min). A custom-manufactured aluminum part connected the pre-separator and split the 60 L/min stream into two; 40 cm Tygon™ tubing (R3603) was used to connect the two outlets with ELPI™ and ACI, each connected to a vacuum pump operating at 30 L/min. Tygon™ tubing is commonly used in aerosol research; unlike other materials, Tygon™ has negligible electrostatic effects (Liu et al., 1985). Deposition of drug in different parts of the experimental setup was determined; deposition in the custom-made part and tubing accounted for <5% of deposition in the ELPI™ and ACI. To prevent particle bounce ACI collection plates were coated with silicon oil. Coated aluminum foils were used with the ELPI™ stages. The apparatus was leak tested prior to each experiment.

Both ELPI™ and ACI were used to classify the particles. In accordance with manufacturer recommendations, the ELPI™ was switched on at least 1 h prior to measurement. Inlet air was not filtered and baseline measurements of charge were collected.

#### 2.6. ELPI™ versus ACI comparison

The ELPI™ was operated with corona charger and trap voltages turned off. Using the experimental arrangement described particle size distributions were obtained from ELPI™ and ACI. Capsules ( $6 \times 30$  mg) containing micronized albuterol, and different formulations ( $10 \times 30$  mg) were actuated with ELPI™ and ACI operating as described. The equipment was then turned off and disassembled, and the stages assayed gravimetrically (for total deposition) and chemically (for drug deposition).

#### 2.7. ELPI™ output versus gravimetric determination

While it is used here for charge measurements, ELPI™ is primarily used for particle sizing. This function was assessed by comparing the particle size distributions recorded by the device with a gravimetric determination of deposited material. For this purpose the ELPI™ was run with charger, trap, and correction (Virtanen et al., 2001) turned on. Capsules containing different formulations ( $10 \times 30$  mg) were actuated sequentially and sampled by ELPI™ and ACI. The ELPI™ was then disassembled and the total deposition on each stage was determined gravimetrically. The particle size distributions acquired by the ELPI™ were compared to the particle size distribution obtained from gravimetric data.

#### 2.8. Particle size analysis

After the ELPI™ was validated with respect to the ACI and gravimetric analysis of its stages, it was used to size the ELPI™ fractions ( $<8.6 \mu\text{m}$ ) from each formulation. These experiments were conducted with the corona charger and trap turned on. Using the Inhalator®, each formulation was dosed in 30 mg-filled capsules in randomized order three times (12 doses). The data collected in each run were used to determine the quanti-

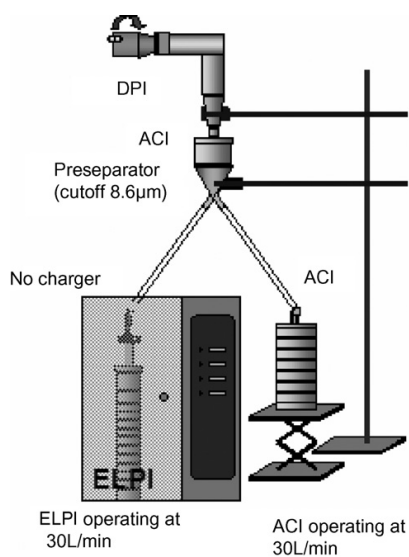


Fig. 1. Experimental set-up.

ties and particle size distributions of ELPI<sup>TM</sup> fractions of the deposited formulations.

### 2.9. Experimental design

The objective of the experimental design was to quantify the contributions of different formulation variables with respect to magnitude and polarity of triboelectrification during DPI actuation. The experimental design was used to investigate the contribution of several common formulation variables:

- (1) *drug load*: 0.5% (w/w) and 1.0% (w/w) albuterol;
- (2) *lactose grade*: sieved lactose and milled lactose;
- (3) *capsule material*: Carrageenan and Gelatin;
- (4) *capsule fill*: 15 mg and 30 mg;
- (5) *inhaler type*: Rotahaler<sup>®</sup> (low resistance) and Inhalator<sup>®</sup> (high resistance device).

The choice of full-factorial design for the above five variables each at two levels/categories yields  $2^5 = 32$  individual data points. Each setting (combination of five factors) was tested at least three times ( $n \geq 3$ ). The experiments were divided into blocks of 16 actuations and the order was randomized. Inhaler and equipment were disassembled and cleaned between blocks.

### 2.10. Environmental conditions

The extent to which triboelectric charging occurs depends in part on the environmental conditions; triboelectrification is only observed at relative humidities of less than 65% (Hinds, 1999). Hence, conditions must be monitored closely. The data for the experimental design were collected over the course of 2 weeks; the conditions during blending, storage, capsule filling, and actuation were constant at a temperature of  $23 \pm 0.5$  °C and a relative humidity of  $39 \pm 1\%$ .

### 2.11. Data analysis

Data were collected by the ELPI<sup>TM</sup> data acquisition system, ELPI<sup>TM</sup>VI 4.0 (Dekati, Tampere, Finland). Raw data were analyzed using Excel software (Microsoft, Seattle, WA). Each actuation was isolated and charge was integrated over the time the actuation had occurred. This data were fed into statistical software Design-Expert 5 (Stat-Ease Corporation, Minneapolis, MN). Total magnitude and polarity (summed across all stages) were designated as response elements. The influence of each of the five factors was determined.

## 3. Results and discussion

### 3.1. Blend uniformity

Blend uniformity was determined by withdrawing five samples (ca. 10 mg each) from each blend and determining the drug content by chemical assay. All blends were within 5% of claim and relative standard deviation of the five samples was <5% in each case.

### 3.2. ELPI<sup>TM</sup> versus ACI comparison

Since the ELPI<sup>TM</sup> is not frequently used for pharmaceutical applications, initial experiments were conducted to assess its ability to classify therapeutic aerosols consistently and in accord with a conventional method, i.e. the ACI. The equipment was validated using micronized albuterol alone and as a component of a 1.0% formulation using two different DPIs. These combinations were chosen to represent scenarios relevant to subsequent studies. After actuations, the equipment was disassembled and stages were weighed or deposition of drug was determined chemically. The details and results of the validation experiments are shown in Table 1. Several capsules were dosed sequentially in each case to ensure sufficient deposition on each stage so discriminating particle size distributions could be obtained. Particle size distributions shown reflect drug deposition only.

The agreement between ELPI<sup>TM</sup> and ACI was good with almost superimposable particle size distributions for drug (represented by cumulative % fines, since the division of intervals differs) and  $d_{50}$  values differing by no more than 0.1  $\mu\text{m}$ . The  $d_{50}$  values of approximately 2.0–2.2  $\mu\text{m}$  are consistent with particle size given by the manufacturer. One representative particle size distribution comparison for drug is shown in Fig. 2; 1.0% albuterol in milled lactose produced identical drug particle size distributions in both measurement devices.

### 3.3. ELPI<sup>TM</sup> output versus gravimetric determination

The particle sizes acquired by the ELPI<sup>TM</sup> compared well to the particle size distribution obtained from gravimetric data. This is shown in Fig. 3, where ELPI<sup>TM</sup> output is compared to the gravimetric determination of its stages. Discrepancy was observed in the lower particle sizes; however, this may be explained by the limited resolution of the gravimetric analysis; deposition on the lower stages ( $\leq 0.39$   $\mu\text{m}$ ) was in the single microgram range, which is the resolution of the analytical balance used. The ELPI<sup>TM</sup> is thought to be more reliable in this

Table 1  
Formulations/device combinations tested for ELPI<sup>TM</sup> ACI comparison and  $d_{50}$  of recovered drug

Formulation	Device	Number of capsules, target fill weight	$d_{50}$ , cumulative undersize
Micronized albuterol	Rotahaler <sup>®</sup>	5 × 6.0 mg capsules	ELPI <sup>TM</sup> : $d_{50} = 2.0$ ; ACI: $d_{50} = 2.1$
1.0% albuterol in milled lactose	Rotahaler <sup>®</sup>	10 × 30 mg capsules	ELPI <sup>TM</sup> : $d_{50} = 2.1$ ; ACI: $d_{50} = 2.2$
	Inhalator <sup>®</sup>	10 × 30 mg capsules	ELPI <sup>TM</sup> : $d_{50} = 2.0$ ; ACI: $d_{50} = 2.1$

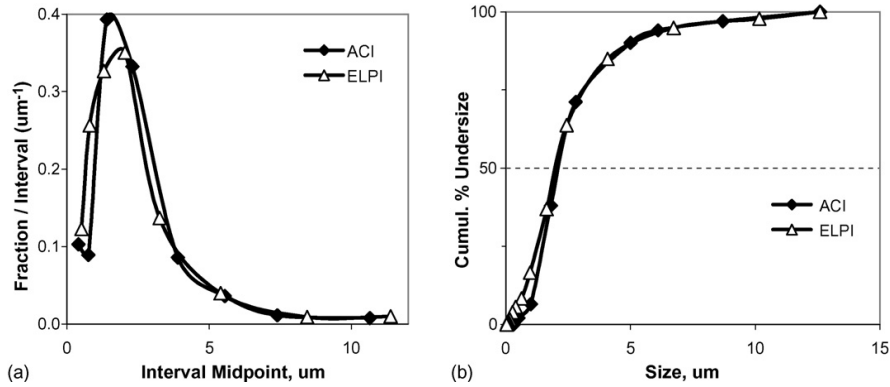


Fig. 2. Particle size distribution of micronized albuterol dosed in 30 mg capsules of 1.0% albuterol in milled lactose via the Inhalator<sup>®</sup> at 60 L/min (determined chemically): (a) fraction per stage normalized for interval width; (b) cumulative % undersize. White triangles represent data collected with ELPI<sup>™</sup>, solid diamonds data collected with ACI.

region. Note that chemical analysis was not used, because total deposition (of drug and lactose) was measured.

3.4. Particle size distributions

The ELPI<sup>™</sup> was in agreement with the ACI (Section 3.2) and the particle size distributions it generates were consistent with gravimetric analysis of the stages (Section 3.3). Having confidence in its ability to size particles, the ELPI<sup>™</sup> was used to determine the particle size distributions of the deposited fines (<8.6 μm) of each of the four formulations. The resulting particle size distributions accounting for both drug and lactose (each the average of three measurements/actuations) are shown in Fig. 4. The particle size distributions are similar, most points are within the standard deviations of the actuations. Standard deviations

on the particle size distributions indicate that particle size distribution varies somewhat from one actuation to the next; the largest variability is observed on the lowest stages, where deposition was very low. The amount of material deposited varied for the formulations; the more disperse milled lactose has a larger portion of fine particles compared with sieved lactose (11.8% versus 7.3% below 8.5 μm, internal data), and therefore resulted in higher deposition on all stages. Total relative depositions are given in Table 2. This deposition pattern is considered in subsequent analyses of electrostatics.

3.5. Charge versus particle size

Charge does not appear to be uniformly distributed with respect to particle size or formulation. Fig. 5 shows five actuations of 0.5% albuterol in milled lactose in 30 mg gelatin

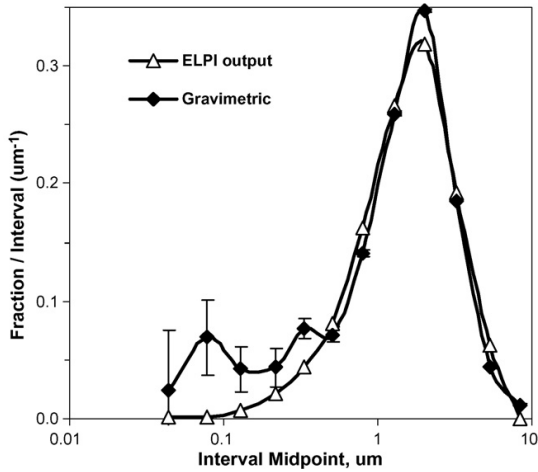


Fig. 3. Particle size distribution of 1.0% albuterol in milled lactose, dosed in 10 × 30 mg capsules delivered by Rotahaler<sup>®</sup> at 60 L/min. Figure shows the size distribution as recorded by ELPI<sup>™</sup> (white triangles) and by gravimetric analysis (black diamond). Conformance is good except in lower region, where resolution of gravimetric analysis is highly limited. Error bar gives resolution of analytical balance, ±0.003 mg.

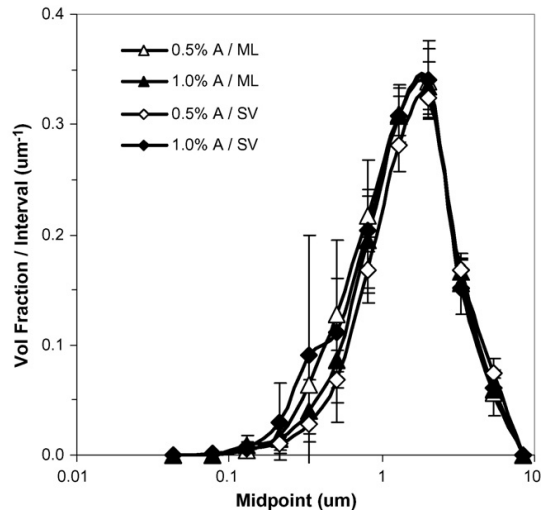


Fig. 4. Particle size distributions of fine particles (<8.6 μm) of the four formulations used as recorded by ELPI<sup>™</sup> (n = 3, mean ± S.D.).

Table 2  
Relative deposition of particles <8.6 μm (entire formulation) in ELPI™

Formulation (drug load and lactose)	Amount deposited average of 3 × 30 mg capsules
0.5% albuterol/SV lactose	100
1.0% albuterol/SV lactose	102
0.5% albuterol/ML lactose	198
1.0% albuterol/ML lactose	240

Deposits relative to 0.5% A/SV. Total deposit for this formulation was 0.5 mg.

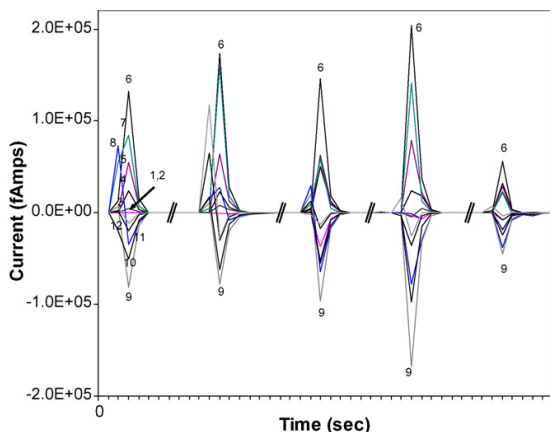


Fig. 5. Five actuations (each performed in different block, i.e. different day, in a different order) of 0.5% albuterol in ML lactose, 30 mg gelatin capsule, dosed via Inhalator®. Double line indicates temporal discontinuity. Capsule emptying and deposition on stages takes about 6 s in each case. The numbers on first actuation indicate the stages on which the electric charge was recorded. While there is some variability, particularly with regards to magnitude, the overall rank/order and polarity is preserved in each trial as shown on the subsequent actuations.

capsules, dosed via Inhalator®. Each actuation was performed in a different experimental block, i.e. on different days (graphs have been merged to facilitate direct comparison). The figure provides insight into formulation delivery by the inhaler. Clearly

there is some variability, however there are many common features. The data provide temporal insight into how emission from the device and deposition in the ELPI™ occurs. Capsule emptying and deposition in the ELPI™ takes about 6 s in each case but deposition on the stages does not occur simultaneously. This temporal data might make ELPI™ a useful screening tool to evaluate formulation and device differences in emission; a thorough discussion of this is beyond the scope of this paper. The numbers (shown on first actuation) indicate the stages on which the charge was recorded. While there is variability with regards to magnitude, the overall rank/order and polarity is preserved in each trial. For example, stage 6 (cut-off size 0.39 μm) is highly positive in each actuation, while stage 9 (cut-off size 1.6 μm) delivers a highly negative charge in each actuation. Actuations of the same formulation/capsule/inhaler combination give a consistent charge distribution which differs for other formulation/capsule/inhaler combinations.

Fig. 6 shows the particle size distribution and total charge observed (integrated over the time course of the actuation) during actuations for two formulations (a) 0.5% albuterol in milled lactose, delivered from 15 mg carrageenan capsule and (b) 1.0% albuterol in sieved lactose, delivered from 30 mg gelatin capsules. Each of the charge profiles is the average of five actuations, performed via the Inhalator® on different days. Particle size distributions were determined separately as described in Section 3.4. Note that the charge profiles of the two formulations are very different. Formulation (a) has a large portion of positively charged particles below stage 9 (cut-off size 1.6 μm), but is negatively charged at and above stage 9. This formulation clearly shows that different size particles can carry opposite charges, as observed by Murtomaa et al. (2004). By contrast, the second graph shows an entirely negative charge distribution. In both graphs, and in most cases observed in these experiments, the largest charge (whether positive or negative) was observed at particle size fractions which accounted for the largest portion of particles by surface area, i.e. stages 7 and 8 (cut-off sizes of 0.63 and 0.97 μm, respectively).

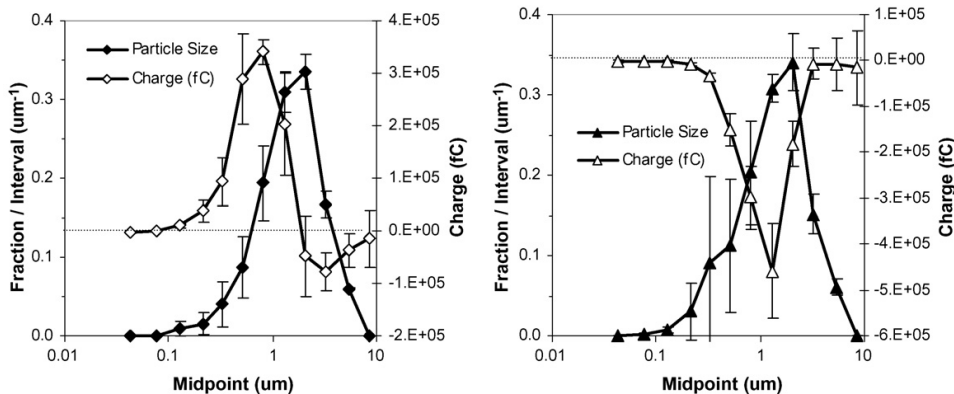


Fig. 6. Particle size distribution ( $n = 3$ , mean  $\pm$  S.D.) (solid) and deposited charge per stage (i.e. current flow) ( $n = 5 \pm$  S.D.) (white) for (a) 1.0% albuterol in milled lactose, delivered from 15 mg carrageenan capsule and (b) 1.0% albuterol in sieved lactose, delivered from 30 mg gelatin capsules, both delivered via Inhalator®. The dashed line indicates charge neutrality.



### 3.6. Experimental design analysis

Magnitude and polarity of electrical charge recorded varied widely depending on the combination of formulation, capsule, and inhaler used. To facilitate statistical analysis, the charges were integrated over time and summed across the different stages, and total charges were recorded as response variables. Using the statistical software, the effects of the five factors (inhaler type, drug load, lactose grade, capsule fill, and capsule material) were evaluated with respect to net charge, as well as to magnitude of charge and polarity ( $-1$  was assigned to each actuation that yielded a net negative charge,  $+1$  where the net charge was positive). The important distinction between net charge and charge magnitude is that opposite charges cancel each other when they are summed to obtain net charge, whereas absolute values, i.e. magnitudes, are summed to obtain charge magnitude.

The results of the experimental analysis, with contribution and significance level for each factor are presented in Table 3. The complete data set with net charge and charge magnitude for the 32 different factor combinations is summarized in Table A1 in Appendix A. The average magnitude for all actuations was  $0.473 \pm 0.337$  nC. Note that electrostatic charge had been measured previously using Faraday cage experiments (not shown); the average recorded charges were in the  $\pm 0.25$  to  $2.0$  nC/g range for several lactose batches and select drugs. Based on the amount of material recovered on the ELPI<sup>TM</sup> stages the expected charge captured by the ELPI<sup>TM</sup> would have been in the  $100$ – $1000$  fC range. However, the charges recorded were at least four orders of magnitude larger in each case, which strongly suggests that triboelectrification during DPI actuation is the main contributor to overall charge.

As can be observed in Table 3, magnitude and polarity of charge are highly correlated with most factors studied. Despite

the inherent variabilities in the data, net charge is highly correlated with all factors except fill weight. There are a number of relevant two-factor interactions. Separation of net charge into absolute magnitude (where negative and positive charges do not cancel each other) and polarity deconvolutes the analysis and allows contributions to be considered separately. Thus, choice of capsule has a large effect on the polarity of the charge but has only a minor (though also statistically significant) effect on the magnitude of the charge. Similarly, fill weight is shown to affect the magnitude (as would be expected) but not the polarity. There are no two-factor interactions that affect polarity, but choice of Inhalator<sup>®</sup> and milled lactose and/or carrageenan capsules has a synergistic effect on charge magnitude.

The effects of drug load and fill weight on magnitude of charge are predictable since they are tied to the amount of material deposited. The effects of lactose can only partly be explained by mass considerations. Milled lactose has a larger fraction of fine particles, so fraction depositing inside the ELPI<sup>TM</sup> is greater, but the contribution of lactose exceeds the effects of drug load and fill weight. It is, therefore, likely that the morphology (shape and surface characteristics) of the milled lactose promotes triboelectric charging (compared to sieved lactose). It has been suggested that different morphology could result in change in polarity of charge (Murtomaa et al., 2004) as observed in the present studies. However, the ELPI<sup>TM</sup> experiments provide additional insight with regards to bipolar charging during single actuations. The effects of inhaler and capsule material cannot be explained by mass considerations alone, since differences in amount of material delivered between the two inhalers were small and there were no differences between the capsules. The increased charge of the Inhalator<sup>®</sup> is likely tied to the increased friction, since the Inhalator<sup>®</sup> has a higher pressure drop, which results in a higher rate of shearing and thus more charge separation (Srichana et al., 1998). The effect

Table 3  
Calculated effects and standard errors for 2<sup>5</sup> factorial ELPI<sup>TM</sup> experimental design

Factors (reference level)	Effect on net charge <sup>a</sup> ± standard error	Effect on absolute polarity of charge ± standard error	Effect on charge magnitude <sup>b</sup> ± standard error
<b>Main effects</b>			
Inhaler (Inhalator <sup>®</sup> )	+0.074 ± 0.025 nC $p=0.0032$	+0.28 ± 0.064*	+0.246 ± 0.029 nC*
Drug load (1.0%)	-0.049 ± 0.021 nC $p=0.022$	No effect	+0.124 ± 0.026 nC*
Lactose (milled)	+0.234 ± 0.022 nC*	+0.65 ± 0.055*	+0.143 ± 0.026 nC*
Fill weight (30 mg)	+0.0055 ± 0.021 (no effect)	No effect	+0.134 ± 0.026 nC*
Capsule (carrageenan)	+0.143 ± 0.034 nC*	+0.29 ± 0.055*	+0.081 ± 0.025 nC $p=0.0017$
<b>Two-factor interactions</b>			
Inhaler × drug load (Inhalator <sup>®</sup> × 1.0%)	No effect	-0.15 ± 0.057 $p=0.0116$	+0.098 ± 0.026 nC $p=0.0003$
Inhaler × lactose (Inhalator <sup>®</sup> × milled lactose)	+0.178 ± 0.022 nC*	No effect	+0.110 ± 0.026 nC*
Inhaler × fill weight (Inhalator <sup>®</sup> × 30 mg)	No effect	No effect	+0.082 ± 0.026 nC $p=0.0021$
Inhaler × capsule (Inhalator <sup>®</sup> × carrageenan)	+0.094 ± 0.022 nC*	No effect	No effect
Drug Load × lactose (1.0% × milled lactose)	+0.142 ± 0.021 nC*	No effect	No effect
Lactose × fill weight (milled lactose × 30 mg)	+0.117 ± 0.021 nC*	No effect	No effect
Lactose × capsule (milled × carrageenan)	+0.089 ± 0.021 nC*	+0.10 ± 0.055 $p=0.0634$	+0.149 ± 0.025 nC*
<b>Three-factor and higher interactions</b>			
	Insignificant		

<sup>a</sup> Net charge refers to the currents summed across stages and integrated over time.

<sup>b</sup> Charge magnitude refers to the absolute values of the currents summed across stages and integrated over time.

\*  $p < 0.0001$ .

of capsule material is perhaps more surprising. Use of capsules made of carrageenan, a carbohydrate polymer, results in higher triboelectric charging than use of gelatin (protein) capsules.

The effects on magnitude of charge are difficult to interpret unequivocally, since they are tied in part to mass deposited inside the ELPI™, which is variable and was not determined for each individual actuation. The effects on absolute polarity are easier to interpret as they are consistent and independent of mass. Use of the Inhalator®, milled lactose, and/or carrageenan increased the formulation's propensity to acquire a positive charge, while Rotahaler®, sieved lactose, and/or gelatin led to negative charging. These effects are statistically highly significant, and these properties could be exploited for delivery purposes. Several studies have implicated electrical charge in lung deposition and have suggested exploiting charge for enhanced delivery (Bailey, 1997; Bailey et al., 1998; Hashish et al., 1994; Wilson, 1947). The results of this study suggest that polarity can be exploited for delivery purposes as well, since it can be controlled quite well and quite easily. Of course there are limitations to the approach. The current study considers only two devices that use single dose capsules to deliver drug, whereas blister packs and reservoirs are more commonly used. Also, storage effects are not considered, but would be expected to play a role.

This paper considers electrical charges of particles in the <8.6 μm range. Note that charged particles can remain in the inhaler and thus result in poor delivery from the device. Only particles that have been emitted from the device, have separated successfully from the carrier particles, and have cleared the preseparator, i.e. particles smaller than 8.6 μm in aerodynamic size (cut-off size of ACI preseparator) are recorded. Despite the fact that these particles account only for a small fraction of the total, the results can help predict situations (e.g. formulation, device) where electrostatics may either be a design advantage or limitation.

#### 4. Conclusions

Triboelectric charging during DPI actuation was quantitatively assessed using an ELPI™. DPI actuation gives rise to significant triboelectric charging, which is orders of magnitude larger than the charge predicted from Faraday cage experiments. The charge magnitude and polarity of fine particles deposited in the ELPI™ was measured and correlated with various formulation variables. Choice of lactose grade, inhaler device, and capsule material have a strong effect on both magnitude and polarity of triboelectrification. These properties could be exploited for therapeutic purposes. The ELPI™ is a device that is not regularly used in pharmaceutical aerosol work. The study has assessed the ELPI™ and validated its measurements against chemical and gravimetric analysis of its stages, and against the more commonly used Anderson cascade impactor. A potentially valuable attribute of the ELPI™ is its ability to provide temporal deposition data across the stages; while not analyzed and discussed thoroughly in the context of this study, this data could help evaluate device and formulation emission and deposition characteristics from a temporal perspective.

#### Acknowledgements

The authors thank Dekati Ltd. for loaning us an ELPI™, and Henna Isherwood from Dekati Ltd. for valuable discussion. The UNC Physics shop is thanked for custom manufacture to specs of the pre-separator attachment. Telko gratefully acknowledges receipt of a U.S. Pharmacopeial Fellowship. The authors are grateful for additional financial support and thoughtful input from John Langridge and Tako Mulder of DMV-Fonterra Excipients, and Richard McLean of Pfizer.

#### Appendix A

See Table A1 .

Table A1  
Results of experimental design studies: net charge and charge magnitude, average value ( $n \geq 3$ )  $\pm$  standard error

Lactose	Drug load (%)	Inhaler	Capsule fill (mg)	Capsule	Net charge (nC) (rank order) <sup>a</sup>	Charge magnitude (nC) (rank order) <sup>b</sup>
Milled	0.50	Inhalator®	30	Gelatin	0.161 $\pm$ 0.195 (7)	0.726 $\pm$ 0.259 (6)
Milled	0.50	Inhalator®	30	Carrageenan	0.809 $\pm$ 0.248 (2)	1.227 $\pm$ 0.331 (3)
Milled	0.50	Inhalator®	15	Gelatin	0.079 $\pm$ 0.057 (9)	0.417 $\pm$ 0.183 (9)
Milled	0.50	Inhalator®	15	Carrageenan	0.351 $\pm$ 0.178 (4)	0.607 $\pm$ 0.233 (8)
Milled	0.50	Rotahaler®	30	Gelatin	-0.076 $\pm$ 0.092 (19)	0.241 $\pm$ 0.139 (17)
Milled	0.50	Rotahaler®	30	Carrageenan	0.073 $\pm$ 0.075 (10)	0.325 $\pm$ 0.087 (13)
Milled	0.50	Rotahaler®	15	Gelatin	-0.031 $\pm$ 0.016 (16)	0.117 $\pm$ 0.075 (26)
Milled	0.50	Rotahaler®	15	Carrageenan	0.021 $\pm$ 0.052 (12)	0.151 $\pm$ 0.117 (21)
Milled	1.00	Inhalator®	30	Gelatin	0.351 $\pm$ 0.348 (5)	0.737 $\pm$ 0.303 (5)
Milled	1.0	Inhalator®	30	Carrageenan	1.403 $\pm$ 0.305 (1)	2.002 $\pm$ 0.532 (1)
Milled	1.0	Inhalator®	15	Gelatin	-0.092 $\pm$ 0.169 (21)	0.368 $\pm$ 0.059 (11)
Milled	1.0	Inhalator®	15	Carrageenan	0.797 $\pm$ 0.107 (3)	1.218 $\pm$ 0.192 (4)
Milled	1.0	Rotahaler®	30	Gelatin	-0.121 $\pm$ 0.050 (24)	0.254 $\pm$ 0.035 (14)
Milled	1.0	Rotahaler®	30	Carrageenan	0.176 $\pm$ 0.047 (6)	0.250 $\pm$ 0.106 (15)
Milled	1.0	Rotahaler®	15	Gelatin	-0.006 $\pm$ 0.058 (14)	0.122 $\pm$ 0.071 (25)
Milled	1.0	Rotahaler®	15	Carrageenan	0.129 $\pm$ 0.019 (8)	0.209 $\pm$ 0.111 (20)

Table A1 (Continued)

Lactose	Drug load (%)	Inhaler	Capsule fill (mg)	Capsule	Net charge (nC) (rank order) <sup>a</sup>	Charge magnitude (nC) (rank order) <sup>b</sup>
Sieved	0.50	Inhalator <sup>®</sup>	30	Gelatin	-0.186 ± 0.156 (26)	0.236 ± 0.174 (18)
Sieved	0.50	Inhalator <sup>®</sup>	30	Carrageenan	0.025 ± 0.062 (11)	0.096 ± 0.042 (27)
Sieved	0.50	Inhalator <sup>®</sup>	15	Gelatin	-0.113 ± 0.080 (23)	0.144 ± 0.065 (22)
Sieved	0.50	Inhalator <sup>®</sup>	15	Carrageenan	0.016 ± 0.060 (13)	0.062 ± 0.030 (30)
Sieved	0.50	Rotahaler <sup>®</sup>	30	Gelatin	-0.106 ± 0.024 (22)	0.131 ± 0.007 (24)
Sieved	0.50	Rotahaler <sup>®</sup>	30	Carrageenan	-0.067 ± 0.013 (18)	0.074 ± 0.010 (29)
Sieved	0.50	Rotahaler <sup>®</sup>	15	Gelatin	-0.049 ± 0.025 (17)	0.051 ± 0.026 (31)
Sieved	0.50	Rotahaler <sup>®</sup>	15	Carrageenan	-0.029 ± 0.013 (15)	0.042 ± 0.009 (32)
Sieved	1.0	Inhalator <sup>®</sup>	30	Gelatin	-1.170 ± 0.228 (32)	1.265 ± 0.263 (2)
Sieved	1.0	Inhalator <sup>®</sup>	30	Carrageenan	-0.653 ± 0.373 (31)	0.725 ± 0.359 (7)
Sieved	1.0	Inhalator <sup>®</sup>	15	Gelatin	-0.356 ± 0.117 (30)	0.379 ± 0.110 (10)
Sieved	1.0	Inhalator <sup>®</sup>	15	Carrageenan	-0.294 ± 0.139 (29)	0.363 ± 0.197 (12)
Sieved	1.0	Rotahaler <sup>®</sup>	30	Gelatin	-0.220 ± 0.070 (28)	0.243 ± 0.060 (16)
Sieved	1.0	Rotahaler <sup>®</sup>	30	Carrageenan	-0.211 ± 0.031 (27)	0.218 ± 0.035 (19)
Sieved	1.0	Rotahaler <sup>®</sup>	15	Gelatin	-0.132 ± 0.021 (25)	0.141 ± 0.025 (23)
Sieved	1.0	Rotahaler <sup>®</sup>	15	Carrageenan	-0.082 ± 0.056 (20)	0.090 ± 0.048 (28)

<sup>a</sup> Determined by addition of all charges across the stages; starts with most positive charge.

<sup>b</sup> Determined by addition of absolute value of all charges across the stages; starts with largest charge.

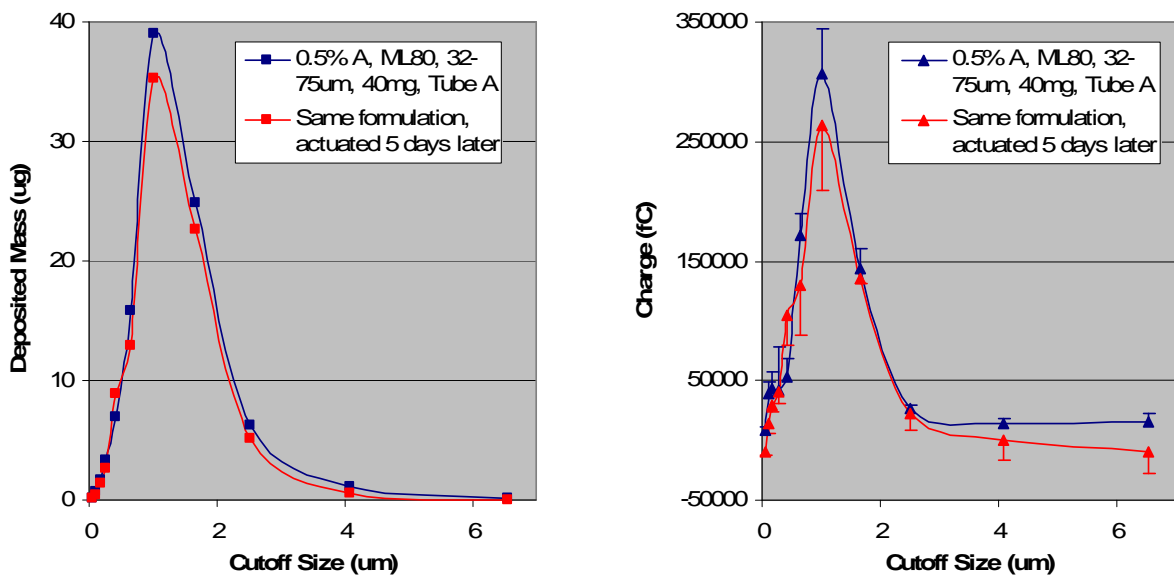
## References

- Bailey, A.G., 1997. The inhalation and deposition of charged particles within the human lung. *J. Electrostat.* 42, 25.
- Bailey, A.G., Hashish, A.H., Williams, T.J., 1998. Drug delivery by inhalation of charged particles. *J. Electrostat.* 44, 3.
- Balachandran, W., Machowski, W., Gaura, E., Hudson, C., 1997. Control of drug aerosol in human airways using electrostatic forces. *J. Electrostat.* 40-1, 579.
- Brouwer, D.H., Gijssbers, J.H., Lurvink, M.W., 2004. Personal exposure to ultra-fine particles in the workplace: exploring sampling techniques and strategies. *Ann. Occup. Hyg.* 48, 439.
- Clark, A.R., Hollingworth, A.M., 1993. The relationship between powder inhaler resistance and peak inspiratory conditions in healthy volunteers—implications for in-vitro testing. *J. Aerosol Med. Deposit. Clear. Eff. Lung* 6, 99.
- Dunbar, C.A., Hickey, A.J., Holzner, P., 1998. Dispersion and characterization of pharmaceutical dry powder aerosols. *KONA* 16, 7.
- Ferge, T., Maguhn, J., Felber, H., Zimmermann, R., 2004. Particle collection efficiency and particle re-entrainment of an electrostatic precipitator in a sewage sludge incineration plant. *Environ. Sci. Technol.* 38, 1545.
- Gonda, I., 2004. Targeting by deposition. In: Hickey, A.J., Wada, K., Hiraki, A. (Eds.), *Pharmaceutical Inhalation Aerosol Technology*. Marcel Dekker, New York.
- Hashish, A.H., Bailey, A.G., Williams, T.J., 1994. Modeling the effect of charge on selective deposition of particles in a diseased lung using aerosol boli. *Phys. Med. Biol.* 39, 2247.
- Hinds, W.C., 1999. *Aerosol Technology: Properties, Behavior and Measurement of Airborne Particles*. John Wiley & Sons, New York.
- Holmen, B.A., Qu, Y., 2004. Uncertainty in particle number modal analysis during transient operation of compressed natural gas, diesel, and trap-equipped diesel transit buses. *Environ. Sci. Technol.* 38, 2413.
- Keskinen, J., Pietarinen, K., Lehtimäki, M., 1992. Electrical low-pressure impactor. *J. Aerosol Sci.* 23, 353.
- Kwok, P.C.L., Glower, W., Chan, H.-K., 2005. Electrostatic charge characteristics of aerosols produced from metered dose inhalers. *J. Pharm. Sci.* 94, 2789.
- Labiris, N.R., Dolovich, M.B., 2003. Pulmonary drug delivery. Part I: physiological factors affecting therapeutic effectiveness of aerosolized medications. *Br. J. Clin. Pharmacol.* 56, 588.
- Lehmann, U., Niemela, V., Mohr, M., 2004. New method for time-resolved diesel engine exhaust particle mass measurement. *Environ. Sci. Technol.* 38, 5704.
- Liu, B.Y., Pui, D.Y., Rubow, K.L., Szymanski, W.W., 1985. Electrostatic effects in aerosol sampling and filtration. *Ann. Occup. Hyg.* 29, 251.
- Maricq, M.M., Chase, R.E., Xu, N., Podsiadlik, D.H., 2002. The effects of the catalytic converter and fuel sulfur level on motor vehicle particulate matter emissions: gasoline vehicles. *Environ. Sci. Technol.* 36, 276.
- Marjamäki, M., Keskinen, J., Chen, D.R., Pui, D.Y.H., 2000. Performance evaluation of the electrical low-pressure impactor (ELPI). *J. Aerosol Sci.* 31, 249.
- Murtomaa, M., Mellin, V., Harjunen, P., Lankinen, T., Laine, E., Lehto, V.P., 2004. Effect of particle morphology on the triboelectrification in dry powder inhalers. *Int. J. Pharm.* 282, 107.
- Murtomaa, M., Strengell, S., Laine, E., Bailey, A., 2003. Measurement of electrostatic charge of an aerosol using a grid-probe. *J. Electrostat.* 58, 197.
- Sanders, P.G., Xu, N., Dalka, T.M., Maricq, M.M., 2003. Airborne brake wear debris: size distributions, composition, and a comparison of dynamometer and vehicle tests. *Environ. Sci. Technol.* 37, 4060.
- Srichana, T., Martin, G.P., Marriott, C., 1998. Dry powder inhalers: the influence of device resistance and powder formulation on drug and lactose deposition in vitro. *Eur. J. Pharm. Sci.* 7, 73.
- Telko, M.J., Hickey, A.J., 2005. Dry powder inhaler formulation. *Respir. Care* 50, 1209.
- Timsina, M.P., Martin, G.P., Marriott, C., Ganderton, D., Yianneskis, M., 1994. Drug-delivery to the respiratory-tract using dry powder inhalers. *Int. J. Pharm.* 101, 1.
- Virtanen, A., Marjamäki, M., Ristimäki, J., Keskinen, J., 2001. Fine particle losses in electrical low-pressure impactor. *J. Aerosol Sci.* 32, 389.
- Wilson, L.B., 1947. The deposition of charged particles in tubes, with reference to the retention of therapeutic aerosols in the human lung. *J. Colloid Sci.* 2, 271.

## APPENDIX D.

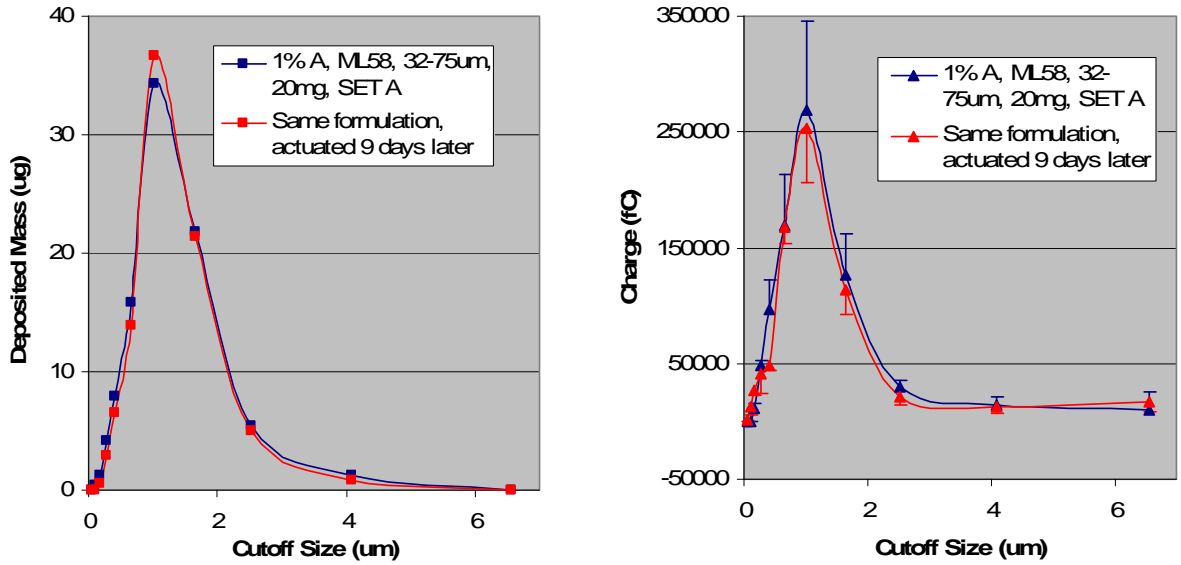
### EFFECT OF STORAGE ON DISPERSION AND CHARGE

To assess storage effects, 20 randomly selected formulations were retested (roughly 1/3 of the experiments). These retests were performed on different days, after varying times of storage in closed glass vials at lab conditions (i.e. 23-24°C and 35±5% RH); varying from hours to 50 days of storage. The following figures show drug depositions (after 3 actuations, determined from chemical assay) and the distribution of charge (average of 3 actuations with standard deviation). Figure D.1 shows a formulation that was retested five days after the original sample was examined; this formulation (0.5% albuterol in 45-75µm ML80 lactose) showed very good reproducibility in both mass deposited (FPF) and charge distribution.



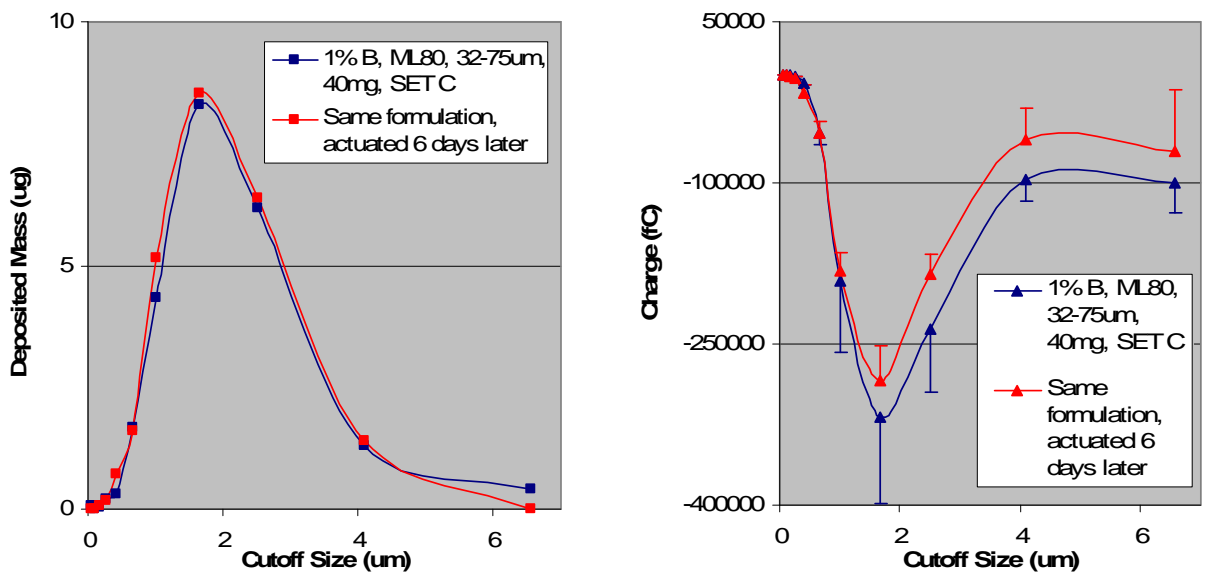
**Figure D.1.** Formulation (0.5% albuterol in 45-75µm ML80 lactose, 40mg) actuated from SET A (three times) on different days, separated by **5 days of storage**. The differences in deposition (actual quantities shown) are minimal. Differences in charge distribution mirror the differences in deposition, and are within a standard deviation from one another.

Figure D.2 also shows excellent reproducibility for a different formulation, with different drug concentration and utilizing a different lactose batch (1% albuterol in 45-75µm ML58 lactose). Retested nine days after the first experiment, the reproducibility of both mass and charge distribution was also excellent in this case.



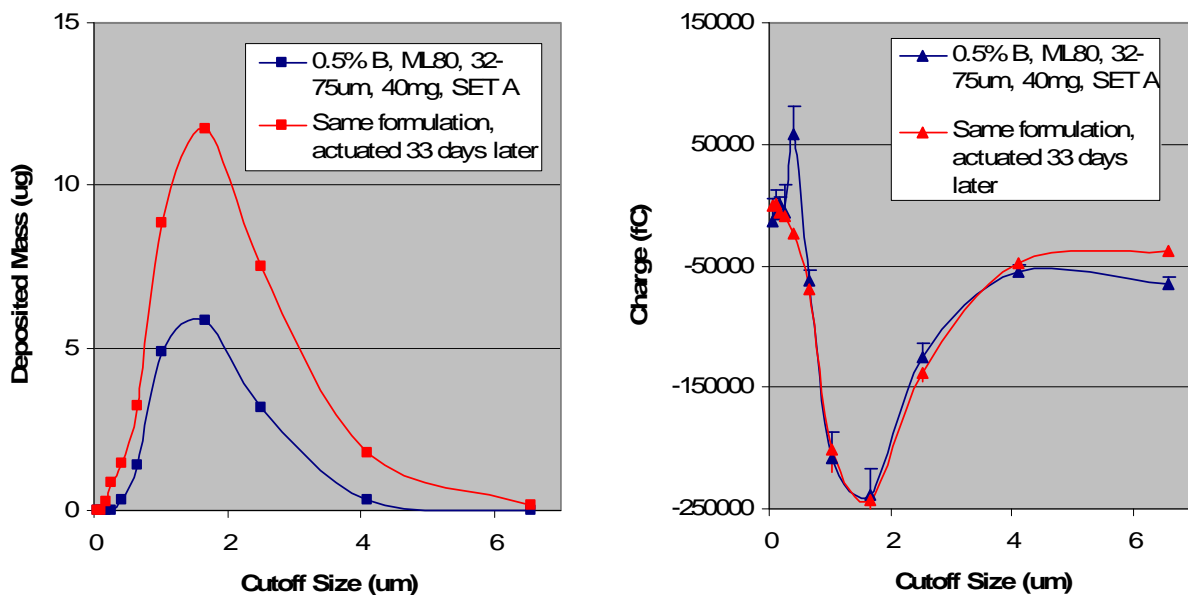
**Figure D.2.** Formulation (1% albuterol in 45-75 $\mu$ m ML58 lactose, 20mg) actuated from SET A (three times) on different days, separated by **9 days of storage**. Reproducibility is very good.

Figure D.3 shows the reproducibility for a formulation containing 1% budesonide (in 45-75 $\mu$ m ML80 lactose); drug deposition and charge distribution are similar after 6 days of storage. However, the lower pressure drop fluidization conditions (SET C) result in larger variability in the charge deposition (or standard deviation) than seen in previous figures.



**Figure D.3.** Same formulation (1% budesonide in 45-75 $\mu$ m ML80 lactose) actuated from SET C (three times) on different days, separated by **6 days of storage**. Differences in deposition (actual quantities shown) are minimal; differences in charge distribution are within standard deviation and follow deposition patterns.

In general, very good reproducibility of both drug deposition and charge was observed when the replicate was performed less than two weeks after the first run; in these cases, the FPF and  $d_{25}$ ,  $d_{50}$ , and  $d_{75}$  values varied by no more than 10% and the total charge recovered varied by no more than 20% from the first actuation. However, an analysis of all 20 replicates and comparison to original actuations revealed in part significant variation in deposition when storage time exceeds approximately two weeks. This suggests the prevalence of significant storage effects. Two such examples are given in Figures C.4 and C.5, which show the reproducibility of a budesonide and an albuterol based formulation after 33 and 49 days of storage, respectively. However, somewhat unexpectedly, both figures show a significant increase in the fine particle fraction after storage. The changes in the charge distributions on the other hand are inconsistent. Figure D.4 shows a virtually identical charge distribution after storage (despite the dramatically larger mass deposited on the stages), while Figure D.5 shows an altogether different charge distribution profile. Clearly, storage affects the triboelectric properties of different formulations differently.



**Figure D.4.** Same formulation (0.5% budesonide in 45-75µm ML80 lactose) actuated from SET A (three times) on different days, separated by **33 days of storage**. The differences in deposition (actual quantities shown) are quite large with significantly more deposition after storage. Despite these differences the charge distributions are virtually the same.

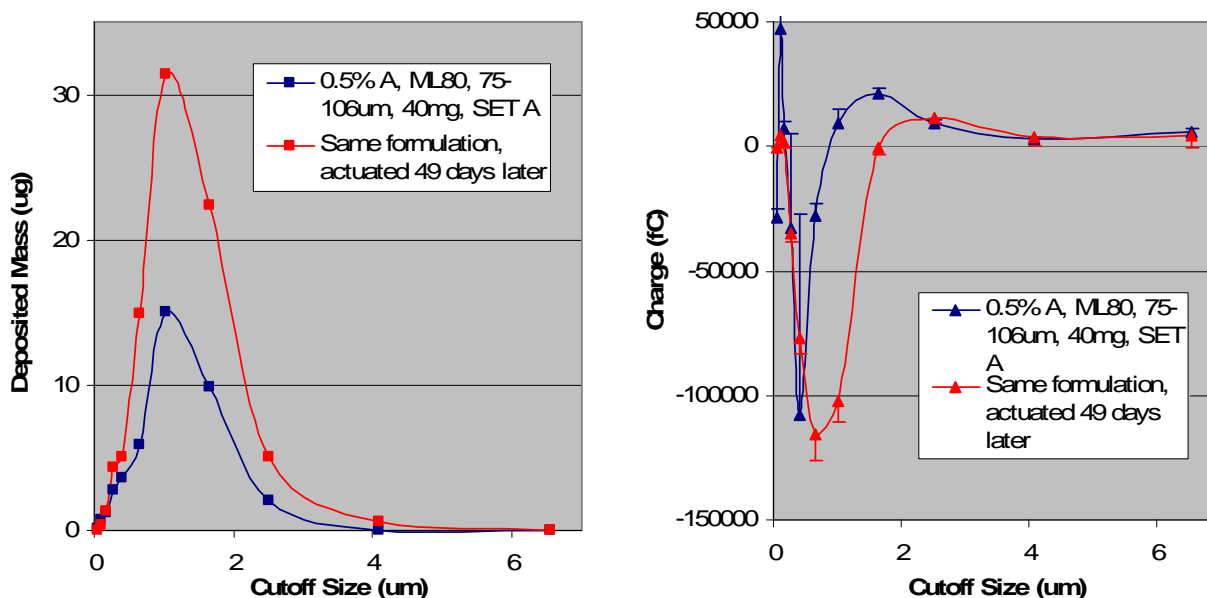


**Figure D.5.** Same formulation (0.5% albuterol in 75-106 $\mu$ m ML80 lactose) actuated from SET A (three times) on different days, separated by **49 days of storage**.

The observation that drug delivery from the formulation improves after storage, highlighted in Figures C.4 and C.5, is counter-intuitive. Yet, it was also observed in many other replicates, though a small number of formulations showed deterioration in delivery. Figure D.6 shows the observed percentage changes in (a) FPF and (b) total charge (sum of actual recovered charges and sum of absolute magnitudes) plotted over storage time for all replicates. Because each point represents a different formulation, it is perhaps difficult to speak of trends; individual formulations respond differently to storage. However, two general observations can be made: (1) The longer the storage time, the more pronounced the changes in FPF. Up to the first two weeks of storage changes in delivery are minor, but increase afterwards. (2) While the data is quite variable, most formulations seem to have better delivery after storage; a line that is fitted to the data has a positive slope, only two formulations show significant deterioration in delivery. The observation seems to hold for both albuterol and budesonide formulations, but the most dramatic improvements are seen with the lactose batches. Note that the changes in the FPF are not accompanied by changes in the normalized particle size distributions ;  $d_{25}$ ,  $d_{50}$ , and  $d_{75}$  remain unchanged.

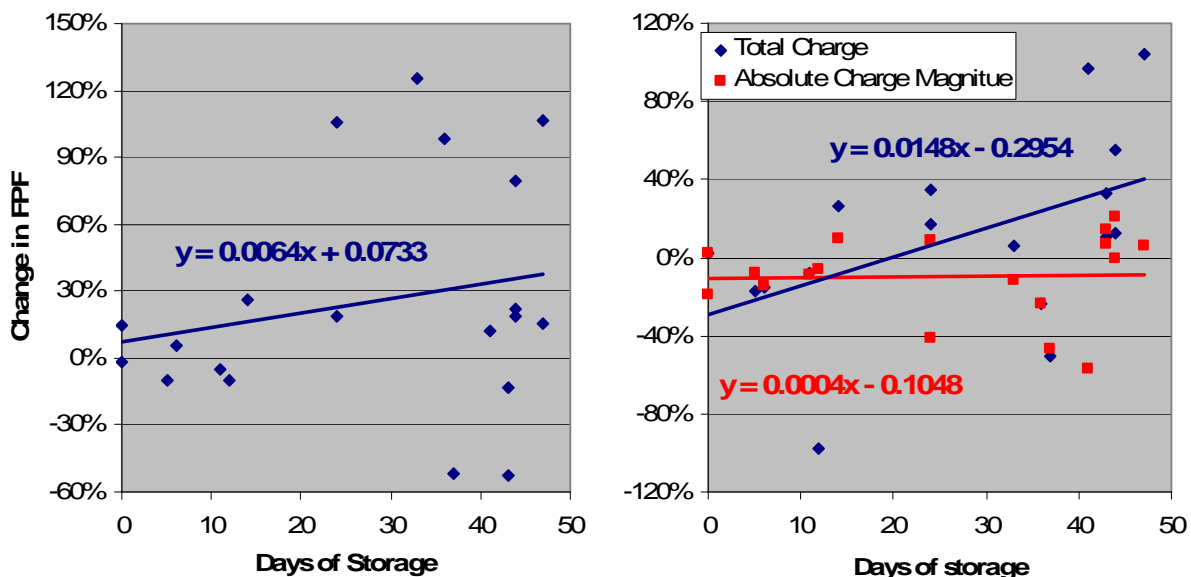


**Figure D.6.** Changes in (a) FPF and (b) charge as a result of storage. Each point in the graph represents a different formulation that was retested after a variable number of days in storage (x-axis). For most formulations, storage seems to increase the FPF, i.e. it results in an improvement of drug/carrier separation. The charge becomes more positive after storage, even though the magnitude remains unchanged.

Figure D.6(b) shows changes in the charge deposition over storage time. Total charge (sum of actual recovered charges) is shown in blue and absolute charge magnitude (sum of absolute value of charges summed across the size fractions) is plotted in red. It appears that after storage, most actuations result in slightly more positive charge deposition, while the magnitude of the charge itself (on average) does not change. The absolute charge magnitude varies little, with most points within 20% of the initial measurements (despite the fact that the magnitude itself varies widely between different actuations); the best-fit line for the change in absolute magnitude is almost horizontal (+0.04%/day), indicating no change on average. This is a surprising result; based on the larger deposition of mass, more charge would be expected. Instead the charges become more positive; yet on a per mass basis they may actually decrease. This is highlighted in Figure D.7, where the changes in charge are plotted against the changes in mass deposition (FPF). The total captured charge becomes more positive as the mass deposition is increased, yet the absolute magnitude of the charge changes little, which actually implies a per particle decrease in charge. One plausible explanation for



this observation is that the charge relaxes upon storage, i.e. the formulation components lose their charge to each other or to their environment (e.g. storage container), and that the reduction in charge results in lower attractive forces and thus better particle separation. This effect requires further investigation with respect to defined formulations.

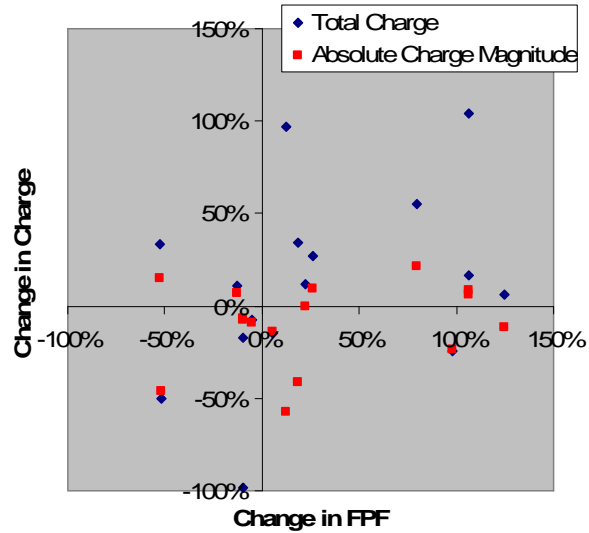


**Figure D.7.** The change in charge plotted against the change in deposited mass. Essentially, the ordinate data in Figures 5.10 (a) and (b) give the abscissa and ordinate in Figure 5.11. The figure indicates more clearly that the total charge becomes more positive but the sum of charges changes little in absolute magnitude.